

Dist: A 1

CASE NO. 0704-0128

1. AGENCY USE ONLY (Leave blank)				2. REPORT DATE 2/15/94		3. REPORT TYPE AND DATES COVERED FINAL 8/15/90-12/14/94	
4. TITLE AND SUBTITLE Micromechanical Prediction of Tensile Damage For Ceramic Matrix Composites Under High-Temperature						5. FUNDING NUMBERS G-AFOSR-90-0341 2306/BS	
6. AUTHOR(S) F. Delale and B. M. Liaw							
7. PERFORMING ORGANIZATION NAME(S) AND ADDRESS(ES) The City College of New York Dept. of Mechanical Engng. 138th Street & Convent Ave. New York, NY 10031						8. PERFORMING ORGANIZATION REPORT NUMBER 447276/3 0701 AFOSR-TR-94 0611	
9. SPONSORING/MONITORING AGENCY NAME(S) AND ADDRESS(ES) Dr. Alexander Pechenik AFOSR/NA Building 410 Bolling AFB, DC 20332-6448						10. SPONSORING/MONITORING AGENCY REPORT NUMBER AFOSR-90-0344	
11. SUPPLEMENTARY NOTES							
12a. DISTRIBUTION/AVAILABILITY STATEMENT Unlimited						12b. DISTRIBUTION CODE A	
13. ABSTRACT (Maximum 200 words) <p>This report documents the experimental and theoretical results obtained in studying the tensile damage behavior of ceramic matrix composites (namely Nicalon/CAS II composites) at room and elevated temperatures.</p> <p>First the composite specimens were machined into dog-bone shape and polished to increase efficacy of observation in the SEM. Then the specimens were placed inside the chamber of a scanning electron microscope (SEM) and subject to tensile loading at room and higher temperatures up to 700 °C. At each temperature, the load was increased until failure of the specimen and the progression of damage was observed and recorded from first crack to total failure. Damage usually started with matrix cracking, followed by debonding along fiber-matrix interface, fiber pullout and finally fiber breakage. At each load level, the displacement was measured, resulting in a stress-strain curve with linear and non-linear portions. Similar behavior was observed at higher temperatures.</p> <p>Theoretical models to predict and simulate the observed behavior were also developed. A singular integral formulation with periodic matrix cracking and interface debonding explains well the fact that embedded matrix cracks almost always propagate to the interface and are arrested by the fibers. The results obtained from finite element model with multiple rows of matrix cracks and debonding at the fiber/matrix interface, compare extremely well with the experimental data.</p> <p>DTIC QUALITY INSPECTED 5</p>							
14. SUBJECT TERMS Ceramic Matrix Composites, matrix cracking, interfacial cracking, fiber pull-out, fiber breaking, tensile damage, high temperature.						15. NUMBER OF PAGES 91	
17. SECURITY CLASSIFICATION OF REPORT Unclassified						18. SECURITY CLASSIFICATION OF THIS PAGE Unclassified	
19. SECURITY CLASSIFICATION OF ABSTRACT Unclassified						20. LIMITATION OF ABSTRACT UL	

Table of contents

Overview.....	1
1. Introduction.....	3
2. The experimental work.....	5
2.1 The testing procedure.....	5
2.2 Experimental results.....	9
2.21 Stress-strain relations.....	9
2.22 Matrix crack density.....	12
2.23 Effect of fiber volume fraction.....	12
2.24 Temperature effects.....	13
2.25 Specimen size effects.....	14
3. Theoretical models.....	16
3.1 Singular integral equations formulation.....	16
3.1.1 Formulation of the problem.....	18
3.1.1.1 Equilibrium equations.....	18
3.1.1.2 Stress-strain relations.....	20
3.1.1.3 Strain-displacement relations.....	20
3.1.2 Boundary and continuity conditions.....	21
3.1.3 Asymptotic analysis of the kernels.....	29
3.1.4 Normalization of the singular integral equations.....	32
3.1.5 Determination of singularities for different crack geometry.....	37
3.1.6 Numerical solutions.....	44
3.1.6.1 Embedded cracks.....	44
3.1.6.2 Matrix cracks touching the interface.....	50
3.1.6.3 H-shaped cracks.....	52
3.1.7 Results and discussion for singular integral equation formulation.....	55
3.2 Finite element analysis.....	60
3.2.1 Description of the H-shaped crack model.....	60
3.2.2 finite element results and discussion.....	61
References.....	63
Figures.....	68
Appendix A.....	i
Appendix B.....	viii
Appendix C.....	xiii
Appendix D.....	xviii
Appendix E.....	xxiii

<input checked="" type="checkbox"/>
<input type="checkbox"/>
<input type="checkbox"/>

by Codes

Dist	Avail and/or Special
A-1	

19941128 027

OVERVIEW

Tensile stress-strain behavior has been widely recognized as the most important single property for ceramic matrix composites. In this study, the tensile failure mechanism of the ceramic matrix composites has been investigated.

First, the dog-bone tensile specimens made of unidirectional ceramic matrix composite namely: Nicalon Fiber ($\text{Si}_3\text{C}_4\text{O}$, β phase) and CAS II ($\text{CaO-Al}_2\text{O}_3\text{-2SiO}_2$) matrix with fiber volume fractions of 30% and 40% were tested in room as well as in elevated temperatures. All tests were conducted inside a chamber of a scanning electron microscope (SEM). Therefore, images at various magnifications revealing the intermediate tensile damage events in the composite specimen were obtained *in-situ* along with other testing data. Since the lens in the SEM is always kept at least one inch away from the specimen during testing, with magnifications ranging from 50x to as high as 3000x, the heat on the specimen won't damage the electron lens. This makes it possible to obtain images while doing tensile testing in high temperature. The damage histories of the specimen at different temperatures were first observed on the monitor of the SEM and then captured immediately either by Polaroid camera or video copy processor. Tensile stress-strain curves were constructed at different temperatures (starting from room temperature, then 250 °C, 400 °C, 600 °C and 700 °C). All tests exhibited a non-linear stress-strain behavior. The effect of specimen size (meaning specimens with different thickness or width in the gauge section) on the failure behavior was discussed. It was found that while thin specimens (about 0.0625 "-0.07 " in either thickness or width) tend to have a tail at failure, retaining some load carrying capability, thick specimens (greater than 0.0725" on both thickness and width) fail catastrophically, breaking into two pieces. The effect of temperature on tensile failure strength was found not quite significant within the temperatures tested. Micrographs taken at different loading and temperatures revealed

the details of damage process from first matrix cracking to multiple matrix cracking, sequential random fiber slipping and fiber breaking to eventual composite failure by sudden fiber pull-out and collective fiber breaking somewhere in the gage section. Matrix crack density versus the stress with different fiber volume fraction and at different temperatures was also studied. The results indicate that, for specimens with 30% fiber volume fraction, the matrix crack initiation stress is less than that of 40% fiber volume fraction. And the matrix crack density (defined as the number of matrix cracks per mm) for specimens of 40% fiber volume fraction is higher than that for those with 30% fiber volume fraction. It is also noted that matrix crack initiation stress was lower in high temperature than in room temperature for specimens of both 30% and 40% fiber volume fraction.

Then, analytical models based on finite element method and the singular integral equation technique were used to explain the tensile damage behavior of the ceramic matrix composites. The H-shaped crack geometry was used in the finite element model to study the interface progression and its effect on the tensile damage behavior. The results from finite element model compare well with the experimental results. The singular behavior at the transverse and interface crack tips were studied using singular integral equations. The stress intensity factors and strain energy release rates were calculated for various crack geometry and were used to explain the failure mechanism of the composites. The results from the singular integral equation technique predict that once the transverse matrix cracks are formed, they will propagate to the fiber/matrix interface. This behavior conforms to the observed behavior. Both models assume that the composite consists of equal spaced fiber strips in the matrix material and the problem is simplified as two dimensional.

1 INTRODUCTION

The research on ceramic matrix composite materials has intensified in recent years due to some of the appealing features of ceramics; such as great stability and resistance to oxidation under hostile (high temperature or corrosive) environments. In comparison to their metallic and polymer counterparts, ceramics, being brittle and low in tensile strength and fracture toughness, traditionally have had little use in structural applications. However, when reinforced with fibers, ceramic matrix composites exhibit an increase in fracture toughness and tensile strength in room as well as high temperatures [1-2]. A variety of ceramic matrix composite systems have been or are being developed for engineering applications ranging from cutting tools to aerospace structures [3-4]. For examples, one can find studies on the following systems of ceramic matrix composites: C/glass [5], C/SiC [6], SiC/glass [7], SiC/LAS glass ceramic [8-13], SiC/BMAS glass-ceramic [13], SiC/alumina [14], SiC/mullite [15], SiC/SiC [16].

In the aforementioned studies, experimental results on damage behaviors of ceramic matrix composites were obtained by failing the specimens with either tensile or three-point bending loading at room or elevated temperature [9-12]. During the thermomechanical testing, the load vs. the displacement (and hence the stress vs. the strain) curves were recorded but only the postmortem damage patterns were identified by either a scanning electron or an optical microscope. It is well known that the stress-strain relations of most ceramic matrix composites under thermomechanical loading usually exhibit nonlinear behaviors. For such ceramic-matrix composites, the failure mechanisms that cause this nonlinear stress-strain relationship is more complex than that of their monolithic counterparts. They come from the results of multiple matrix cracking and sequential fiber breaking due to weak interfacial bonding between the fibers and the matrix. The approaches described above although proved important data to the overall understanding

of the failure mechanisms of the ceramic matrix composites, they fail to correlate the nonlinear stress-strain (and hence the stiffness reduction) behavior with the intermediate damage progression events inside the ceramic matrix composite specimen. A good experimental approach should provide information on the damage history of the specimen that can be used to correlate the nonlinear stress-strain (and hence the stiffness reduction) behavior with the intermediate causative damage events that occurred on the ceramic matrix composite specimen. Recently, in [17-18], the tensile behavior of a Nicalon/CAS II system was studied. Damage patterns were identified and micrographs were taken to capture the matrix crack propagation. However, these micrographs were not taken at the same location and therefore cannot truly correlate the damage progression with the nonlinear stress-strain behavior. And those studies dealt only with room temperature. In this study, experiments were conducted inside the chamber of a scanning electron microscope equipped with a custom designed tensile/heating substage. This made it possible to directly observe and record *in situ* the progressive tensile damage behavior of the ceramic matrix composites from the very first matrix crack to complete fracture of the specimen at any location in the gage section. Test results for both room and elevated temperatures were obtained. One particular advantage of using SEM is for high temperature testing. Since in SEM, unlike in optical microscope, the electronic lens is always kept at least one inch away from the heated specimen, images can be obtained at magnifications as high as 3000x. without damaging the electronic lens during high temperature testing. This makes the technique very appealing for high temperature testing.

Among the factors that affect the overall strength and toughness of the ceramic matrix composites, the following are generally considered the most important: (a) the thermoelastic properties of the constituents (i.e., the matrix and the fibers); (b) the relative strength of the interface between fibers and matrix; (c) the volume fraction and

arrangement of the fibers; and (d) the ambient temperature. Based on the above considerations and observations during the test, two analytical models have been developed. One model utilizes the finite element technique and is based on a periodic multiple-row H-shaped crack configuration. The other uses the singular integral equation method with periodic transverse and interface crack configuration. In both models the real problem is formulated in two dimensional domain.

2 THE EXPERIMENTAL WORK

The experimental work is vital in this study. It provides important insight and data for the understanding of the failure process of this type of composite material. And it also provides the foundation upon which analytical models are based. The technique used in this study is believed to be first developed in the area of experimental mechanics research.

2.1 THE TESTING PROCEDURE

Figure 2.1 shows a schematic drawing of the experimental set-up which uses a scanning electron microscope equipped with a tensile and heating substage to perform the micromechanical tensile testing of a ceramic matrix composite specimen under high temperature. In this study, a Hitachi S-2400 scanning electron microscope is used which is equipped with a custom designed E.F. Fullam tensile/heating combined substage. The specimen used is simple "dog-bone" shaped specimen such as the one shown in Fig. 2.2. The actual experimental set-up and tensile/heating substage are shown in Fig. 2.3. The material used in this study (Nicalon-fiber/CAS II matrix composite) was obtained from Corning Glass Works. Table 2.1 shows the thermomechanical properties of the constituents of the composite. Specimens of both 30% and 40% fiber volume fractions were tested. To study the size effect, we varied either the thickness or the width of the

specimen for specimens with 40% fiber volume fraction. Fibers were unidirectionally aligned with the gage-length direction. The tensile specimens were made by first cutting the large rectangular ceramic matrix composite panel as supplied by Corning Glass Works into smaller rectangular plates using a Leco VC-50 Cari/Cut fine-mesh diamond saw. Then the gage section of the specimens was shaped using the same diamond saw with special a holder. The gage section of the specimens was grounded to its dimensions using a Dremel motorized hand-held grinder with silicon carbide and alumina oxide stones.

Table 1. Properties of Nicalon fiber and CAS II matrix

	CAS II Matrix	Nicalon Fiber
Nominal Composition	CaO-Al ₂ O ₃ -2SiO ₂	Si ₃ C ₄ O
Elastic Modulus Msi(GPa)		
25°C	13.8 (95)	28.3 (195)
1000°C	13.5 (93)	22.9 (158)
1200°C	11.7 (81)	22.5 (155)
Thermal Expansion(10 ⁶ /°C)		
	5.0 (25°-1000°C)	3.1 (25°C-200°C)
	-----	4.0 (25°C-1000°C)
Fracture Toughness K _{IC} (MPa m ^{1/2})		
25°C	2.16±0.11	-----
1000°C	1.30±0.17	-----
Fiber/Matrix Interfacial Shear Strength		
25°C	15.7±2.0 MPa	

To conduct high temperature testing, the bottom surface of the central part of the specimen as shown in Fig. 2.1, was placed in direct contact with the E.F. Fullam heating element (called heater) which is a rectangular plate made of ceramic material with fuse wire circuit inside. The maximum heated area of the heating element is 0.65"x0.25". It can sustain a maximum working temperature of 1100°C and is equipped with a water-cooled heat sink for continuous operation. Temperature is measured by three platinum 30% rhodium-platinum 6% rhodium thermocouples and controlled by a stand-alone DC power supply with adjustable voltage and current knobs. Since the whole operation is conducted inside the chamber of a scanning electron microscope (in this study a Hitachi S-2400) which is usually vacuumed at 1.5×10^{-6} Pa or better, no heat-loss will occur due to thermal convection. The top surface of the specimen was first polished using fine-grade diamond paste containing 15-, 6-, and 1-micron particles until the surface was well finished and the fibers and matrix could be seen clearly under a Nikon UM-2 microscope. Then the specimen was cleaned using a Bronson ultrasonic cleaner for 10 minutes. Finally the bottom surface of the specimen was coated with silver paint to prevent electric charging and to achieve better image before it was mounted into the E.F. Fullam tensile substage. Because it is very difficult to drill holes in a ceramic composite specimen, the top and bottom ends of the specimen were mounted through stainless steel clamps with serrated teeth to the crossheads of the E.F. Fullam tensile substage. To help in alignment and prevent slippage during testing between the ceramic composite specimen and the serrated clamps, cyanoacrylate-based extra-strength epoxy was also applied on the clamp-specimen interfaces. The clamped specimen was then mounted to the tensile substage and was left to cure for at least 20 hours to ensure that the epoxy had hardened and was completely dry before testing.

Finally, the specimen together with the tensile/heating assembly was placed inside the chamber of a Hitachi S-2400 scanning electron microscope which is also equipped with a backscatter detector to enhance the image. By using the X-Y staging control of the scanning electron microscope, micrographical patterns within the central gage area can be observed and recorded. The tensile substage is driven by a variable-speed motor which has a maximum speed of 90 rpm. Through a gear mechanism of 100:1 reduction ratio, the crosshead speed can be controlled within 0.127 mm/min (or 0.005 in/min). The tensile stage can provide a tensile load of up to 455 kgs (1000 lbs). The applied load was increased gradually until the specimen failed totally. The damage to the composite as the load increased was first observed on the monitor of the SEM. Then a sequence of micrographs were taken to get hard copies of various microcracking and damage patterns of the specimen at different loading levels. Since the specimen is very thin thickness (ranges from 1.0 mm to 2.0 mm or 0.04" to .08"), it is expected that failure will occur through the thickness. Thus the recorded micrographs of the surface fracture can represent through-the-thickness failure of the specimen. Quality of the image and hence the quality of the micrographs was further enhanced by transmitting the image signal to a computer which is equipped with an Imaging Technology Advanced Frame Grabber (AFG) digital image analyzer hardware. With the help of the installed software, sharper images were obtained through the contrast and edge enhancement operations. And text can be added to the micrographs.

The tensile stage is designed in such a way that when the load increases, the top and bottom crossheads move in opposite directions to minimize the shift of the observed site. This is achieved by machining the stainless-steel loading columns into worms of reverse directions. Thus searching and refocusing the damaged zone after each load increment are very handy. The applied loads were recorded by a miniature load cell equipped with a

digital readout. The relative displacements of the crossheads were measured by a high-precision, strain-gage-type extensometer which is also fitted with a digital readout. The load-displacement data were recorded and converted into a stress-strain curve. The evolution of damage recorded by micrographs were identified with the corresponding stress and strain. Finally the ruptured specimens were observed under a Nikon UM-2 universal measuring microscope for further postmortem examination.

2.2 EXPERIMENTAL RESULTS

2.2.1 Stress-Strain Relations

Typical stress-strain curves for the room-temperature, tensile damage behavior of a Nicalon/CAS II with 30% and 40% fiber volume fractions are shown in Fig. 2.4 and Fig 2.5 respectively. As depicted in these two figures, the tensile damage behavior of the ceramic matrix composite specimen is characterized by a nonlinear curve made up of three sections. The characteristics are the same for all tests conducted in this study, even though microscopically these specimens might look quite different. Upon load application, the relation between stress and strain was linear and its slope was equivalent to the stiffness of an intact Nicalon/CAS II specimen (18.15 Msi or 125 GPa for $V_f = 30\%$ and 19.6 Msi or 135 GPa for $V_f = 40\%$). For specimens with 30% fiber volume fraction, the slope changed at about 25 ksi (Point A in Fig 2.4). While for 40% fiber volume fraction, the slope changed at about 30 ksi (Point A in Fig. 2.5). First matrix crack is believed to start at or slightly below of point A in both $V_f = 30\%$ and 40% cases. This can be further inferred from the relationship between matrix crack density and tensile stress as will be discussed later in this section. In most cases, matrix cracking initiates either at the edge or at a location where the fiber spacing is maximum. Fig 2.6 shows some micrographs taken during one test. The second micrograph in Fig. 2.6 clearly indicates that matrix crack

initiated not from the voids but from the location where spacing between the two adjacent fibers is the largest. While in Fig. 2.7, matrix cracks initiated from both the edge and a location where fiber spacing is very large if not the largest. The matrix cracks then propagate perpendicular to the fiber direction throughout the whole width of the gage section to form multiple matrix cracks. Unlike the monolithic materials where failure is controlled by a critical crack size, the failure of the composite goes through a process of damage accumulation. The composite is insensitive to the voids and can tolerate very large cracks before failure. At point B (35 ksi for $V_f = 30\%$ and 40 ksi for $V_f = 40\%$), the development of multiple matrix cracks reached a saturated stage. Regularly spaced matrix cracks were formed in the whole gage section of the specimen. This happened with only a small increment of tensile stress (about 10 ksi, as can be seen from point A to point B in both Fig. 2.4 and Fig. 2.5). Further increase of tensile stress creates no or very little additional matrix cracking. Matrix crack opening, fiber debonding, breaking and slipping will dominate the rest of the failure process. Upon reaching point C (about 62 ksi for $V_f = 30\%$ and 58 ksi for $V_f = 40\%$), one surface of the matrix cracks in the gage area started to open up with crack opening displacement far more larger than the rest of the matrix cracks. This then was accompanied by massive fiber breaking and pull-out in that surface. And the eventual separation of the specimen caused the load to drop substantially. Depending on whether the specimen is thin (either in thickness or in width) or thick, there might be a tail in the stress-strain curve at the load drop. Thin specimens tend to have a tail at failure as indicated in Fig. 2.5 where both thin and thick specimens were tested. One explanation is that thin specimens are prone to bending during the test. This might be responsible for the lower failure strength and a tail at failure for thin specimens. For thick specimens, failure is always catastrophic. Fig. 2.8 shows the progression of damage for a thin specimen. At failure, the specimen (this occurred only for thin specimens) was kept in

one piece by the fibers. Further loading after failure was possible as shown in Fig. 2.9. Micrographs in Fig. 2.10 however, show the catastrophic failure of a thick specimen. Upon reaching the maximum stress value, the specimen fails catastrophically with a very big crack opening at the failure surface. Observation on the failure surfaces of the specimens with 30% and 40% fiber volume fractions, indicated that there are significant differences in both the amount and the length of fiber pull-out between the two specimens. For specimens with $V_f = 30\%$, both the amount and the length of fiber pull-out at failure surface are less than those with $V_f = 40\%$ as can be seen from Fig. 2.11 and Fig. 2.12. The lesser amount of fiber pull-out and the shorter fiber pull-out length is an indication of stronger interfacial bonding strength. This explained why the tensile failure strength of $V_f = 30\%$ is slightly higher than that of $V_f = 40\%$. The smoothness of fiber pull-out surface as shown in Fig. 2.13 is evidence of non-chemical bonding between fibers and matrix which generally implies weak interfacial bonding strength. The fiber pull-out length and its amount also deviated substantially among the same batch of specimens as shown in Fig. 2.14, implying that the fiber/matrix interfacial strength may vary for the same batch of ceramic matrix composite specimens. This is also reflected by the fluctuation of the maximum tensile stresses (Point C) among these tests.

Figure 2.15 is a set of micrographs showing typical damage patterns of the specimen at different magnifications after the stress reached point B in the stress-strain curve. At close-up, one can clearly identify the matrix crack opening, fiber breaking, slipping and fiber bridging of the matrix cracks. Also from Fig 2.15, one can observe the typical "H" shaped crack pattern formed by intersection of the transverse matrix cracks with interface cracks during the failure process. This "H" shaped crack configuration will be used in the analytical models discussed later. Besides the easily identified matrix crack patterns, fiber breaking also exhibits some patterns as shown in Fig. 2.16 and Fig. 2.17. In Fig. 2.16, one

fiber breaks at a location away from the matrix cracks first, then a ray of breaking fibers is formed along a line slanted away from the line of matrix cracks. Fiber breaking occurred mostly after the stress reached point B, i.e. after the multiple matrix cracks have been formed. Micrograph in Fig 2.17 gives another pattern of fiber breaking in which fiber breaking is randomly distributed throughout the whole gage section.

The stress-strain relations of the Nicalon/CAS II composite at high temperatures will be discussed later.

2.2.2 Matrix Crack Density

Matrix crack density defined as the number of matrix cracks per 1 mm length in fiber direction, was used to characterize the failure process of the composite. With the help of the scanning electron microscope equipped with a backscatter detector, images reflecting the tensile damage pattern of the composite from the first matrix crack to the eventual failure of the composite were captured. Fig 2.18 and Fig. 2.19 are some micrographs showing the development of matrix cracks with increasing stresses for $V_f = 30\%$ and $V_f = 40\%$ respectively. Based on the number of cracks counted in the frame shown in these micrographs and the associated stress level, the matrix crack density versus tensile stress curve was constructed as shown in Fig 2.20 and Fig 2.21 for 30% and 40% fiber volume fractions respectively. From the matrix crack density curves, it is seen that the matrix crack initiation stress is 25 ksi for $V_f = 30\%$ and 30 ksi for $V_f = 40\%$. These results happen to coincide with point A on the stress-strain curves as shown in both Fig 2.4 and Fig 2.5.

2.2.3 Effect of Fiber Volume Fractions

As can be seen from the stress-strain and matrix crack density curves for specimens of both 30% and 40% fiber volume fractions, the fiber volume fraction affects the tensile behavior substantially. Matrix crack initiation stress is less for specimens with less fiber volume fraction (compare points A in Fig 2.4 and Fig. 2.5). This result is in agreement with that given in [19]. But the tensile failure strength for $V_f = 30\%$ is higher than that for $V_f = 40\%$ (points C in the stress-strain curves). This might be the result of a relatively stronger interfacial bonding strength for specimens with $V_f = 30\%$. The matrix crack density was found to increase with increasing fiber volume fraction of the specimen. This finding also agrees with that reported in [19].

2.2.4 Temperature Effects

The same specimens were tested in the SEM at 250 °C, 400 °C, 600 °C and 700 °C. Fig. 2.22 and Fig. 2.23 show the stress-strain curves obtained at higher temperatures for fiber volume fractions 30% and 40% respectively. Within the temperature range tested (room temperature, 250 °C, 400 °C, 600 °C and 700 °C), no significant changes in ultimate tensile strength have been observed in the stress-strain curves. Fig. 2.24 and Fig. 2.25 show the temperature effects on the ultimate tensile failure strength of the specimens for both 30% and 40% fiber volume fractions. There was a slight increase in tensile failure strength for $V_f = 30\%$ at $T = 250$ °C . Micrographs showing the final failure surfaces of the specimens with $V_f = 30\%$ at different temperatures are compared in Fig. 2.26. It is seen that both the amount and the length of fiber full-out are the smallest for $T = 250$ °C. This might explain why the tensile strength is maximum at $T = 250$ °C. For $V_f = 40\%$, this increase of tensile strength happened at $T = 400$ °C. The phenomenon of slight increase of tensile strength might be the result of release of thermal residual stress and changing of interfacial bonding strength due to temperature. Matrix crack density did not show

significant changes with temperatures for $V_f = 30\%$. Micrographs in Fig. 2.27 show the development of matrix cracks at $T = 600^\circ\text{C}$. Fig. 2.28 shows the relation between the matrix crack density and temperatures (ranging from room to 600°C) for $V_f = 30\%$. But for $V_f = 40\%$, it was found that matrix crack density decreased with increasing temperature as shown in micrographs of Fig. 2.29 taken at $T = 400^\circ\text{C}$. Fig. 2.30 plots the relation of matrix crack density versus temperature for $V_f = 40\%$. Matrix crack initiation stress also decreased slightly at high temperatures for $V_f = 40\%$. Micrographs in Fig 2.31 and Fig. 2.32 show the fiber breaking and slipping process in high temperatures. Since this composite is basically a glass based material, the stress-strain behavior is expected to be quite different when temperature reaches over 800°C .

2.2.5 Specimen Sizing Effects

To study the size effect, specimens of 40% fiber volume fraction with different thickness and width combination were used in the tests. It was found that specimens with either relatively thin thickness or width (about 0.0625~0.07") tended to have a quite different failure pattern than that with thicker one (greater than 0.0725" in both thickness and width). For thin specimens, first, the tensile strength was quite lower than that of thick specimens; second, when the specimen failed, it had a tail in the stress-strain curve indicating that it still retained some load carrying capability and the specimen was kept in one piece by the fibers. The thick specimens on the other hand always failed catastrophically. A comparison of tensile strength between thin and thick specimens against temperature is shown in Fig 2.33. The discrepancy between the two cases might be the result of bending that might have occurred during the test as explained earlier. Size effect of the specimens on the flexural strength of unidirectional carbon epoxy composites has been reported in the literature [20-21]. Since there are some definite relations between

flexural strength and tensile strength, tensile strength will be affected by the size of the specimen as well. From the standpoint of Weibull failure theory, thick specimens tend to contain large defects, therefore they should fail at a lower tensile loading. Since the composite with a relatively weak interfacial bonding strength is insensitive to the defects, the opposite results were obtained here. The specimen didn't fail by one defect or crack when it reaches the critical size, but through the damage accumulation all over the gage section. For thin Nicalon/CAS II specimens with 40% fiber volume fraction, the stress-strain curves at high temperatures were shown in Fig. 2.34.

3 THEORETICAL MODELS

As explained earlier, during testing, it was found that, after the initiation of transverse matrix cracks at point A (in both Figs. 2.4 and 2.5), with increasing load, regularly spaced multiple transverse cracks were formed. When the tensile stress reached a certain value, almost no new transverse cracks were generated until failure. During this process further transverse matrix cracks opening, fiber debonding, breaking and sliding at the fiber/matrix interface is believed to dominate the failure process. This typical failure feature is best described by the periodic H-cracks configuration shown in Fig. 2.15. Two models, one using singular integral equation technique, and the other using finite element method, are adopted to either explain the failure mechanism or simulate the observed tensile behavior of ceramic matrix composites.

The problem of concern is basically a three dimensional problem because of the distribution of fibers in the matrix. However, if one assumes that the fibers are made of composite strips of width $2H_1$, the problem can be treated in two dimensions.

3.1 Singular Integral Equations Formulation.

It has been shown that the singular integral equation technique is a very powerful tool in dealing with crack problems. Fig. 3.1 is a sketch of the proposed mathematical model. It is assumed that fibers are equally spaced in a ceramic matrix, and that the thermomechanical and fracture properties of the fiber and the matrix are known. The model contains cracks perpendicular to as well as parallel to the fibers at the fiber/matrix interface and which are assumed to be periodic. By choosing different geometrical parameters, one can generate various crack geometries. For example: If one sets $a_1=0$, $a_2=H_2$ and $b_1=0$ in Fig. 3.1, then the model reduces to a geometry with periodic H-shaped cracks as shown in Fig. 3.2. This configuration closely resembles the actual cracked geometry observed in testing.

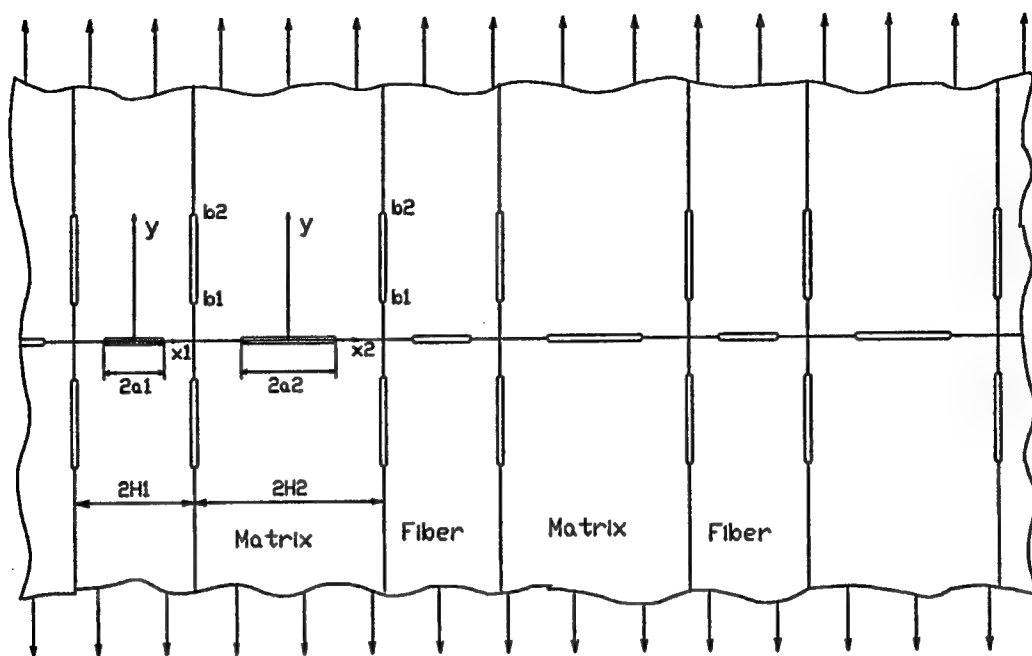


Fig. 3.1 Mathematical model

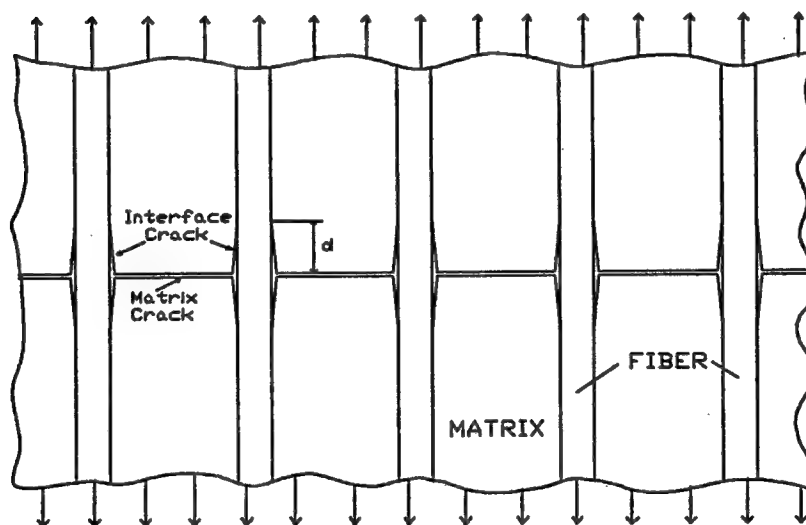


Fig. 3.2 H-shaped cracks

3.1.1 Formulation of the problem

3.1.1.1 Equilibrium equations

The equilibrium equations expressed in terms of displacements for orthotropic materials are as follow:

$$\beta_1 \frac{\partial^2 u}{\partial x^2} + \frac{\partial^2 u}{\partial y^2} + \beta_3 \frac{\partial^2 v}{\partial x \partial y} = 0 \quad (3.1a)$$

$$\frac{\partial^2 v}{\partial x^2} + \beta_2 \frac{\partial^2 v}{\partial y^2} + \beta_3 \frac{\partial^2 u}{\partial x \partial y} = 0 \quad (3.1b)$$

where β_1 , β_2 and β_3 are material constants [23]

Assume that the solutions are of the following forms:

$$u(x,y) = u^{(1)}(x,y) + u^{(2)}(x,y) \quad (3.2a)$$

$$v(x,y) = v^{(1)}(x,y) + v^{(2)}(x,y) \quad (3.2b)$$

where

$$u^{(1)}(x,y) = \frac{2}{\pi} \int_0^\infty f(\alpha,x) \cos \alpha y d\alpha \quad (3.3a)$$

$$v^{(1)}(x,y) = \frac{2}{\pi} \int_0^\infty g(\alpha,x) \sin \alpha y d\alpha \quad (3.3b)$$

and

$$u^{(2)}(x,y) = \frac{2}{\pi} \int_0^\infty h(\alpha,y) \sin \alpha x d\alpha \quad (3.4a)$$

$$v^{(2)}(x,y) = \frac{2}{\pi} \int_0^\infty l(\alpha,y) \cos \alpha x d\alpha \quad (3.4b)$$

here $f(\alpha,x)$, $g(\alpha,x)$, $h(\alpha,y)$ and $l(\alpha,y)$ are shape functions

Substituting (3.3ab) and (3.4ab) into (3.1ab), one gets the following characteristic equation:

$$r^4 + \beta_4 r^2 + \beta_5^2 = 0 \quad (3.5)$$

where $\beta_4 = \frac{\beta_3^2 - \beta_1 \beta_2 - 1}{\beta_1}$ and $\beta_5 = \sqrt{\beta_2 / \beta_1}$

and the roots are obtained as:

$$r_1 = -r_3 = w_1 + iw_2 = \sqrt{(-\beta_4 + \beta_6)/2}$$

$$r_2 = -r_4 = w_3 + iw_4 = \sqrt{(-\beta_4 - \beta_6)/2}$$

where $\beta_6 = \sqrt{\beta_4^2 - 4\beta_5^2}$

Then we have:

$$f(\alpha, x) = A(\alpha)e^{r_1\alpha x} + B(\alpha)e^{-r_1\alpha x} + C(\alpha)e^{r_2\alpha x} + D(\alpha)e^{-r_2\alpha x} \quad (3.6a)$$

$$g(\alpha, x) = \beta_7[A(\alpha)e^{r_1\alpha x} - B(\alpha)e^{-r_1\alpha x}] + \beta_8[C(\alpha)e^{r_2\alpha x} - D(\alpha)e^{-r_2\alpha x}] \quad (3.6b)$$

$$h(\alpha, y) = E(\alpha)e^{r_1\alpha y/\beta_5} + F(\alpha)e^{-r_1\alpha y/\beta_5} + G(\alpha)e^{r_2\alpha y/\beta_5} + H(\alpha)e^{-r_2\alpha y/\beta_5} \quad (3.6c)$$

$$l(\alpha, y) = \beta_9[E(\alpha)e^{r_1\alpha y/\beta_5} - F(\alpha)e^{-r_1\alpha y/\beta_5}] + \beta_{10}[G(\alpha)e^{r_2\alpha y/\beta_5} - H(\alpha)e^{-r_2\alpha y/\beta_5}] \quad (3.6d)$$

Here two types of material will be distinguished according to whether the roots of the characteristic equation are real or complex.

Material type I: where both r_1 and r_2 are real numbers ($w_2=w_4=0$).

Material type II: where r_1 and r_2 are complex numbers.

Applying symmetry conditions:

$$u(x, y) = -u(-x, y) \quad (3.7a)$$

$$v(x, y) = -v(x, -y) \quad (3.7b)$$

we obtain:

$$B(\alpha) = -A(\alpha) \quad D(\alpha) = -C(\alpha) \quad (3.8ab)$$

$$F(\alpha) = -E(\alpha) \quad H(\alpha) = -G(\alpha) \quad (3.8cd)$$

Material type I will be considered because most materials fall into this category..

Based on the fact that both u and v vanish when $y \rightarrow \infty$, and that the problem of concern is symmetrical about the x axis, the displacement functions can be written as:

$$u(x,y) = \frac{4}{\pi} \int_0^\infty [A(\alpha) \sinh(w_1 \alpha x) + C(\alpha) \sinh(w_3 \alpha x)] \cos \alpha y d\alpha \\ + \frac{2}{\pi} \int_0^\infty [E(\alpha) e^{-|w_1| \alpha y / \beta_5} + G(\alpha) e^{-|w_3| \alpha y / \beta_5}] \sin \alpha x d\alpha \quad (3.9a)$$

$$v(x,y) = \frac{4}{\pi} \int_0^\infty [\beta_7 A(\alpha) \cosh(w_1 \alpha x) + \beta_8 C(\alpha) \cosh(w_3 \alpha x)] \sin \alpha y d\alpha \\ - \frac{2}{\pi} \int_0^\infty [\beta_9 \text{sign}(w_1) E(\alpha) e^{-|w_1| \alpha y / \beta_5} + \beta_{10} \text{sign}(w_3) G(\alpha) e^{-|w_3| \alpha y / \beta_5}] \cos \alpha x d\alpha \quad (3.9b)$$

3.1.1.2 Stress-strain relations

$$\text{Let } \Delta = \frac{(1 - v_{xy} v_{yx})}{E_x E_y},$$

then for orthotropic materials, under plane stress conditions'

$$\sigma_x(x,y) = \frac{1}{E_y \Delta} \epsilon_x + \frac{v_{yx}}{E_y \Delta} \epsilon_y \quad (3.10a)$$

$$\sigma_y(x,y) = \frac{v_{xy}}{E_x \Delta} \epsilon_x + \frac{1}{E_x \Delta} \epsilon_y \quad (3.10b)$$

$$\tau_{xy}(x,y) = G_{xy} \gamma_{xy} \quad (3.10c)$$

where E_x , E_y , G_{xy} , v_{xy} and v_{yx} are the orthotropic material constants.

3.1.1.3 Strain-displacement relations

In terms of u and v , the strains are given as:

$$\epsilon_x = \frac{\partial u}{\partial x}, \quad \epsilon_y = \frac{\partial v}{\partial y} \quad \text{and} \quad \gamma_{xy} = \left(\frac{\partial u}{\partial y} + \frac{\partial v}{\partial x} \right) \quad (3.11abc)$$

Substituting eqns (3.9ab) into (3.11) and then into (3.10), the stress can be written

as:

$$\frac{\pi(1 - v_{xy} v_{yx})}{2E_x} \sigma_x(x,y) = \int_0^\infty [\gamma_1 E(\alpha) e^{-|w_1| \alpha y / \beta_5} + \gamma_2 G(\alpha) e^{-|w_3| \alpha y / \beta_5}] \alpha \cos \alpha x d\alpha \\ + \int_0^\infty [2\gamma_3 A(\alpha) \cosh(w_1 \alpha x) + 2\gamma_4 C(\alpha) \cosh(w_3 \alpha x)] \alpha \cos \alpha y d\alpha \quad (3.12a)$$

$$\frac{\pi(1 - v_{xy} v_{yx})}{2E_y} \sigma_y(x,y) = \int_0^\infty [\gamma_5 E(\alpha) e^{-|w_1| \alpha y / \beta_5} + \gamma_6 G(\alpha) e^{-|w_3| \alpha y / \beta_5}] \alpha \cos \alpha x d\alpha$$

$$+ \int_0^\infty [2\gamma_7 A(\alpha) \cosh(w_1 \alpha x) + 2\gamma_8 C(\alpha) \cosh(w_3 \alpha x)] \alpha \cos \alpha y d\alpha \quad (3.12b)$$

$$\begin{aligned} \frac{\pi}{2G_{xy}} \tau_{xy}(x,y) = & \int_0^\infty [\gamma_{11} E(\alpha) e^{-lw_1 |\alpha y/\beta_5} + \gamma_{12} G(\alpha) e^{-lw_3 |\alpha y/\beta_5}] \alpha \sin \alpha x d\alpha \\ & + \int_0^\infty [2\gamma_9 A(\alpha) \sinh(w_1 \alpha x) + 2\gamma_{10} C(\alpha) \sinh(w_3 \alpha x)] \alpha \sin \alpha y d\alpha \end{aligned} \quad (3.12c)$$

The above expressions are for plane stress problems. It can also be used for plane strain problems with the following substitutions:

$$\begin{aligned} v_{yx} &= -\frac{E_x}{E_y} v_{yx}, & v_{xy} &= -\frac{E_y}{E_x} v_{xy}, \\ E_y \Delta &= E_x & \text{and} & \quad E_x \Delta = E_y. \end{aligned}$$

3.1.2 Boundary and continuity conditions

At the interface ($x_1 = H_1$, $x_2 = -H_2$)

$$\sigma_{1xx}(H_1, y) = \sigma_{2xx}(-H_2, y) \quad 0 < y < \infty \quad (3.13a)$$

$$\tau_{1xy}(H_1, y) = \tau_{2xy}(-H_2, y) \quad 0 < y < \infty \quad (3.13b)$$

$$u_1(H_1, y) = u_2(-H_2, y) \quad 0 < y < b_1 \text{ or } b_2 < y < \infty \quad (3.14a)$$

$$v_1(H_1, y) = v_2(-H_2, y) \quad 0 < y < b_1 \text{ or } b_2 < y < \infty \quad (3.14b)$$

$$\sigma_{1xx}(H_1, y) = p_3(y) \quad b_1 < y < b_2 \quad (3.15a)$$

$$\tau_{1xy}(H_1, y) = p_4(y) \quad b_1 < y < b_2 \quad (3.15b)$$

At $y = 0$ (cracks normal to the interface)

$$v_1(x_1, 0) = 0 \quad -H_1 < x_1 < -a_1 \text{ and } a_1 < x_1 < H_1 \quad (3.16a)$$

$$v_2(x_2, 0) = 0 \quad -H_2 < x_2 < -a_2 \text{ and } a_2 < x_2 < H_2 \quad (3.16b)$$

$$\sigma_{1yy}(x_1, 0) = -p_1(x_1) \quad -a_1 < x_1 < a_1 \quad (3.17a)$$

$$\sigma_{2yy}(x_2, 0) = -p_2(x_2) \quad -a_2 < x_2 < a_2 \quad (3.17b)$$

$$\tau_{1xy}(x_1, 0) = 0 \quad -H_1 < x_1 < H_1 \quad (3.18a)$$

$$\tau_{2xy}(x_2, 0) = 0 \quad -H_2 < x_2 < H_2 \quad (3.18b)$$

At $x_1 = 0$ or $x_2 = 0$

$$u_1(0, y) = 0 \quad 0 \leq y \leq \infty \quad (3.19a)$$

$$u_2(0,y)=0 \quad 0 \leq y \leq \infty \quad (3.19b)$$

$$\tau_{1xy}(0,y)=0 \quad 0 \leq y \leq \infty \quad (3.20a)$$

$$\tau_{2xy}(0,y)=0 \quad 0 \leq y \leq \infty \quad (3.20b)$$

where $p_1(x_1)$ is the normal traction on the fiber crack surfaces ($-a_1 < x_1 < a_1$ and $y=0$), $p_2(x_2)$ is the normal traction on matrix crack surfaces ($-a_2 < x_2 < a_2$ and $y=0$), $p_3(y)$ is the normal traction on crack surfaces along the interface ($x_1=H_1$, $b_1 < y < b_2$) and $p_4(y)$ is the shear traction on crack surfaces along the interface ($x_1=H_1$, $b_1 < y < b_2$).

Define:

$$\begin{aligned} \phi_1(x_1) &= \frac{\partial v_1(x_1, 0)}{\partial x_1}, & \phi_2(x_2) &= \frac{\partial v_2(x_2, 0)}{\partial x_2} \\ \phi_3(y) &= \frac{\partial}{\partial y}[v_1(+H_1, y) - v_2(-H_2, y)], & \phi_4(y) &= \frac{\partial}{\partial y}[u_1(+H_1, y) - u_2(-H_2, y)] \end{aligned} \quad (3.21abcd)$$

Then, from (3.14ab) and (3.16ab), one can write:

$$\phi_1(x_1) = 0 \quad a_1 < |x_1| < H_1 \quad (3.22a)$$

$$\phi_2(x_2) = 0 \quad a_2 < |x_2| < H_2 \quad (3.22b)$$

$$\phi_3(y) = 0 \quad 0 < y < b_1 \quad \& \quad b_2 < y < \infty \quad (3.22c)$$

$$\phi_4(y) = 0 \quad 0 < y < b_1 \quad \& \quad b_2 < y < \infty \quad (3.22d)$$

Using eqn(3.9a) and (3.12c), eqns(3.19a,b) and (3.20a,b) are satisfied identically.

Substituting eqns(3.18a,b) into (3.12c) we have:

$$E(\alpha) = -\frac{\gamma_{12}}{\gamma_{11}}G(\alpha), \quad E^*(\alpha) = -\frac{\gamma_{12}^*}{\gamma_{11}^*}G^*(\alpha)$$

Then eqns(3.9a,b) and (3.12a,b,c) become:

$$\begin{aligned} u(x,y) &= \frac{4}{\pi} \int_0^\infty [A(\alpha) \sinh(w_1 \alpha x) + C(\alpha) \sinh(w_3 \alpha x)] \cos \alpha y d\alpha \\ &+ \frac{2}{\pi} \int_0^\infty E(\alpha) [e^{-|w_1| \alpha y / \beta_5} - \frac{\gamma_{11}}{\gamma_{12}} e^{-|w_3| \alpha y / \beta_5}] \sin \alpha x d\alpha \end{aligned} \quad (3.9a^*)$$

$$v(x,y) = \frac{4}{\pi} \int_0^\infty [\beta_7 A(\alpha) \cosh(w_1 \alpha x) + \beta_8 C(\alpha) \cosh(w_3 \alpha x)] \sin \alpha y d\alpha$$

$$-\frac{2}{\pi} \int_0^\infty E(\alpha) [\beta_9 \text{sign}(w_1) e^{-|w_1|\alpha y/\beta_5} - \frac{\gamma_{11}}{\gamma_{12}} \beta_{10} \text{sign}(w_3) e^{-|w_3|\alpha y/\beta_5}] \cos \alpha x d\alpha \quad (3.9b^*)$$

$$\begin{aligned} \frac{\pi(1-v_{xy}v_{yx})}{2E_x} \sigma_x(x,y) &= \int_0^\infty E(\alpha) [\gamma_1 e^{-|w_1|\alpha y/\beta_5} - \gamma_2 \frac{\gamma_{11}}{\gamma_{12}} e^{-|w_3|\alpha y/\beta_5}] \alpha \cos \alpha x d\alpha \\ &+ \int_0^\infty [2\gamma_3 A(\alpha) \cosh(w_1 \alpha x) + 2\gamma_4 C(\alpha) \cosh(w_3 \alpha x)] \alpha \cos \alpha y d\alpha \end{aligned} \quad (3.12a^*)$$

$$\begin{aligned} \frac{\pi(1-v_{xy}v_{yx})}{2E_y} \sigma_y(x,y) &= \int_0^\infty E(\alpha) [\gamma_5 e^{-|w_1|\alpha y/\beta_5} - \gamma_6 \frac{\gamma_{11}}{\gamma_{12}} e^{-|w_3|\alpha y/\beta_5}] \alpha \cos \alpha x d\alpha \\ &+ \int_0^\infty [2\gamma_7 A(\alpha) \cosh(w_1 \alpha x) + 2\gamma_8 C(\alpha) \cosh(w_3 \alpha x)] \alpha \cos \alpha y d\alpha \end{aligned} \quad (3.12b^*)$$

$$\begin{aligned} \frac{\pi}{2G_{xy}} \tau_{xy}(x,y) &= \int_0^\infty E(\alpha) \gamma_{11} [e^{-|w_1|\alpha y/\beta_5} - e^{-|w_3|\alpha y/\beta_5}] \alpha \sin \alpha x d\alpha \\ &+ \int_0^\infty [2\gamma_9 A(\alpha) \sinh(w_1 \alpha x) + 2\gamma_{10} C(\alpha) \sinh(w_3 \alpha x)] \alpha \sin \alpha y d\alpha \end{aligned} \quad (3.12c^*)$$

Applying eqns(3.16a,b), at $y = 0$, one obtains:

$$v_1(x_1,0) = -\frac{2}{\pi} \int_0^\infty E(\alpha) [\beta_9 \text{sign}(w_1) - \frac{\gamma_{11}}{\gamma_{12}} \beta_{10} \text{sign}(w_3)] \cos \alpha x_1 d\alpha \quad a_1 < x_1 < H_1 \quad (3.23a)$$

$$v_2(x_2,0) = -\frac{2}{\pi} \int_0^\infty E^*(\alpha) [\beta_9^* \text{sign}(w_1^*) - \frac{\gamma_{11}^*}{\gamma_{12}^*} \beta_{10}^* \text{sign}(w_3^*)] \cos \alpha x_2 d\alpha \quad a_2 < x_2 < H_2 \quad (3.23b)$$

with

$$\phi_1(x_1) = \frac{\partial v_1(x_1,0)}{\partial x_1} = \frac{2}{\pi} \int_0^\infty \gamma_{13} E(\alpha) \alpha \sin \alpha x_1 d\alpha,$$

$$\phi_2(x_2) = \frac{\partial v_2(x_2,0)}{\partial x_2} = \frac{2}{\pi} \int_0^\infty \gamma_{13}^* E^*(\alpha) \alpha \sin \alpha x_2 d\alpha$$

The inverse Fourier transform gives:

$$E(\alpha) = \frac{1}{\gamma_{13} \alpha} \int_0^{a_1} \phi_1(x_1) \sin \alpha x_1 dx_1 \quad (3.24a)$$

$$E^*(\alpha) = \frac{1}{\gamma_{13}^* \alpha} \int_0^{a_2} \phi_2(x_2) \sin \alpha x_2 dx_2 \quad (3.24b)$$

Substituting eqns(3.24a,b) into eqn(3.9b) respectively and applying eqns(3.17a,b), one can derive:

$$\begin{aligned} & \gamma_{14} \int_{-a_1}^{a_1} \frac{\phi_1(t)}{t-x_1} dt + \int_0^\infty [2\gamma_7 A(\alpha) \cosh(w_1 \alpha x_1) + 2\gamma_8 C(\alpha) \cosh(w_3 \alpha x_1)] \alpha d\alpha \\ &= -\frac{\pi(1-v_{xy}v_{yx})}{2E_y} p_1(x_1) \end{aligned} \quad (3.25a)$$

$$\begin{aligned} & \gamma_{14}^* \int_{-a_2}^{a_2} \frac{\phi_2(t)}{t-x_2} dt + \int_0^\infty [2\gamma_7^* A^*(\alpha) \cosh(w_1^* \alpha x_2) + 2\gamma_8^* C^*(\alpha) \cosh(w_3^* \alpha x_2)] \alpha d\alpha \\ &= -\frac{\pi(1-v_{xy}v_{yx})}{2E_y^*} p_2(x_2) \end{aligned} \quad (3.25b)$$

where γ_i and γ_i^* are given in Appendix B.

Substituting eqns (3.24a,b) into eqns(3.15a,b), one has:

$$\begin{aligned} \frac{\pi(1-v_{xy}v_{yx})}{2E_x} p_3(y) &= \lim_{x_i \rightarrow H_i} \int_0^\infty \int_0^{a_1} \frac{\phi_1(t)}{\gamma_{13}} \sin \alpha t dt [\gamma_1 e^{-lw_1| \alpha y / \beta_5} - \gamma_2 \frac{\gamma_{11}}{\gamma_{12}} e^{-lw_3| \alpha y / \beta_5}] \cos \alpha x_1 d\alpha \\ &+ \lim_{x_i \rightarrow H_i} \int_0^\infty [2\gamma_3 A(\alpha) \cosh(w_1 \alpha x_1) + 2\gamma_4 C(\alpha) \cosh(w_3 \alpha x_1)] \alpha \cos \alpha y d\alpha \quad b_1 < y < b_2 \end{aligned} \quad (3.26a)$$

$$\begin{aligned} \frac{\pi}{2G_{xy}} p_4(y) &= \lim_{x_i \rightarrow H_i} \int_0^\infty \int_0^{a_1} \frac{\phi_1(t)}{\gamma_{13}} \sin \alpha t dt \gamma_{11} [e^{-lw_1| \alpha y / \beta_5} - e^{-lw_3| \alpha y / \beta_5}] \sin \alpha x_1 d\alpha \\ &+ \lim_{x_i \rightarrow H_i} \int_0^\infty [2\gamma_9 A(\alpha) \sinh(w_1 \alpha x_1) + 2\gamma_{10} C(\alpha) \sinh(w_3 \alpha x_1)] \alpha \sin \alpha y d\alpha \quad b_1 < y < b_2 \end{aligned} \quad (3.26b)$$

Applying eqns(A.5a,b), eqns(3.26a,b) can be further reduced to:

$$\begin{aligned} & \int_{-a_1}^{a_1} \frac{\phi_1(t)}{2\gamma_{13}} \left[-\gamma_1 \frac{H_1-t}{\beta_5^2 + (H_1-t)^2} + \gamma_2 \left(\frac{\gamma_{11}}{\gamma_{12}} \right) \frac{H_1-t}{\beta_5^2 + (H_1-t)^2} \right] dt \\ &+ \lim_{x_i \rightarrow H_i} \int_0^\infty [2\gamma_3 A(\alpha) \cosh(w_1 \alpha x_1) + 2\gamma_4 C(\alpha) \cosh(w_3 \alpha x_1)] \alpha \cos \alpha y d\alpha \\ &= \frac{\pi(1-v_{xy}v_{yx})}{2E_x} p_3(y) \quad b_1 < y < b_2 \end{aligned} \quad (3.26a^*)$$

and

$$\begin{aligned}
& \int_{-a_1}^{a_1} \frac{\gamma_{11}\phi_1(t)}{2\gamma_{13}} \left[\frac{\frac{|w_1|y}{\beta_5}}{\frac{(|w_1|y)^2}{\beta_5^2} + (H_1-t)^2} - \frac{\frac{|w_3|y}{\beta_5}}{\frac{(|w_3|y)^2}{\beta_5^2} + (H_1-t)^2} \right] dt \\
& + \lim_{x_i \rightarrow H_1} \int_0^\infty [2\gamma_9 A(\alpha) \sinh(w_1 \alpha x_1) + 2\gamma_{10} C(\alpha) \sinh(w_3 \alpha x_1)] \alpha \sin \alpha y d\alpha \\
& = \frac{\pi}{2G_{xy}} p_4(y) \quad b_1 < y < b_2 \quad (3.26b*)
\end{aligned}$$

Applying eqns(3.14a,b), (3.13a,b) and (3.21a,b,c,d), one obtains:

$$\begin{aligned}
& A(\alpha) \sinh(w_1 \alpha H_1) + C(\alpha) \sinh(w_3 \alpha H_1) \\
& + A^*(\alpha) \sinh(w_1^* \alpha H_2) + C^*(\alpha) \sinh(w_3^* \alpha H_2) = R_1(\alpha) \quad (3.27a)
\end{aligned}$$

$$\begin{aligned}
& \beta_7 A(\alpha) \cosh(w_1 \alpha H_1) + \beta_8 C(\alpha) \cosh(w_3 \alpha H_1) \\
& - \beta_7^* A^*(\alpha) \cosh(w_1^* \alpha H_2) - \beta_8^* C^*(\alpha) \cosh(w_3^* \alpha H_2) = R_2(\alpha) \quad (3.27b)
\end{aligned}$$

$$\begin{aligned}
& [\gamma_3 A(\alpha) \cosh(w_1 \alpha H_1) + \gamma_4 C(\alpha) \cosh(w_3 \alpha H_1) \\
& - \lambda_1 \gamma_3^* A^*(\alpha) \cosh(w_1^* \alpha H_2) - \lambda_1 \gamma_4^* C^*(\alpha) \cosh(w_3^* \alpha H_2)] \alpha = R_3(\alpha) \quad (3.27c)
\end{aligned}$$

$$\begin{aligned}
& [\gamma_9 A(\alpha) \sinh(w_1 \alpha H_1) + \gamma_{10} C(\alpha) \sinh(w_3 \alpha H_1) \\
& + \lambda_2 \gamma_9^* A^*(\alpha) \sinh(w_1^* \alpha H_2) + \lambda_2 \gamma_{10}^* C^*(\alpha) \sinh(w_3^* \alpha H_2)] \alpha = R_4(\alpha) \quad (3.27d)
\end{aligned}$$

where $R_1(\alpha)$, $R_2(\alpha)$, $R_3(\alpha)$ and $R_4(\alpha)$ are given in Appendix A.

Solving eqns(3.27abcd) for $A(\alpha)$, $C(\alpha)$, $A^*(\alpha)$ and $C^*(\alpha)$, we have:

$$A(\alpha) = \frac{1}{\cosh(w_1 \alpha H_1)} \left[\frac{R_1(\alpha)}{f(\alpha)} g_1(\alpha) + \frac{R_2(\alpha)}{f(\alpha)} h_1(\alpha) + \frac{R_3(\alpha)}{f(\alpha)} m_1(\alpha) + \frac{R_4(\alpha)}{f(\alpha)} n_1(\alpha) \right] \quad (3.28a)$$

$$C(\alpha) = \frac{1}{\cosh(w_3 \alpha H_1)} \left[\frac{R_1(\alpha)}{f(\alpha)} g_2(\alpha) + \frac{R_2(\alpha)}{f(\alpha)} h_2(\alpha) + \frac{R_3(\alpha)}{f(\alpha)} m_2(\alpha) + \frac{R_4(\alpha)}{f(\alpha)} n_2(\alpha) \right] \quad (3.28b)$$

$$A^*(\alpha) = \frac{1}{\cosh(w_1^* \alpha H_2)} \left[\frac{R_1(\alpha)}{f(\alpha)} g_3(\alpha) + \frac{R_2(\alpha)}{f(\alpha)} h_3(\alpha) + \frac{R_3(\alpha)}{f(\alpha)} m_3(\alpha) + \frac{R_4(\alpha)}{f(\alpha)} n_3(\alpha) \right] \quad (3.28c)$$

$$C^*(\alpha) = \frac{1}{\cosh(w_3^* \alpha H_2)} \left[\frac{R_1(\alpha)}{f(\alpha)} g_4(\alpha) + \frac{R_2(\alpha)}{f(\alpha)} h_4(\alpha) + \frac{R_3(\alpha)}{f(\alpha)} m_4(\alpha) + \frac{R_4(\alpha)}{f(\alpha)} n_4(\alpha) \right] \quad (3.28d)$$

where $f(\alpha)$, $g_i(\alpha)$, $h_i(\alpha)$, $m_i(\alpha)$ and $n_i(\alpha)$ ($i=1,2,3,4$) are given in Appendix C.

Substituting (3.28a,b,c,d) into (3.25a,b) and (3.26a*,b*):

$$\begin{aligned}
& \frac{1}{\pi} \int_{-a_1}^{a_1} \left[\frac{1}{t-x_1} + \pi K_{11}(x_1, t) \right] \phi_1(t) dt + \int_{-a_2}^{a_2} K_{12}(x_1, t) \phi_2(t) dt \\
& + \int_{b_1}^{b_2} K_{13}(x_1, t) \phi_3(t) dt + \int_{b_1}^{b_2} K_{14}(x_1, t) \phi_4(t) dt \\
& = - \frac{(1-v_{xy}v_{yx})}{2\gamma_{14}E_y} p_1(x_1) \quad -a_1 < x_1 < a_1 \quad (3.29a)
\end{aligned}$$

$$\begin{aligned}
& \int_{-a_1}^{a_1} K_{21}(x_2, t) \phi_1(t) dt + \frac{1}{\pi} \int_{-a_2}^{a_2} \left[\frac{1}{t-x_2} + \pi K_{22}(x_2, t) \right] \phi_2(t) dt \\
& + \int_{b_1}^{b_2} K_{23}(x_2, t) \phi_3(t) dt + \int_{b_1}^{b_2} K_{24}(x_2, t) \phi_4(t) dt \\
& = - \frac{(1-v_{xy}^*v_{yx}^*)}{2\gamma_{14}^*E_y^*} p_2(x_2) \quad -a_2 < x_2 < a_2 \quad (3.29b)
\end{aligned}$$

$$\begin{aligned}
& \int_{-a_1}^{a_1} K_{31}(y, t) \phi_1(t) dt + \int_{-a_2}^{a_2} K_{32}(y, t) \phi_2(t) dt \\
& + \int_{b_1}^{b_2} K_{33}'(y, t) \phi_3(t) dt + \int_{b_1}^{b_2} K_{34}'(y, t) \phi_4(t) dt \\
& = \frac{(1-v_{xy}v_{yx})}{2E_x} p_3(y) \quad b_1 < y < b_2 \quad (3.29c)
\end{aligned}$$

$$\begin{aligned}
& \int_{-a_1}^{a_1} K_{41}(y, t) \phi_1(t) dt + \int_{-a_2}^{a_2} K_{42}(y, t) \phi_2(t) dt \\
& + \int_{b_1}^{b_2} K_{43}'(y, t) \phi_3(t) dt + \int_{b_1}^{b_2} K_{44}'(y, t) \phi_4(t) dt
\end{aligned}$$

$$= \frac{1}{2G_{xy}} p_4(y) \quad b_1 < y < b_2 \quad (3.29d)$$

where

$$\begin{aligned} K_{11}(x_1, t) &= \frac{1}{\gamma_{14}\pi} \int_0^\infty [k_1(x_1, \alpha) e^{-\alpha(H_1-t)\beta_5/w_1} + k_2(x_1, \alpha) e^{-\alpha(H_1-t)\beta_5/w_3}] d\alpha \\ K_{12}(x_1, t) &= \frac{1}{\gamma_{14}\pi} \int_0^\infty [k_3(x_1, \alpha) e^{-\alpha(H_2-t)\beta_5^*/w_1^*} + k_4(x_1, \alpha) e^{-\alpha(H_2-t)\beta_5^*/w_3^*}] d\alpha \\ K_{13}(x_1, t) &= \frac{1}{\gamma_{14}\pi} \int_0^\infty [J_1(x_1, \alpha) + J_2(x_1, \alpha)] \cos \alpha t d\alpha \\ K_{14}(x_1, t) &= \frac{1}{\gamma_{14}\pi} \int_0^\infty [J_3(x_1, \alpha) + J_4(x_1, \alpha)] \sin \alpha t d\alpha \end{aligned} \quad (3.30abcd)$$

$$\begin{aligned} K_{21}(x_2, t) &= \frac{1}{\gamma_{14}^*\pi} \int_0^\infty [k_5(x_2, \alpha) e^{-\alpha(H_1-t)\beta_5/w_1} + k_6(x_2, \alpha) e^{-\alpha(H_1-t)\beta_5/w_3}] d\alpha \\ K_{22}(x_2, t) &= \frac{1}{\gamma_{14}^*\pi} \int_0^\infty [k_7(x_2, \alpha) e^{-\alpha(H_2-t)\beta_5^*/w_1^*} + k_8(x_2, \alpha) e^{-\alpha(H_2-t)\beta_5^*/w_3^*}] d\alpha \\ K_{23}(x_2, t) &= \frac{1}{\gamma_{14}^*\pi} \int_0^\infty [J_5(x_2, \alpha) + J_6(x_2, \alpha)] \cos \alpha t d\alpha \\ K_{24}(x_2, t) &= \frac{1}{\gamma_{14}^*\pi} \int_0^\infty [J_7(x_2, \alpha) + J_8(x_2, \alpha)] \sin \alpha t d\alpha \end{aligned} \quad (3.31abcd)$$

$$\begin{aligned} K_{31}(y, t) &= \frac{1}{2\gamma_{13}\pi} \left[-\gamma_{11} \frac{H_1-t}{\frac{(w_1 y)^2}{\beta_5^2} + (H_1-t)^2} + \gamma_{12} \frac{\gamma_{11}}{\gamma_{12}} \frac{H_1-t}{\frac{(w_3 y)^2}{\beta_5^2} + (H_1-t)^2} \right] \\ &\quad + \lim_{x_1 \rightarrow H_1} \frac{1}{\pi} \int_0^\infty [k_9(y, x_1, \alpha) e^{-\alpha(H_1-t)\beta_5/w_1} + k_{10}(y, x_1, \alpha) e^{-\alpha(H_1-t)\beta_5/w_3}] d\alpha \\ K_{32}(y, t) &= \lim_{x_1 \rightarrow H_1} \frac{1}{\pi} \int_0^\infty [k_{11}(y, x_1, \alpha) e^{-\alpha(H_2-t)\beta_5^*/w_1^*} + k_{12}(y, x_1, \alpha) e^{-\alpha(H_2-t)\beta_5^*/w_3^*}] d\alpha \\ K_{33}'(y, t) &= \lim_{x_1 \rightarrow H_1} \frac{1}{\pi} \int_0^\infty \left[\frac{\text{ch}(w_1 \alpha x_1)}{\text{ch}(w_1 \alpha H_1)} J_9(y, \alpha) + \frac{\text{ch}(w_3 \alpha x_1)}{\text{ch}(w_3 \alpha H_1)} J_{10}(y, \alpha) \right] \cos \alpha t d\alpha \\ K_{34}'(y, t) &= \lim_{x_1 \rightarrow H_1} \frac{1}{\pi} \int_0^\infty \left[\frac{\text{ch}(w_1 \alpha x_1)}{\text{ch}(w_1 \alpha H_1)} J_{11}(y, \alpha) + \frac{\text{ch}(w_3 \alpha x_1)}{\text{ch}(w_3 \alpha H_1)} J_{12}(y, \alpha) \right] \sin \alpha t d\alpha \quad (3.32abcd) \\ K_{41}(y, t) &= \frac{\gamma_{11}}{2\gamma_{13}\pi} \left[\frac{\frac{w_1 y}{\beta_5}}{\frac{(w_1 y)^2}{\beta_5^2} + (H_1-t)^2} - \frac{\frac{w_3 y}{\beta_5}}{\frac{(w_3 y)^2}{\beta_5^2} + (H_1-t)^2} \right] \\ &\quad + \lim_{x_1 \rightarrow H_1} \frac{1}{\pi} \int_0^\infty [k_{13}(y, x_1, \alpha) e^{-\alpha(H_1-t)\beta_5/w_1} + k_{14}(y, x_1, \alpha) e^{-\alpha(H_1-t)\beta_5/w_3}] d\alpha \end{aligned}$$

$$\begin{aligned}
K_{42}(y,t) &= \lim_{x_1 \rightarrow H_1} \frac{1}{\pi} \int_0^\infty [k_{15}(y,x_1,\alpha) e^{-\alpha(H_2-t)\beta_5^*/|w_1^*|} + k_{16}(y,x_1,\alpha) e^{-\alpha(H_2-t)\beta_5^*/|w_3^*|}] d\alpha \\
K_{43}'(y,t) &= \lim_{x_1 \rightarrow H_1} \frac{1}{\pi} \int_0^\infty \left[\frac{\text{sh}(w_1 \alpha x_1)}{\text{ch}(w_1 \alpha H_1)} J_{13}(y,\alpha) + \frac{\text{sh}(w_3 \alpha x_1)}{\text{ch}(w_3 \alpha H_1)} J_{14}(y,\alpha) \right] \cos \alpha t d\alpha \\
K_{44}'(y,t) &= \lim_{x_1 \rightarrow H_1} \frac{1}{\pi} \int_0^\infty \left[\frac{\text{sh}(w_1 \alpha x_1)}{\text{ch}(w_1 \alpha H_1)} J_{15}(y,\alpha) + \frac{\text{sh}(w_3 \alpha x_1)}{\text{ch}(w_3 \alpha H_1)} J_{16}(y,\alpha) \right] \sin \alpha t d\alpha \quad (3.33abcd)
\end{aligned}$$

The derivation of the terms k_i and J_i ($i=1$ to 16) are given in Appendix C.

Note that for $t = y$ the integrals (3.32c,d) and (3.33c,d) are divergent. These divergent parts must be studied and separated by analyzing the asymptotic behavior of the integrands.

After separating the singular parts in (3.32c,d) and (3.33c,d), eqns(3.29c,d) are finally reduced to:

$$\begin{aligned}
& \int_{-a_1}^{a_1} K_{31}(y,t) \phi_1(t) dt + \int_{-a_2}^{a_2} K_{32}(y,t) \phi_2(t) dt + \frac{\rho_1}{2} \phi_3(y) + \int_{b_1}^{b_2} K_{33}(y,t) \phi_3(t) dt \\
& - \frac{\rho_2}{2\pi} \int_{b_1}^{b_2} \left(\frac{1}{t-y} + \frac{1}{t+y} \right) \phi_4(t) dt + \int_{b_1}^{b_2} K_{34}(y,t) \phi_4(t) dt \\
& = \frac{(1-\nu_{xy}\nu_{yx})}{2E_X} p_3(y) \quad b_1 < y < b_2 \quad (3.29c*)
\end{aligned}$$

$$\begin{aligned}
& \int_{-a_1}^{a_1} K_{41}(y,t) \phi_1(t) dt + \int_{-a_2}^{a_2} K_{42}(y,t) \phi_2(t) dt + \frac{\rho_3}{2\pi} \int_{b_1}^{b_2} \left(\frac{-1}{t-y} + \frac{1}{t+y} \right) \phi_3(t) dt \\
& + \int_{b_1}^{b_2} K_{43}(y,t) \phi_3(t) dt - \frac{\rho_4}{2} \phi_4(y) + \int_{b_1}^{b_2} K_{44}(y,t) \phi_4(t) dt \\
& = \frac{1}{2G_{xy}} p_4(y) \quad b_1 < y < b_2 \quad (3.29d*)
\end{aligned}$$

where ρ_1 , ρ_2 , ρ_3 and ρ_4 and $K_{33}(y,t)$, $K_{34}(y,t)$, $K_{43}(y,t)$ and $K_{44}(y,t)$ are defined in Appendix D The additional single-valueness conditions for each crack configuration will be discussed later.

3.1.3 Asymptotic Analysis of the kernels

Depending on the crack geometries, some or all of the kernels might be unbounded as $\alpha \rightarrow \infty$. The unbounded kernels will affect the values of singularities at the crack tips. Therefore an asymptotic analysis is necessary to determine these singularities.

Generally a kernel can be expressed as:

$$K_{ij} = K_{ijs} + K_{ijf} \quad (i, j = 1, 2, 3, 4) \quad (3.34)$$

where K_{ijs} is the unbounded part and K_{ijf} is the bounded part.

Let $k_{i\infty}(x_1, \alpha)$ ($i=1-8$) be the asymptotic part of $k_i(x_1, \alpha)$, when $\alpha \rightarrow \infty$, then we have:

$$\begin{aligned} K_{11S}(x_1, t) &= \frac{1}{\gamma_{14}\pi} \int_0^\infty [k_{1\infty}(x_1, \alpha) e^{-\alpha(H_1-t)\beta_5/|w_1|} + k_{2\infty}(x_1, \alpha) e^{-\alpha(H_1-t)\beta_5/|w_3|}] d\alpha \\ &= \frac{\gamma_7 \lambda_{81}}{\pi \gamma_{13} \gamma_{14} \lambda_{80}} \int_0^\infty \cosh(w_1 \alpha x_1) e^{-\alpha[(H_1-t)\beta_5/|w_1| + H_1|w_1|]} d\alpha \\ &\quad + \frac{\gamma_8 \lambda_{82}}{\pi \gamma_{13} \gamma_{14} \lambda_{80}} \int_0^\infty \cosh(w_3 \alpha x_1) e^{-\alpha[(H_1-t)\beta_5/|w_1| + H_1|w_3|]} d\alpha \\ &\quad + \frac{\gamma_7 \lambda_{83}}{\pi \gamma_{13} \gamma_{14} \lambda_{80}} \int_0^\infty \cosh(w_1 \alpha x_1) e^{-\alpha[(H_1-t)\beta_5/|w_3| + H_1|w_1|]} d\alpha \\ &\quad + \frac{\gamma_8 \lambda_{84}}{\pi \gamma_{13} \gamma_{14} \lambda_{80}} \int_0^\infty \cosh(w_3 \alpha x_1) e^{-\alpha[(H_1-t)\beta_5/|w_3| + H_1|w_3|]} d\alpha \\ &= \frac{1}{\pi} \lambda_{85} \frac{(H_1-t)\beta_5/|w_1| + H_1|w_1|}{[(H_1-t)\beta_5/|w_1| + H_1|w_1|]^2 - (w_1 x_1)^2} \\ &\quad + \frac{1}{\pi} \lambda_{86} \frac{(H_1-t)\beta_5/|w_1| + H_1|w_3|}{[(H_1-t)\beta_5/|w_1| + H_1|w_3|]^2 - (w_3 x_1)^2} \\ &\quad + \frac{1}{\pi} \lambda_{87} \frac{(H_1-t)\beta_5/|w_3| + H_1|w_1|}{[(H_1-t)\beta_5/|w_3| + H_1|w_1|]^2 - (w_1 x_1)^2} \\ &\quad + \frac{1}{\pi} \lambda_{88} \frac{(H_1-t)\beta_5/|w_3| + H_1|w_3|}{[(H_1-t)\beta_5/|w_3| + H_1|w_3|]^2 - (w_3 x_1)^2} \end{aligned} \quad (3.35)$$

Similarly one can derive:

$$\begin{aligned}
 K_{12S}(x_1, t) = & \frac{1}{\pi} \lambda_{93} \frac{(H_2 - t) \beta_5^* / |w_1^*| + H_1 |w_1|}{[(H_2 - t) \beta_5^* / |w_1^*| + H_1 |w_1|]^2 - (w_1 x_1)^2} \\
 & + \frac{1}{\pi} \lambda_{94} \frac{(H_2 - t) \beta_5^* / |w_1^*| + H_1 |w_3|}{[(H_2 - t) \beta_5^* / |w_1^*| + H_1 |w_3|]^2 - (w_3 x_1)^2} \\
 & + \frac{1}{\pi} \lambda_{95} \frac{(H_2 - t) \beta_5^* / |w_3^*| + H_1 |w_1|}{[(H_2 - t) \beta_5^* / |w_3^*| + H_1 |w_1|]^2 - (w_1 x_1)^2} \\
 & + \frac{1}{\pi} \lambda_{96} \frac{(H_2 - t) \beta_5^* / |w_3^*| + H_1 |w_3|}{[(H_2 - t) \beta_5^* / |w_3^*| + H_1 |w_3|]^2 - (w_3 x_1)^2}
 \end{aligned} \tag{3.36}$$

$$\begin{aligned}
 K_{21S}(x_2, t) = & \frac{1}{\pi} \lambda_{101} \frac{(H_1 - t) \beta_5 / |w_1| + H_2 |w_1^*|}{[(H_1 - t) \beta_5 / |w_1| + H_2 |w_1^*|]^2 - (w_1^* x_2)^2} \\
 & + \frac{1}{\pi} \lambda_{102} \frac{(H_1 - t) \beta_5 / |w_1| + H_2 |w_3^*|}{[(H_1 - t) \beta_5 / |w_1| + H_2 |w_3^*|]^2 - (w_3^* x_2)^2} \\
 & + \frac{1}{\pi} \lambda_{103} \frac{(H_1 - t) \beta_5 / |w_3| + H_2 |w_1^*|}{[(H_1 - t) \beta_5 / |w_3| + H_2 |w_1^*|]^2 - (w_1^* x_2)^2} \\
 & + \frac{1}{\pi} \lambda_{104} \frac{(H_1 - t) \beta_5 / |w_3| + H_2 |w_3^*|}{[(H_1 - t) \beta_5 / |w_3| + H_2 |w_3^*|]^2 - (w_3^* x_2)^2}
 \end{aligned} \tag{3.37}$$

$$\begin{aligned}
 K_{22S}(x_2, t) = & \frac{1}{\pi} \lambda_{109} \frac{(H_2 - t) \beta_5^* / |w_1^*| + H_2 |w_1^*|}{[(H_2 - t) \beta_5^* / |w_1^*| + H_2 |w_1^*|]^2 - (w_1^* x_2)^2} \\
 & + \frac{1}{\pi} \lambda_{110} \frac{(H_2 - t) \beta_5^* / |w_1^*| + H_2 |w_3^*|}{[(H_2 - t) \beta_5^* / |w_1^*| + H_2 |w_3^*|]^2 - (w_3^* x_2)^2} \\
 & + \frac{1}{\pi} \lambda_{111} \frac{(H_2 - t) \beta_5^* / |w_3^*| + H_2 |w_1^*|}{[(H_2 - t) \beta_5^* / |w_3^*| + H_2 |w_1^*|]^2 - (w_1^* x_2)^2} \\
 & + \frac{1}{\pi} \lambda_{112} \frac{(H_2 - t) \beta_5^* / |w_3^*| + H_2 |w_3^*|}{[(H_2 - t) \beta_5^* / |w_3^*| + H_2 |w_3^*|]^2 - (w_3^* x_2)^2}
 \end{aligned} \tag{3.37}$$

The asymptotic expressions for $K_{31}(y, t)$, $K_{32}(y, t)$, $K_{41}(y, t)$ and $K_{42}(y, t)$ are obtained as follow:

$$\begin{aligned}
K_{31S}(y,t) &= \frac{1}{2\gamma_{13}\pi} \left[-\gamma_1 \frac{H_1-t}{\beta_5^2 + (H_1-t)^2} + \gamma_2 \left(\frac{\gamma_{11}}{\gamma_{12}} \right) \frac{H_1-t}{\beta_5^2 + (H_1-t)^2} \right] \\
&+ \lim_{x_1 \rightarrow \infty} \frac{1}{\pi} \int_0^\infty [k_{9\infty}(y, x_1, \alpha) e^{-\alpha(H_1-t)\beta_5/|w_1|} + k_{10\infty}(y, x_1, \alpha) e^{-\alpha(H_1-t)\beta_5/|w_3|}] d\alpha \\
&= \frac{1}{2\gamma_{13}\pi} \left[-\gamma_1 \frac{H_1-t}{\beta_5^2 + (H_1-t)^2} + \gamma_2 \left(\frac{\gamma_{11}}{\gamma_{12}} \right) \frac{H_1-t}{\beta_5^2 + (H_1-t)^2} \right] \\
&+ \lim_{x_1 \rightarrow \infty} \frac{\gamma_3 \lambda_{81} + \gamma_4 \lambda_{82}}{\pi \gamma_{13} \lambda_{80}} \int_0^\infty \cos(\alpha y) e^{-\alpha[(H_1-t)\beta_5/|w_1| + (H_1-x_1)|w_1|]} d\alpha \\
&+ \lim_{x_1 \rightarrow \infty} \frac{\gamma_3 \lambda_{83} + \gamma_4 \lambda_{84}}{\pi \gamma_{13} \lambda_{80}} \int_0^\infty \cos(\alpha y) e^{-\alpha[(H_1-t)\beta_5/|w_3| + (H_1-x_1)|w_3|]} d\alpha \\
&= \frac{1}{2\gamma_{13}\pi} \left[-\gamma_1 \frac{H_1-t}{\beta_5^2 + (H_1-t)^2} + \gamma_2 \left(\frac{\gamma_{11}}{\gamma_{12}} \right) \frac{H_1-t}{\beta_5^2 + (H_1-t)^2} \right] \\
&+ \rho_5 \frac{(H_1-t)\beta_5/|w_1|}{[(H_1-t)\beta_5/|w_1|]^2 + y^2} + \rho_6 \frac{(H_1-t)\beta_5/|w_3|}{[(H_1-t)\beta_5/|w_3|]^2 + y^2} \quad (3.38)
\end{aligned}$$

$$K_{32S}(y,t) = \rho_7 \frac{(H_2-t)\beta_5^*/|w_1^*|}{[(H_2-t)\beta_5^*/|w_1^*|]^2 + y^2} + \rho_8 \frac{(H_2-t)\beta_5^*/|w_3^*|}{[(H_2-t)\beta_5^*/|w_3^*|]^2 + y^2} \quad (3.39)$$

$$\begin{aligned}
K_{41S}(y,t) &= \frac{\gamma_{11}}{2\gamma_{13}\pi} \left[\frac{\frac{|w_1|y}{\beta_5}}{\beta_5^2 + (H_1-t)^2} - \frac{\frac{|w_3|y}{\beta_5}}{\beta_5^2 + (H_1-t)^2} \right] \\
&- \rho_9 \frac{y}{[(H_1-t)\beta_5/|w_1|]^2 + y^2} - \rho_{10} \frac{y}{[(H_1-t)\beta_5/|w_3|]^2 + y^2} \quad (3.40)
\end{aligned}$$

$$K_{42S}(y,t) = -\rho_{11} \frac{y}{[(H_2-t)\beta_5^*/|w_1^*|]^2 + y^2} - \rho_{12} \frac{y}{[(H_2-t)\beta_5^*/|w_3^*|]^2 + y^2} \quad (3.41)$$

Let $J_{i\infty}(x_1, \alpha)$ ($i=1-8$) be the asymptotic parts of $J_i(x_1, \alpha)$, as $\alpha \rightarrow \infty$, then we have:

$$\begin{aligned}
K_{13S}(x_1, t) &= \frac{1}{\gamma_{14}\pi} \int_0^\infty [J_{1\infty}(x_1, \alpha) + J_{2\infty}(x_1, \alpha)] \cos \alpha t d\alpha \\
&= \frac{\gamma_7(\lambda_{73} + \lambda_{74} + \lambda_{75})}{\pi \gamma_{14} \lambda_{80}} \int_0^\infty \cos(\alpha t) e^{-\alpha w_1(H_1-x_1)} d\alpha
\end{aligned}$$

$$\begin{aligned}
& + \frac{\gamma_8(\lambda_{61} + \lambda_{62} + \lambda_{63})}{\pi\gamma_{14}\lambda_{80}} \int_0^\infty \cos(\alpha t) e^{-\alpha w_3(H_1 - x_1)} d\alpha \\
& = \rho_{13} \frac{w_1(H_1 - x_1)}{[w_1(H_1 - x_1)]^2 + t^2} + \rho_{14} \frac{w_3(H_1 - x_1)}{[w_3(H_1 - x_1)]^2 + t^2}
\end{aligned} \quad (3.42)$$

Using the same technique we can derive:

$$K_{14S}(x_1, t) = \rho_{15} \frac{t}{[w_1(H_1 - x_1)]^2 + t^2} + \rho_{16} \frac{t}{[w_3(H_1 - x_1)]^2 + t^2} \quad (3.43)$$

$$K_{23S}(x_2, t) = \rho_{17} \frac{w_1^*(H_2 - x_2)}{[w_1^*(H_2 - x_2)]^2 + t^2} + \rho_{18} \frac{w_3^*(H_2 - x_2)}{[w_3^*(H_2 - x_2)]^2 + t^2} \quad (3.44)$$

$$K_{24S}(x_2, t) = \rho_{19} \frac{t}{[w_1^*(H_2 - x_2)]^2 + t^2} + \rho_{20} \frac{t}{[w_3^*(H_2 - x_2)]^2 + t^2} \quad (3.45)$$

The coefficients λ_i ($i=85-112$) and ρ_j ($j=5-20$) are given in Appendix B.

The asymptotic analysis for kernel $K_{33}'(y, t)$, $K_{34}'(y, t)$, $K_{43}'(y, t)$ and $K_{44}'(y, t)$ is given in Appendix D.

3.1.4 Normalization of the singular integral equations

Using the following transformation formulae:

$$\begin{aligned}
x_1 &= a_1 r, \quad t = a_1 s, \quad x_2 = a_2 r, \quad t = a_2 s, & -1 \leq r \leq 1, \quad -1 \leq s \leq 1 \\
y &= \frac{1}{2}(b_2 - b_1)r + \frac{1}{2}(b_2 + b_1), \quad t = \frac{1}{2}(b_2 - b_1)s + \frac{1}{2}(b_2 + b_1). \\
\text{then } t+y &= \frac{1}{2}(b_2 - b_1)[s+r+b_0], \quad b_0 = \frac{2(b_2 + b_1)}{(b_2 - b_1)} & -1 \leq r \leq 1, \quad -1 \leq s \leq 1
\end{aligned}$$

Substituting above into the four singular integral equations, we obtain:

$$\begin{aligned}
& \frac{1}{\pi} \int_{-1}^1 \left[\frac{1}{s-r} + \pi a_1 k_{11}^o(r, s) \right] \phi_1^o(s) ds + \int_{-1}^1 a_2 k_{12}^o(r, s) \phi_2^o(s) ds \\
& + \frac{b_2 - b_1}{2} \int_{-1}^1 k_{13}^o(r, s) \phi_3^o(s) ds + \frac{b_2 - b_1}{2} \int_{-1}^1 k_{14}^o(r, s) \phi_4^o(s) ds = -\frac{(1 - v_{xy} v_{yx})}{2\gamma_{14} E_y} p_1^o(r) \quad (3.46a) \\
& \int_{-1}^1 a_1 k_{21}^o(r, s) \phi_1^o(s) ds + \frac{1}{\pi} \int_{-1}^1 \left[\frac{1}{s-r} + \pi a_2 k_{22}^o(r, s) \right] \phi_2^o(s) ds
\end{aligned}$$

$$+ \frac{b_2 - b_1}{2} \int_{-1}^1 k_{23}^o(r, s) \phi_3^o(s) ds + \frac{b_2 - b_1}{2} \int_{-1}^1 k_{24}^o(r, s) \phi_4^o(s) ds = - \frac{(1 - v_{xy}^* v_{yx}^*)}{2\gamma_{14}^* E_y^*} p_2^o(r) \quad (3.46b)$$

$$\int_{-1}^1 a_1 k_{31}^o(r, s) \phi_1^o(s) ds + \int_{-1}^1 a_2 k_{32}^o(r, s) \phi_2^o(s) ds + \frac{\rho_1}{2} \phi_3^o(r) + \frac{b_2 - b_1}{2} \int_{-1}^1 k_{33}^o(r, s) \phi_3^o(s) ds \\ - \frac{\rho_2}{2\pi} \int_{-1}^1 \left(\frac{1}{s-r} + \frac{1}{s+r+b_o} \right) \phi_4^o(s) ds + \frac{b_2 - b_1}{2} \int_{-1}^1 k_{34}^o(r, s) \phi_4^o(s) ds = \frac{1 - v_{xy} v_{yx}}{2E_x} p_3^o(r) \quad (3.46c)$$

$$\int_{-1}^1 a_1 k_{41}^o(r, s) \phi_1^o(s) ds + \int_{-1}^1 a_2 k_{42}^o(r, s) \phi_2^o(s) ds + \frac{\rho_3}{2\pi} \int_{-1}^1 \left(\frac{-1}{s-r} + \frac{1}{s+r+b_o} \right) \phi_3^o(s) ds \\ \frac{b_2 - b_1}{2} \int_{-1}^1 k_{34}^o(r, s) \phi_3^o(s) ds - \frac{\rho_4}{2} \phi_4^o(r) + \frac{b_2 - b_1}{2} \int_{-1}^1 k_{44}^o(r, s) \phi_4^o(s) ds = \frac{1}{2G_{xy}} p_4^o(r) \quad (3.46d)$$

where superscript "o" is used to denote the normalized quantities.

For orthotropic materials, the dominant parts of eqns (3.46c) and (3.46d) are coupled. In order to solve the singular integral equations numerically, it is necessary to decouple these dominant parts of eqns (3.46c) and (3.46d). Using the technique described in [22], first let:

$$\phi = \begin{Bmatrix} \phi_3^o \\ \phi_4^o \end{Bmatrix}, \quad \theta = \begin{Bmatrix} \phi_1^o \\ \phi_2^o \end{Bmatrix},$$

$$\text{and } A = \begin{bmatrix} \frac{\rho_1}{2} & 0 \\ 0 & -\frac{\rho_4}{2} \end{bmatrix}, \quad B = \begin{bmatrix} 0 & -\frac{\rho_2}{2} i \\ -\frac{\rho_3}{2} i & 0 \end{bmatrix}, \quad B' = \begin{bmatrix} 0 & -\frac{\rho_2}{2} i \\ \frac{\rho_3}{2} i & 0 \end{bmatrix},$$

$$C = \begin{bmatrix} a_1 k_{31}^o & a_2 k_{32}^o \\ a_1 k_{41}^o & a_2 k_{42}^o \end{bmatrix}, \quad K = \frac{b_2 - b_1}{2} \begin{bmatrix} k_{33}^o & k_{34}^o \\ k_{43}^o & k_{44}^o \end{bmatrix}, \quad P = \begin{bmatrix} \frac{1 - v_{xy} v_{yx}}{2E_x} p_3^o \\ \frac{1}{2G_{xy}} p_4^o \end{bmatrix}.$$

then eqns (3.46c) and (3.46d) are combined into:

$$A\phi + \frac{B}{\pi i} \int_{-1}^1 \frac{\phi ds}{s-r} + \frac{B'}{\pi i} \int_{-1}^1 \frac{\phi ds}{s+r+b_o} + \int_{-1}^1 C\theta ds + \int_{-1}^1 K\phi ds = P \quad (3.47)$$

Multiplying both sides of eqn (3.47) by A^{-1} gives:

$$\phi + \frac{1}{\pi i} \int_{-1}^1 \frac{A^{-1}B\phi ds}{s-r} + \frac{1}{\pi i} \int_{-1}^1 \frac{A^{-1}B'\phi ds}{s+r+b_0} + \int_{-1}^1 A^{-1}C\theta ds + \int_{-1}^1 A^{-1}K\phi ds = A^{-1}P \quad (3.48)$$

$$\text{Let } D = A^{-1}B = \begin{bmatrix} 0 & -i\frac{\rho_2}{\rho_1} \\ i\frac{\rho_3}{\rho_4} & 0 \end{bmatrix}, \quad D' = A^{-1}B' = \begin{bmatrix} 0 & -i\frac{\rho_2}{\rho_1} \\ -i\frac{\rho_3}{\rho_4} & 0 \end{bmatrix}$$

then the eigenvalues $\mu_{1,2}$ of D can be determined from:

$$D - \mu I = 0 \quad (3.49)$$

$$\text{giving: } \mu^2 - \frac{\rho_2\rho_3}{\rho_1\rho_4} = 0 \rightarrow \mu_{1,2} = \pm \sqrt{\frac{\rho_2\rho_3}{\rho_1\rho_4}} = \pm \frac{1}{\zeta}$$

Now let R be a square matrix such that:

$$DR = RA \quad (3.50)$$

$$\text{where: } \Lambda = \begin{bmatrix} \zeta^{-1} & 0 \\ 0 & -\zeta^{-1} \end{bmatrix}$$

$$\text{then we have } R = \begin{bmatrix} 1 & i\sqrt{\frac{\eta_1}{\eta_2}} \\ i\sqrt{\frac{\eta_2}{\eta_1}} & 1 \end{bmatrix} \quad \text{where } \eta_1 = \frac{\rho_2}{\rho_1}, \text{ and } \eta_2 = \frac{\rho_3}{\rho_4}$$

Introducing : $\phi = R\psi$, where $\psi = \begin{bmatrix} \psi_3^o \\ \psi_4^o \end{bmatrix}$, then eqn (3.48) is reduced to:

$$\begin{aligned} \psi + \frac{1}{\pi i} \int_{-1}^1 \frac{\Lambda\psi ds}{s-r} + \frac{1}{\pi i} \int_{-1}^1 \frac{R^{-1}A^{-1}B'R\psi ds}{s+r+b_0} + \int_{-1}^1 R^{-1}A^{-1}C\theta ds \\ + \int_{-1}^1 R^{-1}A^{-1}K\phi ds = R^{-1}A^{-1}P \end{aligned} \quad (3.51)$$

$$\text{where } R^{-1}A^{-1}C = \begin{bmatrix} a_1c_1(r,s) & a_2c_2(r,s) \\ a_1c_3(r,s) & a_2c_4(r,s) \end{bmatrix}$$

$$= \begin{bmatrix} a_1 \left(\frac{k_{31}^o}{\rho_1} + \frac{ik_{41}^o}{\rho_4} \sqrt{\frac{\eta_1}{\eta_2}} \right) & a_2 \left(\frac{k_{32}^o}{\rho_1} + \frac{ik_{42}^o}{\rho_4} \sqrt{\frac{\eta_1}{\eta_2}} \right) \\ a_1 \left(-\frac{k_{41}^o}{\rho_4} - \frac{ik_{31}^o}{\rho_1} \sqrt{\frac{\eta_2}{\eta_1}} \right) & a_2 \left(-\frac{k_{42}^o}{\rho_4} - \frac{ik_{32}^o}{\rho_1} \sqrt{\frac{\eta_2}{\eta_1}} \right) \end{bmatrix} \quad (3.52)$$

$$R^{-1}A^{-1}KR = \frac{b_2 - b_1}{2} \begin{bmatrix} k_1^o(r, s) & k_2^o(r, s) \\ k_3^o(r, s) & k_4^o(r, s) \end{bmatrix}$$

$$= \frac{b_2 - b_1}{2} \begin{bmatrix} \left(\frac{k_{33}^o}{\rho_1} - \frac{k_{44}^o}{\rho_4} \right) + i \left(\sqrt{\frac{\eta_2}{\eta_1}} \frac{k_{34}^o}{\rho_1} + \sqrt{\frac{\eta_1}{\eta_2}} \frac{k_{43}^o}{\rho_4} \right) & \left(\frac{k_{34}^o}{\rho_1} - \frac{\eta_1}{\eta_2} \frac{k_{43}^o}{\rho_4} \right) + i \sqrt{\frac{\eta_1}{\eta_2}} \left(\frac{k_{33}^o}{\rho_1} + \frac{k_{44}^o}{\rho_4} \right) \\ \left(\frac{\eta_2}{\eta_1} \frac{k_{34}^o}{\rho_4} - \frac{k_{43}^o}{\rho_4} \right) - i \sqrt{\frac{\eta_2}{\eta_1}} \left(\frac{k_{33}^o}{\rho_1} + \frac{k_{44}^o}{\rho_4} \right) & \left(\frac{k_{33}^o}{\rho_1} - \frac{k_{44}^o}{\rho_4} \right) - i \left(\sqrt{\frac{\eta_2}{\eta_1}} \frac{k_{34}^o}{\rho_1} + \sqrt{\frac{\eta_1}{\eta_2}} \frac{k_{43}^o}{\rho_4} \right) \end{bmatrix} \quad (3.53)$$

and

$$R^{-1}A^{-1} = \begin{bmatrix} m_1 & im_2 \\ -im_1 & -m_2 \end{bmatrix} = \begin{bmatrix} \frac{1}{\rho_1} & -i \sqrt{\frac{\rho_2}{\rho_1 \rho_3 \rho_4}} \\ -i \sqrt{\frac{\rho_3}{\rho_1 \rho_2 \rho_4}} & -\frac{1}{\rho_4} \end{bmatrix} \quad (3.54)$$

Finally eqns (3.46c) and (3.46d) are reduced to:

$$\begin{aligned} \psi_3^o(r) + \frac{\zeta^{-1}}{\pi i} \int_{-1}^1 \psi_3^o(s) \frac{ds}{s-r} - \frac{\zeta^{-1}}{\pi} \int_{-1}^1 \psi_4^o(s) \frac{ds}{s+r+b_o} + \int_{-1}^1 a_1 c_1(r, s) \phi_1^o(s) ds + \int_{-1}^1 a_2 c_2(r, s) \phi_2^o(s) ds \\ + \frac{b_2 - b_1}{2} \int_{-1}^1 k_1^o(r, s) \psi_3^o(s) ds + \frac{b_2 - b_1}{2} \int_{-1}^1 k_2^o(r, s) \psi_4^o(s) ds \\ = m_1 \frac{1 - v_{xy} v_{yx}}{2E_x} p_3(r) + im_2 \frac{1}{2G_{xy}} p_4(r) \end{aligned} \quad (3.55)$$

$$\begin{aligned} \psi_4^o(r) - \frac{\zeta^{-1}}{\pi i} \int_{-1}^1 \psi_4^o(s) \frac{ds}{s-r} - \frac{\zeta^{-1}}{\pi} \int_{-1}^1 \psi_3^o(s) \frac{ds}{s+r+b_o} + \int_{-1}^1 a_1 c_3(r, s) \phi_1^o(s) ds + \int_{-1}^1 a_2 c_4(r, s) \phi_2^o(s) ds \\ + \frac{b_2 - b_1}{2} \int_{-1}^1 k_3^o(r, s) \psi_3^o(s) ds + \frac{b_2 - b_1}{2} \int_{-1}^1 k_4^o(r, s) \psi_4^o(s) ds \end{aligned}$$

$$= -im_1 \frac{1 - v_{xy} v_{yx}}{2E_x} p_3(r) - m_2 \frac{1}{2G_{xy}} p_4(r) \quad (3.56)$$

Note that the functions $\psi_3^o(r)$ and $\psi_4^o(r)$ are related by the following relations:

$$\psi_3^o(r) = \frac{1}{2} [\phi_3^o(r) - i \sqrt{\frac{\eta_1}{\eta_2}} \phi_4^o(r)] \quad (3.57a)$$

$$\psi_4^o(r) = \frac{1}{2} [-i \sqrt{\frac{\eta_2}{\eta_1}} \phi_3^o(r) + \phi_4^o(r)] = -i \sqrt{\frac{\eta_2}{\eta_1}} \bar{\psi}_3^o(r) \quad (3.57b)$$

If both materials are isotropic, it is found that $\sqrt{\frac{\eta_2}{\eta_1}} = 1$, and the above relations

reduce to:

$$\psi_3^o(r) = \frac{1}{2} [\phi_3^o(r) - i \phi_4^o(r)] \quad (3.57a^*)$$

$$\psi_4^o(r) = \frac{1}{2} [-i \phi_3^o(r) + \phi_4^o(r)] = -i \bar{\psi}_3^o(r) \quad (3.57b^*)$$

Now to expressing eqns (3.46a,b) also in terms of $\psi_3^o(r)$ and $\psi_4^o(r)$, we have:

$$\begin{aligned} & \frac{1}{\pi} \int_{-1}^1 \left[\frac{1}{s-r} + \pi a_1 k_{11}^o(r, s) \right] \phi_1^o(s) ds + \int_{-1}^1 a_2 k_{12}^o(r, s) \phi_2^o(s) ds \\ & + \frac{b_2 - b_1}{2} \int_{-1}^1 [T_1 \psi_3^o(s) ds + \bar{T}_1 \bar{\psi}_3^o(s)] ds = \frac{1 - v_{xy} v_{yx}}{2\gamma_{14} E_y} p_1^o(r) \end{aligned} \quad (3.46a^*)$$

$$\begin{aligned} & \int_{-1}^1 a_1 k_{21}^o(r, s) \phi_1^o(s) ds + \frac{1}{\pi} \int_{-1}^1 \left[\frac{1}{s-r} + \pi a_2 k_{22}^o(r, s) \right] \phi_2^o(s) ds \\ & + \frac{b_2 - b_1}{2} \int_{-1}^1 [T_2 \psi_3^o(s) ds + \bar{T}_2 \bar{\psi}_3^o(s)] ds = \frac{1 - v_{xy}^* v_{yx}^*}{2\gamma_{14}^* E_y^*} p_2^o(r) \end{aligned} \quad (3.46b^*)$$

where

$$\begin{aligned} T_1 &= k_{13}^o + i \sqrt{\frac{\eta_2}{\eta_1}} k_{14}^o & \bar{T}_1 &= k_{13}^o - i \sqrt{\frac{\eta_2}{\eta_1}} k_{14}^o \\ T_2 &= k_{23}^o + i \sqrt{\frac{\eta_2}{\eta_1}} k_{24}^o & \bar{T}_2 &= k_{23}^o - i \sqrt{\frac{\eta_2}{\eta_1}} k_{24}^o \end{aligned} \quad (3.58abcd)$$

3.1.5 Determination of singularities for different crack geometry

The stress singularity at the crack tip varies with the crack geometry.

a) Embedded cracks ($|a_1| < H_1$, $|a_2| < H_2$ and $b_1 > 0$)

For embedded cracks, the crack density functions are of the following forms:

$$\begin{aligned}\phi_1^o(t) &= \frac{F_1^o(t)}{(1+t)^{\alpha_1}(1-t)^{\beta_1}}, & \phi_2^o(t) &= \frac{F_2^o(t)}{(1+t)^{\alpha_2}(1-t)^{\beta_2}} \\ \psi_3^o(t) &= \frac{F_3^o(t)}{(1+t)^{\alpha_3}(1-t)^{\beta_3}}, & \psi_4^o(t) &= \frac{F_4^o(t)}{(1+t)^{\alpha_4}(1-t)^{\beta_4}}\end{aligned}\quad (3.59abcd)$$

where $F_i^o(t)$ ($i=1,2,3,4$) are bounded at crack tips. and because of symmetry $\alpha_1=\beta_1$ and $\alpha_2=\beta_2$.

Substituting eqns (3.59a,b,c,d) into eqns (3.29a,b,c,d) and using the following formula [33]:

$$\begin{aligned}\psi_n(z) &= \frac{1}{\pi} \int_{z_1}^{z_2} \frac{\phi_n(t)}{t-z} dt = \frac{1}{\pi} \int_{z_1}^{z_2} \frac{F_n(t)}{(t-z_1)^{\alpha_n}(z_2-t)^{\beta_n}(t-z)} dt \\ &= \frac{F_n(z_1) \cot(\pi\alpha_n)}{(z_2-z_1)^{\beta_n}(z-z_1)^{\alpha_n}} - \frac{F_n(z_2) \cot(\pi\beta_n)}{(z_2-z_1)^{\alpha_n}(z_2-z)^{\beta_n}} + G_n(z)\end{aligned}\quad (3.60)$$

where $G_n(z)$ is bounded at the crack tips.

Then eqns (3.29a,b,c,d) give:

$$\frac{F_1^o(-1) \cot(\pi\alpha_1)}{(2)^{\alpha_1}(r+1)^{\alpha_1}} - \frac{F_1^o(1) \cot(\pi\alpha_1)}{(2)^{\alpha_1}(1-r)^{\alpha_1}} = -\frac{(1-\nu_{xy}\nu_{yx})}{2\gamma_{14}E_y} p_1(r) + \text{bounded terms} \quad (3.61)$$

$$\frac{F_2^o(-1) \cot(\pi\alpha_2)}{(2)^{\alpha_2}(r+1)^{\alpha_2}} - \frac{F_2^o(1) \cot(\pi\alpha_2)}{(2)^{\alpha_2}(1-r)^{\alpha_2}} = -\frac{\pi(1-\nu_{xy}^*\nu_{yx}^*)}{2\gamma_{14}^*E_y^*} p_2(r) + \text{bounded terms} \quad (3.62)$$

$$\begin{aligned}\frac{F_3^o(r)}{(1+r)^{\alpha_3}(1-r)^{\beta_3}} + \frac{\zeta^{-1}}{i} \left[\frac{F_3^o(-1) \cot(\pi\alpha_3)}{(2)^{\beta_3}(1+r)^{\alpha_3}} - \frac{F_3^o(1) \cot(\pi\beta_3)}{(2)^{\alpha_3}(1-r)^{\beta_3}} \right] \\ = m_1 p_3(r) + im_2 p_4(r) + \text{bounded terms} \quad b_1 < y < b_2\end{aligned}\quad (3.63)$$

$$\frac{F_4(r)}{(1+r)^{\alpha_4}(1-r)^{\beta_4}} - \frac{\zeta^{-1}}{i} \left[\frac{F_4^o(-1) \cot(\pi\alpha_4)}{(2)^{\beta_4}(1+r)^{\alpha_4}} - \frac{F_4^o(1) \cot(\pi\beta_4)}{(2)^{\alpha_4}(1-r)^{\beta_4}} \right]$$

$$= -im_1p_3(r) - m_2p_4(r) + \text{bounded terms} \quad b_1 < y < b_2 \quad (3.64)$$

From eqns (3.61) and (3.62), it can be easily shown that:

$$\alpha_1 = \beta_1 = \frac{1}{2}, \quad \alpha_2 = \beta_2 = \frac{1}{2} \quad (3.65)$$

These are the known results for cracks perpendicular to the interface [23].

Similarly, from eqns (3.63) and (3.64) we can derive:

$$\begin{aligned} \cot(\pi\alpha_3) &= -i\zeta = -i\sqrt{\frac{\rho_1\rho_4}{\rho_2\rho_3}}, & \cot(\pi\beta_3) &= i\zeta = i\sqrt{\frac{\rho_1\rho_4}{\rho_2\rho_3}} \\ \cot(\pi\alpha_4) &= i\zeta = i\sqrt{\frac{\rho_1\rho_4}{\rho_2\rho_3}}, & \cot(\pi\beta_4) &= -i\zeta = -i\sqrt{\frac{\rho_1\rho_4}{\rho_2\rho_3}} \end{aligned}$$

Using the formula:

$$\cot^{-1}(z) = \frac{1}{2i} \log \frac{z+i}{z-i} \quad (3.66)$$

We then have:

$$\begin{aligned} \alpha_3 &= \frac{1}{2} + i\omega, & \beta_3 &= \frac{1}{2} - i\omega, \\ \alpha_4 &= \frac{1}{2} - i\omega, & \beta_4 &= \frac{1}{2} + i\omega, \end{aligned} \quad (3.67abcd)$$

where

$$\omega = \frac{1}{2\pi} \log \left(\frac{1+\zeta}{1-\zeta} \right)$$

Eqns (3.67a-d) are of the same form as those obtained for interface cracks between two isotropic dissimilar media [24-29].

b) Matrix crack touching the interface ($a_1=H_1, b_1>0$ and $a_2<H_2$)

In this case, as x_1 and t approach to H_1 , the kernel $k_{11}(x_1, t)$ becomes unbounded.

Let $k_{11s}^o(r, s)$ be the normalized kernel of $k_{11s}(x_1, t)$, that is:

$$k_{11s}^o(r, s) = \lambda_{85} \frac{H_1(1-s)\beta_5/|w_1| + H_1|w_1|}{[H_1(1-s)\beta_5/|w_1| + H_1|w_1|]^2 - H_1^2(w_1r)^2}$$

$$\begin{aligned}
& + \lambda_{86} \frac{H_1(1-s)\beta_5/|w_1|+H_1|w_3|}{[H_1(1-s)\beta_5/|w_1|+H_1|w_3|]^2 - H_1^2(w_3r)^2} \\
& + \lambda_{87} \frac{H_1(1-s)\beta_5/|w_3|+H_1|w_1|}{[H_1(1-s)\beta_5/|w_3|+H_1|w_1|]^2 - H_1^2(w_1r)^2} \\
& + \lambda_{88} \frac{H_1(1-s)\beta_5/|w_3|+H_1|w_3|}{[H_1(1-s)\beta_5/|w_3|+H_1|w_3|]^2 - H_1^2(w_3r)^2} \\
& = \frac{\lambda_{85}|w_1|}{2\beta_5} \left[\frac{1}{H_1(1-s+(1+r)\frac{|w_1|^2}{\beta_5})} + \frac{1}{H_1(1-s+(1-r)\frac{|w_1|^2}{\beta_5})} \right] \\
& \quad \frac{\lambda_{86}|w_1|}{2\beta_5} \left[\frac{1}{H_1(1-s+(1+r)\frac{|w_1||w_3|}{\beta_5})} + \frac{1}{H_1(1-s+(1-r)\frac{|w_1||w_3|}{\beta_5})} \right] \\
& \quad \frac{\lambda_{87}|w_3|}{2\beta_5} \left[\frac{1}{H_1(1-s+(1+r)\frac{|w_1||w_3|}{\beta_5})} + \frac{1}{H_1(1-s+(1-r)\frac{|w_1||w_3|}{\beta_5})} \right] \\
& \quad \frac{\lambda_{88}|w_3|}{2\beta_5} \left[\frac{1}{H_1(1-s+(1+r)\frac{|w_3|^2}{\beta_5})} + \frac{1}{H_1(1-s+(1-r)\frac{|w_3|^2}{\beta_5})} \right] \tag{3.68}
\end{aligned}$$

Substituting eqn(3.68) into eqn(3.29a) and moving the bounded terms to the right hand side of the equation, we have:

$$\begin{aligned}
& \frac{1}{\pi} \int_{-1}^1 \left\{ \frac{1}{s-r} + \pi H_1 \frac{\lambda_{85}|w_1|}{2\beta_5} \left[\frac{1}{H_1(1-s+(1+r)\frac{|w_1|^2}{\beta_5})} + \frac{1}{H_1(1-s+(1-r)\frac{|w_1|^2}{\beta_5})} \right] \right. \\
& \quad \left. + \pi H_1 \frac{\lambda_{86}|w_1|}{2\beta_5} \left[\frac{1}{H_1(1-s+(1+r)\frac{|w_1||w_3|}{\beta_5})} + \frac{1}{H_1(1-s+(1-r)\frac{|w_1||w_3|}{\beta_5})} \right] \right.
\end{aligned}$$

$$\begin{aligned}
& + \pi H_1 \frac{\lambda_{87} |w_3|}{2\beta_5} \left[\frac{1}{H_1(1-s+(1+r)\frac{|w_1||w_3|}{\beta_5})} + \frac{1}{H_1(1-s+(1-r)\frac{|w_1||w_3|}{\beta_5})} \right] \\
& + \pi H_1 \frac{\lambda_{88} |w_3|}{2\beta_5} \left[\frac{1}{H_1(1-s+(1+r)\frac{|w_3|^2}{\beta_5})} + \frac{1}{H_1(1-s+(1-r)\frac{|w_3|^2}{\beta_5})} \right] \phi_1^\circ(s) ds \\
& = \frac{1-v_{xy}v_{yz}}{2\gamma_{14}E_y} p_1(r) + \text{bounded terms} \tag{3.69}
\end{aligned}$$

Applying eqns (3.59a) and (3.60) to (3.69), and setting $\alpha_1=\beta_1=\gamma$, we have:

$$\begin{aligned}
& \frac{F_1^\circ(-1)\cot(\pi\gamma)}{(2)^\gamma(1+r)^\gamma} - \frac{F_1^\circ(1)\cot(\pi\gamma)}{(2)^\gamma(1-r)^\gamma} + \frac{\lambda_{85} |w_1|}{2\beta_5} \frac{F_1^\circ(1)}{(2)^\gamma \sin(\pi\gamma) \left[\frac{w_1^2}{\beta_5} \right]^\gamma} \left[\frac{1}{(1+r)^\gamma} + \frac{1}{(1-r)^\gamma} \right] \\
& + \frac{\lambda_{86} |w_1|}{2\beta_5} \frac{F_1^\circ(1)}{(2)^\gamma \sin(\pi\gamma) \left[\frac{|w_1||w_3|}{\beta_5} \right]^\gamma} \left[\frac{1}{(1+r)^\gamma} + \frac{1}{(1-r)^\gamma} \right] \\
& + \frac{\lambda_{87} |w_3|}{2\beta_5} \frac{F_1^\circ(1)}{(2)^\gamma \sin(\pi\gamma) \left[\frac{|w_1||w_3|}{\beta_5} \right]^\gamma} \left[\frac{1}{(1+r)^\gamma} + \frac{1}{(1-r)^\gamma} \right] \\
& + \frac{\lambda_{88} |w_3|}{2\beta_5} \frac{F_1^\circ(1)}{(2)^\gamma \sin(\pi\gamma) \left[\frac{w_3^2}{\beta_5} \right]^\gamma} \left[\frac{1}{(1+r)^\gamma} + \frac{1}{(1-r)^\gamma} \right] \\
& = \frac{1-v_{xy}v_{yz}}{2\gamma_{14}E_y} p_1(r) + \text{bounded terms} \tag{3.70}
\end{aligned}$$

Multiplying both sides of eqn (3.70) by $(1+r)^\gamma$ and letting $r \rightarrow -1$, we have:

$$\begin{aligned}
& -2\cos(\pi\gamma) + \lambda_{85} \frac{|w_1|}{\beta_5} \frac{1}{\left[\frac{w_1^2}{\beta_5}\right]^\gamma} + \lambda_{86} \frac{|w_1|}{\beta_5} \frac{1}{\left[\frac{|w_1||w_3|}{\beta_5}\right]^\gamma} \\
& + \lambda_{87} \frac{|w_3|}{\beta_5} \frac{1}{\left[\frac{|w_1||w_3|}{\beta_5}\right]^\gamma} + \lambda_{88} \frac{|w_3|}{\beta_5} \frac{1}{\left[\frac{w_3^2}{\beta_5}\right]^\gamma} = 0
\end{aligned} \tag{3.71}$$

This result is the same as that given in [23].

c) H-shaped cracks ($a_1=H_1$, $b_1=0$ and $a_2>0$)

As $a_1 \rightarrow H_1$ and $b_1 \rightarrow 0$, the transverse crack intersects with the interface crack and the kernels K_{11} , K_{13} , K_{14} , K_{31} and K_{41} become unbounded. Let α be the index of singularity at the point of intersection, then we have:

$$\phi_1(t) = \frac{F_1(t)}{(H_1^2 - t^2)^\alpha}, \quad \phi_3(t) = \frac{F_3(t)}{t^\alpha (H_1 - t)^{\beta_3}} \quad \text{and} \quad \phi_4(s) = \frac{F_4(t)}{t^\alpha (H_1 - t)^{\beta_4}}$$

Substituting above expressions into eqns (3.29a,c,d), we have:

$$\begin{aligned}
& \frac{1}{\pi} \int_{-H_1}^{H_1} \left\{ \frac{1}{t - x_1} + \pi \frac{\lambda_{85}|w_1|}{2\beta_5} \left[\frac{1}{(H_1 - t + (H_1 + x_1) \frac{|w_1|^2}{\beta_5})} + \frac{1}{(H_1 - t + (H_1 - x_1) \frac{|w_1|^2}{\beta_5})} \right] \right. \\
& + \pi \frac{\lambda_{86}|w_1|}{2\beta_5} \left[\frac{1}{(H_1 - t + (H_1 + x_1) \frac{|w_1||w_3|}{\beta_5})} + \frac{1}{(H_1 - t + (H_1 - x_1) \frac{|w_1||w_3|}{\beta_5})} \right] \\
& + \pi \frac{\lambda_{87}|w_3|}{2\beta_5} \left[\frac{1}{(H_1 - t + (H_1 + x_1) \frac{|w_1||w_3|}{\beta_5})} + \frac{1}{(H_1 - t + (H_1 - x_1) \frac{|w_1||w_3|}{\beta_5})} \right] \\
& \left. + \pi \frac{\lambda_{88}|w_3|}{2\beta_5} \left[\frac{1}{(H_1 - t + (H_1 + x_1) \frac{|w_3|^2}{\beta_5})} + \frac{1}{(H_1 - t + (H_1 - x_1) \frac{|w_3|^2}{\beta_5})} \right] \right\} \frac{F_1(t)}{(H_1^2 - t^2)^\alpha} dt
\end{aligned}$$

$$\begin{aligned}
& + \int_0^{b_2} [\rho_{13} \frac{|w_1|(H_1 - x_1)}{|w_1|^2 (H_1 - x_1)^2 + t^2} + \rho_{14} \frac{|w_3|(H_1 - x_1)}{|w_3|^2 (H_1 - x_1)^2 + t^2}] \frac{F_3(t)}{t^\alpha (b_2 - t)^{\beta_3}} dt \\
& + \int_0^{b_2} [\rho_{15} \frac{t}{|w_1|^2 (H_1 - x_1)^2 + t^2} + \rho_{16} \frac{t}{|w_3|^2 (H_1 - x_1)^2 + t^2}] \frac{F_4(t)}{t^\alpha (b_2 - t)^{\beta_4}} dt \\
& = \frac{1 - v_{xy} v_{yx}}{2\gamma_{14} E_x} p_1(r) + \text{bounded terms}
\end{aligned} \tag{3.72}$$

$$\begin{aligned}
& \int_{-H_1}^{H_1} \left\{ \frac{1}{2\gamma_{13}\pi} \left[-\gamma_1 \frac{H_1 - t}{\frac{|w_1|^2 y^2}{\beta_5^2} + (H_1 - t)^2} + \frac{\gamma_2 \gamma_{11}}{\gamma_{12}} \frac{H_1 - t}{\frac{|w_3|^2 y^2}{\beta_5^2} + (H_1 - t)^2} \right] \right. \\
& \left. + \rho_5 \frac{\frac{(H_1 - t)\beta_5}{|w_1|}}{\frac{(H_1 - t)^2 \beta_5^2}{|w_1|^2} + y^2} + \rho_6 \frac{\frac{(H_1 - t)\beta_5}{|w_3|}}{\frac{(H_1 - t)^2 \beta_5^2}{|w_3|^2} + y^2} \right\} \frac{F_1(t)}{(H_1^2 - t^2)^\alpha} dt \\
& + \frac{\rho_1}{2} \phi_3(y) + \frac{\rho_2}{2\pi} \int_0^{b_2} \left(\frac{1}{t-y} + \frac{1}{t+y} \right) \frac{F_4(t)}{t^\alpha (b_2 - t)^{\beta_4}} dt \\
& = \frac{1 - v_{xy} v_{yx}}{2E_x} p_3(y) + \text{bounded terms}
\end{aligned} \tag{3.73}$$

$$\begin{aligned}
& \int_{-H_1}^{H_1} \left\{ \frac{\gamma_{11}}{2\gamma_{13}\pi} \left[\frac{\frac{|w_1|y}{\beta_5}}{\frac{|w_1|^2 y^2}{\beta_5^2} + (H_1 - t)^2} + \frac{\frac{|w_3|y}{\beta_5}}{\frac{|w_3|^2 y^2}{\beta_5^2} + (H_1 - t)^2} \right] \right. \\
& \left. + \rho_9 \frac{\frac{y}{(H_1 - t)^2 \beta_5^2}}{\frac{|w_1|^2}{(H_1 - t)^2 \beta_5^2} + y^2} + \rho_{10} \frac{\frac{y}{(H_1 - t)^2 \beta_5^2}}{\frac{|w_3|^2}{(H_1 - t)^2 \beta_5^2} + y^2} \right\} \frac{F_1(t)}{(H_1^2 - t^2)^\alpha} dt \\
& + \frac{\rho_4}{2} \phi_4(y) + \frac{\rho_3}{2\pi} \int_0^{b_2} \left(-\frac{1}{t-y} + \frac{1}{t+y} \right) \frac{F_3(t)}{t^\alpha (b_2 - t)^{\beta_3}} dt \\
& = \frac{1}{2G_{xy}} p_4(y) + \text{bounded terms}
\end{aligned} \tag{3.74}$$

Multiplying both sides of eqns (3.72-74) by t^α and letting $t \rightarrow 0$, we then have the following three algebraic equations for $F_1(H_1)$, $F_3(0)$ and $F_4(0)$ with α yet to be determined.

$$\begin{aligned} & \left\{ -\frac{\cot(\pi\alpha)}{(2H_1)^\alpha} + \frac{\lambda_{85} |w_1|}{2 \beta_5} \frac{1}{(2H_1)^\alpha \sin(\pi\alpha) \left[\frac{w_1^2}{\beta_5} \right]^\alpha} + \frac{\lambda_{86} |w_1|}{2 \beta_5} \frac{1}{(2H_1)^\alpha \sin(\pi\alpha) \left[\frac{|w_1||w_3|}{\beta_5} \right]^\alpha} \right. \\ & + \frac{\lambda_{87} |w_3|}{2 \beta_5} \frac{1}{(2H_1)^\alpha \sin(\pi\alpha) \left[\frac{|w_1||w_3|}{\beta_5} \right]^\alpha} + \left. \frac{\lambda_{88} |w_3|}{2 \beta_5} \frac{1}{(2H_1)^\alpha \sin(\pi\alpha) \left[\frac{w_3^2}{\beta_5} \right]^\alpha} \right\} F_1(H_1) \\ & + \frac{\pi}{2b_2^\beta \cos(\frac{\pi\alpha}{2})} \left[\frac{\rho_{13}}{|w_1|^\alpha} + \frac{\rho_{14}}{|w_3|^\alpha} \right] F_3(0) + \frac{\pi}{2b_2^\beta \sin(\frac{\pi\alpha}{2})} \left[\frac{\rho_{15}}{|w_1|^\alpha} + \frac{\rho_{16}}{|w_3|^\alpha} \right] F_4(0) = 0 \end{aligned} \quad (3.75a)$$

$$\begin{aligned} & - \left\{ \frac{1}{2\gamma_{13}} \left[-\gamma_1 \left(\frac{\beta_5}{|w_1|} \right)^\alpha + \gamma_2 \frac{\gamma_{11}}{\gamma_{12}} \left(\frac{\beta_5}{|w_3|} \right)^\alpha \right] + \right. \\ & \left. \pi \left[\rho_5 \frac{|w_1|}{\beta_5} \left(\frac{\beta_5}{|w_1|} \right)^\alpha + \rho_6 \frac{|w_3|}{\beta_5} \left(\frac{\beta_5}{|w_3|} \right)^\alpha \right] \right\} \frac{1}{(2H_1)^\alpha \sin(\frac{\pi\alpha}{2})} F_1(H_1) + \frac{\rho_1}{b_2^\beta} F_3(0) \\ & + \frac{\rho_2}{b_2^\beta} \left[\cot(\pi\alpha) + \frac{1}{\sin(\pi\alpha)} \right] F_4(0) = 0 \end{aligned} \quad (3.75b)$$

$$\begin{aligned} & - \left\{ \frac{\gamma_{11}}{2\gamma_{13}} \left[\left(\frac{\beta_5}{|w_1|} \right)^\alpha + \left(\frac{\beta_5}{|w_3|} \right)^\alpha \right] + \pi \left[\rho_9 \frac{|w_1|}{\beta_5} \left(\frac{\beta_5}{|w_1|} \right)^\alpha + \rho_{10} \frac{|w_3|}{\beta_5} \left(\frac{\beta_5}{|w_3|} \right)^\alpha \right] \right\} \frac{1}{(2H_1)^\alpha \cos(\frac{\pi\alpha}{2})} F_1(H_1) \\ & + \frac{\rho_3}{b_2^\beta} \left[-\cot(\pi\alpha) + \frac{1}{\sin(\pi\alpha)} \right] F_3(0) + \frac{\rho_4}{b_2^\beta} F_4(0) = 0 \end{aligned} \quad (3.75c)$$

Since $F_1(H_1)$, $F_3(0)$ and $F_4(0)$ are generally assumed nonzero, therefore the characteristic equation associated with eqns (3.75abc) has to be zero. Numerical calculations indicate that α is 0 as expected.

3.1.6 Numerical solutions

In this section, numerical procedures are outlined for solving the singular integral equations for different crack configurations as discussed in the previous section. The goal is to determine the stress intensity factors and the strain energy release rates for each crack configuration, at the crack tips.

3.1.6.1 Embedded cracks

Figure 3.1 shows the embedded crack geometry. In this case, the normalized singular integral equations take the following form as derived earlier in section 3.1.4:

$$\begin{aligned} & \frac{1}{\pi} \int_{-1}^1 \left[\frac{1}{s-r} + \pi a_1 k_{11}^o(r, s) \right] \phi_1^o(s) ds + \int_{-1}^1 a_2 k_{12}^o(r, s) \phi_2^o(s) ds \\ & + \frac{b_2 - b_1}{2} \int_{-1}^1 [T_1 \psi_3^o(s) ds + \bar{T}_1 \bar{\psi}_3^o(s)] ds = \frac{1 - \nu_{xy} \nu_{yx}}{2\gamma_{14} E_y} p_1^o(r) \end{aligned} \quad (3.76a)$$

$$\begin{aligned} & \int_{-1}^1 a_1 k_{21}^o(r, s) \phi_1^o(s) ds + \frac{1}{\pi} \int_{-1}^1 \left[\frac{1}{s-r} + \pi a_2 k_{22}^o(r, s) \right] \phi_2^o(s) ds \\ & + \frac{b_2 - b_1}{2} \int_{-1}^1 [T_2 \psi_3^o(s) ds + \bar{T}_2 \bar{\psi}_3^o(s)] ds = \frac{1 - \nu_{xy}^* \nu_{yx}^*}{2\gamma_{14}^* E_y^*} p_2^o(r) \end{aligned} \quad (3.76b)$$

$$\begin{aligned} & \psi_3^o(r) + \frac{\zeta^{-1}}{\pi i} \int_{-1}^1 \psi_3^o(s) \frac{ds}{s-r} - \frac{\zeta^{-1}}{\pi} \int_{-1}^1 \psi_4^o(s) \frac{ds}{s+r+b_o} + \int_{-1}^1 a_1 c_1(r, s) \phi_1^o(s) ds + \int_{-1}^1 a_2 c_2(r, s) \phi_2^o(s) ds \\ & + \frac{b_2 - b_1}{2} \int_{-1}^1 k_1^o(r, s) \psi_3^o(s) ds + \frac{b_2 - b_1}{2} \int_{-1}^1 k_2^o(r, s) \psi_4^o(s) ds \\ & = m_1 \frac{1 - \nu_{xy} \nu_{yx}}{2E_x} p_3(r) + im_2 \frac{1}{2G_{xy}} p_4(r) \end{aligned} \quad (3.76c)$$

$$\begin{aligned} & \psi_4^o(r) - \frac{\zeta^{-1}}{\pi i} \int_{-1}^1 \psi_4^o(s) \frac{ds}{s-r} - \frac{\zeta^{-1}}{\pi} \int_{-1}^1 \psi_3^o(s) \frac{ds}{s+r+b_o} + \int_{-1}^1 a_1 c_3(r, s) \phi_1^o(s) ds + \int_{-1}^1 a_2 c_4(r, s) \phi_2^o(s) ds \\ & + \frac{b_2 - b_1}{2} \int_{-1}^1 k_3^o(r, s) \psi_3^o(s) ds + \frac{b_2 - b_1}{2} \int_{-1}^1 k_4^o(r, s) \psi_4^o(s) ds \\ & = -im_1 \frac{1 - \nu_{xy} \nu_{yx}}{2E_x} p_3(r) - m_2 \frac{1}{2G_{xy}} p_4(r) \end{aligned} \quad (3.76d)$$

All the quantities are defined in section 3.1.4. Among the four equations given above, only three are independent since $\psi_3^0(r)$ and $\psi_4^0(r)$ are related through eqn (3.57b). The first three will be used.

Equations (3.76a) and (3.76b) are Fredholm equations of first kind. Thus Lobatto-Chebyshev integration formula is used. Equation (3.76c) is a Fredholm equation of the second kind, and thus a Lobatto-Jacobi quadrature integration formula is used.

$$\text{Let } \phi_1^0(s) = \frac{F_1^0(s)}{\sqrt{1-s^2}}, \quad \phi_2^0(s) = \frac{F_2^0(s)}{\sqrt{1-s^2}}$$

$$\text{and } \psi_3^0(s) = \frac{F_3(s)}{(1+s)^{\alpha_3}(1-s)^{\beta_3}} = (1-s)^\alpha(1+s)^\beta \sum_{l=0}^N d_l P_l^{(\alpha,\beta)}(s)$$

$$\text{here } \alpha = -\beta_3, \quad \beta = -\alpha_3, \quad F_3(s) = \sum_{l=0}^N d_l P_l^{(\alpha,\beta)}(s) \quad \text{and} \quad d_l = (d_{xl} + i d_{yl})$$

Using the methods described in [30,37], we have:

$$\begin{aligned} & \sum_{k=1}^n \left\{ \frac{W_k}{\pi} \left[\frac{1}{s_k - r_i} + \pi a_1 K_{11}^0(r_i, s_k) \right] F_1^0(s_k) + a_2 W_k K_{12}^0(r_i, s_k) F_2^0(s_k) \right\} \\ & + \frac{b_2 - b_1}{2} \sum_{l=0}^N \sum_{j=1}^n [T_1(r_i, s_{yj}) W_{yj} d_l P_l^{(\alpha,\beta)}(s_{yj}) + \bar{T}_1(r_i, s_{yj}) \bar{W}_{yj} \bar{d}_l \bar{P}_l^{(\alpha,\beta)}(s_{yj})] = \frac{1 - v_{xy}^* v_{yz}^*}{2\gamma_{14}^* E_y} p_1^0(r_i) \end{aligned} \quad (3.77a)$$

$$\begin{aligned} & \sum_{k=1}^n \left\{ a_1 W_k K_{21}^0(r_i, s_k) F_1^0(s_k) + \frac{W_k}{\pi} \left[\frac{1}{s_k - r_i} + \pi a_2 K_{22}^0(r_i, s_k) \right] F_2^0(s_k) \right\} \\ & + \frac{b_2 - b_1}{2} \sum_{l=0}^N \sum_{j=1}^n [T_2(r_i, s_{yj}) W_{yj} d_l P_l^{(\alpha,\beta)}(s_{yj}) + \bar{T}_2(r_i, s_{yj}) \bar{W}_{yj} \bar{d}_l \bar{P}_l^{(\alpha,\beta)}(s_{yj})] = \frac{1 - v_{xy}^* v_{yz}^*}{2\gamma_{14}^* E_y} p_2^0(r_i) \end{aligned} \quad (3.77b)$$

$$\begin{aligned} & \frac{\zeta^{-1}}{\pi i} \sum_{l=0}^N \sum_{j=1}^n \frac{W_{yj} d_l P_l^{(\alpha,\beta)}(s_{yj})}{s_{yj} - r_{yi}} - \frac{\zeta^{-1}}{\pi} \sum_{l=0}^N \sum_{j=1}^n \frac{\bar{W}_{yj} \bar{d}_l \bar{P}_l^{(\alpha,\beta)}(s_{yj})}{s_{yj} + r_{yi} + b_0} \\ & + \sum_{k=1}^n [a_1 c_1(r_i, s_k) F_1^0(s_k) + a_2 c_2(r_i, s_k) F_2^0(s_k)] W_k \end{aligned}$$

$$\begin{aligned}
& + \frac{b_2 - b_1}{2} \sum_{l=0}^N \sum_{j=1}^n [T_3(r_{yi}, s_{yj}) W_{yj} d_1 P_1^{(\alpha, \beta)}(s_{yj}) + T_4(r_{yi}, s_{yj}) \bar{W}_{yj} \bar{d}_1 \bar{P}_1^{(\alpha, \beta)}(s_{yj})] \\
& = m_1 \frac{1 - v_{xy} v_{yx}}{2E_x} P_3(r_{yi}) + im_2 \frac{1}{2G_{xy}} P_4(r_{yi}) \quad (3.77c)
\end{aligned}$$

where $T_3 = k_1^\circ(r_{yi}, s_{yj})$, $T_4 = -i \sqrt{\frac{\eta_2}{\eta_1}} k_2^\circ(r_{yi}, s_{yj})$ and

$$W_k = \frac{1}{2} \frac{\pi}{n-1} \quad (k = 1, n)$$

$$W_k = \frac{\pi}{n-1} \quad (k = 2, \dots, n-1)$$

$$s_k = \cos\left[\frac{\pi(k-1)}{(n-1)}\right] \quad (k = 1, \dots, n)$$

$$r_i = \cos\left[\frac{\pi(2i-1)}{2(n-1)}\right] \quad (i = 1, \dots, n-1)$$

$$W_{yj} = \frac{2^{\alpha+\beta+1} N! [\Gamma(\beta+1)]^2 \Gamma(\alpha+N+2)}{\Gamma(\beta+N+2) \Gamma(\alpha+\beta+N+3)} (1+\beta) \quad (yj = 0)$$

$$W_{yj} = \frac{2^{\alpha+\beta+1} N! [\Gamma(\alpha+1)]^2 \Gamma(\beta+N+2)}{\Gamma(\alpha+N+2) \Gamma(\alpha+\beta+N+3)} (1+\alpha) \quad (yj = N+1)$$

$$W_{yj} = \frac{2^{\alpha+\beta+1} \Gamma(\alpha+N+2) \Gamma(\beta+N+2)}{(N+1)(N+1)! \Gamma(\alpha+\beta+N+3)} \frac{1}{[P_N^{(\alpha, \beta)}(s_{yj})]^2} \quad (yj = 1, \dots, N)$$

the abscissa s_{yj} are the roots of the following equation:

$$(1 - s_{yj}^2) P_{N-1}^{(\alpha+1, \beta+1)}(s_{yj}) = 0$$

and the collocation points r_{yi} satisfies the equation of the N -th order Jacobi polynomial:

$$P_N^{(-\alpha-1, -\beta-1)}(r_{yi}) = 0$$

\bar{W}_{yj} and $\bar{P}_1^{(\alpha, \beta)}(s_{yj})$ ($l=0, \dots, N$) are the complex conjugates of W_{yj} and $P_1^{(\alpha, \beta)}(s_{yj})$ respectively.

At the interface, since α and β are complex numbers, the weight W_{yj} , the abscissa s_{yj} and the collocation point r_{yi} will also be complex. The technique of using the complex weight, abscissa and the collocation points are not new. One can refer to [36-39].

Note that generally d_l ($l = 0, \dots, N$) are complex numbers, and equation (3.77c) actually provides two sets of equations (for the real and imaginary parts). Together, equations (3.77a-c) provide $2(n-1)+2(N)$ equations. Since there are $2(n)+2(N+1)$ unknowns to be determined, the following additional equations are required to insure the single valueness of the solution:

$$\int_{-1}^1 \phi_1^o(s) ds = 0, \quad \int_{-1}^1 \phi_2^o(s) ds = 0 \quad \text{and} \quad \int_{-1}^1 \psi_3^o(s) ds = 0$$

These in turn provide four additional linear equations:

$$\sum_{k=1}^n W_k F_1^o(t_k) = 0$$

$$\sum_{k=1}^n W_k F_2^o(t_k) = 0$$

$$\sum_{l=0}^N \sum_{j=1}^n W_j d_l P_1^{(\alpha, \beta)}(s_{yj}) = 0 \quad (3.78abcd)$$

Note also that the last expression provides two sets of equations

Once the values of $F_1^o(t_k)$, $F_2^o(t_k)$ ($k=1, \dots, n$) and $d_l = d_{lx} + i d_{ly}$ ($l = 0, \dots, N$) are determined, the stress intensity factors can easily be calculated (see appendix E for details of the derivation):

Defining the stress intensity factors as follow:

for transverse crack in matrix and fiber

$$\text{at } x_1 = a_1: \quad k(a_1) = \lim_{x_1 \rightarrow a_1} \sqrt{2(x_1 - a_1)} \sigma_{1y}(x_1, 0)$$

$$\text{at } x_2 = a_2: \quad k(a_2) = \lim_{x_2 \rightarrow a_2} \sqrt{2(x_2 - a_2)} \sigma_{2y}(x_2, 0)$$

for interface cracks:

$$\text{at } y = b_1: \quad \frac{1}{\rho_3} \frac{1}{2G_{xy}} k_2(b_1) - i \sqrt{\frac{\rho_4}{\rho_1 \rho_2 \rho_3}} \frac{1 - \nu_{xy} \nu_{yx}}{2E_x} k_1(b_1)$$

$$= \lim_{y \rightarrow b_1} (b_1 - y)^{\alpha_3} (y - b_2)^{\beta_3} \left[\frac{1}{\rho_3} \frac{1}{2G_{xy}} \sigma_{1xy}(H_1, y) - i \sqrt{\frac{\rho_4}{\rho_1 \rho_2 \rho_3}} \frac{1 - \nu_{xy} \nu_{yx}}{2E_x} \sigma_{1xx}(H_1, y) \right]$$

$$\text{at } y = b_2: \quad \frac{1}{\rho_3} \frac{1}{2G_{xy}} k_2(b_2) - i \sqrt{\frac{\rho_4}{\rho_1 \rho_2 \rho_3}} \frac{1 - \nu_{xy} \nu_{yx}}{2E_x} k_1(b_2)$$

$$= \lim_{y \rightarrow b_2} (b_1 - y)^{\alpha_3} (y - b_2)^{\beta_3} \left[\frac{1}{\rho_3} \frac{1}{2G_{xy}} \sigma_{1xy}(H_1, y) - i \sqrt{\frac{\rho_4}{\rho_1 \rho_2 \rho_3}} \frac{1 - \nu_{xy} \nu_{yx}}{2E_x} \sigma_{1xx}(H_1, y) \right]$$

After some lengthy calculations (see Appendix E), we have

$$k(a_1) = - \frac{2\gamma_{14} E_y \sqrt{a_1}}{(1 - \nu_{xy} \nu_{yx})} F_1^0(1), \quad k(a_2) = - \frac{2\gamma_{14}^* E_y^* \sqrt{a_2}}{(1 - \nu_{xy}^* \nu_{yx}^*)} F_2^0(1) \quad (3.79ab)$$

$$\frac{1}{\rho_3} \frac{1}{2G_{xy}} k_2(b_1) - i \sqrt{\frac{\rho_4}{\rho_1 \rho_2 \rho_3}} \frac{1 - \nu_{xy} \nu_{yx}}{2E_x} k_1(b_1) = \sqrt{1 - \zeta^2} F_3^0(-1) \quad (3.79c)$$

$$\frac{1}{\rho_3} \frac{1}{2G_{xy}} k_2(b_2) - i \sqrt{\frac{\rho_4}{\rho_1 \rho_2 \rho_3}} \frac{1 - \nu_{xy} \nu_{yx}}{2E_x} k_1(b_2) = -\sqrt{1 - \zeta^2} F_3^0(1) \quad (3.79d)$$

If the materials of both layers are isotropic, it can be shown numerically that

$$\frac{1}{\rho_3} \frac{1}{2G_{xy}} = \sqrt{\frac{\rho_4}{\rho_1 \rho_2 \rho_3}} \frac{1 - \nu_{xy} \nu_{yx}}{2E_x}$$

and eqns (3.79c,d) reduce to

$$k_2(b_1) - i k_1(b_1) = 2G_{xy} \rho_3 \sqrt{1 - \zeta^2} F_3^0(-1) \quad (3.79c^*)$$

$$k_2(b_2) - i k_1(b_2) = -2G_{xy} \rho_3 \sqrt{1 - \zeta^2} F_3^0(1) \quad (3.79d^*)$$

The strain energy release rate at the interface crack tip can be derived as follows:

$$\frac{\Delta E}{\Delta y} = \frac{2\pi}{\sqrt{1 - \zeta^2}} \left[\frac{1 - \nu_{xy} \nu_{yx}}{2E_x} \frac{1}{\rho_2} k_1^2 + \frac{1}{2G_{xy}} \frac{1}{\rho_3} k_2^2 \right] \quad (3.80)$$

Again if both layers are made of isotropic materials, the above equation reduces to

$$\frac{\Delta E}{\Delta y} = \frac{2\pi}{\sqrt{1 - \zeta^2}} \frac{1}{2G_{xy}} \frac{1}{\rho_3} (k_1^2 + k_2^2) \quad (3.80^*)$$

It should be noted that when upper and lower interface cracks meet (that is $b_1=0$), eqns (3.76a-d) should be modified before proceeding to the numerical solution. First the integral limits for interface cracks should be extended from $(0, b_2)$ to $(-b_2, b_2)$. Then, using the following relations:

$$\begin{aligned}\phi_3^o(t) &= \phi_3^o(-t) & \phi_4^o(t) &= -\phi_4^o(-t) \\ K_{i3}(x_i, t) &= K_{i3}(x_i, -t) & K_{i4}(x_i, t) &= K_{i4}(x_i, -t) \quad (i = 1, 2) \\ K_{j3}(y, t) &= K_{j3}(y, -t) \quad \text{and} \quad K_{j4}(y, t) &= K_{j4}(y, -t) \quad (j = 3, 4)\end{aligned}$$

eqns (3.76a-d) can be reduced to:

$$\begin{aligned}& \frac{1}{\pi} \int_{-1}^1 \left[\frac{1}{s-r} + \pi a_1 k_{11}^o(r, s) \right] \phi_1^o(s) ds + \int_{-1}^1 a_2 k_{12}^o(r, s) \phi_2^o(s) ds \\ & + \frac{b_2}{2} \int_{-1}^1 [T_1 \psi_3^o(s) ds + \bar{T}_1 \bar{\psi}_3^o(s)] ds = \frac{1 - v_{xy} v_{yx}}{2 \gamma_{14} E_y} p_1^o(r)\end{aligned}\quad (3.81a)$$

$$\begin{aligned}& \int_{-1}^1 a_1 k_{21}^o(r, s) \phi_1^o(s) ds + \frac{1}{\pi} \int_{-1}^1 \left[\frac{1}{s-r} + \pi a_2 k_{22}^o(r, s) \right] \phi_2^o(s) ds \\ & + \frac{b_2}{2} \int_{-1}^1 [T_2 \psi_3^o(s) ds + \bar{T}_2 \bar{\psi}_3^o(s)] ds = \frac{1 - v_{xy}^* v_{yx}^*}{2 \gamma_{14}^* E_y^*} p_2^o(r)\end{aligned}\quad (3.81b)$$

$$\begin{aligned}\psi_3^o(r) &+ \frac{\zeta^{-1}}{\pi i} \int_{-1}^1 \psi_3^o(s) \frac{ds}{s-r} + \int_{-1}^1 a_1 c_1(r, s) \phi_1^o(s) ds + \int_{-1}^1 a_2 c_2(r, s) \phi_2^o(s) ds \\ &+ \frac{b_2}{2} \int_{-1}^1 [k_1^o(r, s) \psi_3^o(s) + k_2^o(r, s) \psi_4^o(s)] ds \\ &= m_1 \frac{1 - v_{xy} v_{yx}}{2 E_x} p_3(r) + i m_2 \frac{1}{2 G_{xy}} p_4(r)\end{aligned}\quad (3.81c)$$

$$\begin{aligned}\psi_4^o(r) &- \frac{\zeta^{-1}}{\pi i} \int_{-1}^1 \psi_4^o(s) \frac{ds}{s-r} + \int_{-1}^1 a_1 c_3(r, s) \phi_1^o(s) ds + \int_{-1}^1 a_2 c_4(r, s) \phi_2^o(s) ds \\ &+ \frac{b_2}{2} \int_{-1}^1 [k_3^o(r, s) \psi_3^o(s) + k_4^o(r, s) \psi_4^o(s)] ds \\ &= -i m_1 \frac{1 - v_{xy} v_{yx}}{2 E_x} p_3(r) - m_2 \frac{1}{2 G_{xy}} p_4(r)\end{aligned}\quad (3.81d)$$

The above numerical procedure and the single valuedness conditions can also be applied to solve eqns (3.81a-c).

3.1.6.2 Matrix cracks touching the interface ($a_1=H_1$, $b_1>0$)

When matrix cracks touch the interface, the kernel $F_{11}^o(x_1, t)$ becomes unbounded. And the singular behavior at the crack tip changes. Now, redefining $\phi_1^o(s)$ as:

$$\phi_1^o(s) = \frac{F_1^o(s)}{(1-s^2)^\gamma}$$

the power of singularity γ can be determined from eqn (3.71).

Since γ is generally different than 0.5, in the numerical procedures described for eqns (3.78a-c), we now use the Lobatto-Jacobi quadrature for integrals containing $\phi_1^o(s)$. The rest of the definitions and numerical calculations in eqns (3.78a-c) remain the same. The modified version takes the following form:

$$\begin{aligned} & \sum_{k=1}^n \left\{ \frac{W'_k}{\pi} \left[\frac{1}{s_k - r_i} + \pi a_1 K_{11}^o(r_i, s_k) \right] F_1^o(s_k) + W'_k a_1 K_{11}^o(r_i, s_k) F_1^o(s_k) + a_2 W_k K_{12}^o(r_i, s_k) F_2^o(s_k) \right\} \\ & + \frac{b_2 - b_1}{2} \sum_{l=0}^N \sum_{j=1}^n [T_1(r_i, s_{yj}) W_{yj} d_1 P_1^{(\alpha, \beta)}(s_{yj}) + \bar{T}_1(r_i, s_{yj}) \bar{W}_{yj} \bar{d}_1 \bar{P}_1^{(\alpha, \beta)}(s_{yj})] = \frac{1 - v_{xy} v_{yx}}{2 \gamma_{14} E_y} P_1^o(r_i) \end{aligned} \quad (3.82a)$$

$$\begin{aligned} & \sum_{k=1}^n \left\{ a_1 W'_k K_{21}^o(r_i, s_k) F_1^o(s_k) + \frac{W_k}{\pi} \left[\frac{1}{s_k - r_i} + \pi a_2 K_{22}^o(r_i, s_k) \right] F_2^o(s_k) \right\} \\ & + \frac{b_2 - b_1}{2} \sum_{l=0}^N \sum_{j=1}^n [T_2(r_i, s_{yj}) W_{yj} d_1 P_1^{(\alpha, \beta)}(s_{yj}) + \bar{T}_2(r_i, s_{yj}) \bar{W}_{yj} \bar{d}_1 \bar{P}_1^{(\alpha, \beta)}(s_{yj})] = \frac{1 - v_{xy}^* v_{yx}^*}{2 \gamma_{14}^* E_y^*} P_2^o(r_i) \end{aligned} \quad (3.82b)$$

$$\begin{aligned} & \frac{\zeta^{-1}}{\pi i} \sum_{l=0}^N \sum_{j=1}^n \frac{W_{yj} d_1 P_1^{(\alpha, \beta)}(s_{yj})}{s_{yj} - r_{yi}} - \frac{\zeta^{-1}}{\pi} \sum_{l=0}^N \sum_{j=1}^n \frac{\bar{W}_{yj} \bar{d}_1 \bar{P}_1^{(\alpha, \beta)}(s_{yj})}{s_{yj} + r_{yi} + b_o} \\ & + \sum_{k=1}^n [a_1 c_1(r_{yi}, s_k) F_1^o(s_k) W'_k + a_2 c_2(r_{yi}, s_k) F_2^o(s_k) W_k] \end{aligned}$$

$$\begin{aligned}
& + \frac{b_2 - b_1}{2} \sum_{l=0}^N \sum_{j=1}^n [T_3(r_{yi}, s_{yj}) W_{yj} d_l P_1^{(\alpha, \beta)}(s_{yj}) + T_4(r_{yi}, s_{yj}) \bar{W}_{yj} \bar{d}_l \bar{P}_1^{(\alpha, \beta)}(s_{yj})] \\
& = m_1 \frac{1 - v_{xy} v_{yx}}{2E_x} p_3(r_{yi}) + i m_2 \frac{1}{2G_{xy}} p_4(r_{yi})
\end{aligned} \tag{3.82c}$$

where

$$W'_k = \frac{2^{1-\gamma-\gamma}(n-1)! [\Gamma(1-\gamma)]^2}{\Gamma(n+2-2\gamma)} (1-\gamma) \quad (k=1, n)$$

$$W'_k = \frac{2^{1-\gamma-\gamma}(n-1)! [\Gamma(1-\gamma)]^2}{\Gamma(n+2-2\gamma)} \frac{1}{[P_{n-1}^{(-\gamma, -\gamma)}(s'_k)]^2} \quad (k=2, \dots, n-1)$$

the abscissa s'_k are the roots of the following equation:

$$(1 - s'^2_k) P_{n-2}^{(1-\gamma, 1-\gamma)}(s'_k) = 0$$

and the collocation points r'_i are the roots of the following equation

$$P_{n-1}^{(\gamma-1, \gamma-1)}(r'_i) = 0$$

The methods of evaluating the weight, abscissa W_k , t_k for Lobatto-Chebyshev integration rule, W_j , s_{yj} for Lobatto-Jacobi integration rule and their collocation points r_i and r_{yi} will be the same as those described in section 3.1.6.1.

The single valuedness conditions become:

$$\sum_{k=1}^n W'_k F_1^o(t_k) = 0$$

$$\sum_{k=1}^n W_k F_2^o(t_k) = 0$$

$$\sum_{l=0}^N \sum_{j=1}^n W_j d_l P_1^{(\alpha, \beta)}(s_{yj}) = 0 \tag{3.83abcd}$$

The expressions for stress intensity factors and strain energy release rates given in the previous section can still be used in this case except for $k(a_1)$

$$\text{Redefining} \quad k(a_1) = \lim_{x_2 \rightarrow H_2} 2^\gamma (x_2 + H_2)^\gamma \sigma_{2y}(x_2, 0)$$

we have (see Appendix E):

$$\begin{aligned}
k(a_1) = & \frac{(H_1)^{2\gamma} \gamma_{14}^* E_y^* F_1^*(1)}{(1 - v_{xy}^* v_{yx}^*) \sin(\pi\gamma)} \left[\lambda_{101} \frac{|w_1|/\beta_5}{[w_1^* |w_1|/\beta_5]^\gamma} + \lambda_{102} \frac{|w_1|/\beta_5}{[w_3^* |w_1|/\beta_5]^\gamma} \right. \\
& \left. + \lambda_{103} \frac{|w_3|/\beta_5}{[w_3^* |w_1|/\beta_5]^\gamma} + \lambda_{101} \frac{|w_3|/\beta_5}{[w_3^* |w_3|/\beta_5]^\gamma} \right] \quad (3.84)
\end{aligned}$$

3.1.6.3 H-shaped cracks ($a_1=H_1$, $b_1=0$)

When $a_1 = H_1$ and $b_1 = 0$, the transverse matrix cracks intersect with the interface crack to form H-shaped cracks as shown in Fig. 3.2. This configuration has been observed during the tensile test of the uniaxial ceramic matrix composites. Since the power of singularity at the point of intersection is zero, which has been confirmed numerically, $\phi_1^0(s)$ will no longer be singular at this crack tip. Also, the kernels K_{11} , K_{13} , K_{14} , K_{31} and K_{41} become unbounded. In this case, because $b_1 = 0$, the numerical calculations will be based on eqns (3.81a-c) instead of eqns (3.76a-c).

First, the singular parts of the kernels K_{11} , K_{13} , K_{14} , K_{31} and K_{41} in eqns (3.81a-c) will be extracted and integrated in closed form. Then the modified equations take the following form:

$$\begin{aligned}
& \frac{1}{\pi} \int_{-1}^1 \left[\frac{1}{s-r} + \pi a_1 k_{11s}^0(r,s) \right] \phi_1^0(s) ds + \int_{-1}^1 a_1 [k_{11}^0(r,s) - k_{11s}^0(r,s)] \phi_1^0(s) ds \\
& + \int_{-1}^1 a_2 k_{12}^0(r,s) \phi_2^0(s) ds + \frac{b_2}{2} \int_{-1}^1 [T_{1s} \psi_3^0(s) ds + \bar{T}_{1s} \bar{\psi}_3^0(s)] ds \\
& + \frac{b_2}{2} \int_{-1}^1 [(T_1 - T_{1s}) \psi_3^0(s) ds + (\bar{T}_1 - \bar{T}_{1s}) \bar{\psi}_3^0(s)] ds = \frac{1 - v_{xy}^* v_{yx}^*}{2\gamma_{14} E_y} p_1^0(r) \quad (3.85a)
\end{aligned}$$

$$\begin{aligned}
& \int_{-1}^1 a_1 k_{21}^0(r,s) \phi_1^0(s) ds + \frac{1}{\pi} \int_{-1}^1 \left[\frac{1}{s-r} + \pi a_2 k_{22}^0(r,s) \right] \phi_2^0(s) ds \\
& + \frac{b_2}{2} \int_{-1}^1 [T_2 \psi_3^0(s) ds + \bar{T}_2 \bar{\psi}_3^0(s)] ds = \frac{1 - v_{xy}^* v_{yx}^*}{2\gamma_{14} E_y} p_2^0(r) \quad (3.85b)
\end{aligned}$$

$$\begin{aligned}
\psi_3^o(r) + \frac{\zeta^{-1}}{\pi i} \int_{-1}^1 \psi_3^o(s) \frac{ds}{s-r} + \int_{-1}^1 a_1 c_{1s}(r,s) \phi_1^o(s) ds + \int_{-1}^1 a_1 [c_1(r,s) - c_{1s}(r,s)] \phi_1^o(s) ds \\
+ \int_{-1}^1 a_2 c_{2s}(r,s) \phi_2^o(s) ds + \frac{b_2}{2} \int_{-1}^1 [k_1^o(r,s) \psi_3^o(s) + k_2^o(r,s) \psi_4^o(s)] ds \\
= m_1 \frac{1 - v_{xy} v_{yx}}{2E_x} p_3(r) + i m_2 \frac{1}{2G_{xy}} p_4(r)
\end{aligned} \quad (3.85c)$$

$$\text{where} \quad T_{1s} = k_{13s}^o + i \sqrt{\frac{\eta_2}{\eta_1}} k_{14s}^o \quad \bar{T}_{1s} = k_{13s}^o - i \sqrt{\frac{\eta_2}{\eta_1}} k_{14s}^o$$

$$\text{and} \quad c_{1s}(r,s) = \left[\frac{k_{31s}^o}{\rho_1} + i \frac{k_{41s}^o}{\rho_4} \sqrt{\frac{\eta_1}{\eta_2}} \right]$$

Now defining $\phi_1^o(s) = F_1^o(s)$, the definitions for the rest of the displacement density functions remain the same as in section 3.1.6.1. Then we have:

$$\begin{aligned}
\sum_{k=1}^n \left\{ \frac{W_k'}{\pi} \left[\frac{1}{s_k - r_i} + \pi a_1 K_{11s}^o(r_i', s_k') \right] F_1^o(s_k') + a_1 W_k' [K_{11}^o(r_i', s_k') - K_{11s}^o(r_i', s_k')] F_1^o(s_k') \right. \\
\left. + a_2 W_k K_{12}^o(r_i, s_k) F_2^o(s_k) \right\} + \frac{b_2}{2} \sum_{i=0}^N \sum_{j=1}^n [T_{1s}(r_i, s_{yj}) W_{yj} d_1 P_1^{(\alpha, \beta)}(s_{yj}) + \bar{T}_{1s}(r_i, s_{yj}) \bar{W}_{yj} \bar{d}_1 \bar{P}_1^{(\alpha, \beta)}(s_{yj})] \\
\frac{b_2}{2} \sum_{i=0}^N \sum_{j=1}^n \{ [T_1(r_i, s_{yj}) - T_{1s}(r_i, s_{yj})] W_{yj} d_1 P_1^{(\alpha, \beta)}(s_{yj}) + [\bar{T}_1(r_i, s_{yj}) - \bar{T}_{1s}(r_i, s_{yj})] \bar{W}_{yj} \bar{d}_1 \bar{P}_1^{(\alpha, \beta)}(s_{yj}) \} \\
= \frac{1 - v_{xy} v_{yx}}{2\gamma_{14} E_y} p_1^o(r_i')
\end{aligned} \quad (3.77a)$$

$$\begin{aligned}
\sum_{k=1}^n \left\{ a_1 W_k' K_{21}^o(r_i', s_k') F_1^o(s_k') + \frac{W_k}{\pi} \left[\frac{1}{s_k - r_i} + \pi a_2 K_{22}^o(r_i, s_k) \right] F_2^o(s_k) \right\} \\
+ \frac{b_2}{2} \sum_{i=0}^N \sum_{j=1}^n [T_2(r_i, s_{yj}) W_{yj} d_1 P_1^{(\alpha, \beta)}(s_{yj}) + \bar{T}_2(r_i, s_{yj}) \bar{W}_{yj} \bar{d}_1 \bar{P}_1^{(\alpha, \beta)}(s_{yj})] = \frac{1 - v_{xy}^* v_{yx}^*}{2\gamma_{14}^* E_y^*} p_2^o(r_i)
\end{aligned} \quad (3.77b)$$

$$\frac{\zeta^{-1}}{\pi i} \sum_{i=0}^N \sum_{j=1}^n \frac{W_{yj} d_1 P_1^{(\alpha, \beta)}(s_{yj})}{s_{yj} - r_{yi}} - \frac{\zeta^{-1}}{\pi} \sum_{i=0}^N \sum_{j=1}^n \frac{\bar{W}_{yj} \bar{d}_1 \bar{P}_1^{(\alpha, \beta)}(s_{yj})}{s_{yj} + r_{yi} + b_o}$$

$$\begin{aligned}
& + \sum_{k=1}^n W'_k a_1 c_{1s}(r'_1, s'_k) F_1^o(s'_k) + \sum_{k=1}^n W'_k a_1 [c_1(r'_1, s'_k) - c_{1s}(r'_1, s'_k) F_1^o(s'_k)] \\
& + \sum_{k=1}^n W'_k a_2 c_2(r_i, s_k) F_2^o(s_k) + \frac{b_2}{2} \sum_{l=0}^N \sum_{j=1}^n [T_3(r_{yi}, s_{yj}) W_{yj} d_1 P_1^{(\alpha, \beta)}(s_{yj}) \\
& + T_4(r_{yi}, s_{yj}) \bar{W}_{yj} \bar{d}_1 \bar{P}_1^{(\alpha, \beta)}(s_{yj})] = m_1 \frac{1 - v_{xy} v_{yz}}{2E_x} p_3(r_{yi}) + im_2 \frac{1}{2G_{xy}} p_4(r_{yi}) \quad (3.77c)
\end{aligned}$$

where

$$W'_k = \frac{2}{n(n-1)} \quad (k=1, n)$$

$$W'_k = \frac{2}{n(n-1)} \frac{1}{[P_{n-1}(s'_k)]^2} \quad (k=2, \dots, n-1)$$

the abscissa s'_k are the roots of the following equation:

$$(1 - s_k'^2) P_{n-2}^{(1,1)}(s'_k) = 0$$

W'_k and s'_k are the weights and abscissa of the Lobatto-Legendre integration rule.

The collocation points r'_1 are the roots of the following equation

$$P_{n-1}^{(-1,-1)}(r'_1) = 0$$

Again, the methods of evaluating the weight and abscissa W_k , t_k for Lobatto-Chebyshev integration rule; W_j , s_{yj} for Lobatto-Jacobi integration rule and their collocation points r_i and r_{yi} remain the same as those given in section 3.1.6.1.

The remaining four additional equations take the following form:

$$F_1^o(-1) = 0 \quad (3.86a)$$

$$F_1^o(1) = 0 \quad (3.86b)$$

$$\int_{-1}^1 \phi_2^o(s) ds = 0 \quad (3.86c)$$

$$\text{and} \quad \int_{-H_1}^{H_1} \phi_1(s) ds = \int_0^{b_2} \phi_3(s) ds \quad (3.86d)$$

The first two equations originate from the requirement that $\phi_1^o(s)$ remains finite at both crack tips. The third equation is deduced from the single valuedness condition for

embedded cracks in the fiber if a_2 is not zero. And the last equation states the condition of continuity of displacement at the point of intersection.

Eqns (3.86ab) can be directly used in the numerical calculations. Eqn (3.86c) can be written as:

$$\sum_{k=1}^n W_k F_2^o(t_k) = 0 \quad (3.86c^*)$$

Using the fact that

$$\begin{aligned} \int_0^{b_2} \phi_3(s) ds &= \frac{b_2}{2} \int_{-1}^1 \phi_3^o(s) ds \\ &= -i \frac{b_2}{2} \int_{-1}^1 \psi_3^o(s) ds \\ &= -i \frac{b_2}{2} d_0 \frac{\pi}{\cosh(\pi\omega)}, \end{aligned}$$

we have

$$\int_{-H_1}^{H_1} \phi_1(s) ds = -i \frac{b_2}{2} d_0 \frac{\pi}{\cosh(\pi\omega)}$$

Since $\int_{-H_1}^{H_1} \phi_1(s) ds$ is real, therefore,

$$\text{Re}(d_0) = 0 \quad (3.86d^*)$$

This result gives the last equation that is needed for the numerical calculations.

The calculation of the stress intensity factors at the embedded crack tips remain the same, and needs no further elaboration.

3.1.7 Results and discussion for singular integration formulation

It is well known that the interface bonding strength contributes to the toughness of ceramic matrix composites. A "weak" bonding strength generally improves the toughness of the composite. A direct indication of weak bonding between the matrix and the fiber interface is the existence of interface crack or defects either due to manufacturing or due to debonding during loading. In the experiment, it was observed that under tensile loading,

matrix cracks generated first and then propagated to the interface. Once the matrix cracks reached the interface, they did not penetrate through the fibers. This means the fracture energy available at the crack tip is less than the fracture energy of the fiber, and is larger than the fracture energy along the interface due the weak interface. Thus, the energy is released along the interface causing interface debonding or generating interface cracks. The actual role that the interface plays has drawn a lot of attention by both involved in research and manufacturing of ceramic composites. One can refer to [45,46] for detailed discussions. The goal here is to explain or simulate the damage mechanism of ceramic matrix composites by analyzing the interactions between matrix and interface cracks using different crack configurations.

The numerical calculation for embedded crack configuration has been carried out first. To check the correctness of the numerical procedure, some simple crack configurations have been studied first. For periodic transverse cracks in the matrix and the fibers without interface cracks, the results match those given in [23,44]; For interface cracks without transverse cracks, if both H_1 and H_2 are set very large and the materials of both layers are isotropic, the problem is reduced to an interface crack in an infinite domain and the results from [25,43] for stress intensity factor at the interface were recovered. Table 3.1 gives the results of stress intensity factors at the interface for four different materials combinations. As can be seen from the table, the two results are almost identical. Also, the strain energy release rates at the interface for the above four material combinations were calculated using eqn (3.80*). For isotropic materials, the exact expression of the strain energy release rate at the interface was first given in [40] as follows:

$$\frac{\Delta E}{\Delta y} = \frac{\pi}{2} \frac{(\mu_1 + \kappa_1 \mu_2)(\mu_2 + \kappa_2 \mu_1)}{\mu_1 \mu_2 [(1 + \kappa_1)\mu_2 + (1 + \kappa_2)\mu_1]} (k_1^2 + k_2^2) \quad (3.87)$$

where μ_1 and μ_2 are the shear moduli of the fiber and the matrix respectively.

Table 3.1 Comparison of stress intensity factors

Materials		$\frac{K_1(b)}{\sigma_0\sqrt{b}}$		$\frac{K_2(b)}{\sigma_0\sqrt{b}}$	
Layer 1	Layer 2	Results from [25]	Results from eqn (3.79d)	Results from [25]	Results from eqn (3.79d)
Aluminum	Epoxy	1	1.0000	-0.1342	-0.13421
Steel	Epoxy	1	1.0000	-0.1443	-0.14431
Steel	Aluminum	1	1.0000	-0.09158	-0.091576
Nicalon	CAS II	1	1.0000	-0.071076	-0.071074

The results using eqn (3.80*) differed with that given in eqn (3.87) by a factor of $\sqrt{2}$. The strain energy release rates using both eqn (3.80*) and eqn (3.87) are compared in Table 3.2. The error is within 3 percent. Considering the fact that all the derivations are based on the orthotropic materials, and the isotropic behavior was approximated in the calculation, the results are quite good. Table 3.3 gives the Young's moduli and the poisson's ratios for the materials used in the calculation.

Table 3.2 Comparison of strain energy release rates

Materials		Strain energy release rates	
Layer 1	Layer 2	$\frac{2}{\pi} \frac{\Delta E}{\Delta y}$ in (3.87)	$\sqrt{2} \frac{2}{\pi} \frac{\Delta E}{\Delta y}$ in (3.80*)
Aluminum	Epoxy	0.397614×10^{-5}	0.402399×10^{-5}
Steel	Epoxy	0.384227×10^{-5}	0.389954×10^{-5}
Steel	Aluminum	0.239708×10^{-6}	0.239753×10^{-6}
Nicalon	CAS II	0.203262×10^{-6}	0.208256×10^{-6}

Table 3.3 Material constants

Material	Young's modulus E (lb in. $^{-2}$)	Poisson's ratio
Aluminum	1×10^7	0.3
Steel	3×10^7	0.3
Epoxy	4.5×10^5	0.35
Nicalon	2.83×10^7	0.28
CAS II	13.2×10^7	0.28

Next, the effects of the transverse and interface cracks on the tensile damage behavior of the ceramic matrix composite are investigated. Suppose there exist both small transverse matrix cracks and interface cracks or defects. First, let the matrix cracks be allowed to propagate and the interface crack be fixed at a small value $b/H_2=0.01$. The stress intensity factors at both the matrix crack and the interface crack tips are calculated and plotted against the increasing matrix crack length. Fig. 3.3 shows the mode I stress intensity factors at the matrix crack tips versus the matrix crack length for both $V_f = 30\%$ and $V_f = 40\%$. The stress intensity factors increased first and then decreased as the matrix crack approached the interface. The decrease of the stress intensity factors as the matrix crack approached the interface is because of the fiber constraint effect. The mode I stress intensity factors at the interface, however, remained unchanged at first and increased rapidly as shown in Fig. 3.4 when the matrix crack approached the interface. Fig. 3.5 gives the strain energy release rate at the interface versus the matrix crack length for two different fiber volume fractions. The influence of fiber volume fractions can also be noted here. Next, let the matrix crack length be fixed ($a_2=0.9H_2$) and the interface crack length be allowed to increase, then the stress intensity factors at the matrix crack tips and

interface crack tips were calculated and plotted in Fig. 3.6 and Fig. 3.7. respectively. The mode I stress intensity factors at the transverse matrix crack tips exhibited a steady increase until the interface crack length reached a certain value ($b=H_2$). Fig. 3.8 shows the strain energy release rate at the interface versus the interface crack length. The following conclusion can be drawn from the above two cases: If both matrix crack and interface crack exist in the composite, the matrix crack will first propagate because of the increase of stress intensity factors at the matrix crack tips and the low fracture toughness of the matrix. Then the crack will be arrested when it reaches the interface because of the fiber constraint effect. On the other hand, if the fracture toughness along the interface is small, the interface crack will grow due to an increase in the strain energy release rate at the interface. Once the interface crack or debonding length reaches a certain value, the fiber constraint effect is almost lost and the stress intensity factors at the matrix crack tips start to grow again as can be seen from Fig. 3.9 where $b/H_2 = 0.55$. Eventually the matrix crack will reach the interface boundary. This has been observed during testing. Another important role that the interface crack plays, is to prevent the matrix cracks from extending self-similarly into the fibers. As can be seen from the test results, fibers do not break at the same locations as the matrix resulting in longer fiber pull-out length. The variations of the stress intensity factors versus the increase of matrix crack length for two different values of interface crack length are shown in Figure 3.9a and Figure 3.9b for fiber volume fractions of 30% and 40% respectively.

3.2 Finite Element analysis

The H-shaped crack configuration is adopted and used to study the effects of interface cracking and its progression on the tensile behavior of ceramic matrix composites.

3.2.1 Description of the H-shaped crack model

From the experiments, it is observed that, after the appearance of initial transverse matrix cracks, the stress-strain behavior starts to become nonlinear. With certain increase of the tensile load (about 10 ksi), a regularly spaced multiple transverse matrix crack pattern is formed. Once this stage is reached, further increase of load generates few new matrix cracks until final failure. Therefore, during the period from which saturated matrix crack formed to eventual failure, interface debonding, matrix crack opening and sequential fiber breaking dominate the failure process. To capture the effect of damage accumulation due to interface debonding, a configuration of periodic H-cracks as shown in Fig. 3.2 is used where the interface crack length is allowed to increase with increasing load. The popular ABAQUS finite element code is used with strain energy release rate as the criterion for the interface crack propagation. First, the strain energy was calculated for a certain interface crack length, then the interface crack length is allowed to increase by releasing the node at the crack tip and the strain energy is again calculated. Thus an estimation of the strain energy release rate G at the interface crack tip can be determined using the following expression:

$$G = \frac{U_n - U_{n+1}}{t\Delta D} \quad (n=0,1,2, \dots)$$

where U_n and U_{n+1} are the strain energies associated with the two subsequent crack lengths, ΔD is the interface crack increment and t is the thickness of the specimen. If this G value is greater than G_{cr} (critical strain energy release rate), then the crack is assumed

to propagate. In practice, the G_{CT} value at the interface is extremely difficult to measure. Here we estimate G_{CT} by matching one point of the stress-strain curve with the calculated value. Table 3.4 shows the computed G_{CT} for both $V_f = 30\%$ and $V_f = 40\%$.

Table 3.4 Estimated critical strain energy release rate G_{CT}

Fiber volume fraction	$L/2H_2$	Estimated G_{CT}
30%	2.5	85.36 (lbs/in)
40%	3.0	62.70 (lbs/in)

3.2.2 Finite element results and discussion

Before the finite element calculation is carried out, one has to determine the matrix crack spacing L and the fiber spacing $2H_2$ used in the model as shown in Fig. 3.10. The ratio $L/2H_2$ affects the results significantly. Matrix crack spacing is determined by averaging the matrix crack length from the micrographs taken during the experiment. It is found that the matrix crack spacing decreases with increasing fiber volume fraction of the specimen. The average matrix crack spacing for $V_f = 30\%$ was found to be $L = 166 \mu\text{m}$. And for $V_f = 40\%$, the value is $L = 111 \mu\text{m}$. The fiber spacing varies with fiber volume fraction, the fiber diameter and how evenly the fiber filament is distributed in the matrix media. The average fiber diameter for Nicalon fiber is about $16 \mu\text{m}$ as measured from the test results. Consider the case where fibers are evenly distributed in the matrix media, then for $V_f = 30\%$, $2H_2 = (0.7)(16)/0.3 = 37.3 \mu\text{m}$ and for $V_f = 40\%$, $2H_2 = (0.6)(16)/0.4 = 24 \mu\text{m}$. Therefore we have:

$$\frac{L}{2H_2} = 166/37 = 4.44 \quad \text{for } V_f = 30\%$$

and
$$\frac{L}{2H_2} = 111/24 = 4.625 \quad \text{for } V_f = 40\%$$

Considering the fact that fibers are randomly distributed in the matrix and that the fiber diameter is not constant, the above ratios were varied between 2.0 to 3.0 in the calculations. Fig 3.11 is a comparison of finite element results with the test results for $V_f = 30\%$. Fig. 3.12 shows the comparison for $V_f = 40\%$. It can be seen that finite element results match the test results quite well at the start of the non-linear stress-strain curve. Then the two results deviate somewhat as the load is further increased. This is because at higher loading the fibers start to break as can be seen from the micrographs taken during the tests. This contributes to the flattening of the actual stress-strain curve. It may also be noted that the finite element results for $V_f = 30\%$ match the stress-strain diagram better than those for $V_f = 40\%$. This can be explained as follows: with more fibers in the 40% fiber volume fraction specimen, more sequential fiber breakings occurred during the final stage of the experiment after the saturated multiple matrix crack pattern was formed. This can not be simulated by considering interface cracks only. Fig. 3.13 gives the stress distribution in both fiber and matrix near the interface crack tips. Fig. 3.14 gives the normal stress distribution along the interface

REFERENCES

- [1] Schioler, L. J. and Stiglich, J. J., Jr. "Ceramic matrix composites: a literature review." Ceramic Bull. **65**, 289-292, 1986.
- [2] Cornie, J. A., Chiang, Y., M., Uhlmann, D. R., Mortensen, A. and Collins, J. M. "Processing of metal and ceramic matrix composites." Ceramic Bull. **65**, 293-304, 1986.
- [3] Ichinose, N. (Editor) Introduction to Fine Ceramics Applications in Engineering. Wiley, New York, 1987.
- [4] Wachtman, J. B., Jr (Editor) Structural Ceramics. Treatise on Materials Science and Technology, Vol. 29, 1989. Academic Press, New York.
- [5] Phillips, D. C. "The fracture energy of carbon-fiber reinforced glass." J. Mater. Sci. **7**, 1175-1191, 1972.
- [6] Gomina, M., Chermant, J. L., Osterstock, F., Bernhart, G. and Mace, J. "Applicability of fracture mechanics to fiber-reinforced CVD-ceramic composites." Fracture Mechanics of Ceramics (Edited by R. C. Bradt *et al.*), Vol. 7, pp. 17-32, 1986. Plenum Press, New York.
- [7] Prewo, K. M. and Brennan, J. J. "High-strength silicon carbide fiber-reinforced glass-matrix composites." J. Mater. Sci. **15**, 463-468, 1980
- [8] Brennan, J. J. and Prewo, K. M. "Silicon carbide fiber reinforced glass-ceramic matrix composites exhibiting high strength and toughness." J. Mater. Sci. **17**, 2371-2383, 1982.
- [9] Mah, T., Mendioretta, M. G., Katz, A. P., Ruh, R. and Mazdiasni, K. S. "Room-temperature mechanical behavior of fiber-reinforced glass-ceramic-matrix composites." J. Am. Ceramic Soc. **68**, C27-C30, 1985.

- [10] Mah, T., Mendioretta, M. G., Katz, A. P., Ruh, R. and Mazdiyasni, K. S. "High-temperature mechanical behavior of fiber-reinforced glass-ceramic-matrix composites." *J. Am. Ceramic Soc.* **68**, C248-C251, 1985.
- [11] Marshall, D. B. and Evans, A. G. "Failure mechanisms in ceramic-fiber/ceramic-matrix composites." *J. Am. Ceramic Soc.* **68**, 225-231, 1985.
- [12] Marshall, D. B. and Evans, A. G. "The tensile strength of uniaxially reinforced ceramic fiber composites." In *Fracture Mechanics of Ceramics* (Edited by R. C. Bradt, *et al.*), Vol. 7, pp. 1-15, 1986. Plenum Press, New York.
- [13] Stewart, R. L., Chyung, K., Taylor, M. P. and Cooper, R. F. "Fracture of SiC/glass-ceramic composites as a function of temperature." In *Fracture Mechanics of Ceramics* (Edited by R. C. Bradt, *et al.*), Vol. 7, pp. 33-51, 1986. Plenum Press, New York.
- [14] Jenkins, M. G., Kobayashi, A. S., White, K. W. and Bradt, R. C. "Crack initiation and arrest in a SiC whisker/ Al_2O_3 matrix composite." *J. Am. Ceramic Soc.* **70**, 393-395, 1987.
- [15] Singh, R. N. and Gaddipati, A. R. "Mechanical properties of a uniaxially reinforced mullite-silicon carbide composite," *J. Am. Ceramic Soc.* **71**, C100-C103, 1988.
- [16] Xu, Y. L., Delale, F. and Liaw, B. M. "Effect of temperature and fiber distribution on matrix cracking in ceramic matrix composites." *Composites Engng* **2**, 67-79, 1992.
- [17] Karandikar, P. and Chou, T. W. "Characterization and Modeling of Microcracking and Elastic Moduli Changes in Nicalon/CAS Composites." *Composites Science and Technology* Vol 46, 253-263, 1993.

- [18] Daniel, I. M. and Anastassopoulos, G. "The Behavior of Ceramic Matrix Fiber Composites Under Longitudinal Loading." Composites Science and Technology Vol 46, 105-113, 1993.
- [19] Barsoum, M. W., Kangutkar, P. and Wang, A. S. D. "Matrix Crack Initiation in Ceramic Matrix Composites Part I: Experiments and Test Results." Composites Science and Technology Vol 44, 257-269, 1992.
- [19a] A. S. D. Wang, X. G. Huang and Michel W. Barsoum, "Matrix Crack Initiation in Ceramic Matrix Composites Part II: Models and Simulation results", Composites Science and Technology Vol. 44, pp 271-282, 1992.
- [20] Wisnom, M. R. "The Effect of Specimen Size on the Flexural Stength of Unidirectional Cabon Fibre-Epoxy." Composite Structure, 18:47-63, 1991.
- [21] Wisnom, M. R. "Relationship Between Strength Variability and Size Effect in Unidirectional Cabon Fibre-Epoxy." Composites, 22:47-52, 1991.
- [22] F. Erdogan, " Approximate Solutions of Systems of Singular Integral Equations ", SJAM J. Appl. Math. Vol. 17, No. 6. November 1969.
- [23] F. Delale, "Fracture of Composite Orthotropic Plate Containing Periodic Buffer Strips," Ph.D. Dissertation, Lehigh University (1976).
- [24] F. Erdogan and G.D. Gupta, "The Stress Analysis of Multi-Layered Composites with a Flaw," International Journal of Solids and Structures, Vol. 7, p. 39, 1971.
- [25] F. Erdogan and G.D. Gupta, "Layered Composites with an interface Flaw," International Journal of Solids and Structures, Vol. 7, p. 1089, 1971.
- [26] M.C. Lu and F. Erdogan, "Stress Intensity Factors in Two Bonded Elastic Layers Containing cracks Perpendicular to and on the Interface, Part I. Analysis," Engineering Fracture Mechanics, Vol. 18, pp. 491-506, 1983.

- [27] M.C. Lu and F. Erdogan, "Stress Intensity Factors in Two Bonded Elastic Layers Containing cracks Perpendicular to and on the Interface, Part II. Solution and Results," *Engineering Fracture Mechanics*, Vol. 18, pp. 507-528, 1983.
- [28] M. C. Lu, "A Composite of Two Bounded Strips Containing Perpendicular Cracks And An Interface Crack ", Ph.D. Dissertation, Lehigh University (1978).
- [29] F. Erdogan, "Mixed Boundary-Value Problems in Mechanics," *Mechanics Today*, (Edited by S. Nemat-Nasser) Vol. 4, Pergamon Press, Oxford, p. 1, 1978.
- [30] M. A. Golberg, " Numerical Solution of Integral Equations", Plenum Press, New York, 1990.
- [31] A. H. Stroud and D. Secrest, "Gaussian Quadrature Formulas", Prentice-Hall, Englewood Cliffs, New Jersey, 1966.
- [32] P. J. Davis and P. Rabinowitz, " Methods of numerical Integration", Second Edition, Academic Press, New York, New York, 1984.
- [33] N. I. Muskhelishvili, " Singular Integral Equations ", Noordhoff, Groningen, Holland, 1953.
- [34] A. Ghizzetti and A. Ossicini, "Quadrature Formulae", Academic Press, New York, 1970.
- [35] Z. Kopal, "Numerical Alalysis", Second Edition. John Wiley & Sons Inc. New York 1961.
- [36] N. I. Ioakimidis and P. S. Theocaris, "On the Numerical Solution of a Class of Singular Integral Equations", *Journal of Mathematical and Physical Sciences*. Vol. 11, pp 219-235, 1977.
- [37] P. S. Theocaris and N. I. Ioakimidis, " Numerical Solution of Cauchy Type Singular Equations", Transactions of Academy of Athens. Vol. 40, pp 1-39, 1977.

- [38] N. I. Ioakimidis and P. S. Theocaris, "On the Selection of Collocation Points For the Numerical Solution of Singular Integral Equations With Generalized Kernels Appearing in Elasticity Problems", *Computers & Structures*. Vol. 11. pp 289-295. 1978.
- [39] N. I. Ioakimidis and P. S. Theocaris, "Numerical Evaluation of a Class of Generalized Stress Intensity Factors by Use of the Lobatto-Jacobi Numerical Integration Rule", *Int. Journal of Fracture*. Vol. 14. pp 469-484. 1978.
- [40] B. M. Malyshev and R. L. Salganik, "The Strength of Adhesive Joints Using The Theory of Cracks", *Int. Journal of Fracture Mechanics*. Vol. 1. 114-127 1965.
- [41] G. P. Cherepanov, "Mechanics of Brittle Fracture", McGra-Hill, New York, 1979.
- [42] J. R. Rice, "Elastic Fracture Mechanics Concepts for Interface Cracks", *Transactions of ASME*. Vol 55, March 1988.
- [43] J. R. Rice and G. C. Sih, "Plane Problems of Cracks in Dissimilar Media", *Transactions of ASME*. June 1965.
- [44] T. L. Anderson, "Fracture Mechanics: Fundamentals and Applications", CRC Press, Inc. 1991
- [45] M. H. Lewis and V. S. R. Murthy, "Microstructural Characterization of Interfaces in Fibre-Reinforced Ceramics", *Composites Science and Technology*. Vol. 42, pp 221-249, 1991.
- [46] A. G. Evans, F. W. Zok and J. Davis, "The Role of Interfaces in Fiber-Reinforced Brittle Matrix Composites", *Composites Science and Technology*, Vol. 42, pp 3-24, 1991

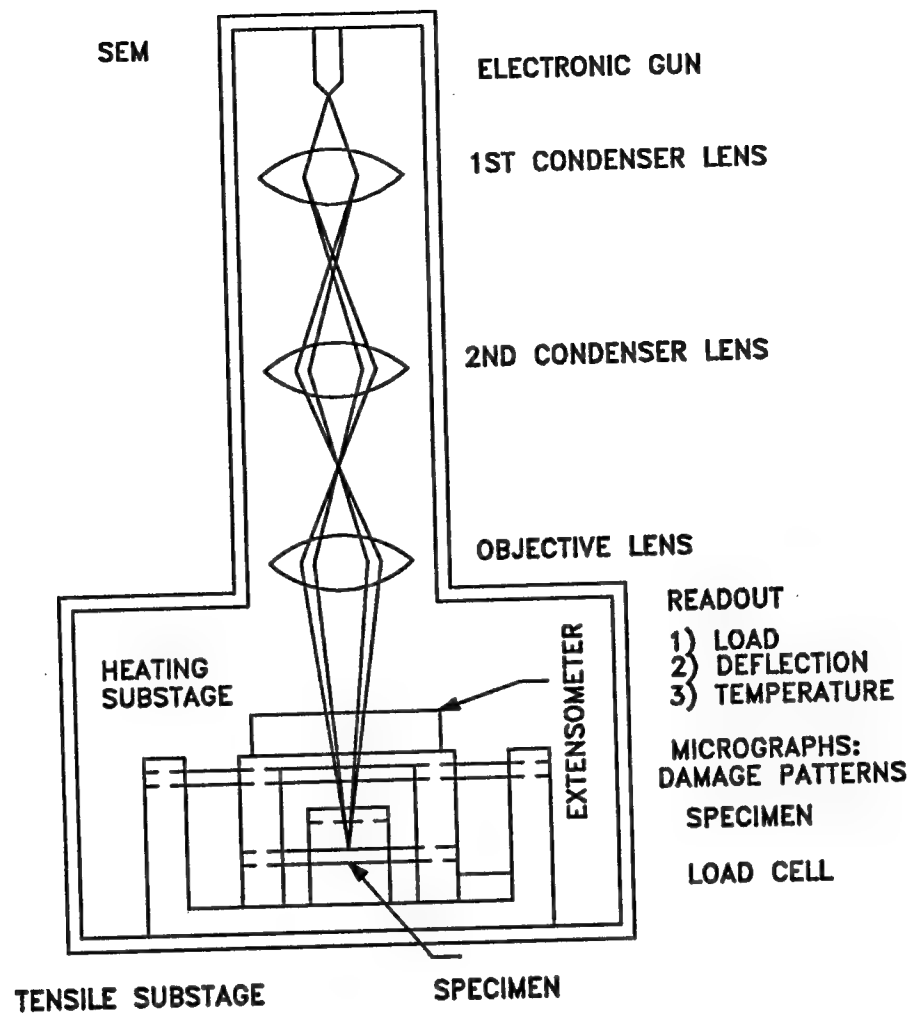


Fig. 2.1 Experimental setup

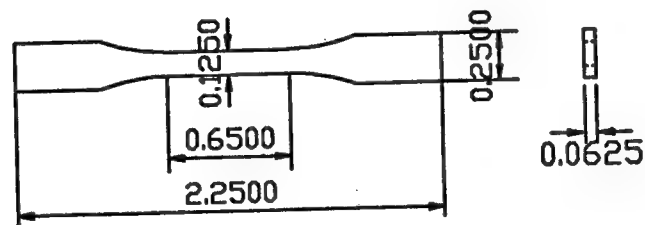


Fig. 2.2 Specimen geometry (Unit in inches)

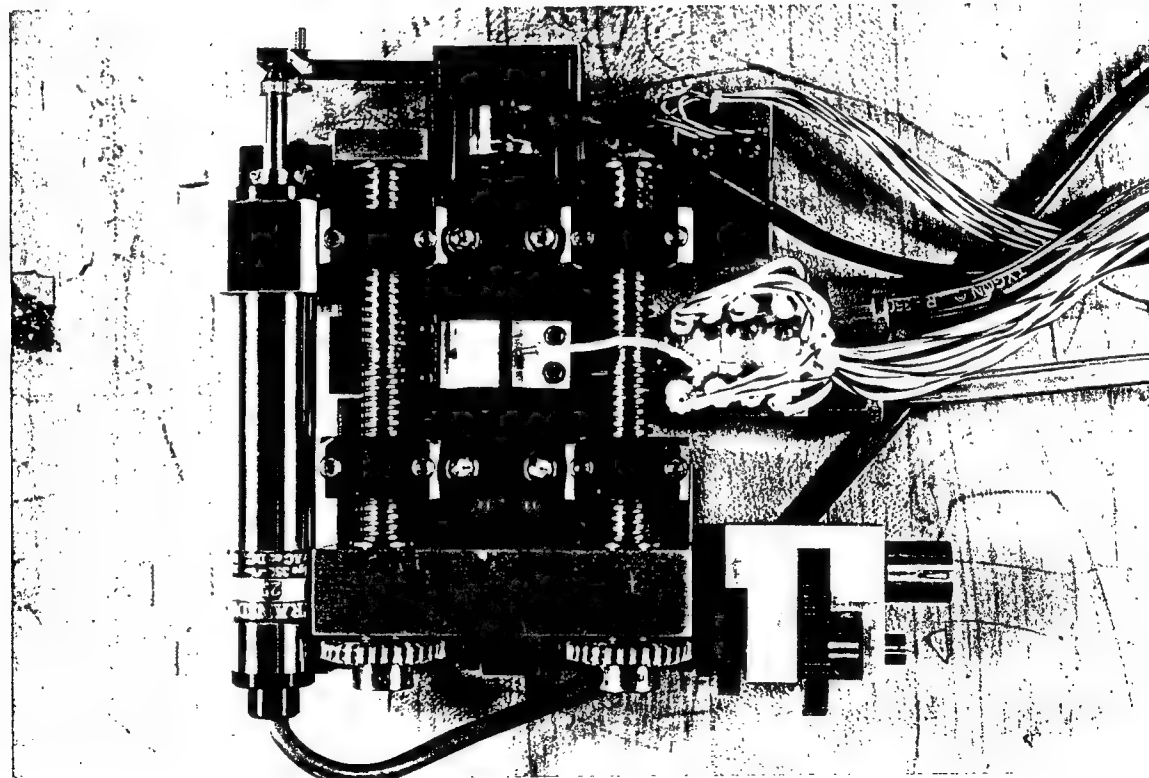
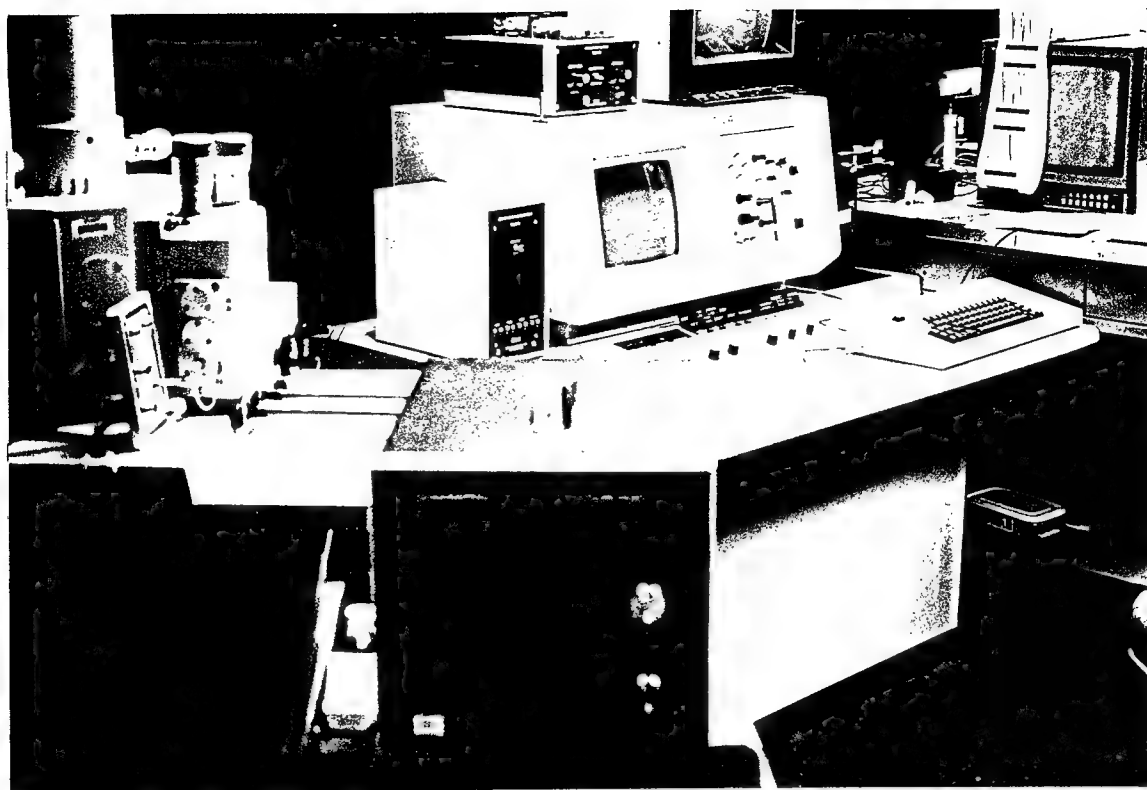


Fig. 2.3 The actual layout of the test equipment and its tensile/heating substage

**Fig. 2.4 Tensile tests on Nicalon/CAS II
with $V_f=30\%$ at room temperature**

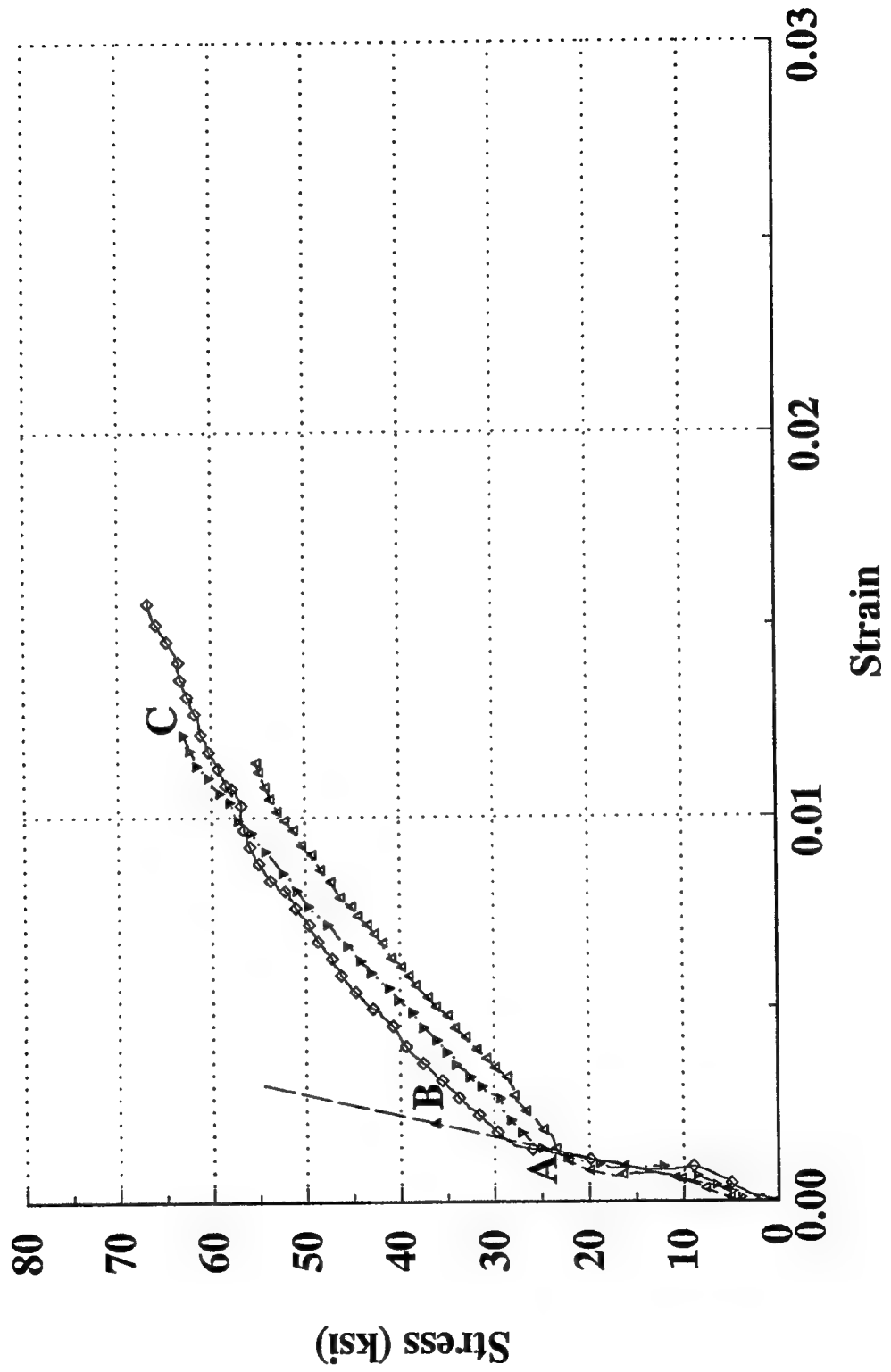
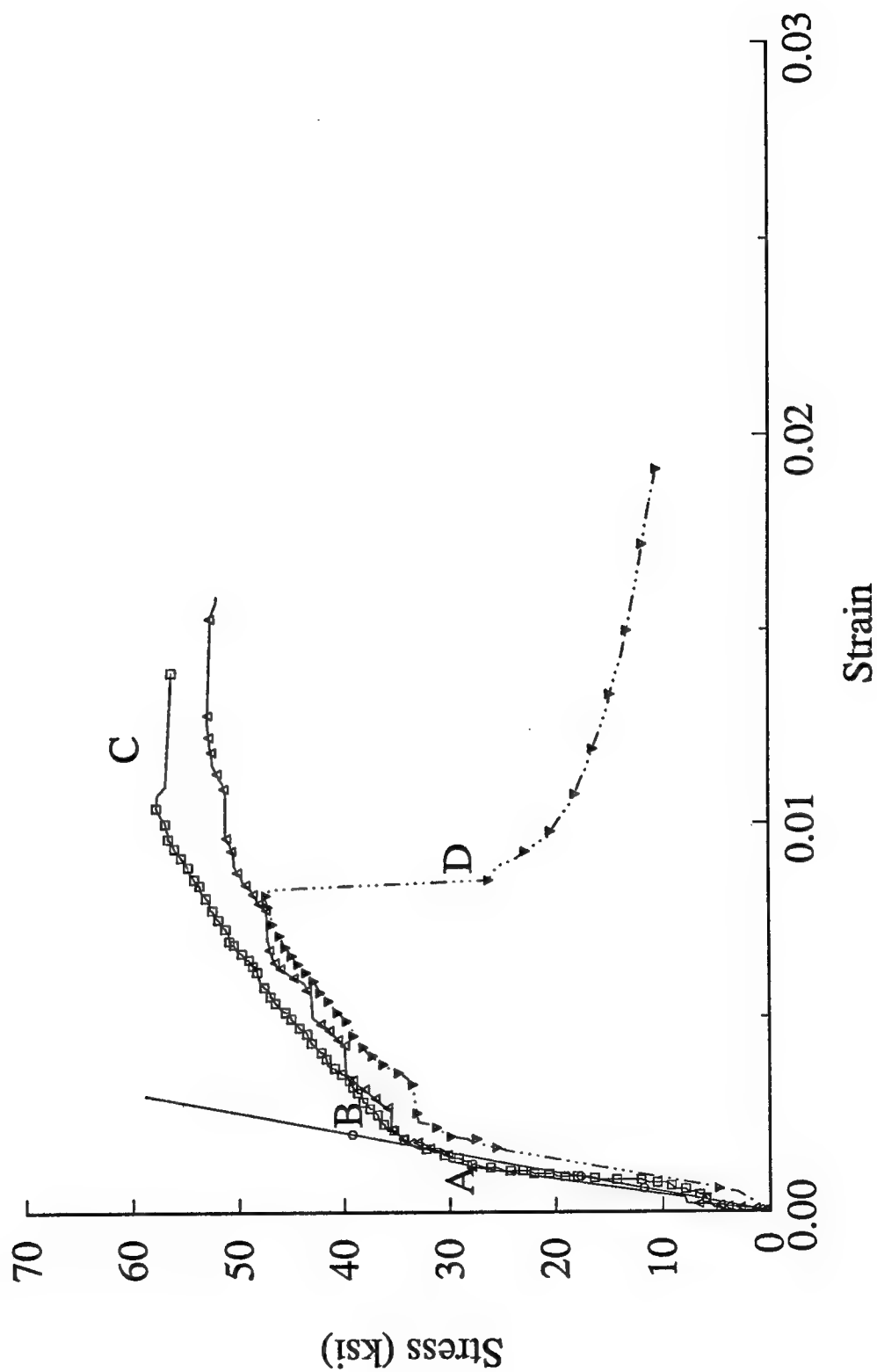
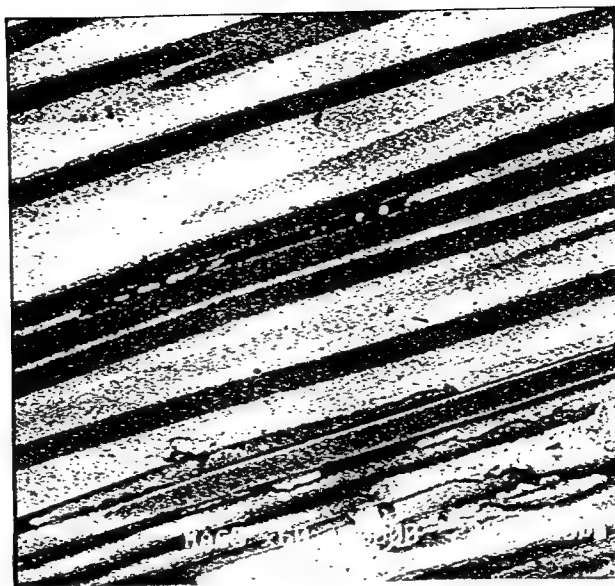
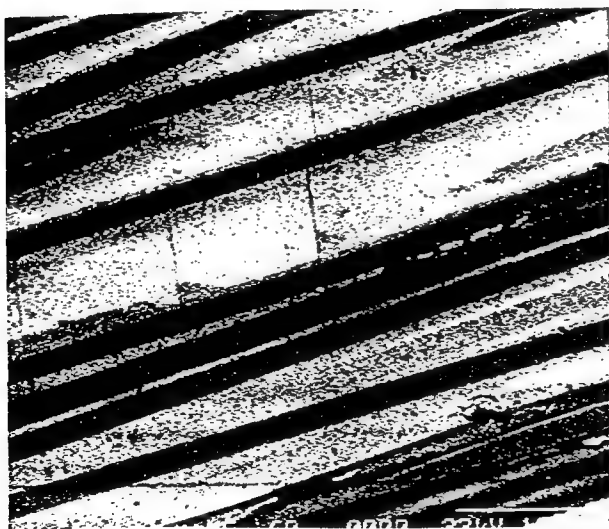


Fig. 2.5 Tensile Tests on Nicalon/CAS II
with $V_f = 40\%$ at room temperature

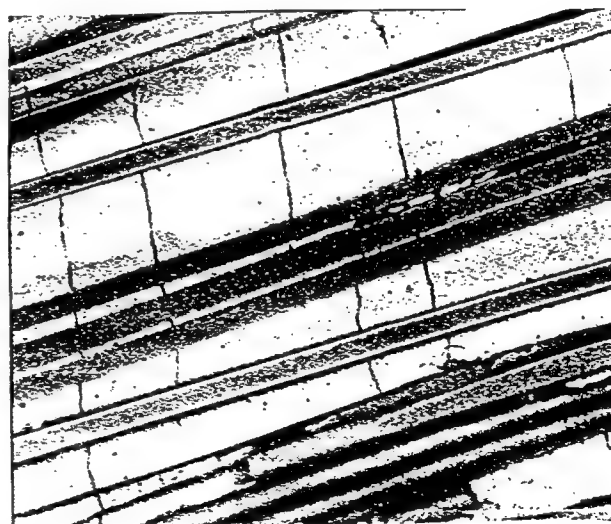




No matrix crack has been observed



**Matrix crack initiated
away from the defects**



Fully developed matrix crack

Fig. 2.6 Another pattern of matrix crack initiation.

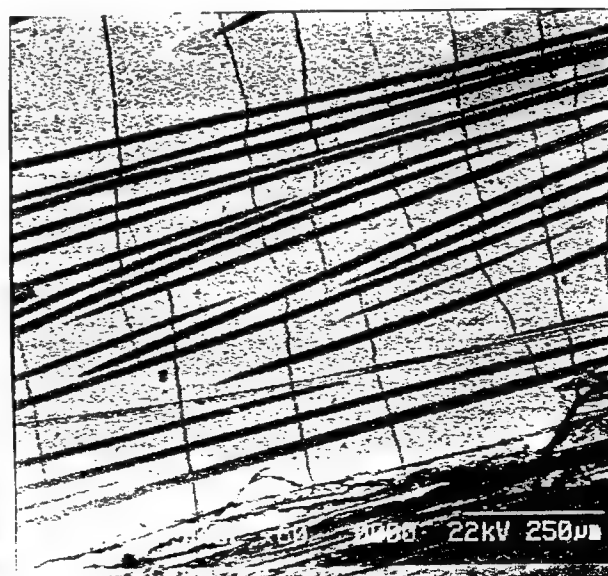
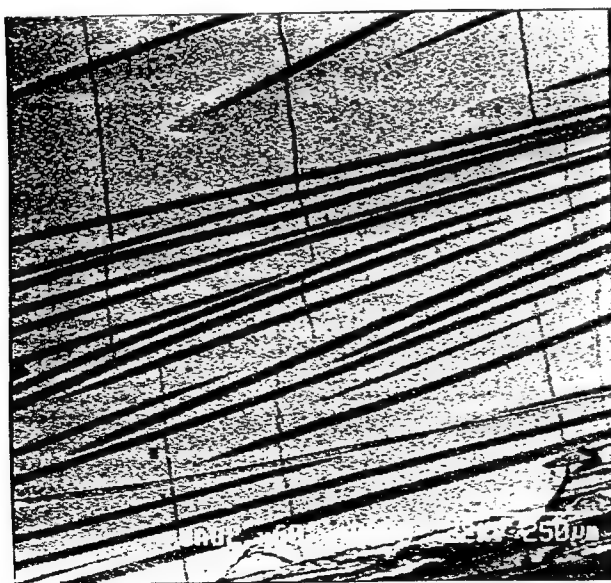
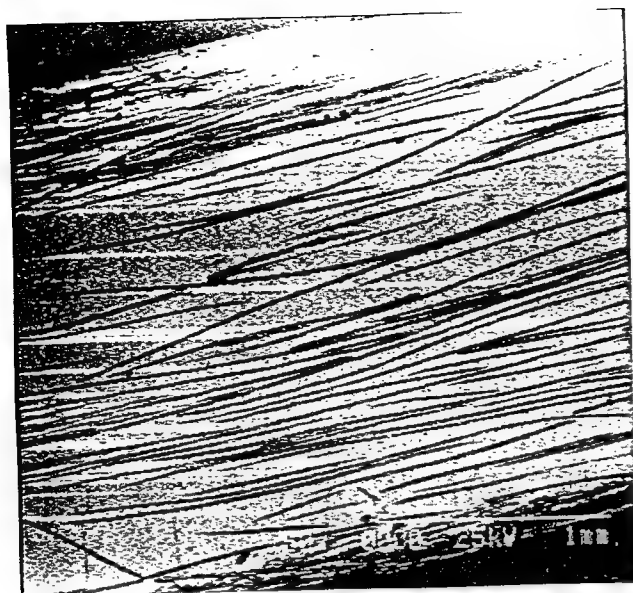


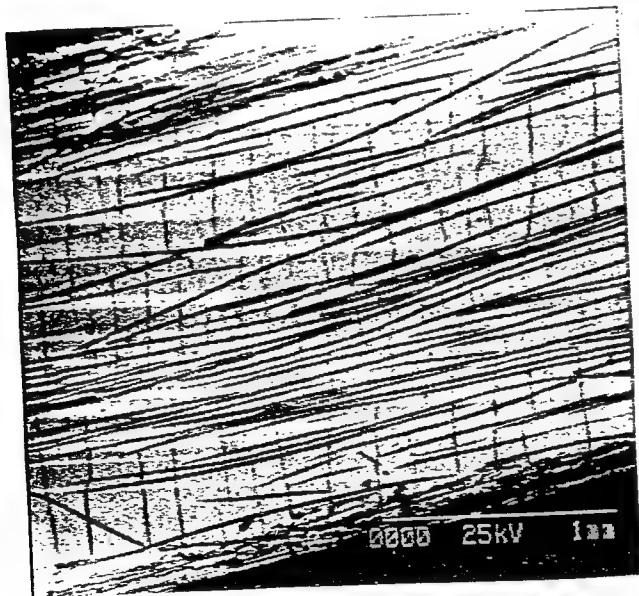
Fig. 2.7 Micrographs showing the location of the first matrix cracks initiation and their development.



(A) at 30 ksi



(B) at 40 ksi

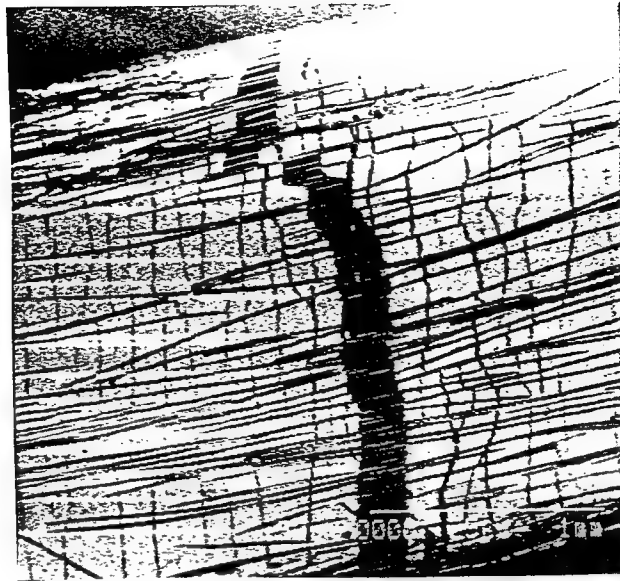


(C) at 55 ksi



(D) at 20 ksi

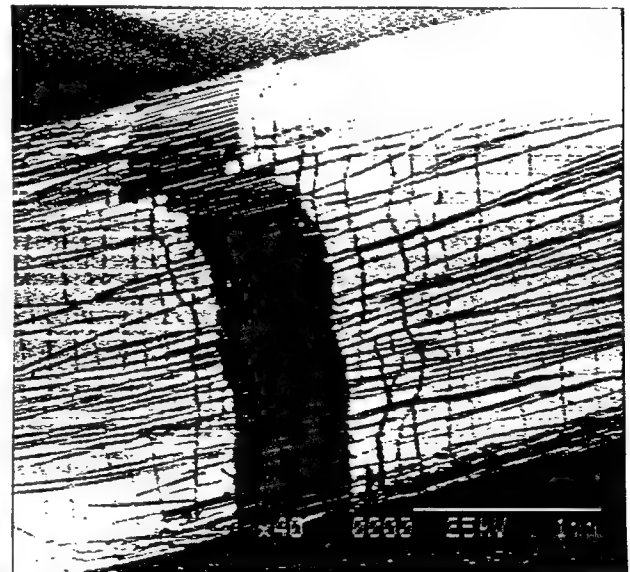
Fig. 2.8 Tensile damage of Nicalon/CAS II specimen with $V_f=40\%$



Load = 60 lbs

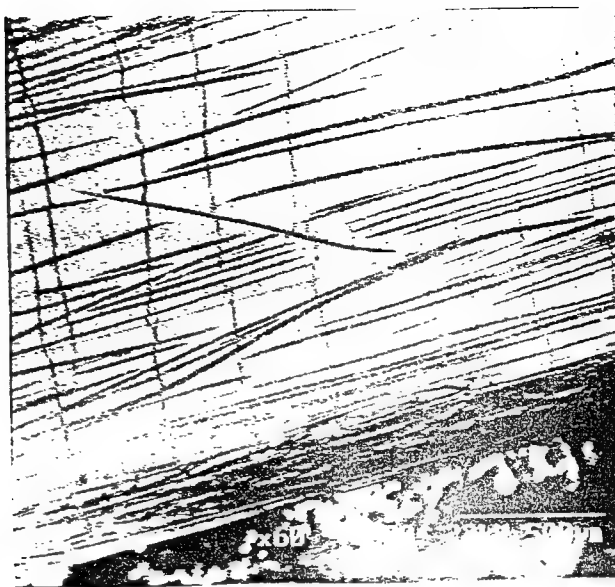


Load = 49.6 lbs

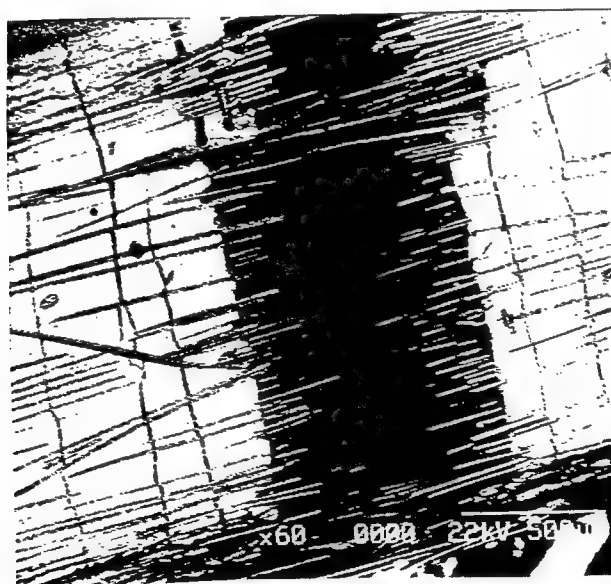


Load = 33 lbs

Fig. 2.9 Further loading of the specimen is possible after failure for thin Nicalon/CAS II specimen.



Location and the damage pattern just before major fracture developed.



Major fracture on the specimen

Fig. 2.10 Brittle behavior of the thick Nicalon/CAS II specimens.

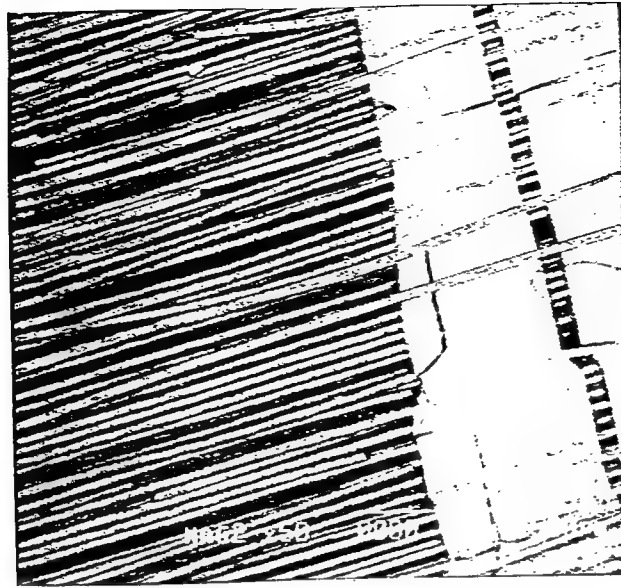


Fig. 2.11 Long fiber full-out length for Nicalon/CAS II with $V_f = 40\%$

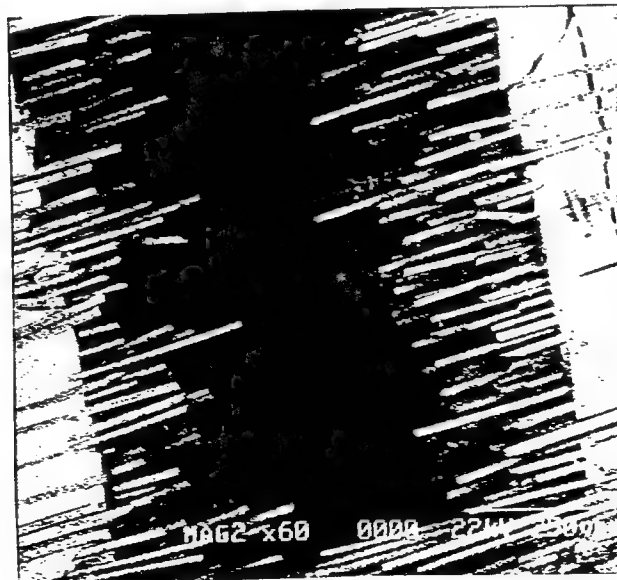


Fig. 2.12 Short fiber pull-out length for Nicalon/CAS II with $V_f = 30\%$.

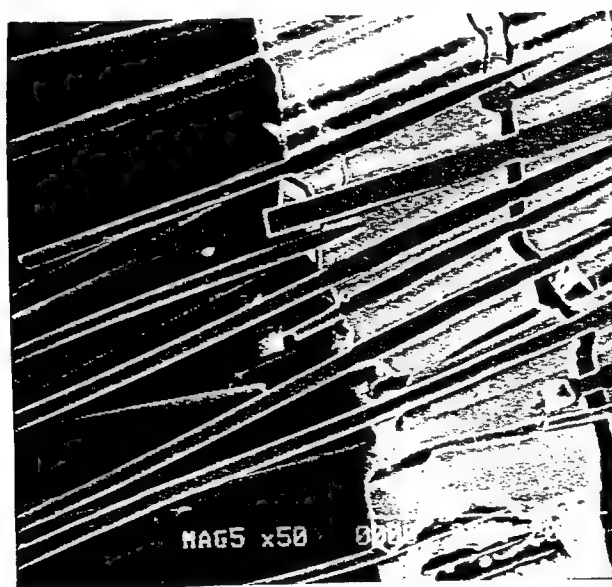
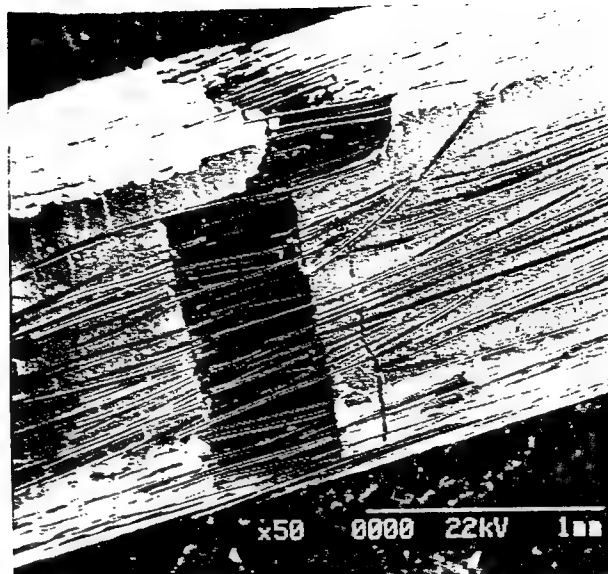


Fig. 2.13 Very smooth surfaces on the fibers being pull-out.

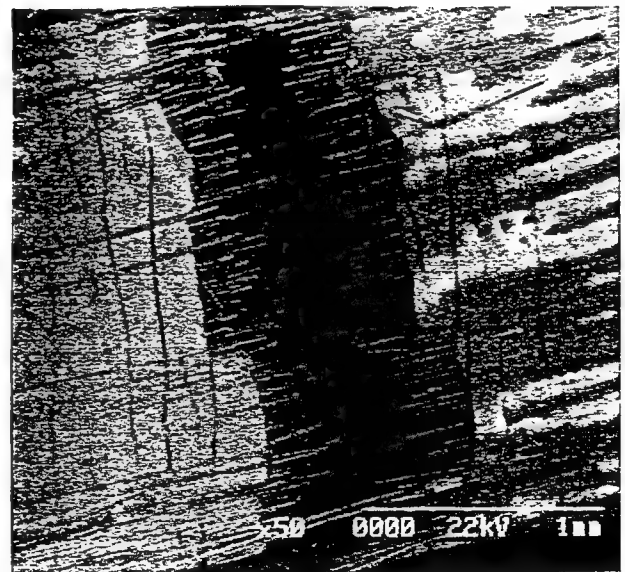
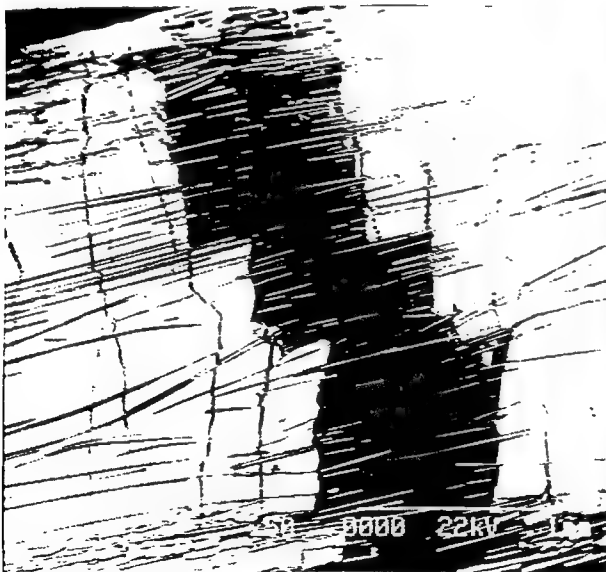
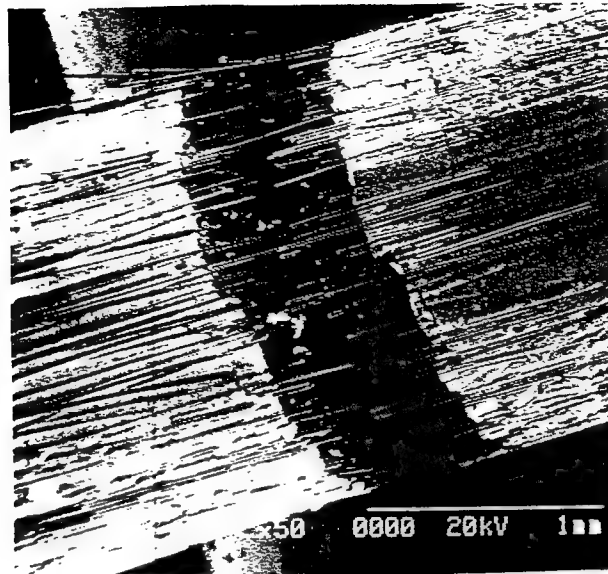
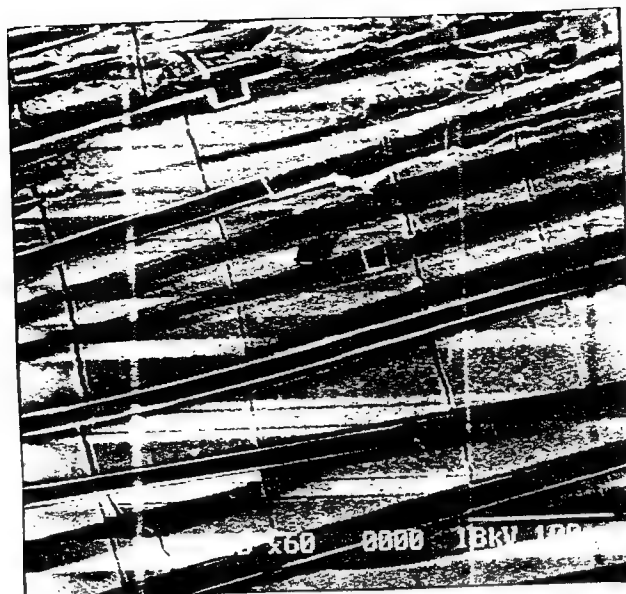
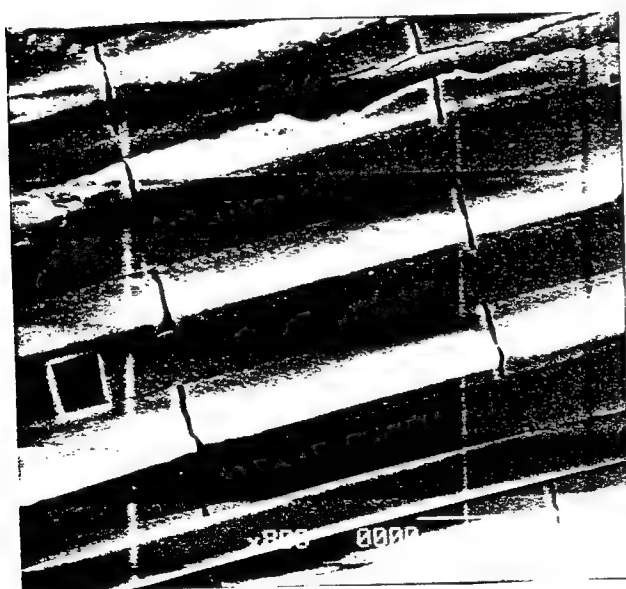


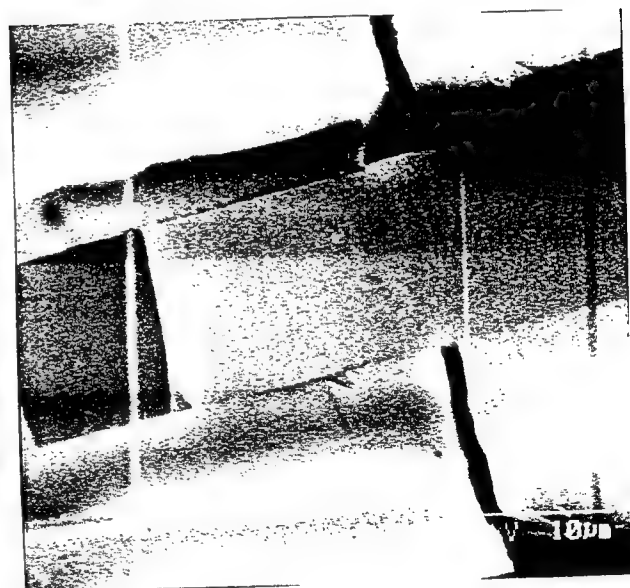
Fig. 2.14 Micrographs selected from three test results for specimen with $V_f = 30\%$ indicating an different amount of fiber pull-out and the fiber pull-out length for different test.



(a)



(b)



(c)

Fig. 2.15 Typical damage pattern for Nicalon/CAS II specimen taken at different magnifications: (a) 300x; (b) 800x; (c) 3000x.

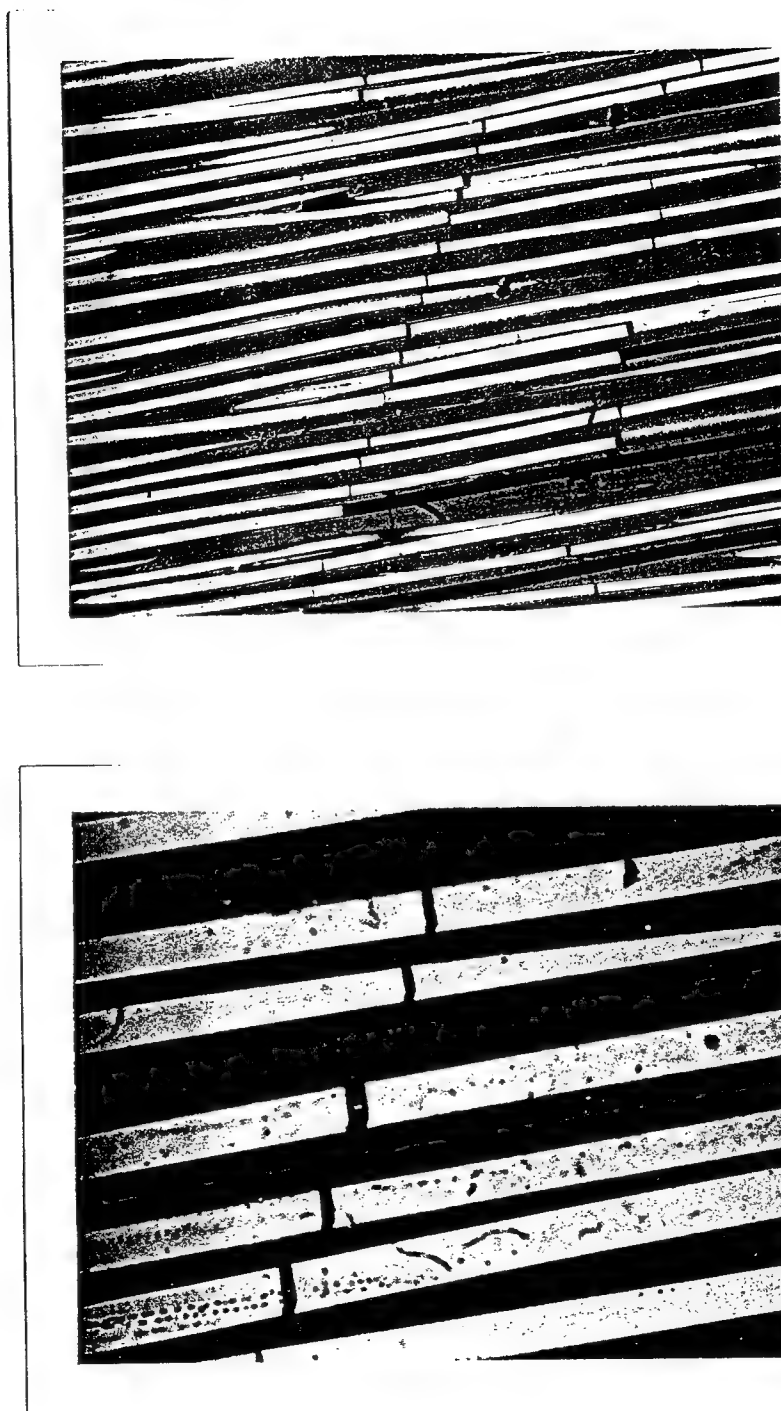


Fig. 2.16 Typical fiber breaking pattern for Nicalon/CAS II specimen.

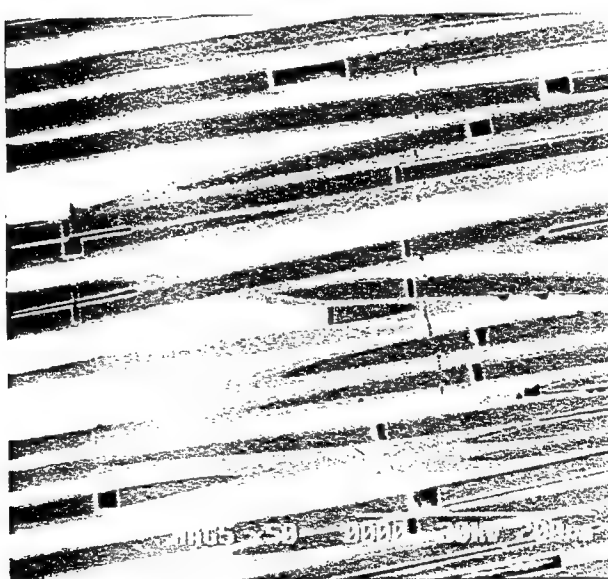
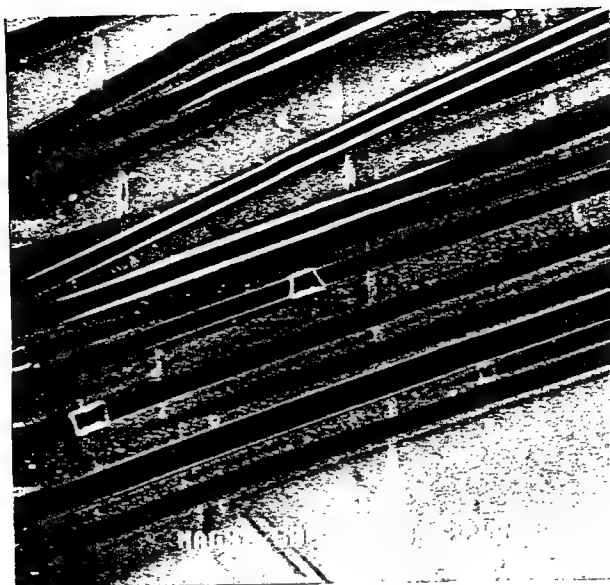


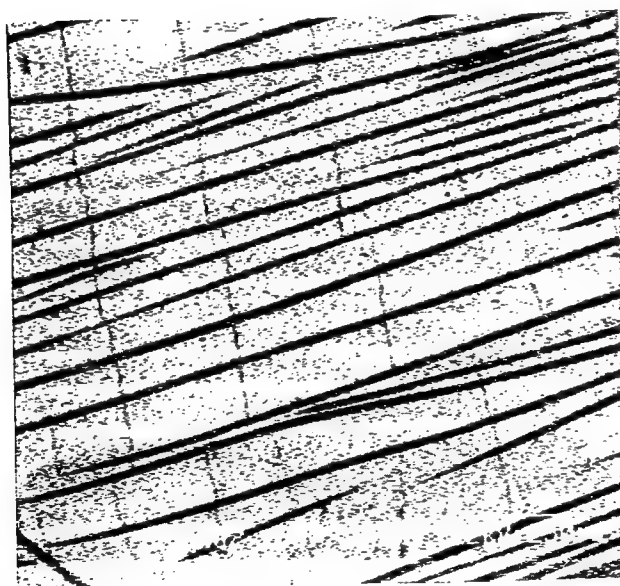
Fig. 2.17 Radom fiber breaking on Nicalon/CAS II specimen.



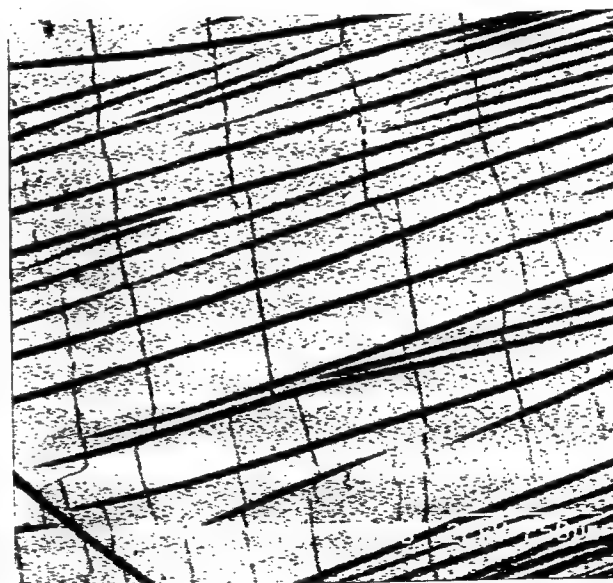
(a) 19.5 ksi



(b) 32.0 ksi



(c) 36.5 ksi

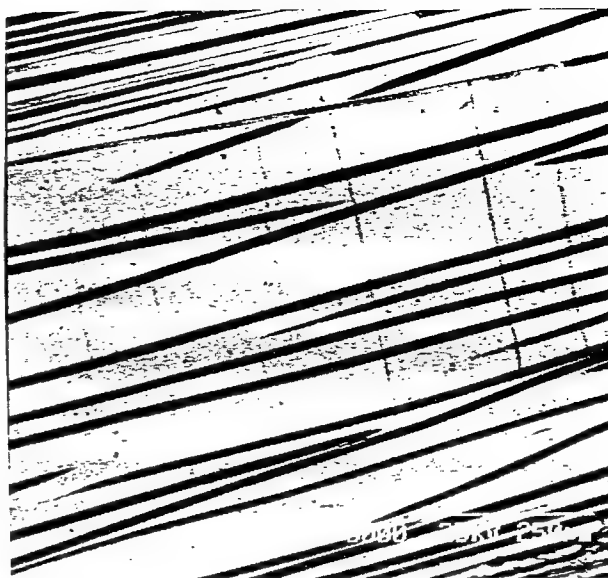


(d) 51.5 ksi

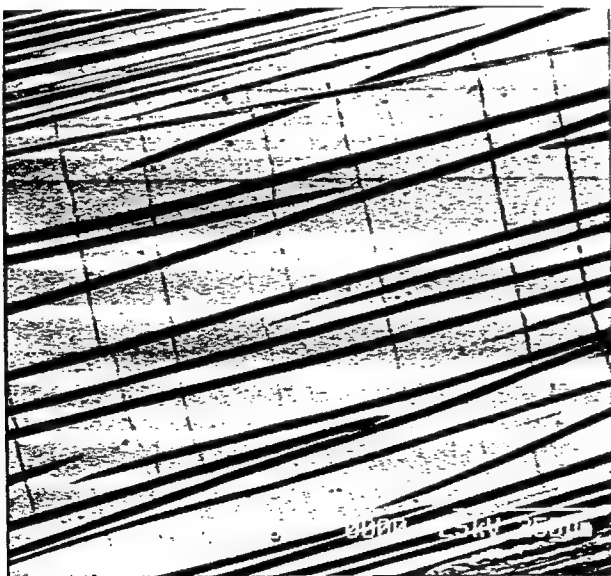
**Fig. 2.18 Matrix cracks density vs. the tensile stress
for Nicalon/CAS II specimen with $V_f=30\%$.**



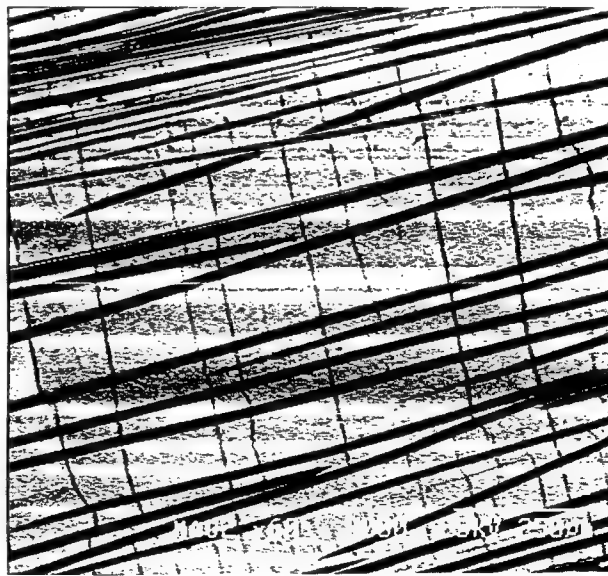
(a) 28.3 ksi



(b) 29.8 ksi



(c) 30.81 ksi



(d) 51.7 ksi

Fig. 2.19 Matrix cracks density vs. the tensile stress at room temperature for Nicalon/CAS II specimen with $V_f=40\%$.

Fig. 2.20 Matrix crack density vs. stress for Nicalon/CAS II specimens with $v_f=30\%$ at room temperature

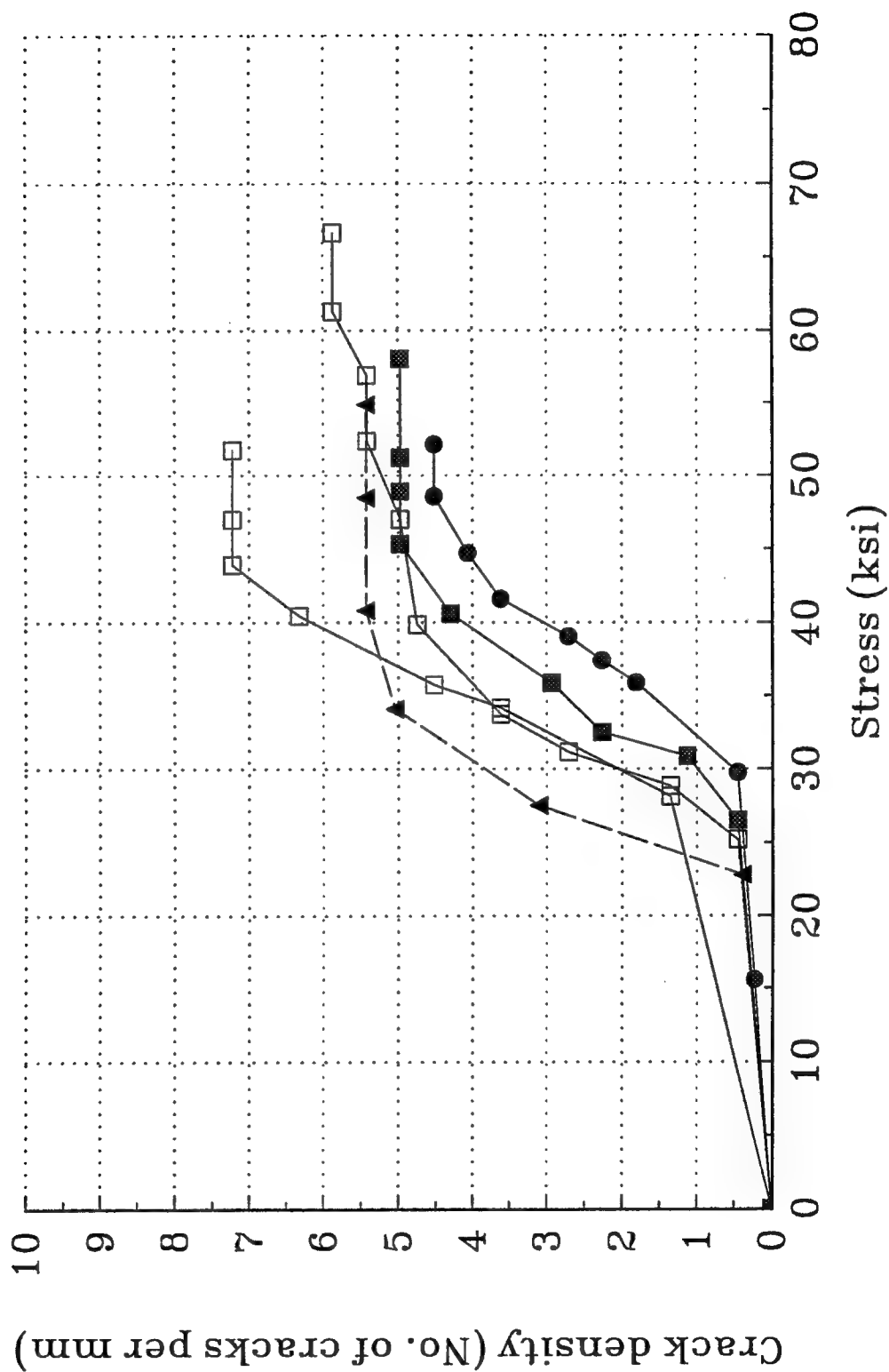


Fig. 2.21 Matrix crack density vs. stress for Nicalon/CAS II specimens with $v_f=40\%$ at room temperature

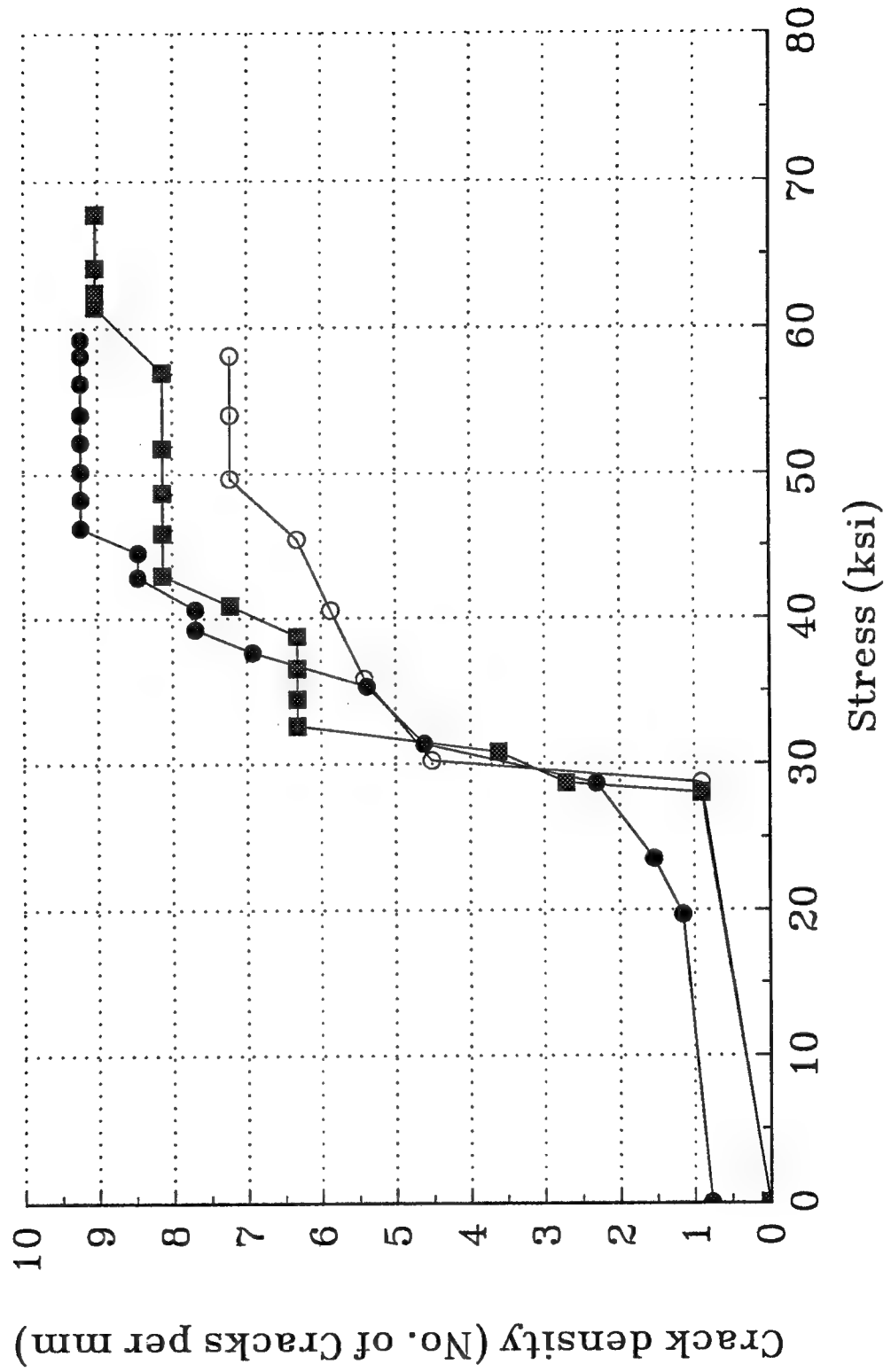


Fig 2.22 Tensile tests on Nicalon/CAS II specimens
with $v_f=30\%$ at high temperatures

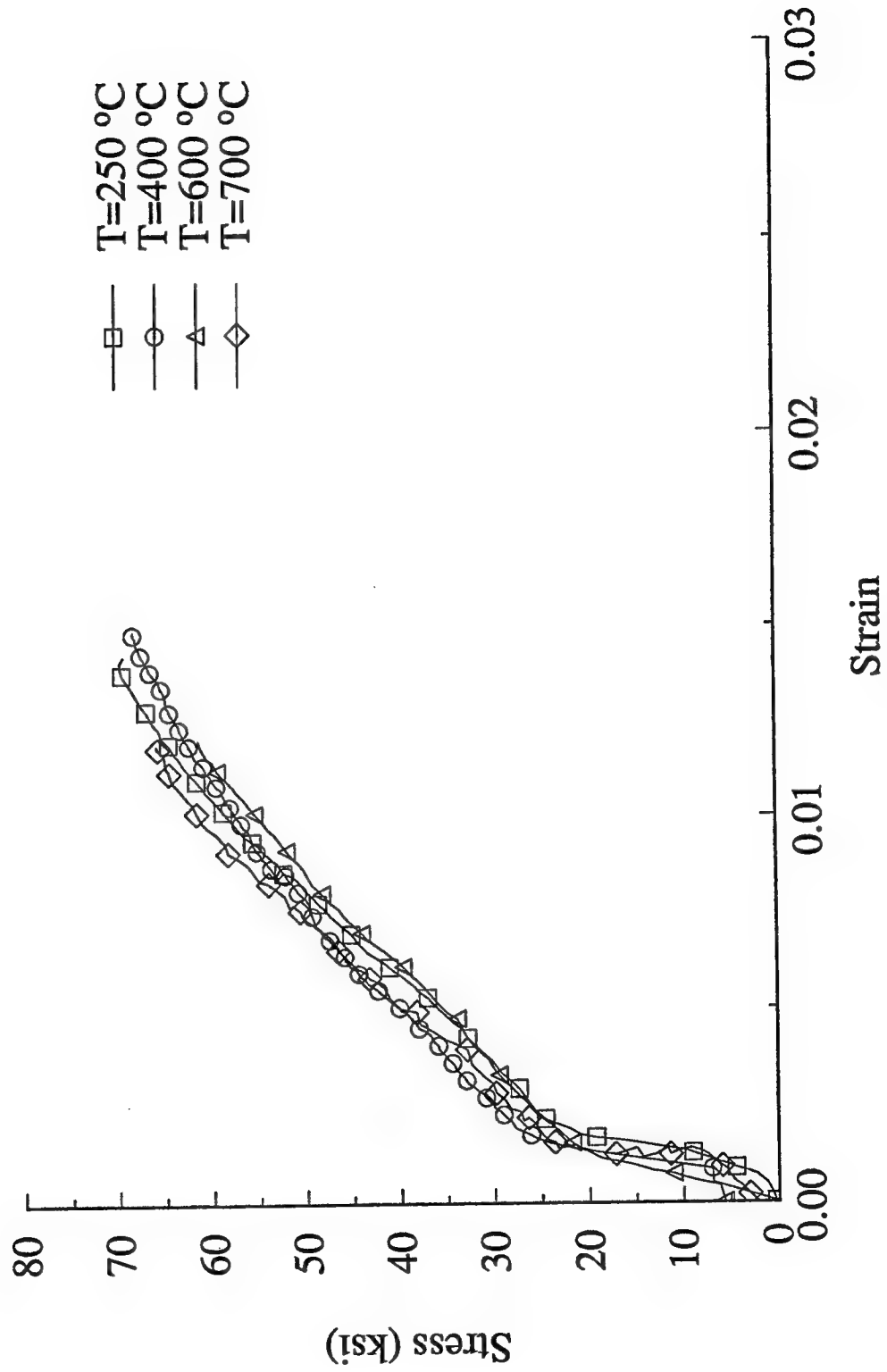


Fig 2.23 Tensile tests on Nicalon/CAS II
with $V_f=40\%$ at high temperatures (thick specimens)

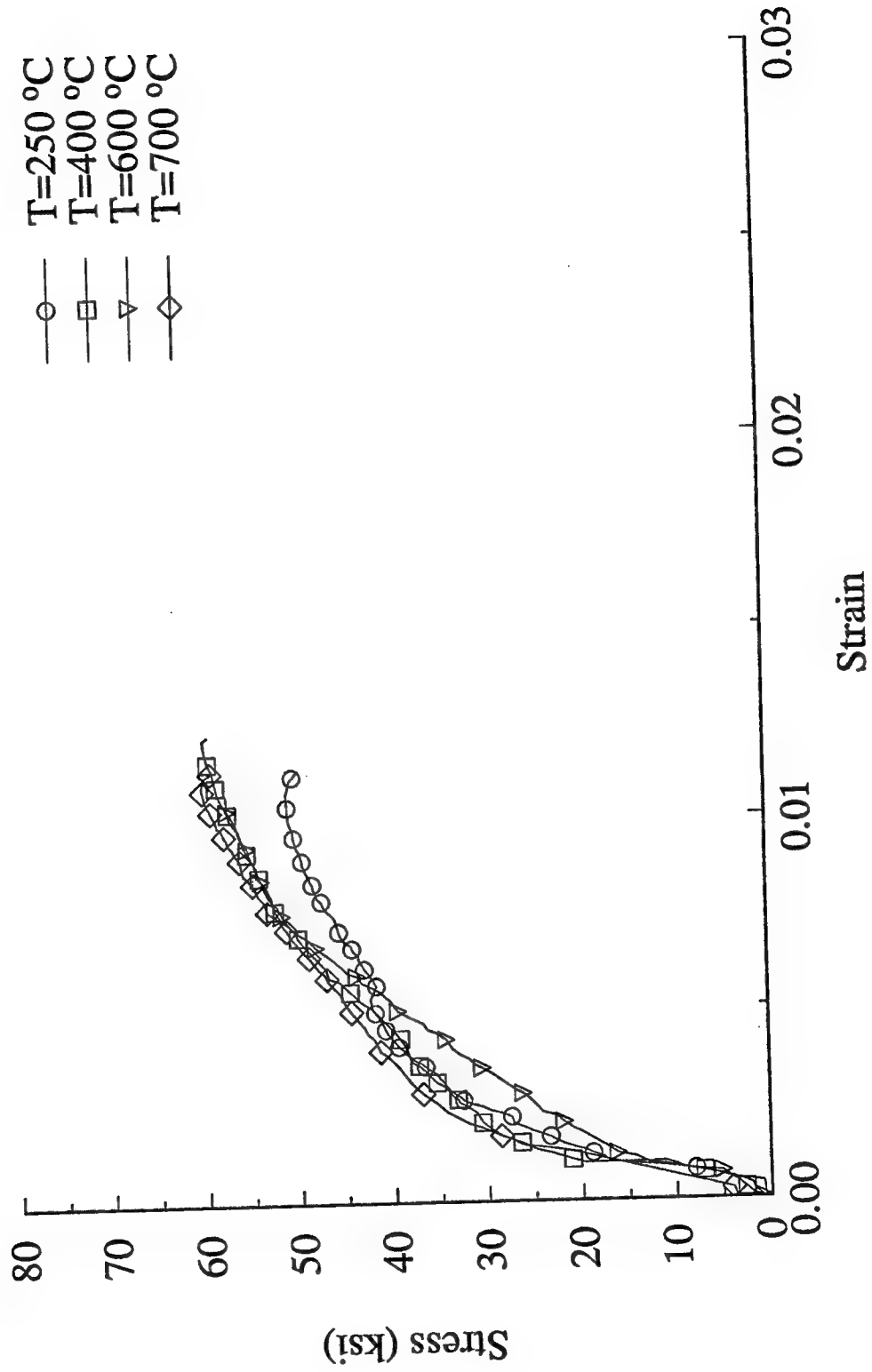


Fig. 2.24 Tensile Strength of Nicalon/CAS II
with $V_f=30\%$ at various temperatures

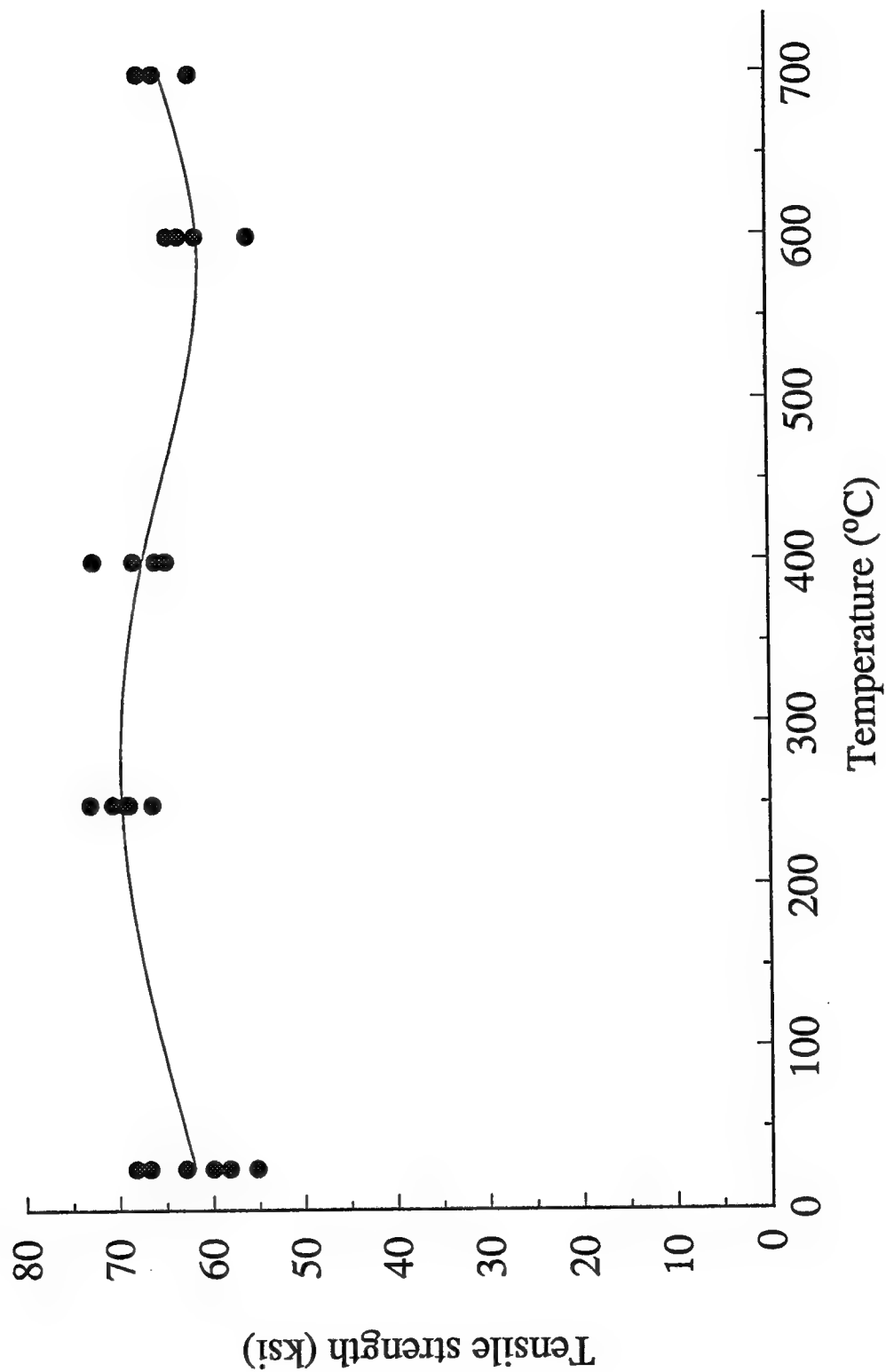
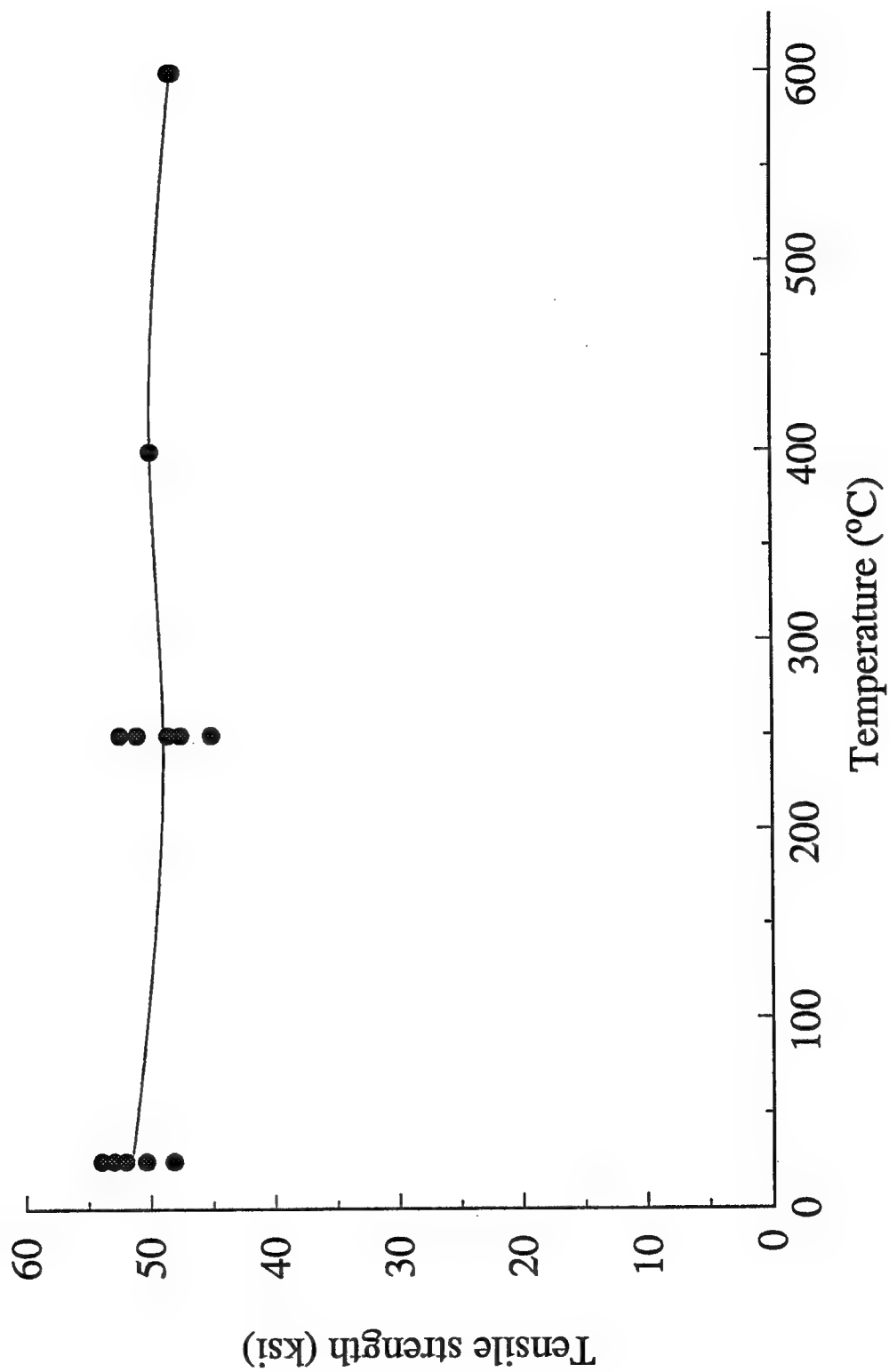


Fig. 2.25 Tensile Strength of Nicalon/CAS II
with $V_f=40\%$ at high temperatures

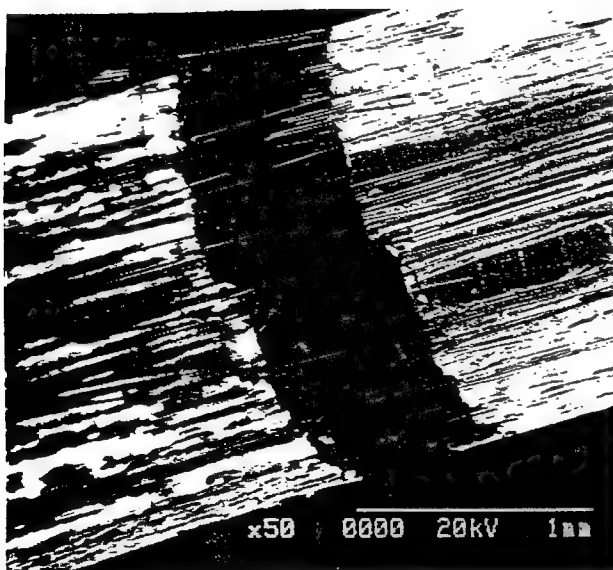




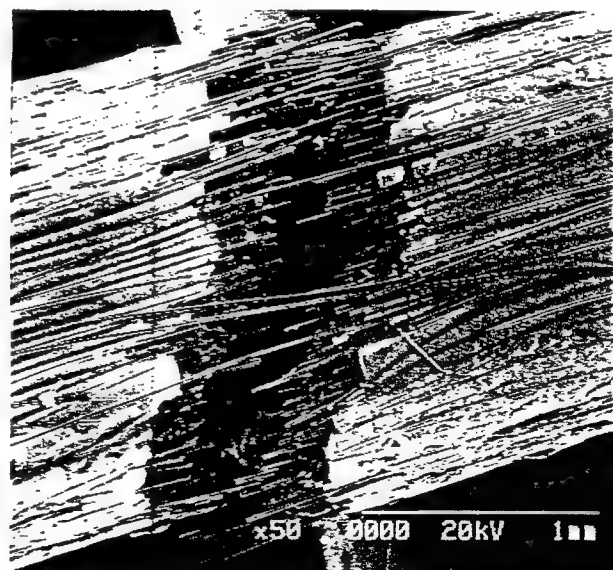
Room temperature



T = 250 °C

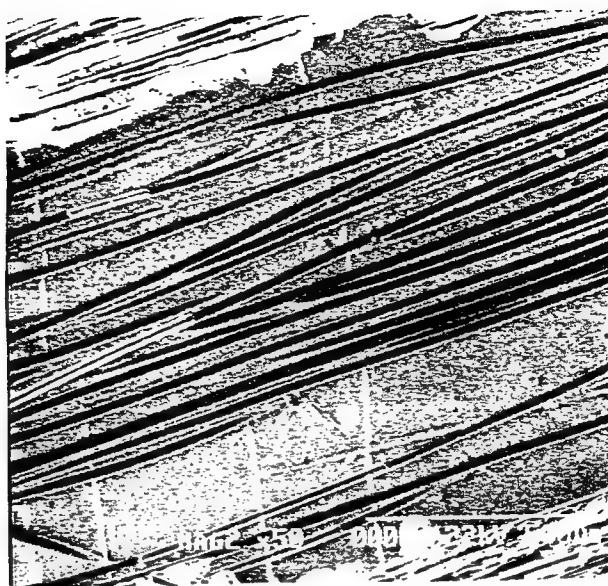


T = 400 °C



T = 600 °C

Fig. 2.26 Final failure surfaces at different temperatures for Nicalon/CAS II with $V_f = 30\%$.



(a) 25.9 ksi



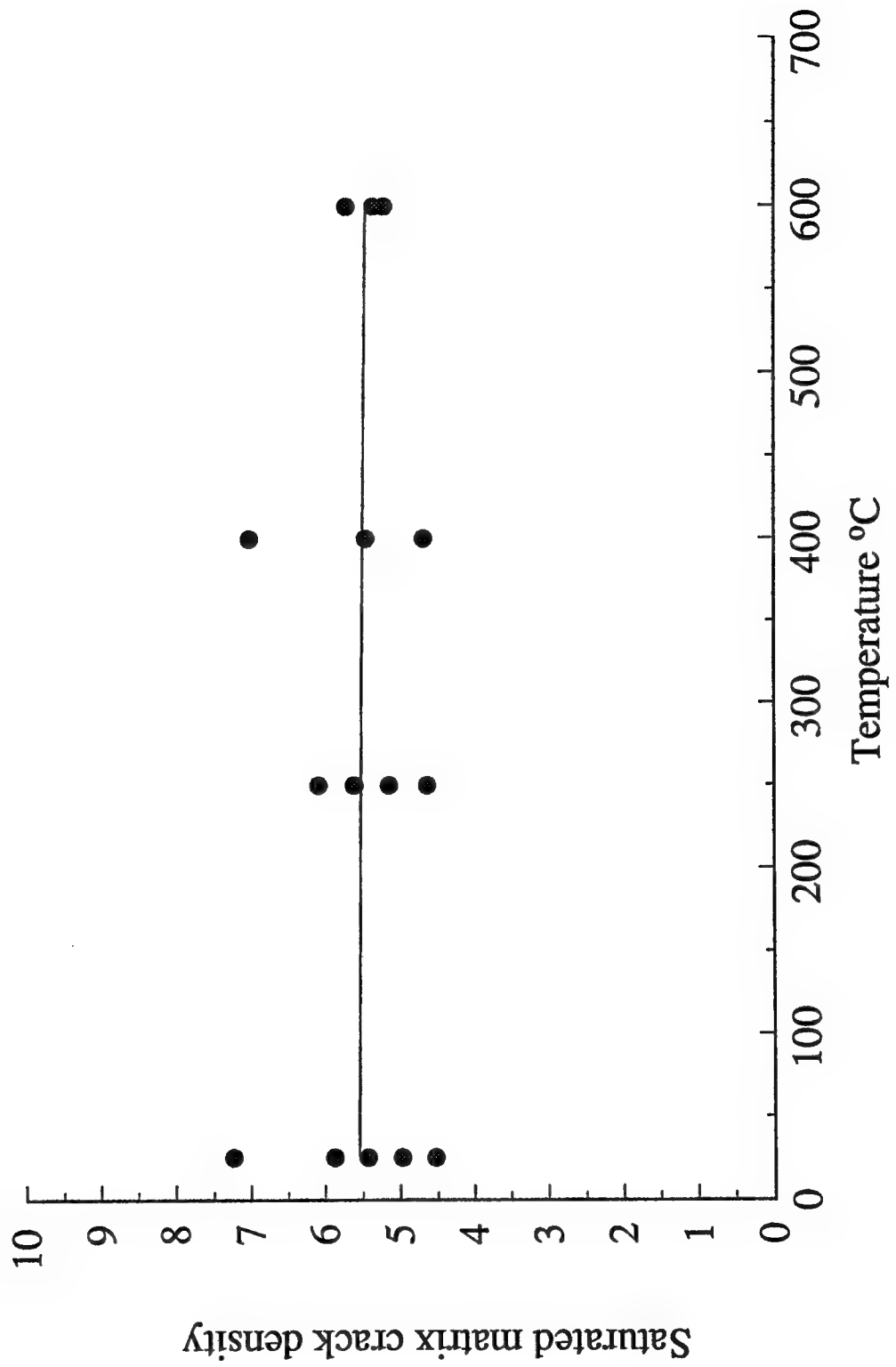
(b) 30.3 ksi



(c) 52.0 ksi

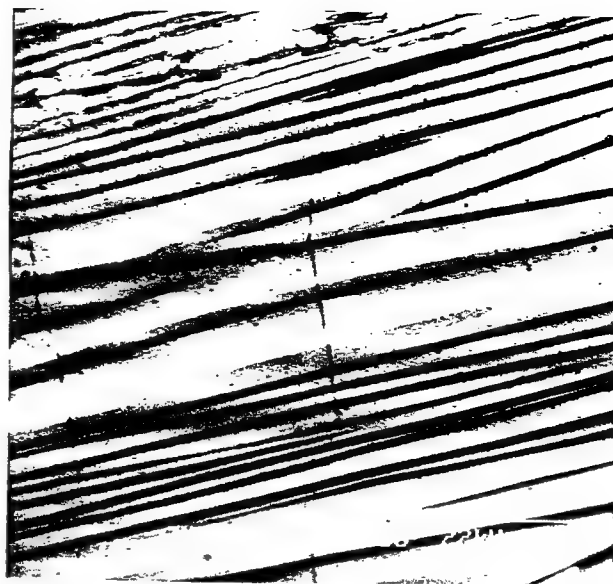
Fig. 2.27 Development of matrix cracks at $T=600^{\circ}\text{C}$ for Nicalon/CAS II specimen with $V_f=30\%$.

Fig. 2.28 Saturated matrix crack density vs. temperatures
for 30% fiber volume fraction

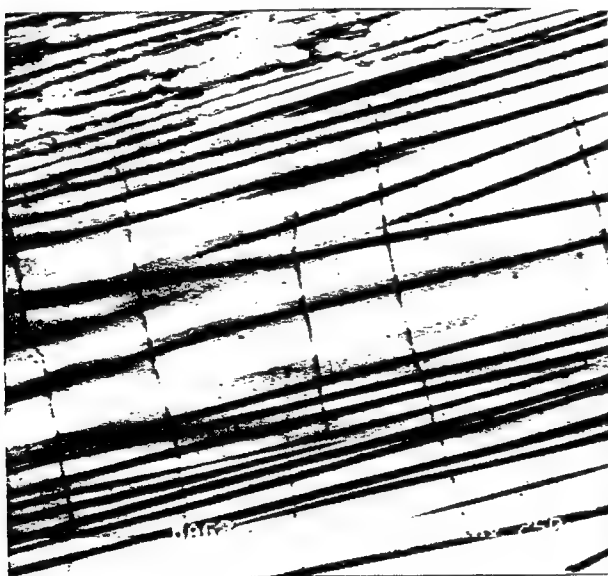




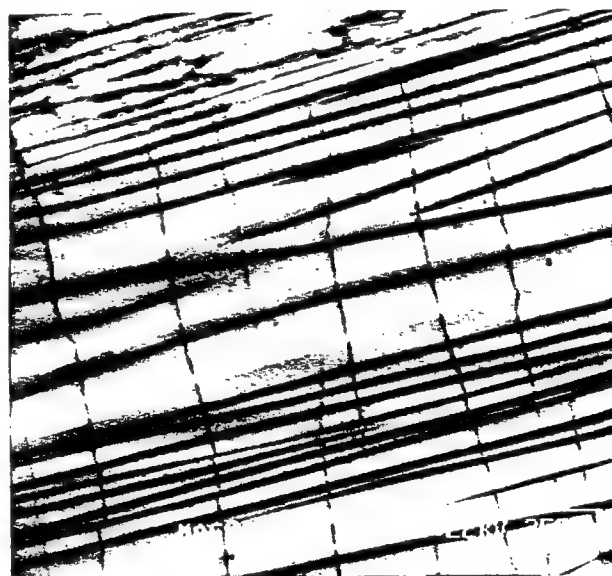
(a) Pre-existing crack
before loading



(b) 21.1 ksi



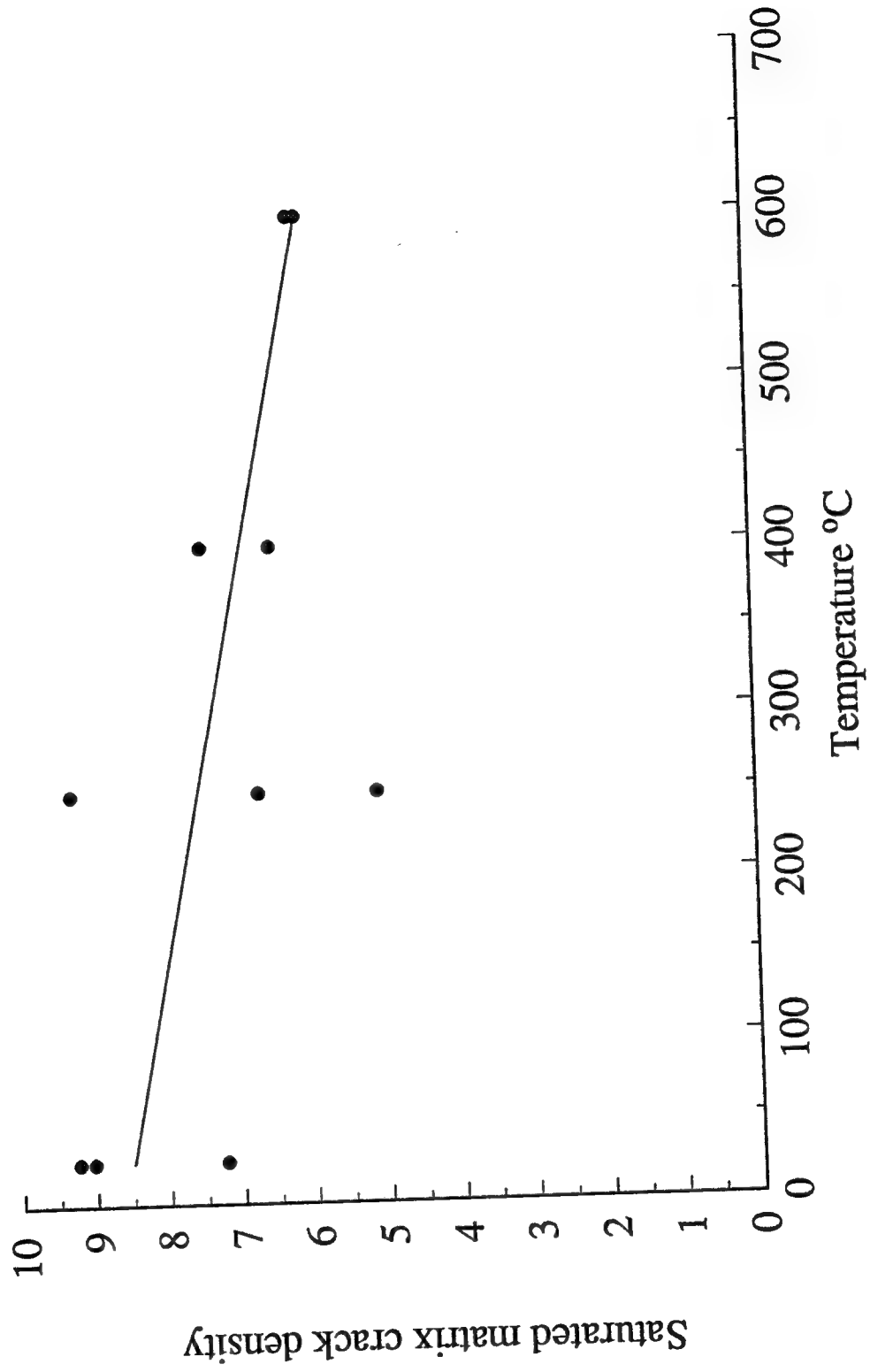
(c) 32.5 ksi

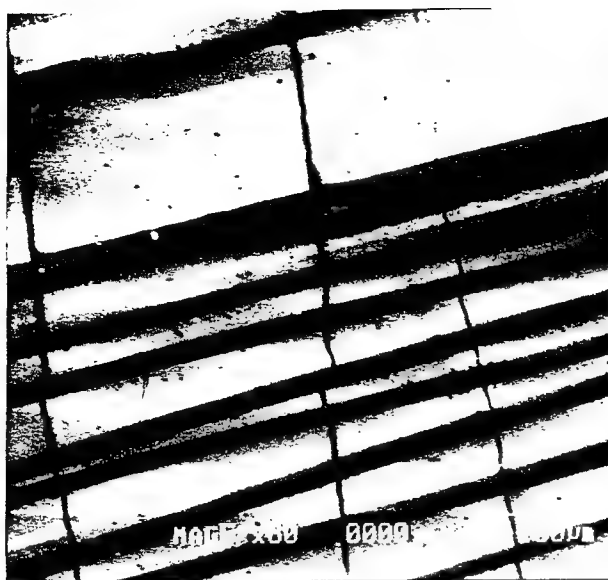


(d) 40.8 ksi

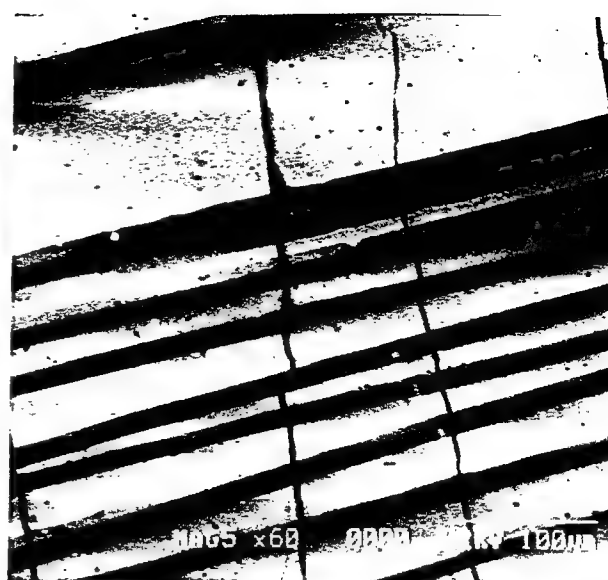
**Fig. 2.29 Development of matrix cracks at $T=400\text{ }^{\circ}\text{C}$
for Nicalon/CAS II specimen with $V_f=40\%$.**

Fig. 2.30 Saturated matrix crack density vs. temperatures
for 40% fiber volume fraction

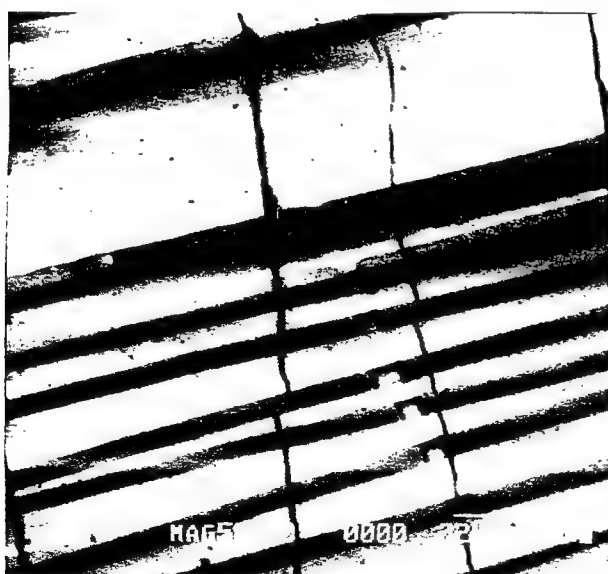




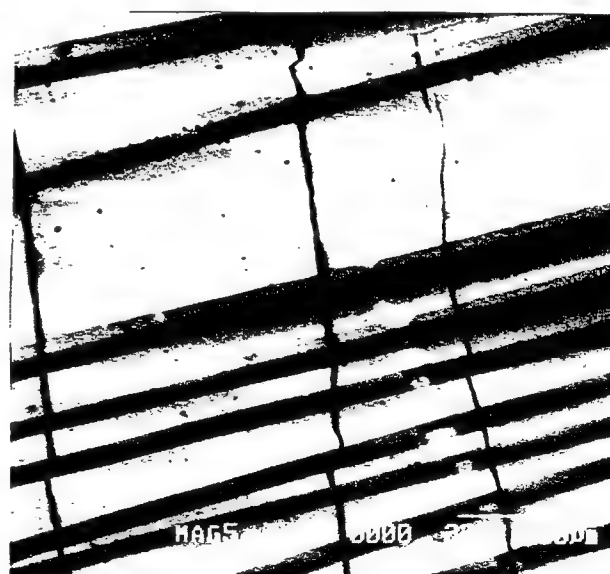
(a) 41.4 ksi



(b) 50.2 ksi

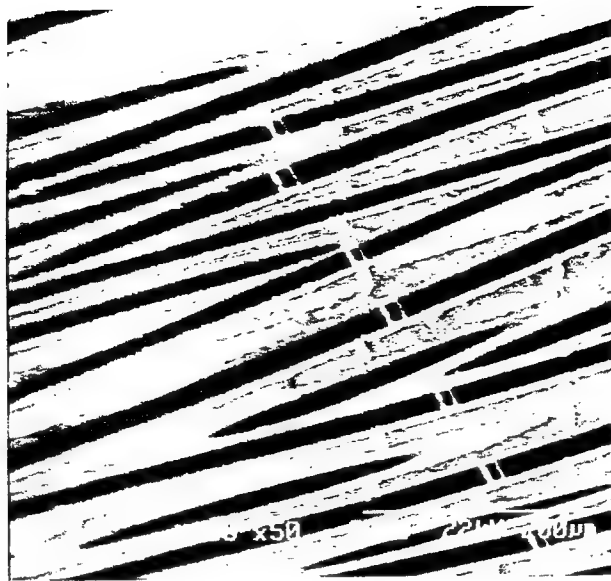


(c) 56.1 ksi

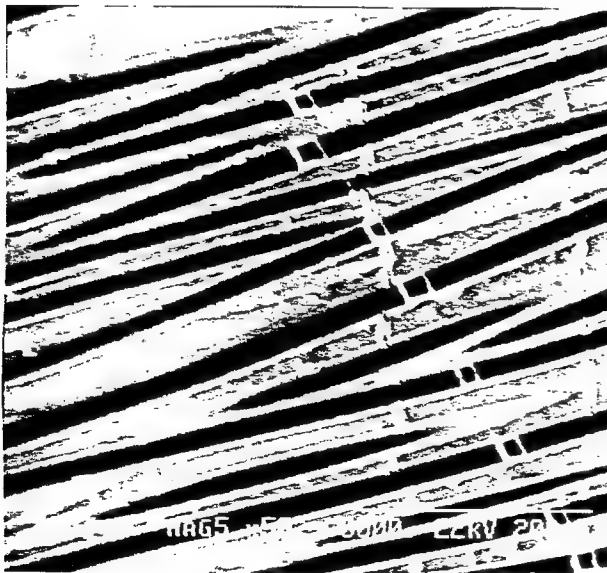


(d) 64.1 ksi

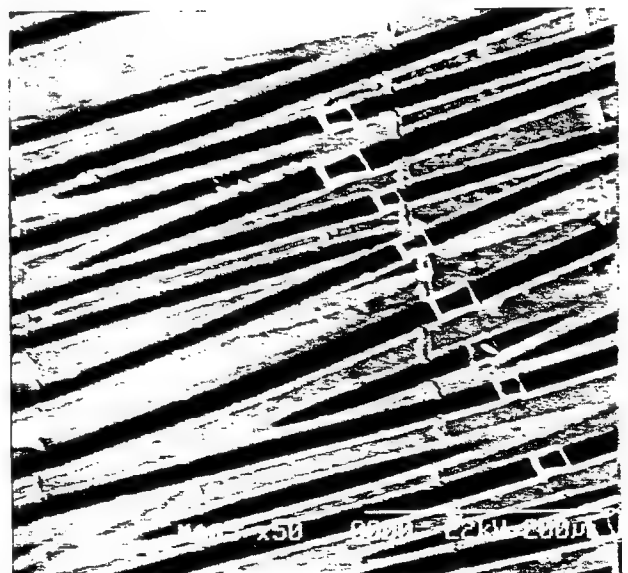
**Fig. 2.31 Progression of fiber crack opening at $T=400^{\circ}\text{C}$
for Nicalon/CAS II specimen with $V_f=40\%$**



(a) 47.4 ksi



(b) 56.5 ksi



(c) 64.1 ksi

**Fig. 2.32 Progression of fiber crack opening at $T=600\text{ }^{\circ}\text{C}$
for Nicalon/CAS II specimen with $V_f=30\%$**

Fig. 2.33 Tensile Strength of Nicalon/CAS II
with $V_f=40\%$ at various temperatures

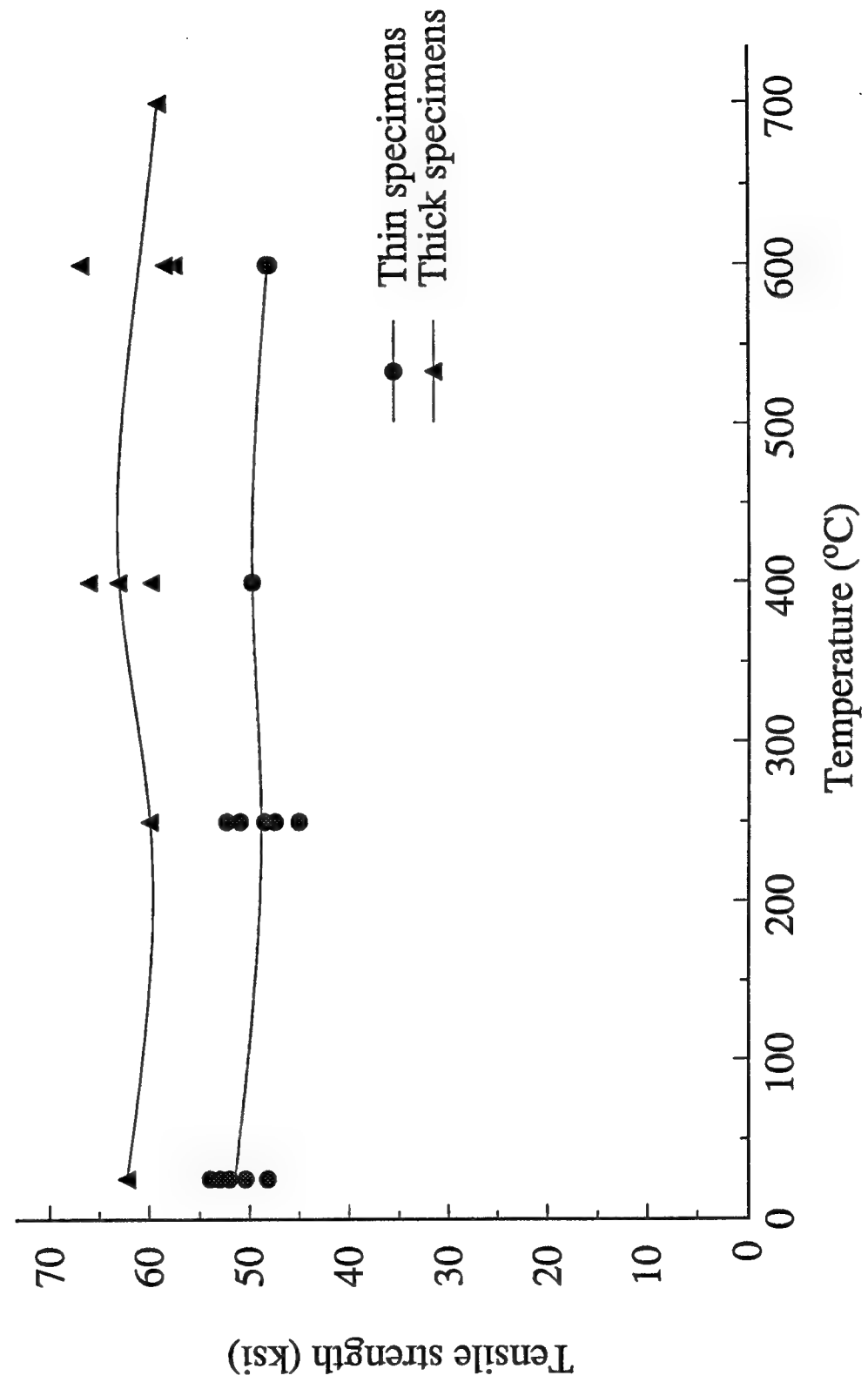


Fig 2.34 Tensile tests on Nicalon/CAS II specimens
with $V_f = 40\%$ at high temperatures (thin specimens)

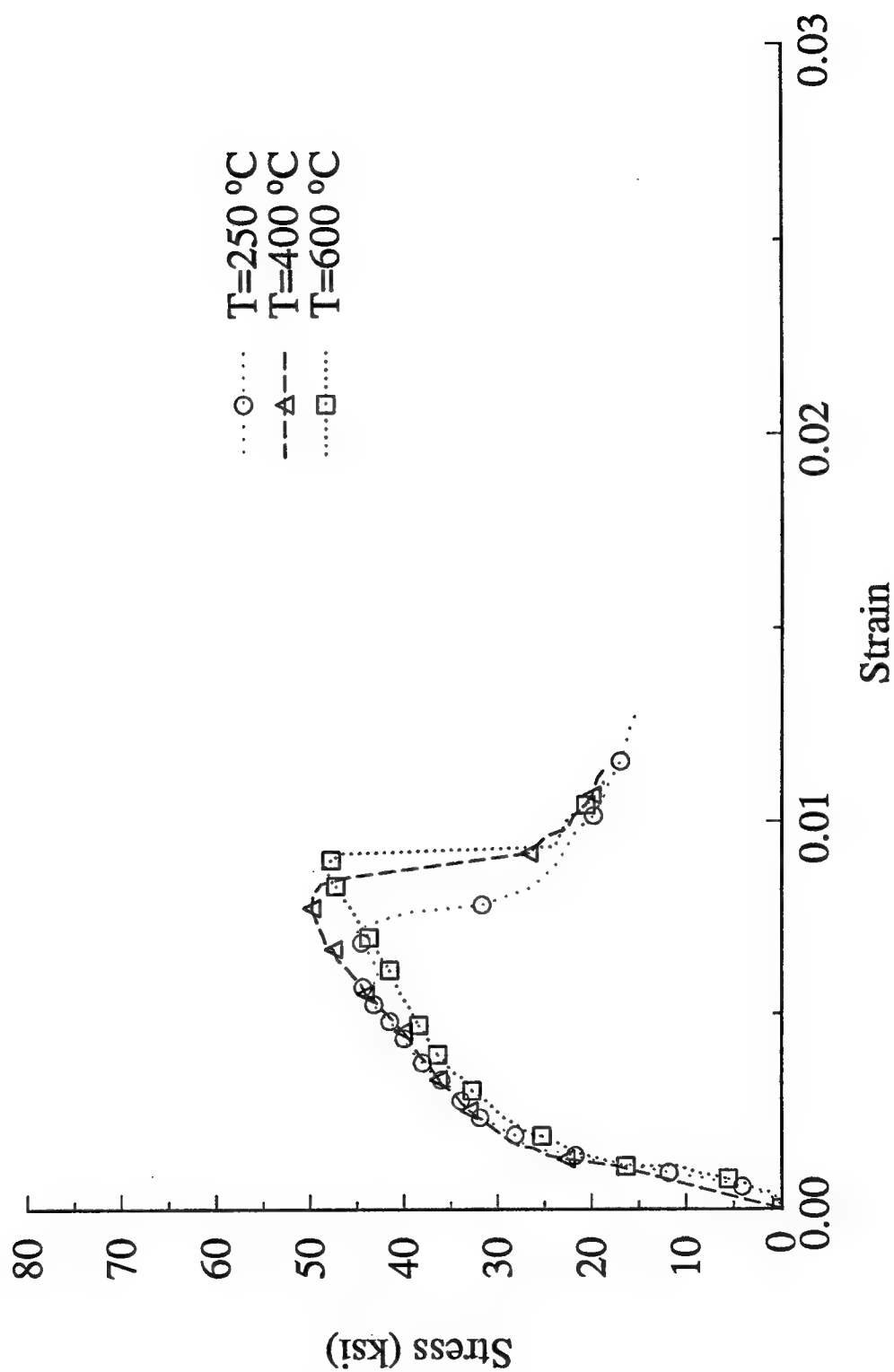


Fig. 3.3 Stress intensity factors at the matrix crack
for Nicalon/CAS II ($b/H_2=0.001$)

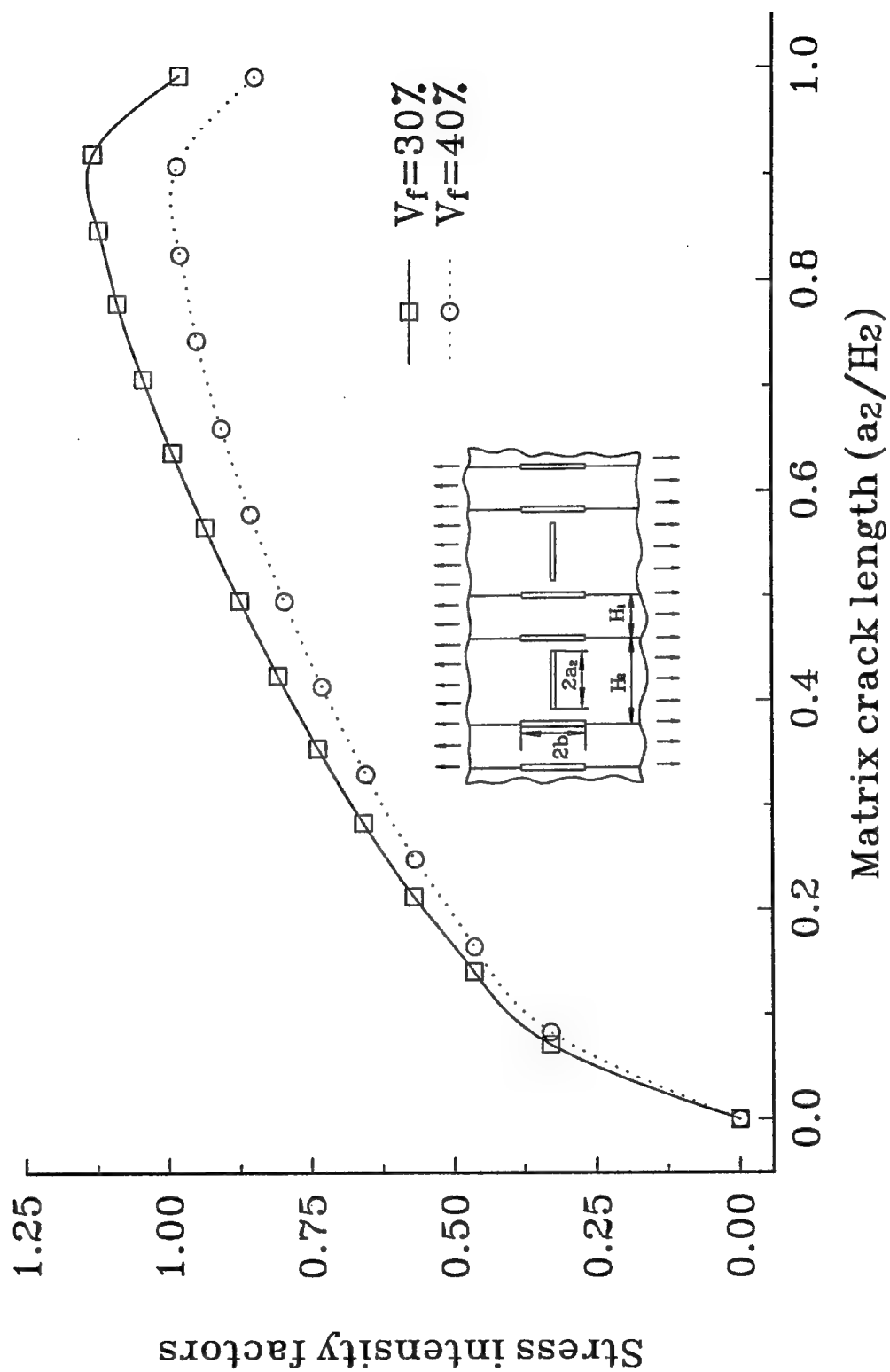


Fig. 3.4 Stress intensity factors at the interface crack for Nicalon/CAS II with ($b/H_2=0.001$)

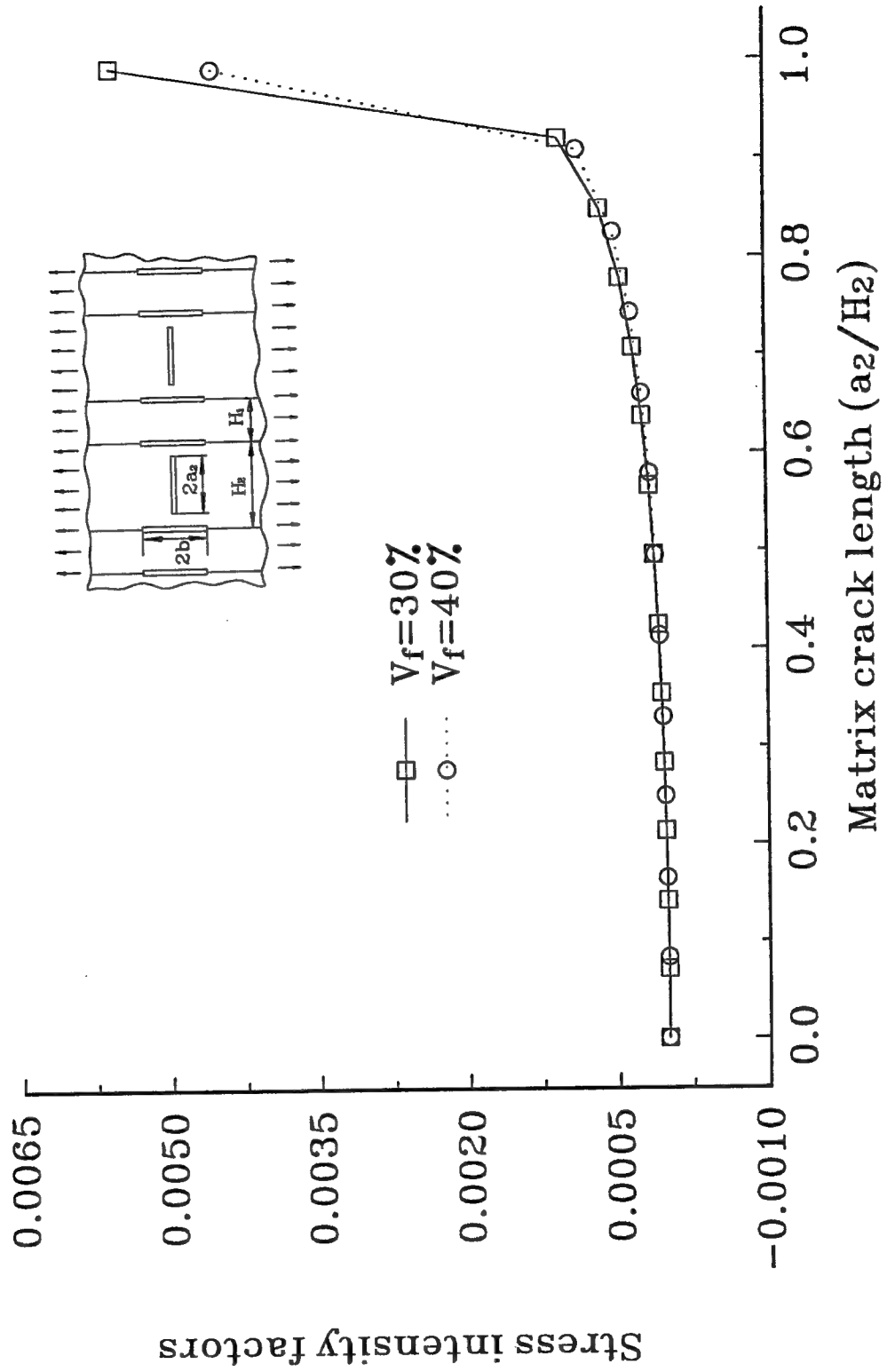


Fig. 3.5 Strain energy release rate at the interface
for Nicalon/CAS II with ($b/H_2=0.001$)

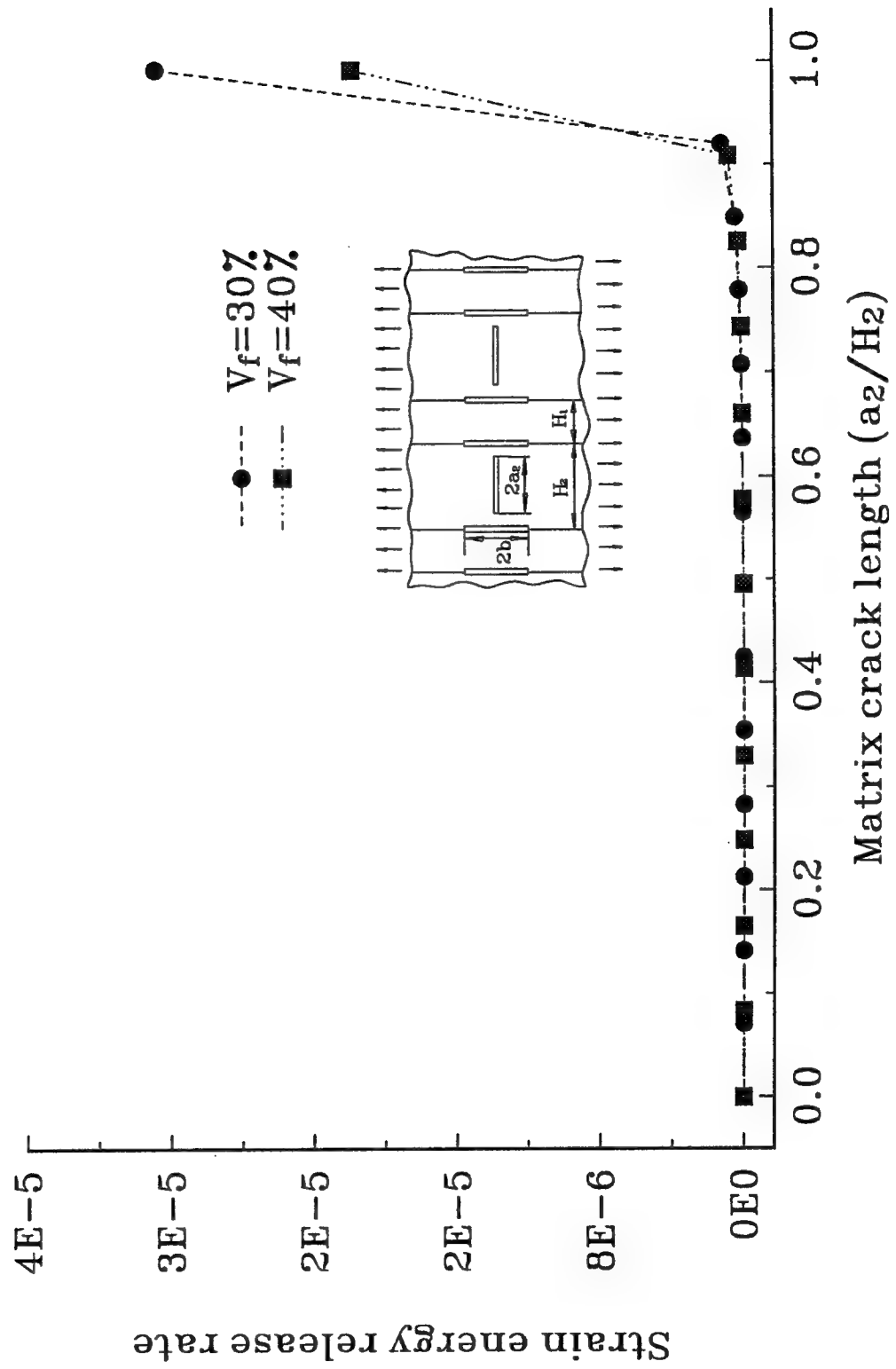


Fig. 3.6 Stress intensity factors at the matrix
for Nicalon/CAS II ($a_2/H_2=0.9$)

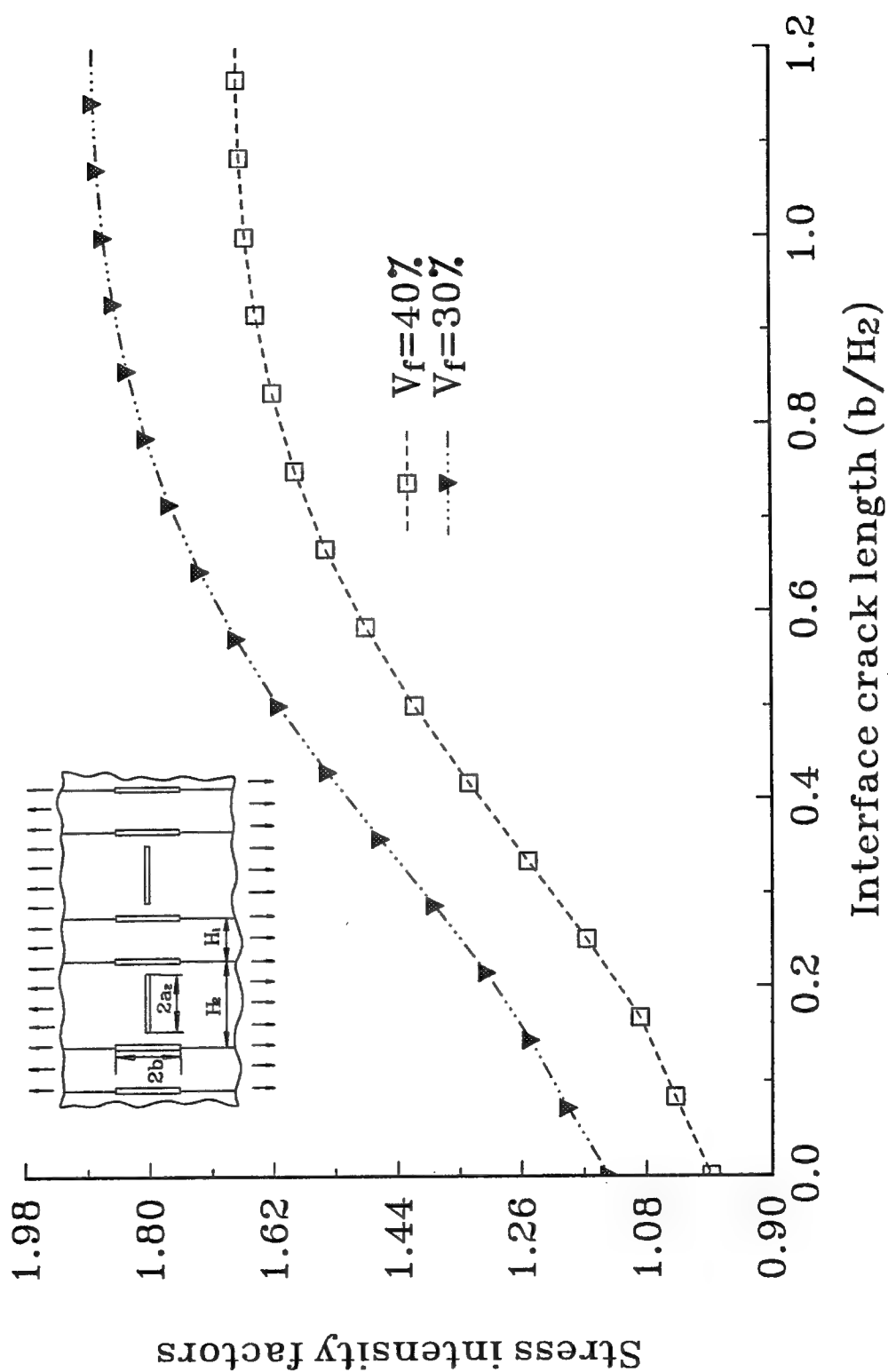


Fig 3.7 Stress intensity factors at the interface
for Nicalon/CAS II ($a_2/H_2=0.9$)

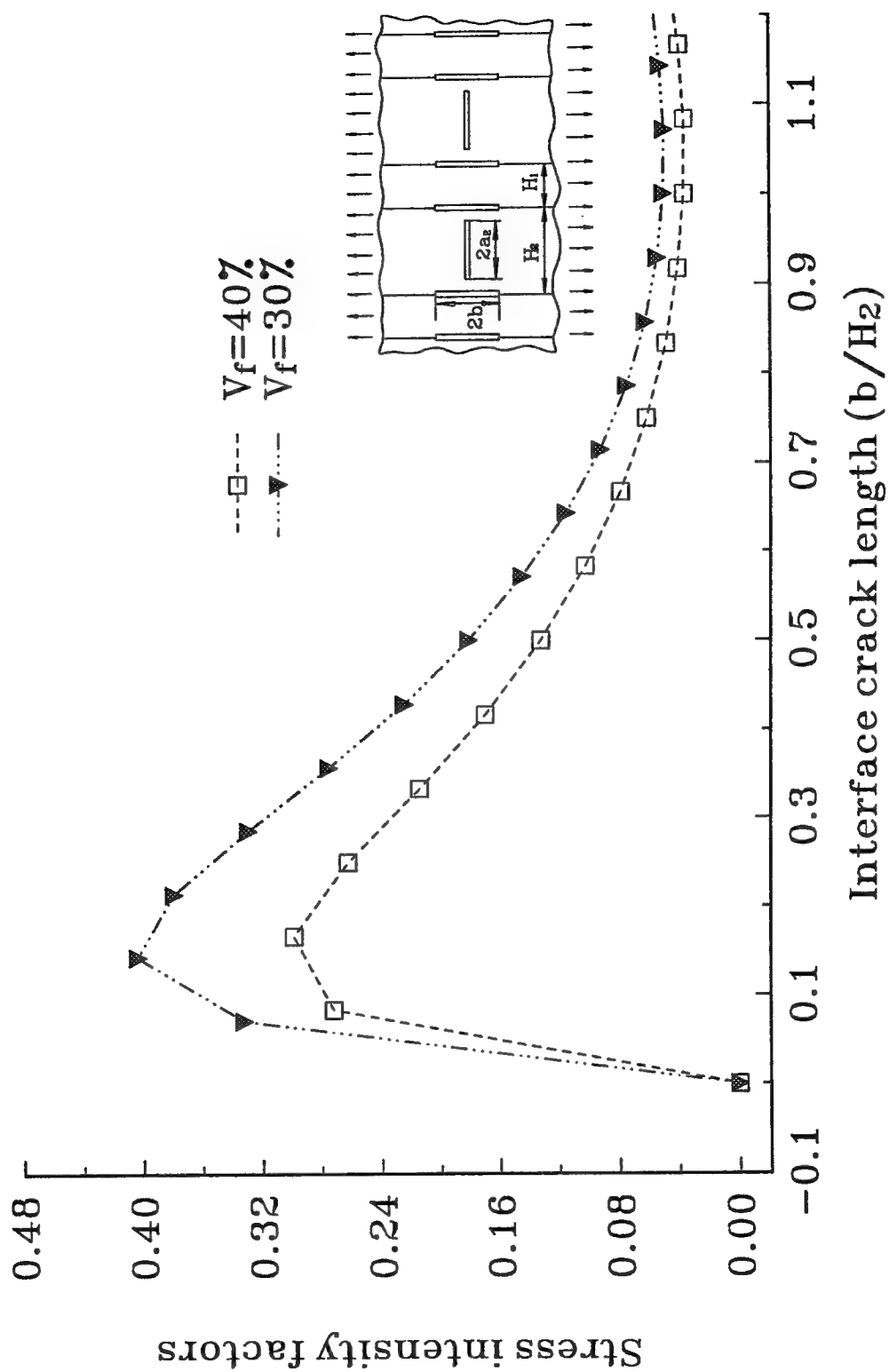


Fig. 3.8 Strain energy release rate at the interface
for Nicalon/CAS II ($a_2/H_2=0.9$)

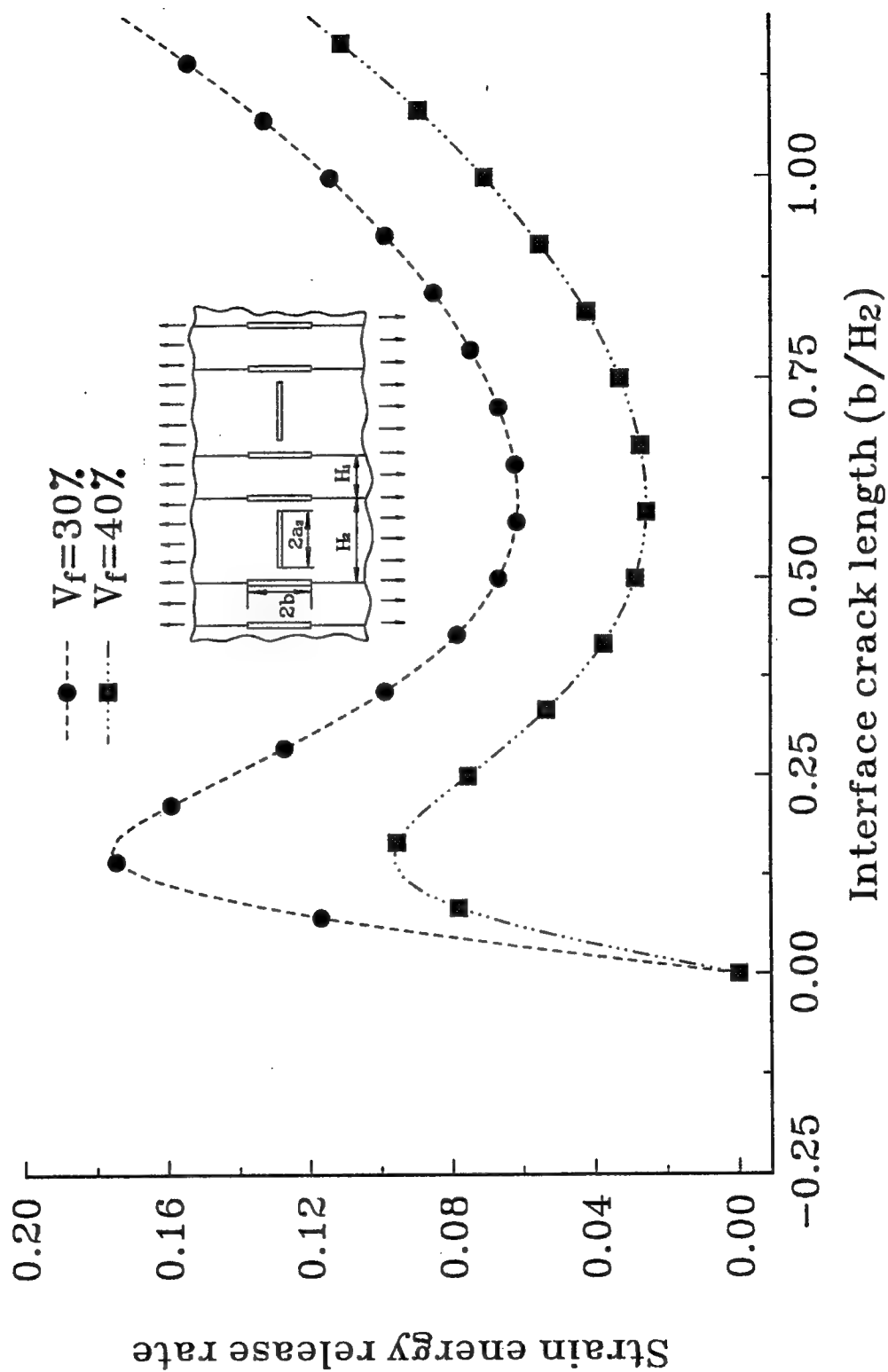


Fig. 3.9 Stress intensity factors at the matrix
for Nicalon/CAS II when $b/H_2=0.55$

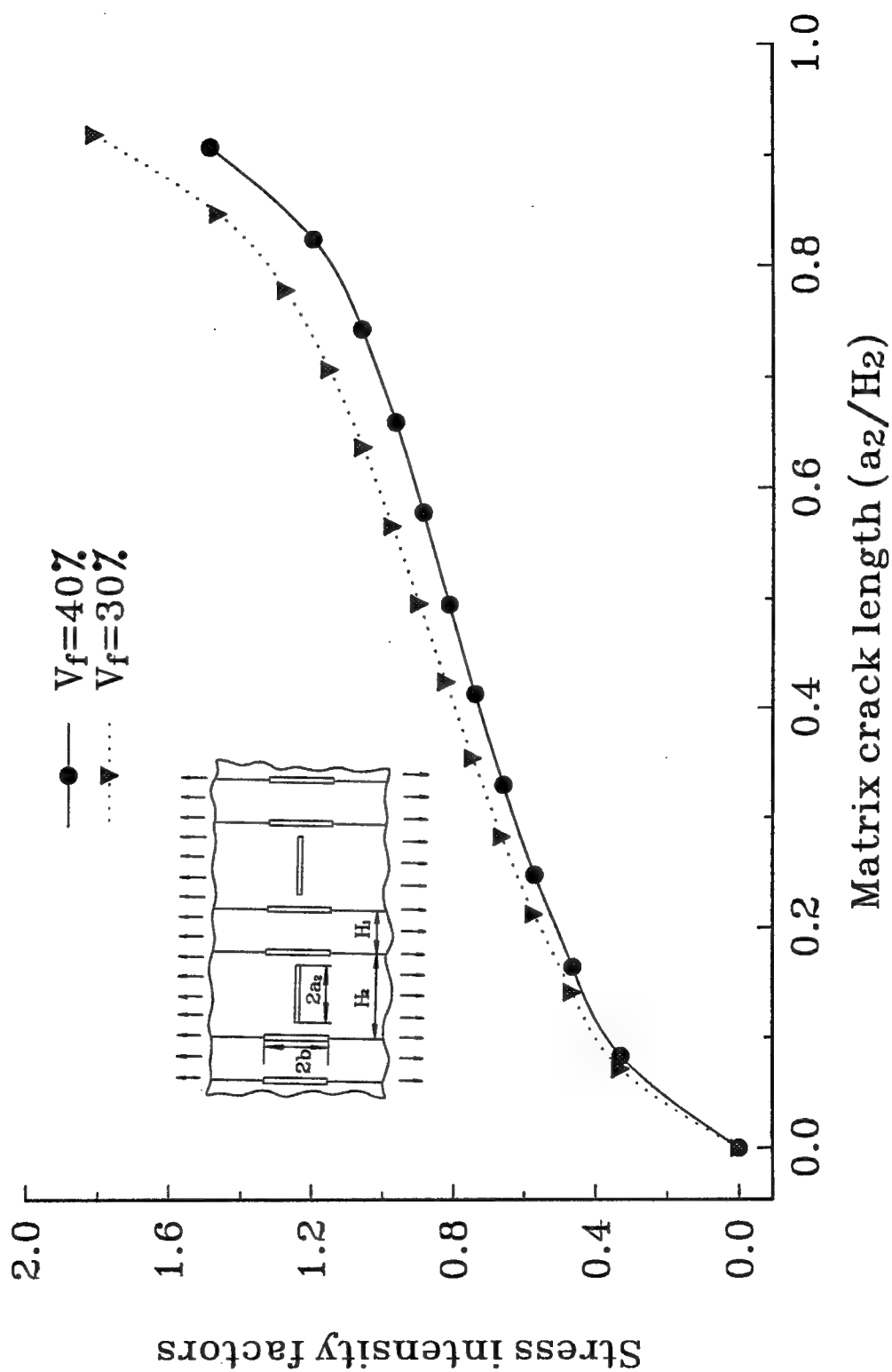


Fig. 3.9a Stress intensity factors at the matrix crack tips
for Nicalon/CAS II with $V_f=30\%$.

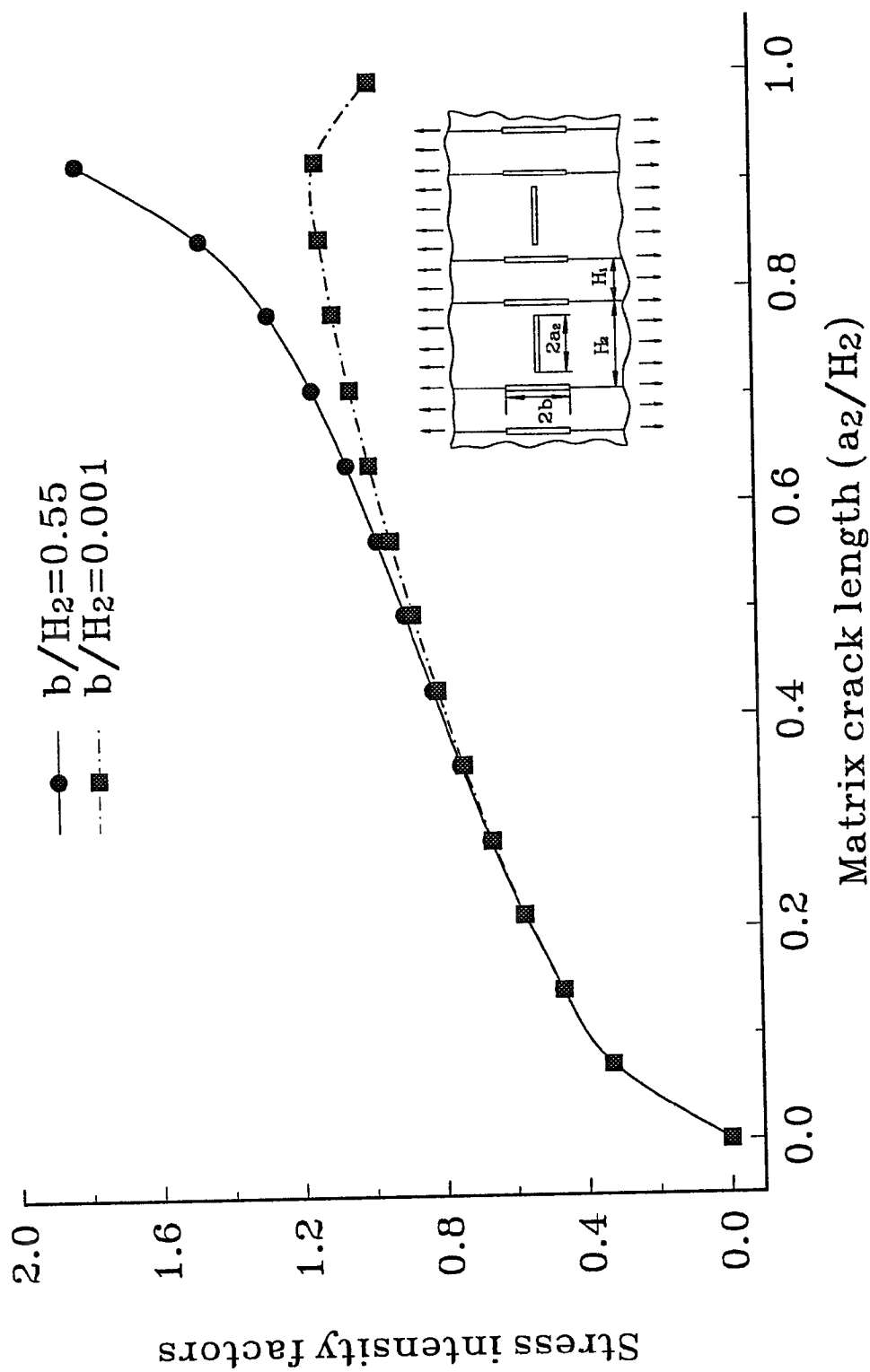
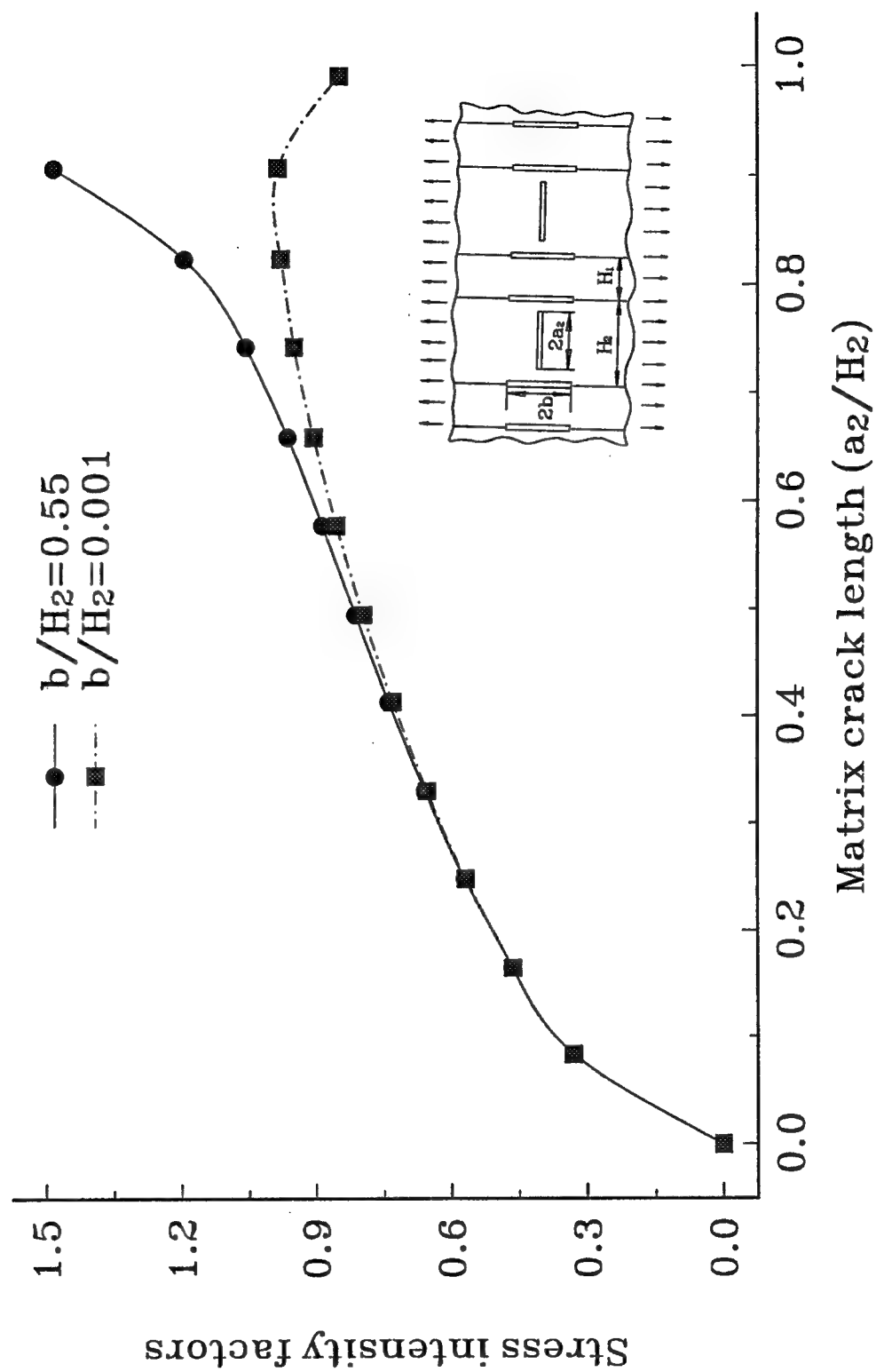


Fig. 3.9b Stress intensity factors at the matrix crack tips
for Nicalon/CAS II with $V_f=40\%$.



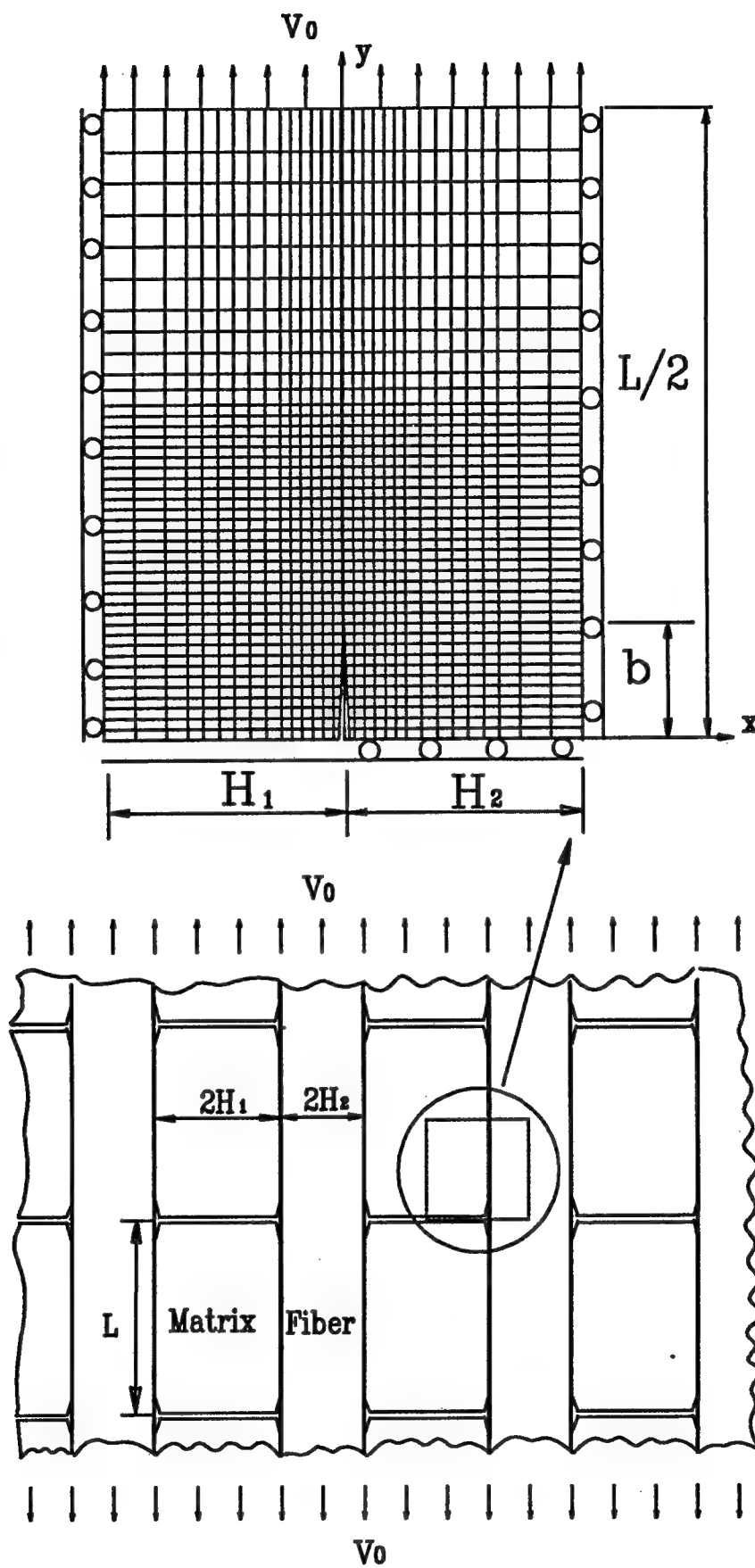


Fig. 3.10 Finite element model

**Fig. 3.11 Tensile tests on Nicalon/CAS II
with $V_f=30\%$ at room temperature**

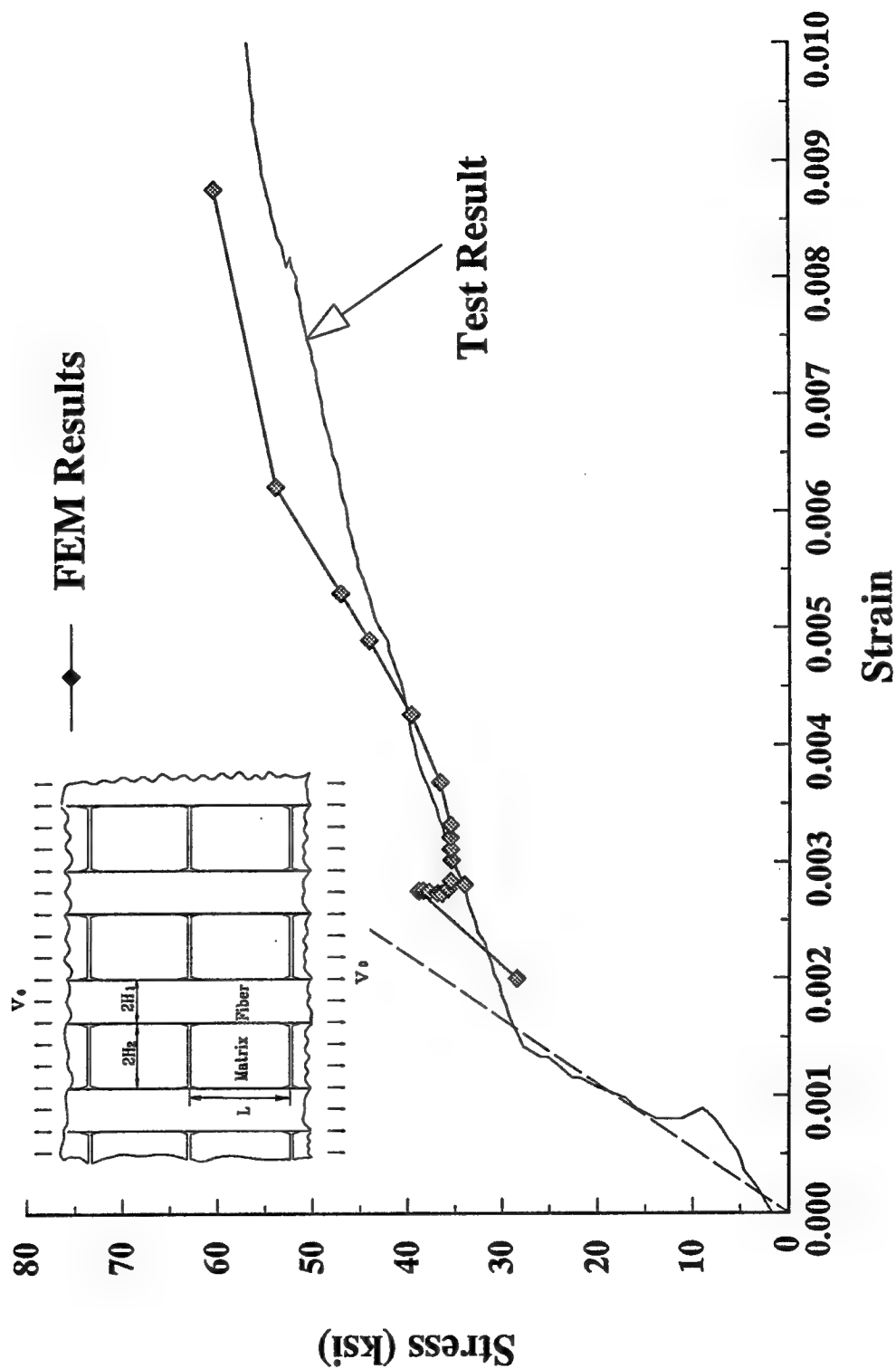


Fig. 3.12 Tensile Tests on Nicalon/CAS II
with $V_f = 40\%$ at room temperature (thick plates)

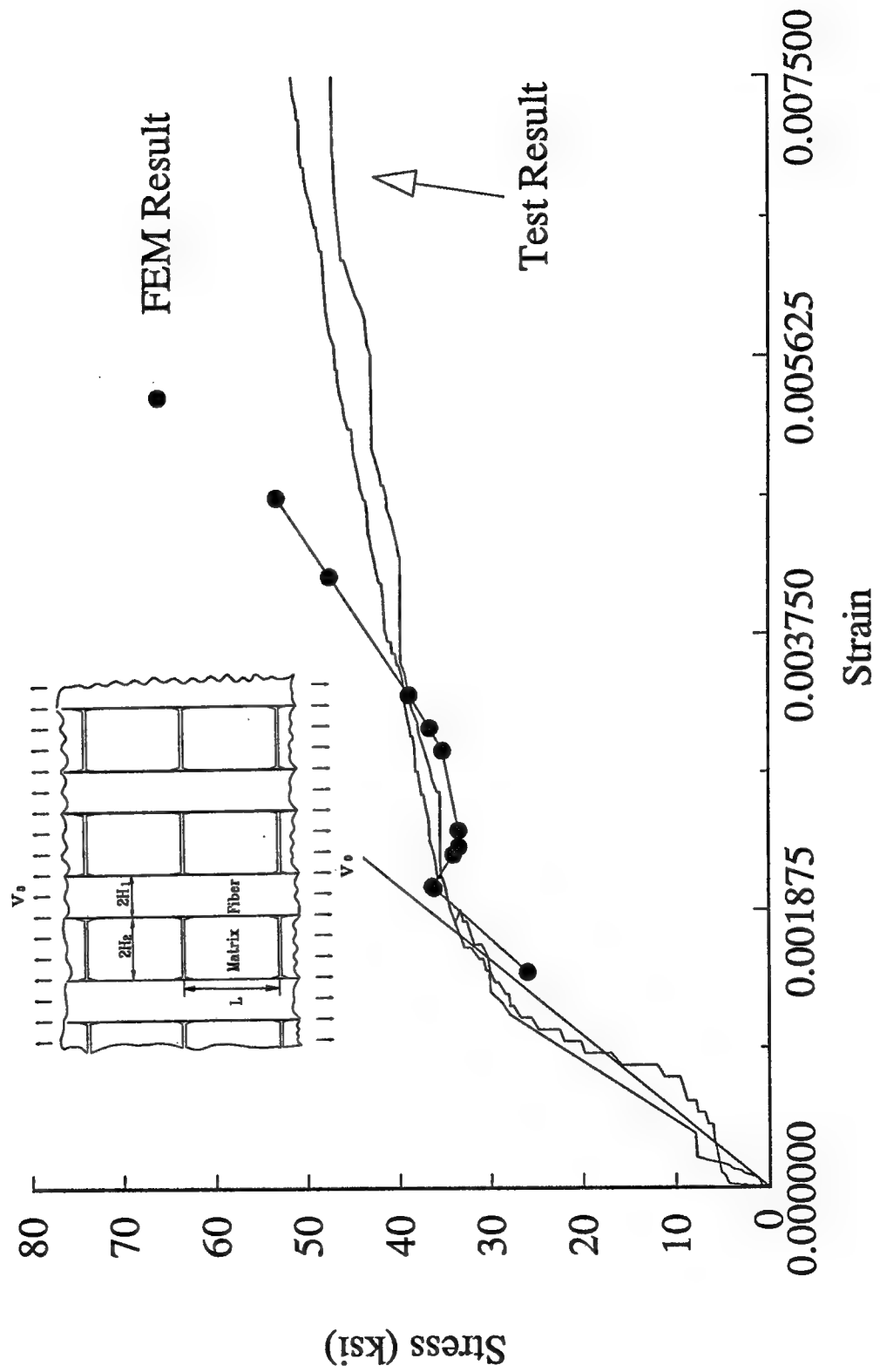
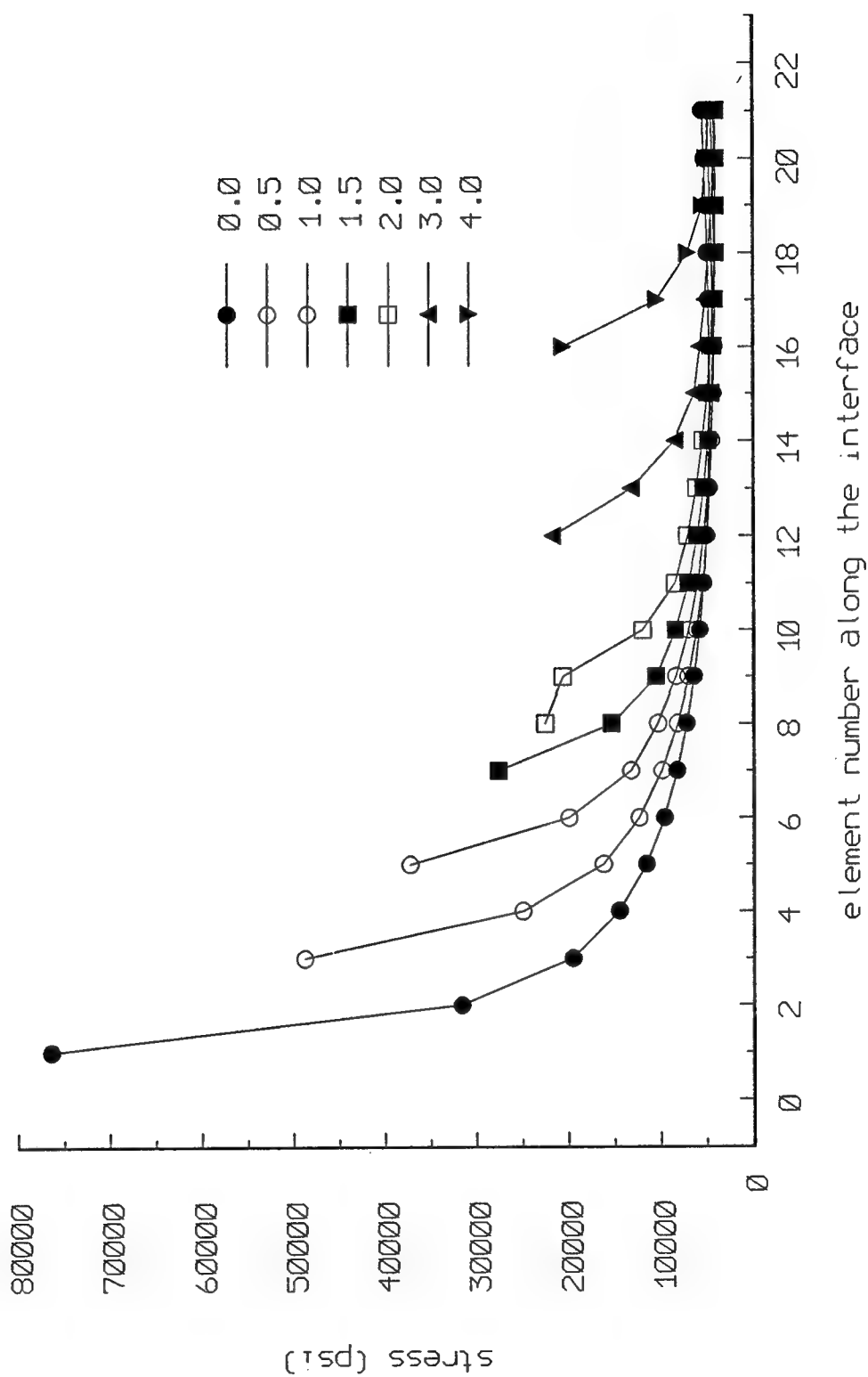


Fig. 3.14 Normal stress distribution at the interface with different interfacial crack length ($L/2H_2=2.5$)



Appendix A

From eqns(1.9ab), one obtains:

$$\begin{aligned} \frac{\partial u_1(H_1, y)}{\partial y} = & -\frac{4}{\pi} \int_0^\infty [A(\alpha) \sinh(w_1 \alpha H_1) + C(\alpha) \sinh(w_3 \alpha H_1)] \alpha \sin \alpha y d\alpha \\ & + \frac{2}{\pi} \int_0^\infty \int_0^{t_1} \frac{\phi_1(t)}{\gamma_{13}} \left[-\frac{|w_1|}{\beta_5} e^{-|w_1| \alpha y / \beta_5} + \frac{|w_3|}{\beta_5} \left(\frac{\gamma_{11}}{\gamma_{12}} \right) e^{-|w_3| \alpha y / \beta_5} \right] \sin \alpha t \sin \alpha H_1 dt d\alpha \quad (A.1) \end{aligned}$$

$$\begin{aligned} \frac{\partial u_2(-H_2, y)}{\partial y} = & \frac{4}{\pi} \int_0^\infty [A^*(\alpha) \sinh(w_1^* \alpha H_2) + C(\alpha) \sinh(w_3^* \alpha H_2)] \alpha \sin \alpha y d\alpha \\ & + \frac{2}{\pi} \int_0^\infty \int_0^{t_2} \frac{\phi_2(t)}{\gamma_{13}^*} \left[-\frac{|w_1^*|}{\beta_5^*} e^{-|w_1^*| \alpha y / \beta_5^*} + \frac{|w_3^*|}{\beta_5^*} \left(\frac{\gamma_{11}^*}{\gamma_{12}^*} \right) e^{-|w_3^*| \alpha y / \beta_5^*} \right] \sin \alpha t \sin \alpha H_2 dt d\alpha \quad (A.2) \end{aligned}$$

$$\begin{aligned} \frac{\partial v_1(H_1, y)}{\partial y} = & \frac{4}{\pi} \int_0^\infty [\beta_7 A(\alpha) \cosh(w_1 \alpha H_1) + \beta_8 C(\alpha) \cosh(w_3 \alpha H_1)] \alpha \cos \alpha y d\alpha \\ & - \frac{2}{\pi} \int_0^\infty \int_0^{t_1} \frac{\phi_1(t)}{\gamma_{13}} \left[-\frac{|w_1|}{\beta_5} \beta_9 \operatorname{sign}(w_1) e^{-|w_1| \alpha y / \beta_5} \right. \\ & \left. + \frac{|w_3|}{\beta_5} \left(\frac{\gamma_{11}}{\gamma_{12}} \right) \beta_{10} \operatorname{sign}(w_3) e^{-|w_3| \alpha y / \beta_5} \right] \sin \alpha t \cos \alpha H_1 dt d\alpha \quad (A.3) \end{aligned}$$

$$\begin{aligned} \frac{\partial v_2(-H_2, y)}{\partial y} = & \frac{4}{\pi} \int_0^\infty [\beta_7^* A^*(\alpha) \cosh(w_1^* \alpha H_2) + \beta_8^* C^*(\alpha) \cosh(w_3^* \alpha H_2)] \alpha \cos \alpha y d\alpha \\ & - \frac{2}{\pi} \int_0^\infty \int_0^{t_2} \frac{\phi_2(t)}{\gamma_{13}^*} \left[-\frac{|w_1^*|}{\beta_5^*} \beta_9^* \operatorname{sign}(w_1^*) e^{-|w_1^*| \alpha y / \beta_5^*} \right. \\ & \left. + \frac{|w_3^*|}{\beta_5^*} \left(\frac{\gamma_{11}^*}{\gamma_{12}^*} \right) \beta_{10}^* \operatorname{sign}(w_3^*) e^{-|w_3^*| \alpha y / \beta_5^*} \right] \sin \alpha t \cos \alpha H_2 dt d\alpha \quad (A.4) \end{aligned}$$

Using the following integral formulas:

$$\int_0^\infty e^{-at} \sin bt \, dt = \frac{b}{a^2 + b^2} \quad \text{and} \quad \int_0^\infty e^{-at} \cos bt \, dt = \frac{a}{a^2 + b^2} \quad a > 0 \quad (A.5ab)$$

equations (A.1-A.4) reduce to:

$$\begin{aligned} \frac{\partial u_1(H_1, y)}{\partial y} = & -\frac{4}{\pi} \int_0^\infty [A(\alpha) \sinh(w_1 \alpha H_1) + C(\alpha) \sinh(w_3 \alpha H_1)] \alpha \sin \alpha y d\alpha \\ & + \frac{2}{\pi} \int_0^{t_1} \frac{\phi_1(t)}{2\gamma_{13}} G_1(t, y) dt \quad (A.1^*) \end{aligned}$$

$$\frac{\partial u_2(-H_2, y)}{\partial y} = \frac{4}{\pi} \int_0^\infty [A^*(\alpha) \sinh(w_1^* \alpha H_2) + C^*(\alpha) \sinh(w_3^* \alpha H_2)] \alpha \sin \alpha y d\alpha$$

$$+ \frac{2}{\pi} \int_0^{a_2} \frac{\phi_2(t)}{2\gamma_{13}^*} G_2(t, y) dt \quad (\text{A.2}^*)$$

$$\begin{aligned} \frac{\partial v_1(H_1, y)}{\partial y} = & \frac{4}{\pi} \int_0^\infty [\beta_7 A(\alpha) \cosh(w_1 \alpha H_1) + \beta_8 C(\alpha) \cosh(w_3 \alpha H_1)] \alpha \cos \alpha y d\alpha \\ & - \frac{2}{\pi} \int_0^{a_1} \frac{\phi_1(t)}{2\gamma_{13}} G_3(t, y) dt \end{aligned} \quad (\text{A.3}^*)$$

$$\begin{aligned} \frac{\partial v_2(-H_2, y)}{\partial y} = & \frac{4}{\pi} \int_0^\infty [\beta_7^* A^*(\alpha) \cosh(w_1^* \alpha H_2) + \beta_8^* C^*(\alpha) \cosh(w_3^* \alpha H_2)] \alpha \cos \alpha y d\alpha \\ & - \frac{2}{\pi} \int_0^{a_2} \frac{\phi_2(t)}{2\gamma_{13}^*} G_4(t, y) dt \end{aligned} \quad (\text{A.4}^*)$$

where

$$\begin{aligned} G_1(t, y) = & -\frac{|w_1|}{\beta_5} \left[\frac{\frac{|w_1|y}{\beta_5}}{\frac{(lw_1|y)^2}{\beta_5^2} + (H_1-t)^2} - \frac{\frac{|w_1|y}{\beta_5}}{\frac{(lw_1|y)^2}{\beta_5^2} + (H_1+t)^2} \right] \\ & + \frac{|w_3|}{\beta_5} \left[\frac{\frac{|w_3|y}{\beta_5}}{\frac{(lw_3|y)^2}{\beta_5^2} + (H_1-t)^2} - \frac{\frac{|w_3|y}{\beta_5}}{\frac{(lw_3|y)^2}{\beta_5^2} + (H_1+t)^2} \right] \end{aligned} \quad (\text{A.6a})$$

$$\begin{aligned} G_2(t, y) = & -\frac{|w_1^*|}{\beta_5^*} \left[\frac{\frac{|w_1^*|y}{\beta_5^*}}{\frac{(lw_1^*|y)^2}{\beta_5^{*2}} + (H_1-t)^2} - \frac{\frac{|w_1^*|y}{\beta_5^*}}{\frac{(lw_1^*|y)^2}{\beta_5^{*2}} + (H_1+t)^2} \right] \\ & + \frac{|w_3^*|}{\beta_5^*} \left[\frac{\frac{|w_3^*|y}{\beta_5^*}}{\frac{(lw_3^*|y)^2}{\beta_5^{*2}} + (H_1-t)^2} - \frac{\frac{|w_3^*|y}{\beta_5^*}}{\frac{(lw_3^*|y)^2}{\beta_5^{*2}} + (H_1+t)^2} \right] \end{aligned} \quad (\text{A.6b})$$

$$\begin{aligned} G_3(t, y) = & \frac{\beta_9 \text{sign}(w_1) |w_1|}{\beta_5} \left[\frac{H_1-t}{\frac{(lw_1|y)^2}{\beta_5^2} + (H_1-t)^2} - \frac{H_1+t}{\frac{(lw_1|y)^2}{\beta_5^2} + (H_1+t)^2} \right] \\ & - \frac{\beta_{10} \text{sign}(w_3) |w_3| \gamma_{11}}{\beta_5 \gamma_{12}} \left[\frac{H_1-t}{\frac{(lw_3|y)^2}{\beta_5^2} + (H_1-t)^2} - \frac{H_1+t}{\frac{(lw_3|y)^2}{\beta_5^2} + (H_1+t)^2} \right] \end{aligned} \quad (\text{A.6c})$$

$$\begin{aligned} G_4(t, y) = & \frac{\beta_9^* \text{sign}(w_1^*) |w_1^*|}{\beta_5^*} \left[\frac{H_2-t}{\frac{(lw_1^*|y)^2}{\beta_5^{*2}} + (H_2-t)^2} - \frac{H_2+t}{\frac{(lw_1^*|y)^2}{\beta_5^{*2}} + (H_2+t)^2} \right] \\ & - \frac{\beta_{10}^* \text{sign}(w_3^*) |w_3^*| \gamma_{11}^*}{\beta_5^* \gamma_{12}^*} \left[\frac{H_2-t}{\frac{(lw_3^*|y)^2}{\beta_5^{*2}} + (H_2-t)^2} - \frac{H_2+t}{\frac{(lw_3^*|y)^2}{\beta_5^{*2}} + (H_2+t)^2} \right] \end{aligned} \quad (\text{A.6d})$$

Applying (3.14ab) and (3.21cd) to eqns(A.1*)-(A.4*):

$$\begin{aligned}\phi_4(y) = & -\frac{4}{\pi} \int_0^\infty [A(\alpha) \sinh(w_1 \alpha H_1) + C(\alpha) \sinh(w_3 \alpha H_1) \\ & + A^*(\alpha) \sinh(w_1^* \alpha H_2) + C^*(\alpha) \sinh(w_3^* \alpha H_2)] \alpha \sin \alpha y d\alpha \\ & + \frac{2}{\pi} \int_0^{t_1} \frac{\phi_1(t)}{2\gamma_{13}} G_1(t, y) dt + \frac{2}{\pi} \int_0^{t_2} \frac{\phi_2(t)}{2\gamma_{13}^*} G_2(t, y) dt\end{aligned}\quad (A.7a)$$

$$\begin{aligned}\phi_3(y) = & \frac{4}{\pi} \int_0^\infty [\beta_7 A(\alpha) \cosh(w_1 \alpha H_1) + \beta_8 C(\alpha) \cosh(w_3 \alpha H_1) \\ & - \beta_7^* A^*(\alpha) \cosh(w_1^* \alpha H_2) - \beta_8^* C^*(\alpha) \cosh(w_3^* \alpha H_2)] \alpha \cos \alpha y d\alpha \\ & - \frac{2}{\pi} \int_0^{t_1} \frac{\phi_1(t)}{2\gamma_{13}} G_3(t, y) dt + \frac{2}{\pi} \int_0^{t_2} \frac{\phi_2(t)}{2\gamma_{13}^*} G_4(t, y) dt\end{aligned}\quad (A.7b)$$

Taking inverse cosine and sine Fourier transforms for both sides of eqn(A.7a) and (A.7b) respectively, one gets:

$$\begin{aligned}A(\alpha) \sinh(w_1 \alpha H_1) + C(\alpha) \sinh(w_3 \alpha H_1) \\ + A^*(\alpha) \sinh(w_1^* \alpha H_2) + C^*(\alpha) \sinh(w_3^* \alpha H_2) = R_1(\alpha)\end{aligned}\quad (A.8a)$$

and

$$\begin{aligned}\beta_7 A(\alpha) \cosh(w_1 \alpha H_1) + \beta_8 C(\alpha) \cosh(w_3 \alpha H_1) \\ - \beta_7^* A^*(\alpha) \cosh(w_1^* \alpha H_2) - \beta_8^* C^*(\alpha) \cosh(w_3^* \alpha H_2) = R_2(\alpha)\end{aligned}\quad (A.8b)$$

where

$$\begin{aligned}R_1(\alpha) = & -\frac{1}{2\alpha} \int_0^\infty \phi_4(y) \sin \alpha y dy + \frac{2}{\pi \alpha} \int_0^\infty \int_0^{t_1} \frac{\phi_1(t)}{4\gamma_{13}} G_1(t, y) \sin \alpha y dt dy \\ & + \frac{2}{\pi \alpha} \int_0^\infty \int_0^{t_2} \frac{\phi_2(t)}{4\gamma_{13}^*} G_2(t, y) \sin \alpha y dt dy\end{aligned}\quad (A.9a)$$

$$\begin{aligned}R_2(\alpha) = & \frac{1}{2\alpha} \int_0^\infty \phi_3(y) \cos \alpha y dy + \frac{2}{\pi \alpha} \int_0^\infty \int_0^{t_1} \frac{\phi_1(t)}{4\gamma_{13}} G_3(t, y) \cos \alpha y dt dy \\ & - \frac{2}{\pi \alpha} \int_0^\infty \int_0^{t_2} \frac{\phi_2(t)}{4\gamma_{13}^*} G_4(t, y) \cos \alpha y dt dy\end{aligned}\quad (A.9b)$$

Using the following integrals:

$$\begin{aligned} \int_0^{\infty} G_1(t,y) \sin \alpha y dy = & -\frac{\pi}{2} (e^{-\alpha(H_1-t)} \beta_5 / w_1 - e^{-\alpha(H_1+t)} \beta_5 / w_1) \\ & + \frac{\pi \gamma_{11}}{2 \gamma_{12}} (e^{-\alpha(H_1-t)} \beta_5 / w_3 - e^{-\alpha(H_1+t)} \beta_5 / w_3) \end{aligned} \quad (A.10a)$$

$$\begin{aligned} \int_0^{\infty} G_2(t,y) \sin \alpha y dy = & -\frac{\pi}{2} (e^{-\alpha(H_2-t)} \beta_5^* / w_1^* - e^{-\alpha(H_2+t)} \beta_5^* / w_1^*) \\ & + \frac{\pi \gamma_{11}^*}{2 \gamma_{12}^*} (e^{-\alpha(H_2-t)} \beta_5^* / w_3^* - e^{-\alpha(H_2+t)} \beta_5^* / w_3^*) \end{aligned} \quad (A.10b)$$

$$\begin{aligned} \int_0^{\infty} G_3(t,y) \cos \alpha y dy = & \frac{\pi}{2} \text{sign}(w_1) \beta_9 (e^{-\alpha(H_1-t)} \beta_5 / w_1 - e^{-\alpha(H_1+t)} \beta_5 / w_1) \\ & - \frac{\pi}{2} \text{sign}(w_3) \beta_{10} \frac{\gamma_{11}}{\gamma_{12}} (e^{-\alpha(H_1-t)} \beta_5 / w_3 - e^{-\alpha(H_1+t)} \beta_5 / w_3) \end{aligned} \quad (A.10c)$$

$$\begin{aligned} \int_0^{\infty} G_4(t,y) \cos \alpha y dy = & \frac{\pi}{2} \text{sign}(w_1^*) \beta_9^* (e^{-\alpha(H_2-t)} \beta_5^* / w_1^* - e^{-\alpha(H_2+t)} \beta_5^* / w_1^*) \\ & - \frac{\pi}{2} \text{sign}(w_3^*) \beta_{10}^* \frac{\gamma_{11}^*}{\gamma_{12}^*} (e^{-\alpha(H_2-t)} \beta_5^* / w_3^* - e^{-\alpha(H_2+t)} \beta_5^* / w_3^*) \end{aligned} \quad (A.10d)$$

eqns(A.9a) and (A.9b) are finally reduced to:

$$\begin{aligned} R_1(\alpha) = & -\frac{1}{2\alpha} \int_{b_1}^{b_2} \phi_4(y) \sin \alpha y dy \\ & + \frac{1}{4\alpha \gamma_{13}} \int_{-a_1}^{a_1} \phi_1(t) [-e^{-\alpha(H_1-t)} \beta_5 / w_1 + \frac{\gamma_{11}}{\gamma_{12}} e^{-\alpha(H_1-t)} \beta_5 / w_3] dt \\ & + \frac{1}{4\alpha \gamma_{13}^*} \int_{-a_2}^{a_2} \phi_2(t) [-e^{-\alpha(H_2-t)} \beta_5^* / w_1^* + \frac{\gamma_{11}^*}{\gamma_{12}^*} e^{-\alpha(H_2-t)} \beta_5^* / w_3^*] dt \end{aligned} \quad (A.11a)$$

and

$$R_2(a) = \frac{1}{2\alpha} \int_{b_1}^{b_2} \phi_3(y) \cos \alpha y dy$$

$$\begin{aligned}
& + \frac{1}{4\alpha\gamma_{13}} \int_{-a_1}^{a_1} \phi_1(t) [\text{sign}(w_1)\beta_9 e^{-\alpha(H_1-t)}\beta_5/|w_1| - \text{sign}(w_3)\beta_{10}\frac{\gamma_{11}}{\gamma_{12}} e^{-\alpha(H_1-t)}\beta_5/|w_3|] dt \\
& - \frac{1}{4\alpha\gamma_{13}^*} \int_{-a_2}^{a_2} \phi_2(t) [\text{sign}(w_1^*)\beta_9^* e^{-\alpha(H_2-t)}\beta_5^*/|w_1^*| \\
& \quad - \text{sign}(w_3^*)\beta_{10}^*\frac{\gamma_{11}^*}{\gamma_{12}^*} e^{-\alpha(H_2-t)}\beta_5^*/|w_3^*|] dt \quad (A.11b)
\end{aligned}$$

Applying the continuity conditions (3.13ab) and (3.14ab), one derives the following:

$$\begin{aligned}
& \int_0^\infty 2[\gamma_3 A(\alpha) \cosh(w_1 \alpha H_1) + \gamma_4 C(\alpha) \cosh(w_3 \alpha H_1) \\
& - \lambda_1 \gamma_3^* A^*(\alpha) \cosh(w_1^* \alpha H_2) - \lambda_1 \gamma_4^* C^*(\alpha) \cosh(w_3^* \alpha H_2)] \alpha \cos \alpha y d\alpha \\
& = - \int_0^\infty \int_0^{a_1} \frac{\phi_1(t)}{\gamma_{13}} \sin \alpha t dt [\gamma_1 e^{-|w_1| \alpha y / \beta_5} - \gamma_2 \frac{\gamma_{11}}{\gamma_{12}} e^{-|w_3| \alpha y / \beta_5}] \cos \alpha H_1 d\alpha \\
& + \int_0^\infty \int_0^{a_1} \frac{\lambda_1 \phi_2(t)}{\gamma_{13}^*} \sin \alpha t dt [\gamma_1^* e^{-|w_1^*| \alpha y / \beta_5^*} - \gamma_2^* \frac{\gamma_{11}^*}{\gamma_{12}^*} e^{-|w_3^*| \alpha y / \beta_5^*}] \cos \alpha H_2 d\alpha \quad (A.12a)
\end{aligned}$$

and

$$\begin{aligned}
& \int_0^\infty 2[\gamma_9 A(\alpha) \sinh(w_1 \alpha H_1) + \gamma_{10} C(\alpha) \sinh(w_3 \alpha H_1) \\
& + \lambda_2 \gamma_9^* A^*(\alpha) \sinh(w_1^* \alpha H_2) + \lambda_2 \gamma_{10}^* C^*(\alpha) \sinh(w_3^* \alpha H_2)] \alpha \sin \alpha y d\alpha \\
& = - \int_0^\infty \int_0^{a_1} \frac{\phi_1(t)}{\gamma_{13}} \sin \alpha t dt \gamma_{11} [e^{-|w_1| \alpha y / \beta_5} - e^{-|w_3| \alpha y / \beta_5}] \sin \alpha H_1 d\alpha \\
& - \int_0^\infty \int_0^{a_1} \frac{\lambda_2 \phi_2(t)}{\gamma_{13}^*} \sin \alpha t dt \gamma_{11}^* [e^{-|w_1^*| \alpha y / \beta_5^*} - e^{-|w_3^*| \alpha y / \beta_5^*}] \sin \alpha H_2 d\alpha \quad (A.12b)
\end{aligned}$$

Applying inverse Fourier cosine and sine transforms to (A.12a,b) respectively, we have:

$$[\gamma_3 A(\alpha) \cosh(w_1 \alpha H_1) + \gamma_4 C(\alpha) \cosh(w_3 \alpha H_1)]$$

$$-\lambda_1\gamma_3^*A^*(\alpha)\cosh(w_1\alpha H_2) - \lambda_1\gamma_4^*C^*(\alpha)\cosh(w_3\alpha H_2)]\alpha = R_3(\alpha) \quad (A.13a)$$

and

$$\begin{aligned} & [\gamma_9A(\alpha)\sinh(w_1\alpha H_1) + \gamma_{10}C(\alpha)\sinh(w_3\alpha H_1) \\ & + \lambda_2\gamma_9^*A^*(\alpha)\sinh(w_1\alpha H_2) + \lambda_2\gamma_{10}^*C^*(\alpha)\sinh(w_3\alpha H_2)]\alpha = R_4(\alpha) \end{aligned} \quad (A.13b)$$

where

$$R_3(\alpha) = -\frac{2}{\pi} \int_0^\infty \int_0^{a_1} \frac{\phi_1(t)}{4\gamma_{13}} S_1(t,y) \cos\alpha y dt dy + \frac{2}{\pi} \int_0^\infty \int_0^{a_1} \frac{\lambda_1\phi_2(t)}{4\gamma_{13}^*} S_2(t,y) \cos\alpha y dt dy \quad (A.14a)$$

$$R_4(\alpha) = -\frac{2}{\pi} \int_0^\infty \int_0^{a_1} \frac{\phi_1(t)}{4\gamma_{13}} S_3(t,y) \sin\alpha y dt dy - \frac{2}{\pi} \int_0^\infty \int_0^{a_1} \frac{\lambda_2\phi_2(t)}{4\gamma_{13}^*} S_4(t,y) \sin\alpha y dt dy \quad (A.14b)$$

and

$$\begin{aligned} S_1(t,y) = & \left[-\gamma_1 \frac{\frac{H_1-t}{\beta_5^2}}{\frac{(lw_1|y)^2}{\beta_5^2} + (H_1-t)^2} + \gamma_2 \left(\frac{\gamma_{11}}{\gamma_{12}} \right) \frac{\frac{H_1-t}{\beta_5^2}}{\frac{(lw_3|y)^2}{\beta_5^2} + (H_1-t)^2} \right] \\ & + \left[\gamma_1 \frac{\frac{H_1+t}{\beta_5^2}}{\frac{(lw_1|y)^2}{\beta_5^2} + (H_1+t)^2} - \gamma_2 \left(\frac{\gamma_{11}}{\gamma_{12}} \right) \frac{\frac{H_1+t}{\beta_5^2}}{\frac{(lw_3|y)^2}{\beta_5^2} + (H_1+t)^2} \right] \end{aligned} \quad (A.15a)$$

$$\begin{aligned} S_2(t,y) = & \left[-\gamma_1^* \frac{\frac{H_2-t}{\beta_5^{*2}}}{\frac{(lw_1^*|y)^2}{\beta_5^{*2}} + (H_2-t)^2} + \gamma_2^* \left(\frac{\gamma_{11}^*}{\gamma_{12}^*} \right) \frac{\frac{H_2-t}{\beta_5^{*2}}}{\frac{(lw_3^*|y)^2}{\beta_5^{*2}} + (H_2-t)^2} \right] \\ & + \left[\gamma_1^* \frac{\frac{H_2+t}{\beta_5^{*2}}}{\frac{(lw_1^*|y)^2}{\beta_5^{*2}} + (H_2+t)^2} - \gamma_2^* \left(\frac{\gamma_{11}^*}{\gamma_{12}^*} \right) \frac{\frac{H_2+t}{\beta_5^{*2}}}{\frac{(lw_3^*|y)^2}{\beta_5^{*2}} + (H_2+t)^2} \right] \end{aligned} \quad (A.15b)$$

$$\begin{aligned} S_3(t,y) = & \gamma_{11} \left[\frac{\frac{\frac{lw_1|y}{\beta_5}}{\frac{(lw_1|y)^2}{\beta_5^2} + (H_1-t)^2}}{\frac{(lw_1|y)^2}{\beta_5^2} + (H_1-t)^2} - \frac{\frac{\frac{lw_3|y}{\beta_5}}{\frac{(lw_3|y)^2}{\beta_5^2} + (H_1-t)^2}}{\frac{(lw_3|y)^2}{\beta_5^2} + (H_1-t)^2} \right] \\ & - \gamma_{11} \left[\frac{\frac{\frac{lw_1|y}{\beta_5}}{\frac{(lw_1|y)^2}{\beta_5^2} + (H_1+t)^2}}{\frac{(lw_1|y)^2}{\beta_5^2} + (H_1+t)^2} - \frac{\frac{\frac{lw_3|y}{\beta_5}}{\frac{(lw_3|y)^2}{\beta_5^2} + (H_1+t)^2}}{\frac{(lw_3|y)^2}{\beta_5^2} + (H_1+t)^2} \right] \end{aligned} \quad (A.15c)$$

$$\begin{aligned} S_4(t,y) = & \gamma_{11}^* \left[\frac{\frac{\frac{lw_1^*|y}{\beta_5^*}}{\frac{(lw_1^*|y)^2}{\beta_5^{*2}} + (H_1-t)^2}}{\frac{(lw_1^*|y)^2}{\beta_5^{*2}} + (H_1-t)^2} - \frac{\frac{\frac{lw_3^*|y}{\beta_5^*}}{\frac{(lw_3^*|y)^2}{\beta_5^{*2}} + (H_1-t)^2}}{\frac{(lw_3^*|y)^2}{\beta_5^{*2}} + (H_1-t)^2} \right] \\ & - \gamma_{11}^* \left[\frac{\frac{\frac{lw_1^*|y}{\beta_5^*}}{\frac{(lw_1^*|y)^2}{\beta_5^{*2}} + (H_1+t)^2}}{\frac{(lw_1^*|y)^2}{\beta_5^{*2}} + (H_1+t)^2} - \frac{\frac{\frac{lw_3^*|y}{\beta_5^*}}{\frac{(lw_3^*|y)^2}{\beta_5^{*2}} + (H_1+t)^2}}{\frac{(lw_3^*|y)^2}{\beta_5^{*2}} + (H_1+t)^2} \right] \end{aligned} \quad (A.15d)$$

With the help of the following integrals:

$$\begin{aligned} \int_0^\infty S_1(t,y) \cos \alpha y dy &= -\frac{\pi \gamma_1 \beta_5}{2 |w_1|} (e^{-\alpha(H_1-t)\beta_5/|w_1|} - e^{-\alpha(H_1+t)\beta_5/|w_1|}) \\ &\quad + \frac{\pi \gamma_2 \gamma_{11} \beta_5}{2 \gamma_{12} |w_3|} (e^{-\alpha(H_1-t)\beta_5/|w_3|} - e^{-\alpha(H_1+t)\beta_5/|w_3|}) \end{aligned} \quad (A.16a)$$

$$\begin{aligned} \int_0^\infty S_2(t,y) \cos \alpha y dy &= -\frac{\pi \gamma_1^* \beta_5^*}{2 |w_1^*|} (e^{-\alpha(H_2-t)\beta_5^*/|w_1^*|} - e^{-\alpha(H_2+t)\beta_5^*/|w_1^*|}) \\ &\quad + \frac{\pi \gamma_2^* \gamma_{11}^* \beta_5^*}{2 \gamma_{12}^* |w_3^*|} (e^{-\alpha(H_2-t)\beta_5^*/|w_3^*|} - e^{-\alpha(H_2+t)\beta_5^*/|w_3^*|}) \end{aligned} \quad (A.16b)$$

$$\begin{aligned} \int_0^\infty S_3(t,y) \sin \alpha y dy &= +\frac{\pi \gamma_{11} \beta_5}{2 |w_1|} (e^{-\alpha(H_1-t)\beta_5/|w_1|} - e^{-\alpha(H_1+t)\beta_5/|w_1|}) \\ &\quad - \frac{\pi \gamma_{11} \beta_5}{2 |w_3|} (e^{-\alpha(H_1-t)\beta_5/|w_3|} - e^{-\alpha(H_1+t)\beta_5/|w_3|}) \end{aligned} \quad (A.16c)$$

$$\begin{aligned} \int_0^\infty S_4(t,y) \sin \alpha y dy &= +\frac{\pi \gamma_{11}^* \beta_5^*}{2 |w_1^*|} (e^{-\alpha(H_2-t)\beta_5^*/|w_1^*|} - e^{-\alpha(H_2+t)\beta_5^*/|w_1^*|}) \\ &\quad - \frac{\pi \gamma_{11}^* \beta_5^*}{2 |w_3^*|} (e^{-\alpha(H_2-t)\beta_5^*/|w_3^*|} - e^{-\alpha(H_2+t)\beta_5^*/|w_3^*|}) \end{aligned} \quad (A.16d)$$

$R_3(\alpha)$ and $R_4(\alpha)$ are finally reduced to:

$$\begin{aligned} R_3(a) &= \frac{1}{4\alpha\gamma_{13}} \int_{-a_1}^{a_1} \phi_1(t) \left[\frac{\gamma_1 \beta_5}{|w_1|} e^{-\alpha(H_1-t)\beta_5/|w_1|} - \frac{\gamma_2 \gamma_{11} \beta_5}{\gamma_{12} |w_3|} e^{-\alpha(H_1-t)\beta_5/|w_3|} \right] dt \\ &\quad + \frac{1}{4\alpha\gamma_{13}^*} \int_{-a_2}^{a_2} \phi_2(t) \lambda_1 \left[-\frac{\gamma_1^* \beta_5^*}{|w_1^*|} e^{-\alpha(H_2-t)\beta_5^*/|w_1^*|} + \frac{\gamma_2^* \gamma_{11}^* \beta_5^*}{\gamma_{12}^* |w_3^*|} e^{-\alpha(H_2-t)\beta_5^*/|w_3^*|} \right] dt \end{aligned} \quad (A.17a)$$

and

$$\begin{aligned} R_4(\alpha) &= \frac{1}{4\alpha\gamma_{13}} \int_{-a_1}^{a_1} \phi_1(t) \gamma_{11} \beta_5 \left[-\frac{1}{|w_1|} e^{-\alpha(H_1-t)\beta_5/|w_1|} + \frac{1}{|w_3|} e^{-\alpha(H_1-t)\beta_5/|w_3|} \right] dt \\ &\quad + \frac{1}{4\alpha\gamma_{13}^*} \int_{-a_2}^{a_2} \phi_2(t) \gamma_{11}^* \beta_5^* \lambda_2 \left[-\frac{1}{|w_1^*|} e^{-\alpha(H_2-t)\beta_5^*/|w_1^*|} + \frac{1}{|w_3^*|} e^{-\alpha(H_2-t)\beta_5^*/|w_3^*|} \right] dt \end{aligned} \quad (A.17b)$$

Appendix B

Definition of material constants for both layers. A superscript * will be used for the material in second layer.

$$\gamma_1 = 1 + \frac{v_{yx} w_1 \beta_9}{\beta_5} \quad \gamma_2 = 1 + \frac{v_{yx} w_3 \beta_{10}}{\beta_5} \quad \gamma_3 = w_1 + v_{xy} \beta_7 \quad \gamma_4 = w_3 + v_{yx} \beta_8$$

$$\gamma_5 = v_{xy} + \frac{\beta_9 w_1}{\beta_5} \quad \gamma_6 = v_{xy} + \frac{\beta_{10} w_3}{\beta_5} \quad \gamma_7 = v_{xy} w_1 + \beta_7 \quad \gamma_8 = v_{xy} w_3 + \beta_8$$

$$\gamma_9 = -1 + \beta_7 w_1 \quad \gamma_{10} = -1 + \beta_8 w_3 \quad \gamma_{11} = -\frac{|w_1|}{\beta_5} + \text{sign}(w_1) \beta_9$$

$$\gamma_{12} = \frac{|w_3|}{\beta_5} + \text{sign}(w_3) \beta_{10} \quad \gamma_{13} = \text{sign}(w_1) \beta_9 - \frac{\gamma_{11}}{\gamma_{12}} \text{sign}(w_3) \beta_{10}$$

$$\gamma_{14} = \frac{1}{2} \left[\frac{\gamma_5}{\gamma_{13}} - \frac{\gamma_6}{\gamma_{13}} \frac{\gamma_{11}}{\gamma_{12}} \right]$$

$$\lambda_1 = \frac{E_x^*}{E_x} \frac{1 - v_{xy} v_{yx}}{1 - v_{xy}^* v_{yx}^*}$$

$$\lambda_2 = \frac{G_{xy}^*}{G_{xy}}$$

$$\lambda_3 = \beta_8 \gamma_3 - \beta_7 \gamma_4$$

$$\lambda_4 = \lambda_1 \gamma_3^* \beta_7 - \beta_7^* \gamma_3$$

$$\lambda_5 = \lambda_1 \gamma_4^* \beta_7 - \beta_8^* \gamma_3$$

$$\lambda_6 = \gamma_9 - \gamma_{10}$$

$$\lambda_7 = \gamma_9 - \gamma_9^* \lambda_2$$

$$\lambda_8 = \gamma_9 - \gamma_{10}^* \lambda_2$$

$$\lambda_9 = \lambda_3 \lambda_7$$

$$\lambda_{10} = \lambda_3 \lambda_8$$

$$\lambda_{11} = \lambda_3 \gamma_9$$

$$\lambda_{12} = \lambda_6 \lambda_4$$

$$\lambda_{13} = \lambda_5 \lambda_6$$

$$\lambda_{14} = \lambda_6 \gamma_3$$

$$\lambda_{15} = \lambda_6 \beta_7$$

$$\lambda_{16} = \lambda_3 \beta_7$$

$$\lambda_{17} = \lambda_3 \beta_7^* + \lambda_4 \beta_8$$

$$\lambda_{18} = \lambda_4 \beta_7$$

$$\lambda_{19} = \lambda_3 \beta_8^* + \lambda_5 \beta_8$$

$$\lambda_{20} = \lambda_5 \beta_7$$

$$\lambda_{21} = \lambda_3 - \gamma_3 \beta_8$$

$$\lambda_{22} = \gamma_3 \beta_7$$

$$\lambda_{23} = \beta_7 \beta_8$$

$$\lambda_{24} = \lambda_{10} \lambda_{16} - \lambda_9 \lambda_{16}$$

$$\lambda_{25} = \lambda_{10} \lambda_{17}$$

$$\lambda_{26} = \lambda_{12} \lambda_{16} - \lambda_{10} \lambda_{18}$$

$$\lambda_{27} = \lambda_9 \lambda_{20} - \lambda_{13} \lambda_{16}$$

$$\lambda_{28} = \lambda_9 \lambda_{19}$$

$$\lambda_{29} = \lambda_{12} \lambda_{19} - \lambda_{13} \lambda_{17}$$

$$\lambda_{30} = \lambda_{13} \lambda_{18} - \lambda_{12} \lambda_{20}$$

$$\lambda_{31} = \lambda_{11} \lambda_{16} - \lambda_9 \lambda_{16}$$

$$\lambda_{32} = \lambda_{11} \lambda_{17}$$

$$\lambda_{33} = \lambda_{16} \lambda_{12} - \lambda_{11} \lambda_{18}$$

$$\lambda_{34} = \lambda_9 \lambda_{22} - \lambda_{14} \lambda_{16}$$

$$\lambda_{35} = \lambda_9 \lambda_{21}$$

$$\lambda_{36} = -\lambda_{14} \lambda_{17} - \lambda_{21} \lambda_{12}$$

$$\lambda_{37} = \lambda_{14} \lambda_{18} - \lambda_{22} \lambda_{12}$$

$$\lambda_{38} = \lambda_{15} \lambda_{16} - \beta_7 \beta_7 \lambda_9$$

$$\lambda_{39} = \lambda_9 \lambda_{23}$$

$$\lambda_{40} = \lambda_{15} \lambda_{17} - \lambda_{12} \lambda_{23}$$

$$\lambda_{41} = \beta_7 \beta_7 \lambda_{12} - \lambda_{15} \lambda_{18}$$

$$\lambda_{42} = \lambda_3 \lambda_{16}$$

$$\lambda_{43} = \lambda_3 \lambda_{17}$$

$$\lambda_{44} = \lambda_3 \lambda_{18}$$

$$\begin{aligned}
\lambda_{45} &= \lambda_{10}\lambda_{16} - \lambda_{11}\lambda_{16} & \lambda_{46} &= \lambda_{11}\lambda_{20} - \lambda_{13}\lambda_{16} & \lambda_{47} &= -\lambda_{11}\lambda_{19} \\
\lambda_{48} &= \lambda_{14}\lambda_{16} - \lambda_{10}\lambda_2 & \lambda_{49} &= \lambda_{13}\lambda_{22} - \lambda_{14}\lambda_{20} & \lambda_{50} &= -\lambda_{10}\lambda_{21} \\
\lambda_{51} &= \lambda_{14}\lambda_{19} + \lambda_{13}\lambda_{21} & \lambda_{52} &= \lambda_{10}\beta_7\beta_7 - \lambda_{15}\lambda_{16} & \lambda_{53} &= \lambda_{15}\lambda_{20} - \lambda_{13}\beta_7\beta_7 \\
\lambda_{54} &= -\lambda_{10}\lambda_{23} & \lambda_{55} &= \lambda_{13}\lambda_{23} - \lambda_{15}\lambda_{19} & \lambda_{56} &= -\lambda_3\lambda_{20} \\
\lambda_{57} &= \lambda_3\lambda_{19} & \lambda_{58} &= -\lambda_4\lambda_{16}(\lambda_8 - \gamma_9) & \lambda_{59} &= -\lambda_5\lambda_{16}(\gamma_9 - \lambda_7) \\
\lambda_{60} &= \gamma_9(\lambda_4\lambda_{19} - \lambda_5\lambda_{17}) & \lambda_{61} &= \gamma_3\beta_7(\lambda_{10} - \lambda_9) & \lambda_{62} &= \lambda_8(\gamma_3\lambda_{17} + \lambda_4\lambda_{21}) \\
\lambda_{63} &= -\lambda_9(\gamma_3\beta_8^* + \lambda_5) & \lambda_{64} &= -\beta_7\beta_7(\lambda_{10} - \lambda_9) & \lambda_{65} &= \lambda_8(\lambda_4\lambda_{23} - \beta_7\lambda_{17}) \\
\lambda_{66} &= \lambda_7(\beta_7\lambda_{19} - \lambda_5\lambda_{23}) & \lambda_{67} &= -\lambda_4\lambda_{16} & \lambda_{68} &= \lambda_5\lambda_{16} \\
\lambda_{69} &= \lambda_5\lambda_{17} - \lambda_4\lambda_{19} & \lambda_{70} &= \lambda_3(\beta_7^*(\lambda_{10} - \lambda_{11}) + \beta_8\lambda_4(\lambda_8 - \gamma_9)) \\
\lambda_{71} &= \lambda_3(\beta_8^*(\lambda_{11} - \lambda_9) + \beta_8\lambda_5(\gamma_9 - \lambda_7)) & \lambda_{72} &= \beta_7^*(\lambda_{11}\lambda_5 - \lambda_3\lambda_{13}) + \beta_8^*(\lambda_3\lambda_{12} - \lambda_{11}\lambda_4) \\
\lambda_{73} &= \lambda_{21}(\lambda_{10} - \lambda_9) & \lambda_{74} &= \lambda_{12}\lambda_3 - \lambda_{10}\lambda_4 + \beta_7^*(\lambda_{14}\lambda_3 - \lambda_{10}\gamma_3) \\
\lambda_{75} &= \lambda_9\lambda_5 - \lambda_{13}\lambda_3 + \beta_8^*(\lambda_9\gamma_3 - \lambda_{14}\lambda_3) & \lambda_{76} &= \lambda_{23}(\lambda_{10} - \lambda_9) \\
\lambda_{77} &= \beta_7^*(\lambda_{10}\beta_7 - \lambda_{15}\lambda_3) & \lambda_{78} &= \beta_8^*(\lambda_{15}\lambda_3 - \beta_7\lambda_9) \\
\lambda_{79} &= \lambda_3(\lambda_4\beta_8^* - \lambda_5\beta_7^*) & \lambda_{80} &= \lambda_{24} + \lambda_{25} + \lambda_{26} + \lambda_{27} - \lambda_{28} + \lambda_{29} \\
\lambda_{81} &= -\lambda_{70} - \lambda_{71} - \lambda_{72} + \text{sign}(w_1)\beta_9(\lambda_{73} + \lambda_{74} + \lambda_{75})
\end{aligned}$$

$$+ \frac{\beta_5\gamma_1}{|w_1|}(\lambda_{76} + \lambda_{77} + \lambda_{78}) - \frac{\gamma_{11}\beta_5}{|w_1|}(\lambda_{43} - \lambda_{57} + \lambda_{79})$$

$$\lambda_{82} = -\lambda_{58} - \lambda_{59} - \lambda_{60} + \text{sign}(w_1)\beta_9(\lambda_{61} + \lambda_{62} + \lambda_{63})$$

$$+ \frac{\beta_5\gamma_1}{|w_1|}(\lambda_{64} + \lambda_{65} + \lambda_{66}) - \frac{\gamma_{11}\beta_5}{|w_1|}(\lambda_{67} + \lambda_{68} + \lambda_{69})$$

$$\lambda_{83} = \frac{\gamma_{11}}{\gamma_{12}}(\lambda_{70} + \lambda_{71} + \lambda_{72}) - \frac{\gamma_{11}}{\gamma_{12}}\text{sign}(w_3)\beta_{10}(\lambda_{73} + \lambda_{74} + \lambda_{75})$$

$$- \frac{\gamma_{11}}{\gamma_{12}} \frac{\beta_5\gamma_2}{|w_3|}(\lambda_{76} + \lambda_{77} + \lambda_{78}) + \frac{\gamma_{11}\beta_5}{|w_3|}(\lambda_{43} - \lambda_{57} + \lambda_{79})$$

$$\lambda_{84} = \frac{\gamma_{11}}{\gamma_{12}}(\lambda_{58} + \lambda_{59} + \lambda_{60}) - \frac{\gamma_{11}}{\gamma_{12}}\text{sign}(w_3)\beta_{10}(\lambda_{61} + \lambda_{62} + \lambda_{63})$$

$$-\frac{\gamma_{11}}{\gamma_{12}} \frac{\beta_5 \gamma_2}{|w_3|} (\lambda_{64} + \lambda_{65} + \lambda_{66}) + \frac{\gamma_{11} \beta_5}{|w_3|} (\lambda_{67} + \lambda_{68} + \lambda_{69})$$

$$\lambda_{85} = \gamma_7 \lambda_{81} \frac{1}{\gamma_{13} \gamma_{14} \lambda_{80}} \quad \lambda_{86} = \gamma_8 \lambda_{82} \frac{1}{\gamma_{13} \gamma_{14} \lambda_{80}} \quad \lambda_{87} = \gamma_7 \lambda_{83} \frac{1}{\gamma_{13} \gamma_{14} \lambda_{80}} \quad \lambda_{88} = \gamma_7 \lambda_{84} \frac{1}{\gamma_{13} \gamma_{14} \lambda_{80}}$$

$$\lambda_{89} = -\lambda_{70} - \lambda_{71} - \lambda_{72} - \text{sign}(w_1^*) \beta_9^* (\lambda_{73} + \lambda_{74} + \lambda_{75})$$

$$-\lambda_1 \gamma_1^* \frac{\beta_5^*}{|w_1^*|} (\lambda_{76} + \lambda_{77} + \lambda_{78}) - \lambda_2 \gamma_{11}^* \frac{\beta_5^*}{|w_1^*|} (\lambda_{43} - \lambda_{57} + \lambda_{79})$$

$$\lambda_{90} = -\lambda_{58} - \lambda_{59} - \lambda_{60} - \text{sign}(w_1^*) \beta_9^* (\lambda_{61} + \lambda_{62} + \lambda_{63})$$

$$-\lambda_1 \gamma_1^* \frac{\beta_5^*}{|w_1^*|} (\lambda_{64} + \lambda_{65} + \lambda_{66}) - \lambda_2 \gamma_{11}^* \frac{\beta_5^*}{|w_1^*|} (\lambda_{67} + \lambda_{68} + \lambda_{69})$$

$$\lambda_{91} = \frac{\gamma_{11}^*}{\gamma_{12}^*} (\lambda_{70} + \lambda_{71} + \lambda_{72}) + \frac{\gamma_{11}^*}{\gamma_{12}^*} \text{sign}(w_3^*) \beta_{10}^* (\lambda_{73} + \lambda_{74} + \lambda_{75})$$

$$+ \lambda_1 \gamma_2^* \frac{\gamma_{11}^*}{\gamma_{12}^*} \frac{\beta_5^*}{|w_3^*|} (\lambda_{76} + \lambda_{77} + \lambda_{78}) + \lambda_2 \gamma_{11}^* \frac{\beta_5^*}{|w_3^*|} (\lambda_{43} - \lambda_{57} + \lambda_{79})$$

$$\lambda_{92} = \frac{\gamma_{11}^*}{\gamma_{12}^*} (\lambda_{58} + \lambda_{59} + \lambda_{60}) + \frac{\gamma_{11}^*}{\gamma_{12}^*} \text{sign}(w_3^*) \beta_{10}^* (\lambda_{61} + \lambda_{62} + \lambda_{63})$$

$$+ \lambda_1 \gamma_2^* \frac{\gamma_{11}^*}{\gamma_{12}^*} \frac{\beta_5^*}{|w_3^*|} (\lambda_{64} + \lambda_{65} + \lambda_{66}) + \lambda_2 \gamma_{11}^* \frac{\beta_5^*}{|w_3^*|} (\lambda_{67} + \lambda_{68} + \lambda_{69})$$

$$\lambda_{93} = \gamma_7 \lambda_{89} \frac{1}{\gamma_{13}^* \gamma_{14}^* \lambda_{80}} \quad \lambda_{94} = \gamma_8 \lambda_{90} \frac{1}{\gamma_{13}^* \gamma_{14}^* \lambda_{80}} \quad \lambda_{95} = \gamma_7 \lambda_{91} \frac{1}{\gamma_{13}^* \gamma_{14}^* \lambda_{80}} \quad \lambda_{96} = \gamma_8 \lambda_{92} \frac{1}{\gamma_{13}^* \gamma_{14}^* \lambda_{80}}$$

$$\lambda_{97} = -\lambda_{45} - \lambda_{46} - \lambda_{47} + \text{sign}(w_1) \beta_9 (\lambda_{48} + \lambda_{50} + \lambda_{51})$$

$$+ \frac{\beta_5 \gamma_1}{|w_1|} (\lambda_{52} + \lambda_{54} + \lambda_{55}) - \frac{\gamma_{11} \beta_5}{|w_1|} (\lambda_{42} + \lambda_{56} + \lambda_{57})$$

$$\lambda_{98} = -\lambda_{31} - \lambda_{32} - \lambda_{33} + \text{sign}(w_1) \beta_9 (\lambda_{34} + \lambda_{35} + \lambda_{36})$$

$$+ \frac{\beta_5 \gamma_1}{|w_1|} (\lambda_{38} + \lambda_{39} + \lambda_{40}) - \frac{\gamma_{11} \beta_5}{|w_1|} (\lambda_{42} + \lambda_{43} + \lambda_{44})$$

$$\lambda_{99} = \frac{\gamma_{11}}{\gamma_{12}}(\lambda_{45} + \lambda_{46} + \lambda_{47}) - \frac{\gamma_{11}}{\gamma_{12}}\text{sign}(w_3)\beta_{10}(\lambda_{48} + \lambda_{50} + \lambda_{51})$$

$$- \frac{\gamma_{11}}{\gamma_{12}} \frac{\beta_5 \gamma_2}{|w_3|}(\lambda_{52} + \lambda_{54} + \lambda_{55}) + \frac{\gamma_{11}\beta_5}{|w_3|}(\lambda_{42} + \lambda_{56} + \lambda_{57})$$

$$\lambda_{100} = \frac{\gamma_{11}}{\gamma_{12}}(\lambda_{31} + \lambda_{32} + \lambda_{33}) - \frac{\gamma_{11}}{\gamma_{12}}\text{sign}(w_3)\beta_{10}(\lambda_{34} + \lambda_{35} + \lambda_{36})$$

$$- \frac{\gamma_{11}}{\gamma_{12}} \frac{\beta_5 \gamma_2}{|w_3|}(\lambda_{38} + \lambda_{39} + \lambda_{40}) + \frac{\gamma_{11}\beta_5}{|w_3|}(-\lambda_{42} - \lambda_{43} + \lambda_{44})$$

$$\lambda_{101} = \lambda_{97}\gamma_7^* \frac{1}{\gamma_{13}\gamma_{14}^*\lambda_{80}} \quad \lambda_{102} = \lambda_{98}\gamma_8^* \frac{1}{\gamma_{13}\gamma_{14}^*\lambda_{80}}$$

$$\lambda_{103} = \lambda_{99}\gamma_7^* \frac{1}{\gamma_{13}\gamma_{14}^*\lambda_{80}} \quad \lambda_{104} = \lambda_{100}\gamma_8^* \frac{1}{\gamma_{13}\gamma_{14}^*\lambda_{80}}$$

$$\lambda_{105} = -\lambda_{45} - \lambda_{46} - \lambda_{47} - \text{sign}(w_1^*)\beta_9^*(\lambda_{48} + \lambda_{50} + \lambda_{51})$$

$$- \lambda_1\gamma_1^* \frac{\beta_5^*}{|w_1^*|}(\lambda_{52} + \lambda_{54} + \lambda_{55}) - \lambda_2\gamma_{11}^* \frac{\beta_5^*}{|w_1^*|}(\lambda_{42} + \lambda_{56} + \lambda_{57})$$

$$\lambda_{106} = -\lambda_{31} - \lambda_{32} - \lambda_{33} - \text{sign}(w_1^*)\beta_9^*(\lambda_{34} + \lambda_{35} + \lambda_{36})$$

$$- \lambda_1\gamma_1^* \frac{\beta_5^*}{|w_1^*|}(\lambda_{38} + \lambda_{39} + \lambda_{40}) - \lambda_2\gamma_{11}^* \frac{\beta_5^*}{|w_1^*|}(-\lambda_{42} - \lambda_{43} + \lambda_{44})$$

$$\lambda_{107} = \frac{\gamma_{11}^*}{\gamma_{12}^*}(\lambda_{45} + \lambda_{46} + \lambda_{47}) + \frac{\gamma_{11}^*}{\gamma_{12}^*}\text{sign}(w_3^*)\beta_{10}^*(\lambda_{48} + \lambda_{50} + \lambda_{51})$$

$$+ \lambda_1\gamma_2^* \frac{\gamma_{11}^* \beta_5^*}{\gamma_{12}^* |w_3^*|}(\lambda_{52} + \lambda_{54} + \lambda_{55}) + \lambda_2\gamma_{11}^* \frac{\beta_5^*}{|w_3^*|}(\lambda_{42} + \lambda_{56} + \lambda_{57})$$

$$\lambda_{108} = \frac{\gamma_{11}^*}{\gamma_{12}^*}(\lambda_{31} + \lambda_{32} + \lambda_{33}) + \frac{\gamma_{11}^*}{\gamma_{12}^*}\text{sign}(w_3^*)\beta_{10}^*(\lambda_{34} + \lambda_{35} + \lambda_{36})$$

$$+ \lambda_1\gamma_2^* \frac{\gamma_{11}^* \beta_5^*}{\gamma_{12}^* |w_3^*|}(\lambda_{38} + \lambda_{39} + \lambda_{40}) + \lambda_2\gamma_{11}^* \frac{\beta_5^*}{|w_3^*|}(-\lambda_{42} - \lambda_{43} + \lambda_{44}) \quad 1$$

$$\lambda_{109} = \lambda_{105} \gamma_7^* \frac{1}{\gamma_{13}^* \gamma_{14}^* \lambda_{80}}$$

$$\lambda_{110} = \lambda_{106} \gamma_8^* \frac{1}{\gamma_{13}^* \gamma_{14}^* \lambda_{80}}$$

$$\lambda_{111} = \lambda_{107} \gamma_7^* \frac{1}{\gamma_{13}^* \gamma_{14}^* \lambda_{80}}$$

$$\lambda_{112} = \lambda_{108} \gamma_8^* \frac{1}{\gamma_{13}^* \gamma_{14}^* \lambda_{80}}$$

$$\rho_5 = \frac{\gamma_3 \lambda_{81} + \gamma_4 \lambda_{82}}{\pi \gamma_{13} \lambda_{80}}$$

$$\rho_6 = \frac{\gamma_3 \lambda_{83} + \gamma_4 \lambda_{84}}{\pi \gamma_{13} \lambda_{80}}$$

$$\rho_7 = \frac{\gamma_3 \lambda_{89} + \gamma_4 \lambda_{90}}{\pi \gamma_{13}^* \lambda_{80}}$$

$$\rho_8 = \frac{\gamma_3 \lambda_{91} + \gamma_4 \lambda_{92}}{\pi \gamma_{13}^* \lambda_{80}}$$

$$\rho_9 = \frac{\gamma_9 \lambda_{81} + \gamma_{10} \lambda_{82}}{\pi \gamma_{13} \lambda_{80}}$$

$$\rho_{10} = \frac{\gamma_9 \lambda_{83} + \gamma_{10} \lambda_{84}}{\pi \gamma_{13} \lambda_{80}}$$

$$\rho_{11} = \frac{\gamma_9 \lambda_{89} + \gamma_{10} \lambda_{90}}{\pi \gamma_{13}^* \lambda_{80}}$$

$$\rho_{12} = \frac{\gamma_9 \lambda_{91} + \gamma_{10} \lambda_{92}}{\pi \gamma_{13}^* \lambda_{80}}$$

$$\rho_{13} = \frac{\gamma_7 (\lambda_{73} + \lambda_{74} + \lambda_{75})}{\pi \gamma_{14} \lambda_{80}}$$

$$\rho_{14} = \frac{\gamma_8 (\lambda_{61} + \lambda_{62} + \lambda_{63})}{\pi \gamma_{14} \lambda_{80}}$$

$$\rho_{15} = \frac{\gamma_7 (\lambda_{70} + \lambda_{71} + \lambda_{72})}{\pi \gamma_{14} \lambda_{80}}$$

$$\rho_{16} = \frac{\gamma_8 (\lambda_{58} + \lambda_{59} + \lambda_{60})}{\pi \gamma_{14} \lambda_{80}}$$

$$\rho_{17} = \frac{\gamma_7^* (\lambda_{48} + \lambda_{50} + \lambda_{51})}{\pi \gamma_{14}^* \lambda_{80}}$$

$$\rho_{18} = \frac{\gamma_8^* (\lambda_{34} + \lambda_{35} + \lambda_{36})}{\pi \gamma_{14}^* \lambda_{80}}$$

$$\rho_{19} = \frac{\gamma_7^* (\lambda_{45} + \lambda_{46} + \lambda_{47})}{\pi \gamma_{14}^* \lambda_{80}}$$

$$\rho_{20} = \frac{\gamma_8^* (\lambda_{31} + \lambda_{32} + \lambda_{33})}{\pi \gamma_{14}^* \lambda_{80}}$$

Appendix C

$$f_1(\alpha) = \tanh(w^*_1 \alpha H_2) \tanh(w^*_3 \alpha H_2) \quad f_2(\alpha) = \tanh(w^*_3 \alpha H_2) \tanh(w_1 \alpha H_1)$$

$$f_3(\alpha) = \tanh(w^*_3 \alpha H_2) \tanh(w_3 \alpha H_1) \quad f_4(\alpha) = \tanh(w^*_1 \alpha H_2) \tanh(w_3 \alpha H_1)$$

$$f_5(\alpha) = \tanh(w^*_1 \alpha H_2) \tanh(w_1 \alpha H_1) \quad f_6(\alpha) = \tanh(w_1 \alpha H_1) \tanh(w_3 \alpha H_1)$$

$$f(\alpha) = \lambda_{24} f_1(\alpha) + \lambda_{25} f_2(\alpha) + \lambda_{26} f_3(\alpha) + \lambda_{27} f_4(\alpha) - \lambda_{28} f_5(\alpha) + \lambda_{29} f_6(\alpha)$$

$$g_1(\alpha) = \lambda_{70} \tanh(w^*_3 \alpha H_2) + \lambda_{71} \tanh(w^*_1 \alpha H_2) + \lambda_{72} \tanh(w_3 \alpha H_1)$$

$$h_1(\alpha) = \lambda_{73} f_1(\alpha) + \lambda_{74} f_3(\alpha) + \lambda_{75} f_4(\alpha)$$

$$m_1(\alpha) = \lambda_{76} f_1(\alpha) + \lambda_{77} f_3(\alpha) + \lambda_{78} f_4(\alpha)$$

$$n_1(\alpha) = \lambda_{43} \tanh(w^*_3 \alpha H_2) - \lambda_{57} \tanh(w^*_1 \alpha H_2) + \lambda_{79} \tanh(w_3 \alpha H_1)$$

$$g_2(\alpha) = \lambda_{58} \tanh(w^*_3 \alpha H_2) + \lambda_{59} \tanh(w^*_1 \alpha H_2) + \lambda_{60} \tanh(w_1 \alpha H_1)$$

$$h_2(\alpha) = \lambda_{61} f_1(\alpha) + \lambda_{62} f_2(\alpha) + \lambda_{63} f_5(\alpha)$$

$$m_2(\alpha) = \lambda_{64} f_1(\alpha) + \lambda_{65} f_2(\alpha) + \lambda_{66} f_5(\alpha)$$

$$n_2(\alpha) = \lambda_{67} \tanh(w^*_3 \alpha H_2) + \lambda_{68} \tanh(w^*_1 \alpha H_2) + \lambda_{69} \tanh(w_1 \alpha H_1)$$

$$g_3(\alpha) = \lambda_{45} \tanh(w^*_3 \alpha H_2) + \lambda_{46} \tanh(w_3 \alpha H_1) + \lambda_{47} \tanh(w_1 \alpha H_1)$$

$$h_3(\alpha) = \lambda_{48} f_3(\alpha) + \lambda_{50} f_2(\alpha) + \lambda_{51} f_6(\alpha)$$

$$m_3(\alpha) = \lambda_{52} f_3(\alpha) + \lambda_{54} f_2(\alpha) + \lambda_{55} f_6(\alpha)$$

$$n_3(\alpha) = \lambda_{42} \tanh(w^*_3 \alpha H_2) + \lambda_{56} \tanh(w_3 \alpha H_1) + \lambda_{57} \tanh(w_1 \alpha H_1)$$

$$g_4(\alpha) = \lambda_{31} \tanh(w^*_1 \alpha H_2) + \lambda_{32} \tanh(w_1 \alpha H_1) + \lambda_{33} \tanh(w_3 \alpha H_1)$$

$$h_4(\alpha) = \lambda_{34} f_4(\alpha) + \lambda_{35} f_5(\alpha) + \lambda_{36} f_6(\alpha)$$

$$m_4(\alpha) = \lambda_{38} f_4(\alpha) + \lambda_{39} f_5(\alpha) + \lambda_{40} f_6(\alpha)$$

$$n_4(\alpha) = -\lambda_{42} \tanh(w^*_1 \alpha H_2) - \lambda_{43} \tanh(w_1 \alpha H_1) + \lambda_{44} \tanh(w_3 \alpha H_1)$$

$$\begin{aligned} k_1(x_1, \alpha) = & \frac{\gamma_7 \cosh(w_1 \alpha x_1)}{2 \cosh(w_1 \alpha H_1) f(\alpha) \gamma_{13}} [-g_1(\alpha) + \text{sign}(w_1) \beta_9 h_1(\alpha) \\ & + \frac{\gamma_1 \beta_5}{|w_1|} m_1(\alpha) - \frac{\gamma_{11} \beta_5}{|w_1|} n_1(\alpha)] + \frac{\gamma_8 \cosh(w_3 \alpha x_1)}{2 \cosh(w_3 \alpha H_1) f(\alpha) \gamma_{13}} [-g_2(\alpha) \\ & + \text{sign}(w_1) \beta_9 h_2(\alpha) + \frac{\gamma_1 \beta_5}{|w_1|} m_2(\alpha) - \frac{\gamma_{11} \beta_5}{|w_1|} n_2(\alpha)] \end{aligned}$$

$$k_2(x_1, \alpha) = \frac{\gamma_7 \cosh(w_1 \alpha x_1)}{2 \cosh(w_1 \alpha H_1) f(\alpha) \gamma_{13}} \left[\frac{\gamma_{11}}{\gamma_{12}} g_1(\alpha) - \frac{\gamma_{11}}{\gamma_{12}} \text{sign}(w_3) \beta_{10} h_1(\alpha) \right. \\ \left. - \frac{\gamma_{11} \gamma_2 \beta_5}{\gamma_{12} |w_3|} m_1(\alpha) + \frac{\gamma_{11} \beta_5}{|w_3|} n_1(\alpha) \right] + \frac{\gamma_8 \cosh(w_3 \alpha x_1)}{2 \cosh(w_3 \alpha H_1) f(\alpha) \gamma_{13}} \left[\frac{\gamma_{11}}{\gamma_{12}} g_2(\alpha) \right. \\ \left. - \frac{\gamma_{11}}{\gamma_{12}} \text{sign}(w_3) \beta_{10} h_2(\alpha) - \frac{\gamma_{11} \gamma_2 \beta_5}{\gamma_{12} |w_3|} m_2(\alpha) + \frac{\gamma_{11} \beta_5}{|w_3|} n_2(\alpha) \right]$$

$$k_3(x_1, \alpha) = \frac{\gamma_7 \cosh(w_1 \alpha x_1)}{2 \cosh(w_1 \alpha H_1) f(\alpha) \gamma_{13}^*} \left[-g_1(\alpha) - \text{sign}(w_1^*) \beta_9^* h_1(\alpha) \right. \\ \left. - \frac{\gamma_1^* \lambda_1 \beta_5^*}{|w_1^*|} m_1(\alpha) - \frac{\gamma_{11}^* \lambda_2 \beta_5^*}{|w_1^*|} n_1(\alpha) \right] + \frac{\gamma_8 \cosh(w_3 \alpha x_1)}{2 \cosh(w_3 \alpha H_1) f(\alpha) \gamma_{13}^*} \left[-g_2(\alpha) \right. \\ \left. - \text{sign}(w_1^*) \beta_9^* h_2(\alpha) - \frac{\gamma_1^* \lambda_1 \beta_5^*}{|w_1^*|} m_2(\alpha) - \frac{\gamma_{11}^* \lambda_2 \beta_5^*}{|w_1^*|} n_2(\alpha) \right]$$

$$k_4(x_1, \alpha) = \frac{\gamma_7 \cosh(w_1 \alpha x_1)}{2 \cosh(w_1 \alpha H_1) f(\alpha) \gamma_{13}^*} \left[\frac{\gamma_{11}^*}{\gamma_{12}^*} g_1(\alpha) + \frac{\gamma_{11}^*}{\gamma_{12}^*} \text{sign}(w_3^*) \beta_{10}^* h_1(\alpha) \right. \\ \left. + \frac{\gamma_{11}^* \gamma_2^* \lambda_1 \beta_5^*}{\gamma_{12}^* |w_3^*|} m_1(\alpha) + \frac{\gamma_{11}^* \lambda_2 \beta_5^*}{|w_1^*|} n_1(\alpha) \right] + \frac{\gamma_8 \cosh(w_3 \alpha x_1)}{2 \cosh(w_3 \alpha H_1) f(\alpha) \gamma_{13}^*} \left[\frac{\gamma_{11}^*}{\gamma_{12}^*} g_2(\alpha) \right. \\ \left. + \frac{\gamma_{11}^*}{\gamma_{12}^*} \text{sign}(w_3^*) \beta_{10}^* h_2(\alpha) + \frac{\gamma_{11}^* \gamma_2^* \lambda_1 \beta_5^*}{\gamma_{12}^* |w_3^*|} m_2(\alpha) + \frac{\gamma_{11}^* \lambda_2 \beta_5^*}{|w_3^*|} n_2(\alpha) \right]$$

$$J_1(x_1, \alpha) = \frac{\gamma_7 \cosh(w_1 \alpha x_1) h_1(\alpha)}{\cosh(w_1 \alpha H_1) f(\alpha)} \quad J_2(x_1, \alpha) = \frac{\gamma_8 \cosh(w_3 \alpha x_1) h_2(\alpha)}{\cosh(w_3 \alpha H_1) f(\alpha)}$$

$$J_3(x_1, \alpha) = -\frac{\gamma_7 \cosh(w_1 \alpha x_1) g_1(\alpha)}{\cosh(w_1 \alpha H_1) f(\alpha)} \quad J_4(x_1, \alpha) = -\frac{\gamma_8 \cosh(w_3 \alpha x_1) g_2(\alpha)}{\cosh(w_3 \alpha H_1) f(\alpha)}$$

$$k_5(x_2, \alpha) = \frac{\gamma_7^* \cosh(w_1^* \alpha x_2)}{2 \cosh(w_1^* \alpha H_2) f(\alpha) \gamma_{13}} \left[-g_3(\alpha) + \text{sign}(w_1) \beta_9 h_3(\alpha) \right. \\ \left. + \frac{\gamma_1 \beta_5}{|w_1|} m_3(\alpha) - \frac{\gamma_{11} \beta_5}{|w_1|} n_3(\alpha) \right] + \frac{\gamma_8^* \cosh(w_3^* \alpha x_2)}{2 \cosh(w_3^* \alpha H_2) f(\alpha) \gamma_{13}} \left[-g_4(\alpha) \right. \\ \left. + \text{sign}(w_1) \beta_9 h_4(\alpha) + \frac{\gamma_1 \beta_5}{|w_1|} m_4(\alpha) - \frac{\gamma_{11} \beta_5}{|w_1|} n_4(\alpha) \right]$$

$$k_6(x_2, \alpha) = \frac{\gamma_7^* \cosh(w_1^* \alpha x_2)}{2 \cosh(w_1^* \alpha H_2) f(\alpha) \gamma_{13}} \left[\frac{\gamma_{11}}{\gamma_{12}} g_3(\alpha) - \frac{\gamma_{11}}{\gamma_{12}} \text{sign}(w_3) \beta_{10} h_3(\alpha) \right. \\ \left. - \frac{\gamma_{11} \gamma_2 \beta_5}{\gamma_{12} |w_3|} m_3(\alpha) + \frac{\gamma_{11} \beta_5}{|w_3|} n_3(\alpha) \right] + \frac{\gamma_8^* \cosh(w_3^* \alpha x_2)}{2 \cosh(w_3^* \alpha H_2) f(\alpha) \gamma_{13}} \left[\frac{\gamma_{11}}{\gamma_{12}} g_4(\alpha) \right. \\ \left. - \frac{\gamma_{11}}{\gamma_{12}} \text{sign}(w_3) \beta_{10} h_4(\alpha) - \frac{\gamma_{11} \gamma_2 \beta_5}{\gamma_{12} |w_3|} m_4(\alpha) + \frac{\gamma_{11} \beta_5}{|w_3|} n_4(\alpha) \right]$$

$$k_7(x_2, \alpha) = \frac{\gamma_7^* \cosh(w_1^* \alpha x_2)}{2 \cosh(w_1^* \alpha H_2) f(\alpha) \gamma_{13}^*} [-g_3(\alpha) - \text{sign}(w_1^*) \beta_9^* h_3(\alpha) - \frac{\gamma_1^* \lambda_1 \beta_5^*}{|w_1^*|} m_3(\alpha) - \frac{\gamma_{11}^* \lambda_2 \beta_5^*}{|w_1^*|} n_3(\alpha)] + \frac{\gamma_8^* \cosh(w_3^* \alpha x_2)}{2 \cosh(w_3^* \alpha H_2) f(\alpha) \gamma_{13}^*} [-g_4(\alpha) - \text{sign}(w_1^*) \beta_9^* h_4(\alpha) - \frac{\gamma_1^* \lambda_1 \beta_5^*}{|w_1^*|} m_4(\alpha) - \frac{\gamma_{11}^* \lambda_2 \beta_5^*}{|w_1^*|} n_4(\alpha)]$$

$$k_8(x_2, \alpha) = \frac{\gamma_7^* \cosh(w_1^* \alpha x_2)}{2 \cosh(w_1^* \alpha H_2) f(\alpha) \gamma_{13}^*} [\frac{\gamma_{11}^*}{\gamma_{12}^*} g_3(\alpha) + \frac{\gamma_{11}^*}{\gamma_{12}^*} \text{sign}(w_3^*) \beta_{10}^* h_3(\alpha) + \frac{\gamma_{11}^* \gamma_2^* \lambda_1 \beta_5^*}{\gamma_{12}^* |w_3^*|} m_3(\alpha) + \frac{\gamma_{11}^* \lambda_2 \beta_5^*}{|w_1^*|} n_3(\alpha)] + \frac{\gamma_8^* \cosh(w_3^* \alpha x_2)}{2 \cosh(w_3^* \alpha H_2) f(\alpha) \gamma_{13}^*} [\frac{\gamma_{11}^*}{\gamma_{12}^*} g_4(\alpha) + \frac{\gamma_{11}^*}{\gamma_{12}^*} \text{sign}(w_3^*) \beta_{10}^* h_4(\alpha) + \frac{\gamma_{11}^* \gamma_2^* \lambda_1 \beta_5^*}{\gamma_{12}^* |w_3^*|} m_4(\alpha) + \frac{\gamma_{11}^* \lambda_2 \beta_5^*}{|w_3^*|} n_4(\alpha)]$$

$$J_5(x_2, \alpha) = \frac{\gamma_7^* \cosh(w_1^* \alpha x_2) h_3(\alpha)}{\cosh(w_1^* \alpha H_2) f(\alpha)} \quad J_6(x_2, \alpha) = \frac{\gamma_8^* \cosh(w_3^* \alpha x_2) h_4(\alpha)}{\cosh(w_3^* \alpha H_2) f(\alpha)}$$

$$J_7(x_2, \alpha) = - \frac{\gamma_7^* \cosh(w_1^* \alpha x_2) g_3(\alpha)}{\cosh(w_1^* \alpha H_2) f(\alpha)} \quad J_8(x_2, \alpha) = - \frac{\gamma_8^* \cosh(w_3^* \alpha x_2) g_4(\alpha)}{\cosh(w_3^* \alpha H_2) f(\alpha)}$$

$$k_9(y, x_1, \alpha) = \frac{\gamma_3 \cos \alpha y \cosh(w_1 \alpha x_1)}{2 f(\alpha) \gamma_{13} \cosh(w_1 \alpha H_1)} [-g_1(\alpha) + \text{sign}(w_1) \beta_9 h_1(\alpha) + \frac{\gamma_1 \beta_5}{|w_1|} m_1(\alpha) - \frac{\gamma_{11} \beta_5}{|w_1|} n_1(\alpha)] + \frac{\gamma_4 \cos \alpha y \cosh(w_3 \alpha x_1)}{2 f(\alpha) \gamma_{13} \cosh(w_3 \alpha H_1)} [-g_2(\alpha) + \text{sign}(w_1) \beta_9 h_2(\alpha) + \frac{\gamma_1 \beta_5}{|w_1|} m_2(\alpha) - \frac{\gamma_{11} \beta_5}{|w_1|} n_2(\alpha)]$$

$$k_{10}(y, x_1, \alpha) = \frac{\gamma_3 \cos \alpha y \cosh(w_1 \alpha x_1)}{2 f(\alpha) \gamma_{13} \cosh(w_1 \alpha H_1)} [\frac{\gamma_{11}}{\gamma_{12}} g_1(\alpha) - \frac{\gamma_{11}}{\gamma_{12}} \text{sign}(w_3) \beta_{10} h_1(\alpha) - \frac{\gamma_{11} \gamma_2 \beta_5}{\gamma_{12} |w_3|} m_1(\alpha) + \frac{\gamma_{11} \beta_5}{|w_3|} n_1(\alpha)] + \frac{\gamma_4 \cos \alpha y \cosh(w_3 \alpha x_1)}{2 f(\alpha) \gamma_{13} \cosh(w_3 \alpha H_1)} [\frac{\gamma_{11}}{\gamma_{12}} g_2(\alpha) - \frac{\gamma_{11}}{\gamma_{12}} \text{sign}(w_3) \beta_{10} h_2(\alpha) - \frac{\gamma_{11} \gamma_2 \beta_5}{\gamma_{12} |w_3|} m_2(\alpha) + \frac{\gamma_{11} \beta_5}{|w_3|} n_2(\alpha)]$$

$$k_{11}(y, x_1, \alpha) = \frac{\gamma_3 \cos \alpha y \cosh(w_1 \alpha x_1)}{2 f(\alpha) \gamma_{13}^* \cosh(w_1 \alpha H_1)} [-g_1(\alpha) - \text{sign}(w_1^*) \beta_9^* h_1(\alpha)]$$

$$- \frac{\gamma_1^* \lambda_1 \beta_5^*}{|w_1^*|} m_1(\alpha) - \frac{\gamma_{11}^* \lambda_2 \beta_5^*}{|w_1^*|} n_1(\alpha) \Big] + \frac{\gamma_4 \cos \alpha y}{2f(\alpha) \gamma_{13}^* \cosh(w_3 \alpha H_1)} \Big[-g_2(\alpha) \\ - \operatorname{sign}(w_1^*) \beta_9^* h_2(\alpha) - \frac{\gamma_1^* \lambda_1 \beta_5^*}{|w_1^*|} m_2(\alpha) - \frac{\gamma_{11}^* \lambda_2 \beta_5^*}{|w_1^*|} n_2(\alpha) \Big]$$

$$k_{12}(y, x_1, \alpha) = \frac{\gamma_3 \cos \alpha y}{2f(\alpha) \gamma_{13}^* \cosh(w_1 \alpha H_1)} \Big[\frac{\gamma_{11}^*}{\gamma_{12}^*} g_1(\alpha) + \frac{\gamma_{11}^*}{\gamma_{12}^*} \operatorname{sign}(w_3^*) \beta_{10}^* h_1(\alpha) \\ + \frac{\gamma_{11}^* \gamma_2^* \lambda_1 \beta_5^*}{\gamma_{12}^* |w_3^*|} m_1(\alpha) + \frac{\gamma_{11}^* \lambda_2 \beta_5^*}{|w_1^*|} n_1(\alpha) \Big] + \frac{\gamma_4 \cos \alpha y}{2f(\alpha) \gamma_{13}^* \cosh(w_3 \alpha H_1)} \Big[\frac{\gamma_{11}^*}{\gamma_{12}^*} g_2(\alpha) \\ + \frac{\gamma_{11}^*}{\gamma_{12}^*} \operatorname{sign}(w_3^*) \beta_{10}^* h_2(\alpha) + \frac{\gamma_{11}^* \gamma_2^* \lambda_1 \beta_5^*}{\gamma_{12}^* |w_3^*|} m_2(\alpha) + \frac{\gamma_{11}^* \lambda_2 \beta_5^*}{|w_3^*|} n_2(\alpha) \Big]$$

$$J_9(y, \alpha) = \frac{\gamma_3 h_1(\alpha)}{f(\alpha)} \cos \alpha y$$

$$J_{10}(y, \alpha) = \frac{\gamma_4 h_2(\alpha)}{f(\alpha)} \cos \alpha y$$

$$J_{11}(y, \alpha) = -\frac{\gamma_3 g_1(\alpha)}{f(\alpha)} \cos \alpha y$$

$$J_{12}(y, \alpha) = -\frac{\gamma_4 g_2(\alpha)}{f(\alpha)} \cos \alpha y$$

$$k_{13}(y, x_1, \alpha) = \frac{\gamma_9 \sin \alpha y}{2f(\alpha) \gamma_{13} \sinh(w_1 \alpha H_1)} \Big[-g_1(\alpha) + \operatorname{sign}(w_1) \beta_9 h_1(\alpha) + \frac{\gamma_1 \beta_5}{|w_1|} m_1(\alpha) \\ - \frac{\gamma_{11} \beta_5}{|w_1|} n_1(\alpha) \Big] + \frac{\gamma_{10} \sin \alpha y}{2f(\alpha) \gamma_{13} \sinh(w_3 \alpha H_1)} \Big[-g_2(\alpha) + \operatorname{sign}(w_1) \beta_9 h_2(\alpha) \\ + \frac{\gamma_1 \beta_5}{|w_1|} m_2(\alpha) - \frac{\gamma_{11} \beta_5}{|w_1|} n_2(\alpha) \Big]$$

$$k_{14}(y, x_1, \alpha) = \frac{\gamma_9 \sin \alpha y}{2f(\alpha) \gamma_{13} \sinh(w_1 \alpha H_1)} \Big[\frac{\gamma_{11}}{\gamma_{12}} g_1(\alpha) - \frac{\gamma_{11}}{\gamma_{12}} \operatorname{sign}(w_3) \beta_{10} h_1(\alpha) \\ - \frac{\gamma_{11} \gamma_2 \beta_5}{\gamma_{12} |w_3|} m_1(\alpha) + \frac{\gamma_{11} \beta_5}{|w_3|} n_1(\alpha) \Big] + \frac{\gamma_{10} \sin \alpha y}{2f(\alpha) \gamma_{13} \sinh(w_3 \alpha H_1)} \Big[\frac{\gamma_{11}}{\gamma_{12}} g_2(\alpha) \\ - \frac{\gamma_{11}}{\gamma_{12}} \operatorname{sign}(w_3) \beta_{10} h_2(\alpha) - \frac{\gamma_{11} \gamma_2 \beta_5}{\gamma_{12} |w_3|} m_2(\alpha) + \frac{\gamma_{11} \beta_5}{|w_3|} n_2(\alpha) \Big]$$

$$k_{15}(y, x_1, \alpha) = \frac{\gamma_9 \sin \alpha y}{2f(\alpha) \gamma_{13}^* \sinh(w_1 \alpha H_1)} \Big[-g_1(\alpha) - \operatorname{sign}(w_1^*) \beta_9^* h_1(\alpha)$$

$$\begin{aligned}
& - \frac{\gamma_1^* \lambda_1 \beta_5^*}{|w_1^*|} m_1(\alpha) - \frac{\gamma_{11}^* \lambda_2 \beta_5^*}{|w_1^*|} n_1(\alpha)] + \frac{\gamma_{10} \sin \alpha y}{2f(\alpha) \gamma_{13}^* \sinh(w_3 \alpha H_1)} [-g_2(\alpha) \\
& - \text{sign}(w_1^*) \beta_9^* h_2(\alpha) - \frac{\gamma_1^* \lambda_1 \beta_5^*}{|w_1^*|} m_2(\alpha) - \frac{\gamma_{11}^* \lambda_2 \beta_5^*}{|w_1^*|} n_2(\alpha)]
\end{aligned}$$

$$\begin{aligned}
k_{16}(y, x_1, \alpha) = & \frac{\gamma_9 \sin \alpha y}{2f(\alpha) \gamma_{13}^* \sinh(w_1 \alpha H_1)} [\frac{\gamma_{11}^*}{\gamma_{12}^*} g_1(\alpha) + \frac{\gamma_{11}^*}{\gamma_{12}^*} \text{sign}(w_3^*) \beta_{10}^* h_1(\alpha) \\
& + \frac{\gamma_{11}^* \gamma_2^* \lambda_1 \beta_5^*}{\gamma_{12}^* |w_3^*|} m_1(\alpha) + \frac{\gamma_{11}^* \lambda_2 \beta_5^*}{|w_3^*|} n_1(\alpha)] + \frac{\gamma_{10} \sin \alpha y}{2f(\alpha) \gamma_{13}^* \sinh(w_3 \alpha H_1)} [\frac{\gamma_{11}^*}{\gamma_{12}^*} g_2(\alpha) \\
& + \frac{\gamma_{11}^*}{\gamma_{12}^*} \text{sign}(w_3^*) \beta_{10}^* h_2(\alpha) + \frac{\gamma_{11}^* \gamma_2^* \lambda_1 \beta_5^*}{\gamma_{12}^* |w_3^*|} m_2(\alpha) - \frac{\gamma_{11}^* \lambda_2 \beta_5^*}{|w_3^*|} n_2(\alpha)]
\end{aligned}$$

$$J_{13}(y, \alpha) = \frac{\gamma_9 h_1(\alpha)}{f(\alpha)} \sin \alpha y$$

$$J_{14}(y, \alpha) = \frac{\gamma_{10} h_2(\alpha)}{f(\alpha)} \sin \alpha y$$

$$J_{15}(y, \alpha) = - \frac{\gamma_9 g_1(\alpha)}{f(\alpha)} \sin \alpha y$$

$$J_{16}(y, \alpha) = - \frac{\gamma_{10} g_2(\alpha)}{f(\alpha)} \sin \alpha y$$

Appendix D

Consider the following integrals in eqns(1.29c,d):

$$\begin{aligned} & \int_{b_1}^{b_2} K_{33}'(y,t)\phi_3(t)dt \quad \int_{b_1}^{b_2} K_{34}'(y,t)\phi_4(t)dt \\ & \int_{b_1}^{b_2} K_{43}'(y,t)\phi_3(t)dt \quad \int_{b_1}^{b_2} K_{44}'(y,t)\phi_4(t)dt \end{aligned} \quad (D.1abcd)$$

where

$$\begin{aligned} K_{33}'(y,t) &= \lim_{x_1 \rightarrow H_1} \frac{1}{\pi} \int_0^\infty \left[\frac{\text{ch}(w_1 \alpha x_1)}{\text{ch}(w_1 \alpha H_1)} J_9(y, \alpha) + \frac{\text{ch}(w_3 \alpha x_1)}{\text{ch}(w_3 \alpha H_1)} J_{10}(y, \alpha) \right] \cos \alpha t d\alpha \\ &= \lim_{x_1 \rightarrow H_1} \frac{1}{\pi} \int_0^\infty \left[\frac{\text{ch}(w_1 \alpha x_1) \gamma_3 h_1(\alpha)}{\text{ch}(w_1 \alpha H_1) f(\alpha)} + \frac{\text{ch}(w_3 \alpha x_1) \gamma_4 h_2(\alpha)}{\text{ch}(w_3 \alpha H_1) f(\alpha)} \right] \cos \alpha y \cos \alpha t d\alpha \\ &= \lim_{x_1 \rightarrow H_1} \frac{1}{2\pi} \int_0^\infty \left[\frac{\text{ch}(w_1 \alpha x_1) \gamma_3 h_1(\alpha)}{\text{ch}(w_1 \alpha H_1) f(\alpha)} + \frac{\text{ch}(w_3 \alpha x_1) \gamma_4 h_2(\alpha)}{\text{ch}(w_3 \alpha H_1) f(\alpha)} \right] [\cos \alpha(t-y) + \cos \alpha(t+y)] d\alpha \end{aligned} \quad (D.2a)$$

$$\begin{aligned} K_{34}'(y,t) &= \lim_{x_1 \rightarrow H_1} \frac{1}{\pi} \int_0^\infty \left[\frac{\text{ch}(w_1 \alpha x_1)}{\text{ch}(w_1 \alpha H_1)} J_{11}(y, \alpha) + \frac{\text{ch}(w_3 \alpha x_1)}{\text{ch}(w_3 \alpha H_1)} J_{12}(y, \alpha) \right] \sin \alpha t d\alpha \\ &= - \lim_{x_1 \rightarrow H_1} \frac{1}{\pi} \int_0^\infty \left[\frac{\text{ch}(w_1 \alpha x_1) \gamma_3 g_1(\alpha)}{\text{ch}(w_1 \alpha H_1) f(\alpha)} + \frac{\text{ch}(w_3 \alpha x_1) \gamma_4 g_2(\alpha)}{\text{ch}(w_3 \alpha H_1) f(\alpha)} \right] \cos \alpha y \sin \alpha t d\alpha \\ &= - \lim_{x_1 \rightarrow H_1} \frac{1}{2\pi} \int_0^\infty \left[\frac{\text{ch}(w_1 \alpha x_1) \gamma_3 g_1(\alpha)}{\text{ch}(w_1 \alpha H_1) f(\alpha)} + \frac{\text{ch}(w_3 \alpha x_1) \gamma_4 g_2(\alpha)}{\text{ch}(w_3 \alpha H_1) f(\alpha)} \right] [\sin \alpha(t-y) + \sin \alpha(t+y)] d\alpha \end{aligned} \quad (D.2b)$$

$$K_{43}'(y,t) = \lim_{x_1 \rightarrow H_1} \frac{1}{\pi} \int_0^\infty \left[\frac{\text{sh}(w_1 \alpha x_1)}{\text{ch}(w_1 \alpha H_1)} J_{13}(y, \alpha) + \frac{\text{sh}(w_3 \alpha x_1)}{\text{ch}(w_3 \alpha H_1)} J_{14}(y, \alpha) \right] \cos \alpha t d\alpha$$

$$\begin{aligned}
&= \lim_{x_1 \rightarrow H_1} \frac{1}{\pi} \int_0^{\infty} \left[\frac{\text{sh}(w_1 \alpha x_1) \gamma_9 h_1(\alpha)}{\text{ch}(w_1 \alpha H_1) f(\alpha)} + \frac{\text{sh}(w_3 \alpha x_1) \gamma_{10} h_2(\alpha)}{\text{ch}(w_3 \alpha H_1) f(\alpha)} \right] \sin \alpha y \cos \alpha t d\alpha \\
&= \lim_{x_1 \rightarrow H_1} \frac{1}{2\pi} \int_0^{\infty} \left[\frac{\text{sh}(w_1 \alpha x_1) \gamma_9 h_1(\alpha)}{\text{ch}(w_1 \alpha H_1) f(\alpha)} + \frac{\text{sh}(w_3 \alpha x_1) \gamma_{10} h_2(\alpha)}{\text{ch}(w_3 \alpha H_1) f(\alpha)} \right] [-\sin \alpha(t-y) + \sin \alpha(t+y)] d\alpha \quad (\text{D.2c})
\end{aligned}$$

$$\begin{aligned}
K_{44}'(y, t) &= \lim_{x_1 \rightarrow H_1} \frac{1}{\pi} \int_0^{\infty} \left[\frac{\text{sh}(w_1 \alpha x_1)}{\text{ch}(w_1 \alpha H_1)} J_{15}(y, \alpha) + \frac{\text{sh}(w_3 \alpha x_1)}{\text{ch}(w_3 \alpha H_1)} J_{16}(y, \alpha) \right] \sin \alpha t d\alpha \\
&= -\lim_{x_1 \rightarrow H_1} \frac{1}{\pi} \int_0^{\infty} \left[\frac{\text{sh}(w_1 \alpha x_1) \gamma_9 g_1(\alpha)}{\text{ch}(w_1 \alpha H_1) f(\alpha)} + \frac{\text{sh}(w_3 \alpha x_1) \gamma_{10} g_2(\alpha)}{\text{ch}(w_3 \alpha H_1) f(\alpha)} \right] \sin \alpha y \sin \alpha t d\alpha \\
&= -\lim_{x_1 \rightarrow H_1} \frac{1}{2\pi} \int_0^{\infty} \left[\frac{\text{sh}(w_1 \alpha x_1) \gamma_9 g_1(\alpha)}{\text{ch}(w_1 \alpha H_1) f(\alpha)} + \frac{\text{sh}(w_3 \alpha x_1) \gamma_{10} g_2(\alpha)}{\text{ch}(w_3 \alpha H_1) f(\alpha)} \right] [\cos \alpha(t-y) - \cos \alpha(t+y)] d\alpha \quad (\text{D.2.d})
\end{aligned}$$

As α approaches infinity, we have:

$$\left[\frac{\text{ch}(w_1 \alpha x_1) \gamma_3 h_1(\alpha)}{\text{ch}(w_1 \alpha H_1) f(\alpha)} + \frac{\text{ch}(w_3 \alpha x_1) \gamma_4 h_2(\alpha)}{\text{ch}(w_3 \alpha H_1) f(\alpha)} \right] \equiv \xi_1 e^{-\alpha w_1 (H_1 - x_1)} + \xi_2 e^{-\alpha w_3 (H_1 - x_1)} \quad (\text{D.3a})$$

$$\left[\frac{\text{ch}(w_1 \alpha x_1) \gamma_3 g_1(\alpha)}{\text{ch}(w_1 \alpha H_1) f(\alpha)} + \frac{\text{ch}(w_3 \alpha x_1) \gamma_4 g_2(\alpha)}{\text{ch}(w_3 \alpha H_1) f(\alpha)} \right] \equiv \xi_3 e^{-\alpha w_1 (H_1 - x_1)} + \xi_4 e^{-\alpha w_3 (H_1 - x_1)} \quad (\text{D.3b})$$

$$\left[\frac{\text{sh}(w_1 \alpha x_1) \gamma_9 h_1(\alpha)}{\text{ch}(w_1 \alpha H_1) f(\alpha)} + \frac{\text{sh}(w_3 \alpha x_1) \gamma_{10} h_2(\alpha)}{\text{ch}(w_3 \alpha H_1) f(\alpha)} \right] \equiv \xi_5 e^{-\alpha w_1 (H_1 - x_1)} + \xi_6 e^{-\alpha w_3 (H_1 - x_1)} \quad (\text{D.3c})$$

$$\left[\frac{\text{sh}(w_1 \alpha x_1) \gamma_9 g_1(\alpha)}{\text{ch}(w_1 \alpha H_1) f(\alpha)} + \frac{\text{sh}(w_3 \alpha x_1) \gamma_{10} g_2(\alpha)}{\text{ch}(w_3 \alpha H_1) f(\alpha)} \right] \equiv \xi_7 e^{-\alpha w_1 (H_1 - x_1)} + \xi_8 e^{-\alpha w_3 (H_1 - x_1)} \quad (\text{D.3d})$$

where $\xi_i (i=1-8)$ are material constants and are expressed as:

$$\xi_1 = \frac{\gamma_3 (\lambda_{73} + \lambda_{74} + \lambda_{75})}{\lambda_{24} + \lambda_{25} + \lambda_{26} + \lambda_{27} - \lambda_{28} + \lambda_{29}} \quad (\text{D.4a})$$

$$\xi_2 = \frac{\gamma_4 (\lambda_{61} + \lambda_{62} + \lambda_{63})}{\lambda_{24} + \lambda_{25} + \lambda_{26} + \lambda_{27} - \lambda_{28} + \lambda_{29}} \quad (\text{D.4b})$$

$$\xi_3 = \frac{\gamma_3 (\lambda_{70} + \lambda_{71} + \lambda_{72})}{\lambda_{24} + \lambda_{25} + \lambda_{26} + \lambda_{27} - \lambda_{28} + \lambda_{29}} \quad (\text{D.4c})$$

$$\xi_4 = \frac{\gamma_4 (\lambda_{58} + \lambda_{59} + \lambda_{60})}{\lambda_{24} + \lambda_{25} + \lambda_{26} + \lambda_{27} - \lambda_{28} + \lambda_{29}} \quad (\text{D.4d})$$

$$\xi_5 = \frac{\gamma_9 (\lambda_{73} + \lambda_{74} + \lambda_{75})}{\lambda_{24} + \lambda_{25} + \lambda_{26} + \lambda_{27} - \lambda_{28} + \lambda_{29}} \quad (\text{D.4e})$$

$$\xi_6 = \frac{\gamma_{10}(\lambda_{61} + \lambda_{62} + \lambda_{63})}{\lambda_{24} + \lambda_{25} + \lambda_{26} + \lambda_{27} - \lambda_{28} + \lambda_{29}} \quad (D.4f)$$

$$\xi_7 = \frac{\gamma_9(\lambda_{70} + \lambda_{71} + \lambda_{72})}{\lambda_{24} + \lambda_{25} + \lambda_{26} + \lambda_{27} - \lambda_{28} + \lambda_{29}} \quad (D.4.g)$$

$$\xi_8 = \frac{\gamma_{10}(\lambda_{58} + \lambda_{59} + \lambda_{60})}{\lambda_{24} + \lambda_{25} + \lambda_{26} + \lambda_{27} - \lambda_{28} + \lambda_{29}} \quad (D.4.h)$$

Using the following formulas:

$$\lim_{x_1 \rightarrow H_1} \int_0^{\infty} e^{-\alpha w_1(H_1 - x_1)} [\cos \alpha(t-y) + \cos \alpha(t+y)] d\alpha = \pi [\delta(t-y) + \delta(t+y)] \quad (D5.a)$$

and

$$\lim_{x_1 \rightarrow H_1} \int_0^{\infty} e^{-\alpha w_1(H_1 - x_1)} [\sin \alpha(t-y) + \sin \alpha(t+y)] d\alpha = \left(\frac{1}{t-y} + \frac{1}{t+y} \right) \quad (D.5b)$$

The asymptotic values of eqns(D.2abcd) become:

$$\begin{aligned} \lim_{x_1 \rightarrow H_1} \frac{1}{2\pi} \int_0^{\infty} [\xi_1 e^{-\alpha w_1(H_1 - x_1)} + \xi_2 e^{-\alpha w_3(H_1 - x_1)}] [\cos \alpha(t-y) + \cos \alpha(t+y)] d\alpha \\ = \frac{\rho_1}{2} [\delta(t-y) + \delta(t+y)] \end{aligned} \quad (D.6a)$$

$$\begin{aligned} - \lim_{x_1 \rightarrow H_1} \frac{1}{2\pi} \int_0^{\infty} [\xi_3 e^{-\alpha w_1(H_1 - x_1)} + \xi_4 e^{-\alpha w_3(H_1 - x_1)}] [\sin \alpha(t-y) + \sin \alpha(t+y)] d\alpha \\ = - \frac{\rho_2}{2\pi} \left(\frac{1}{t-y} + \frac{1}{t+y} \right) \end{aligned} \quad (D.6b)$$

$$\begin{aligned} \lim_{x_1 \rightarrow H_1} \frac{1}{2\pi} \int_0^{\infty} [\xi_5 e^{-\alpha w_1(H_1 - x_1)} + \xi_6 e^{-\alpha w_3(H_1 - x_1)}] [-\sin \alpha(t-y) + \sin \alpha(t+y)] d\alpha \\ = \frac{\rho_3}{2\pi} \left(-\frac{1}{t-y} + \frac{1}{t+y} \right) \end{aligned} \quad (D.6c)$$

$$- \lim_{x_1 \rightarrow H_1} \frac{1}{2\pi} \int_0^{\infty} [\xi_7 e^{-\alpha w_1(H_1 - x_1)} + \xi_8 e^{-\alpha w_3(H_1 - x_1)}] [\cos \alpha(t-y) - \cos \alpha(t+y)] d\alpha$$

$$= -\frac{\rho_4}{2} [\delta(t-y) - \delta(t+y)] \quad (\text{D.6d})$$

where $\rho_1 = \xi_1 + \xi_2$, $\rho_2 = \xi_3 + \xi_4$, $\rho_3 = \xi_5 + \xi_6$ and $\rho_4 = \xi_7 + \xi_8$

For $0 < b_1 \leq t \leq b_2$, one has the following relations:

$$\frac{\rho_1}{2} \int_{b_1}^{b_2} \phi_3(t) \delta(t-y) dt = \frac{\rho_1}{2} \phi_3(y) \quad (\text{D.7a})$$

$$\frac{\rho_1}{2} \int_{b_1}^{b_2} \phi_3(t) \delta(t+y) dt = 0 \quad (\text{D.7b})$$

$$\frac{\rho_4}{2} \int_{b_1}^{b_2} \phi_4(t) \delta(t-y) dt = \frac{\rho_4}{2} \phi_4(y) \quad (\text{D.7c})$$

$$\frac{\rho_4}{2} \int_{b_1}^{b_2} \phi_4(t) \delta(t+y) dt = 0 \quad (\text{D.7d})$$

By adding and subtracting the asymptotic value under the integral signs in eqns(D.2a-d), and substituting them back into eqns(D.a-d) respectively, we obtain:

$$\int_{b_1}^{b_2} K_{33}'(y,t) \phi_3(t) dt = \frac{\rho_1}{2} \phi_3(y) + \int_{b_1}^{b_2} K_{33}(y,t) \phi_3(t) dt \quad (\text{D.8a})$$

$$\int_{b_1}^{b_2} K_{34}'(y,t) \phi_4(t) dt = -\frac{\rho_2}{2\pi} \int_{b_1}^{b_2} \left(\frac{1}{t-y} + \frac{1}{t+y} \right) \phi_4(t) dt + \int_{b_1}^{b_2} K_{34}(y,t) \phi_4(t) dt \quad (\text{D.8b})$$

$$\int_{b_1}^{b_2} K_{43}'(y,t) \phi_3(t) dt = \frac{\rho_3}{2\pi} \int_{b_1}^{b_2} \left(-\frac{1}{t-y} + \frac{1}{t+y} \right) \phi_3(t) dt + \int_{b_1}^{b_2} K_{43}(y,t) \phi_3(t) dt \quad (\text{D.8c})$$

$$\int_{b_1}^{b_2} K_{44}'(y,t)\phi_4(t)dt = -\frac{p_4}{2}\phi_4(y) + \int_{b_1}^{b_2} K_{44}(y,t)\phi_4(t)dt \quad (D.8d)$$

where

$$K_{33}(y,t) = \lim_{x_1 \rightarrow H_1} \frac{1}{2\pi} \int_0^\infty \left\{ \left[\frac{\text{ch}(w_1 \alpha x_1) \gamma_3 h_1(\alpha)}{\text{ch}(w_1 \alpha H_1) f(\alpha)} + \frac{\text{ch}(w_3 \alpha x_1) \gamma_4 h_2(\alpha)}{\text{ch}(w_3 \alpha H_1) f(\alpha)} \right] \right. \\ \left. - [\xi_1 e^{-\alpha w_1 (H_1 - x_1)} + \xi_2 e^{-\alpha w_3 (H_1 - x_1)}] [\cos \alpha(t-y) + \cos \alpha(t+y)] \right\} d\alpha \quad (D.9a)$$

$$K_{34}(y,t) = - \lim_{x_1 \rightarrow H_1} \frac{1}{2\pi} \int_0^\infty \left\{ \left[\frac{\text{ch}(w_1 \alpha x_1) \gamma_3 g_1(\alpha)}{\text{ch}(w_1 \alpha H_1) f(\alpha)} + \frac{\text{ch}(w_3 \alpha x_1) \gamma_4 g_2(\alpha)}{\text{ch}(w_3 \alpha H_1) f(\alpha)} \right] \right. \\ \left. - [\xi_3 e^{-\alpha w_1 (H_1 - x_1)} + \xi_4 e^{-\alpha w_3 (H_1 - x_1)}] [\sin \alpha(t-y) + \sin \alpha(t+y)] \right\} d\alpha \quad (D.9b)$$

$$K_{43}(y,t) = \lim_{x_1 \rightarrow H_1} \frac{1}{2\pi} \int_0^\infty \left\{ \left[\frac{\text{sh}(w_1 \alpha x_1) \gamma_9 h_1(\alpha)}{\text{ch}(w_1 \alpha H_1) f(\alpha)} + \frac{\text{sh}(w_3 \alpha x_1) \gamma_{10} h_2(\alpha)}{\text{ch}(w_3 \alpha H_1) f(\alpha)} \right] \right. \\ \left. - [\xi_5 e^{-\alpha w_1 (H_1 - x_1)} + \xi_6 e^{-\alpha w_3 (H_1 - x_1)}] [-\sin \alpha(t-y) + \sin \alpha(t+y)] \right\} d\alpha \quad (D.9c)$$

$$K_{44}(y,t) = - \lim_{x_1 \rightarrow H_1} \frac{1}{2\pi} \int_0^\infty \left\{ \left[\frac{\text{sh}(w_1 \alpha x_1) \gamma_9 g_1(\alpha)}{\text{ch}(w_1 \alpha H_1) f(\alpha)} + \frac{\text{sh}(w_3 \alpha x_1) \gamma_{10} g_2(\alpha)}{\text{ch}(w_3 \alpha H_1) f(\alpha)} \right] \right. \\ \left. - [\xi_7 e^{-\alpha w_1 (H_1 - x_1)} + \xi_8 e^{-\alpha w_3 (H_1 - x_1)}] [\cos \alpha(t-y) - \cos \alpha(t+y)] \right\} d\alpha \quad (D.9d)$$

Appendix E Derivation of stress intensity factors and strain energy release rates

i) Case of embedded cracks

The stress intensity factors at the transverse crack tips are defined as:

$$\text{at } x_1 = a_1: \quad k(a_1) = \lim_{x_1 \rightarrow a_1} \sqrt{2(x_1 - a_1)} \sigma_{1y}(x_1, 0) \quad (\text{E.1a})$$

$$\text{at } x_2 = a_2: \quad k(a_2) = \lim_{x_2 \rightarrow a_2} \sqrt{2(x_2 - a_2)} \sigma_{2y}(x_2, 0) \quad (\text{E.1b})$$

From eqns (3.29a), for $|x_1| > a_1$ we obtain:

$$\sigma_{1y}(x_1, 0) = \frac{2\gamma_{14}E_y}{\pi(1 - v_{xy}v_{yx})} \int_{-a_1}^{a_1} \frac{\phi_1(t)}{t - x_1} dt + \sigma_{1y}^o(x_1, 0) \quad (\text{E.2})$$

where $\sigma_{1y}^o(x_1, 0)$ is a bounded function, and

$$\phi(t) = \frac{F_1(t)}{\sqrt{a_1^2 - t^2}} = \frac{F_1(t)e^{i\pi/2}}{(t - a_1)^{1/2}(t + a_1)^{1/2}}$$

From [33] if we introduce the sectionally holomorphic function $\varphi(z)$ as

$$\varphi(z) = \frac{1}{\pi} \int_{-a_1}^{a_1} \frac{\phi_1(t)}{t - z} dt$$

then we have:

$$\varphi(z) = \frac{F_1(-a_1)e^{i\pi/2}}{(2a_1)^{1/2}(z + a_1)^{1/2}} - \frac{F_1(a_1)}{(2a_1)^{1/2}(z - a_1)^{1/2}} + \varphi_o(z) \quad (\text{E.3})$$

Substituting (E.3) into (E.2) and from the definition of (E.1a), we have:

$$k(a_1) = - \frac{2\gamma_{14}E_y}{\pi(1 - v_{xy}v_{yx})} \frac{1}{\sqrt{a_1}} F_1(a_1) = - \frac{2\gamma_{14}E_y}{\pi(1 - v_{xy}v_{yx})} \sqrt{a_1} F_1^o(1)$$

Similarly

$$k(a_2) = - \frac{2\gamma_{14}^*E_y^*}{\pi(1 - v_{xy}^*v_{yx}^*)} \frac{1}{\sqrt{a_2}} F_2(a_2) = - \frac{2\gamma_{14}^*E_y^*}{\pi(1 - v_{xy}^*v_{yx}^*)} \sqrt{a_2} F_2^o(1)$$

Now consider the stress intensity factors on the interface.

From Eqn (3.55), we obtain:

$$\sqrt{\frac{\rho_4}{\rho_1\rho_2\rho_3}} \frac{1 - v_{xy}v_{yx}}{2E_x} \sigma_{xx}(H_1, r) + i \frac{1}{\rho_3} \frac{1}{2G_{xy}} \sigma_{xy}(H_1, r) = \frac{1}{\pi i} \int_{-1}^1 \frac{\psi_3^o(s)}{s - r} ds \quad |r| > 1$$

where $\psi_3^o(s) = \frac{F_3^o(s)e^{in\beta_3}}{(s+1)^{\alpha_3}(s-1)^{\beta_3}}$

Again from [33], we obtain:

$$\frac{1}{\pi i} \int_{-1}^1 \frac{\psi_3^o(s)}{s-r} ds = i\sqrt{1-\zeta^2} \left[\frac{1}{(r+1)^{\alpha_3}(r-1)^{\beta_3}} F_3^o(r) + F_n(r) \right]$$

where $F_n(r)$ is the principal part of $\psi_3^o(r)$ at infinity and is bounded. Therefore:

$$\frac{1-v_{xy}v_{yx}}{2E_x} \sqrt{\frac{\rho_4}{\rho_1\rho_2\rho_3}} \sigma_{xx}(H_1, r) + i \frac{1}{\rho_3} \frac{1}{2G_{xy}} \sigma_{xy}(H_1, r) = i\sqrt{1-\zeta^2} \left[\frac{1}{(r+1)^{\alpha_3}(r-1)^{\beta_3}} F_3^o(r) \right]$$

Multiply both sides of the above equation by $-i$, then we have:

$$\frac{1}{\rho_3} \frac{1}{2G_{xy}} \sigma_{xy}(H_1, r) - i \frac{1-v_{xy}v_{yx}}{2E_x} \sqrt{\frac{\rho_4}{\rho_1\rho_2\rho_3}} \sigma_{xx}(H_1, r) = \sqrt{1-\zeta^2} \left[\frac{1}{(r+1)^{\alpha_3}(r-1)^{\beta_3}} F_3^o(r) \right]$$

Now if we define the following stress intensity factors at the interface:

$$\begin{aligned} & \frac{1}{\rho_3} \frac{1}{2G_{xy}} k_2(r) - i \sqrt{\frac{\rho_4}{\rho_1\rho_2\rho_3}} \frac{1-v_{xy}v_{yx}}{2E_x} k_1(r) \\ &= \lim_{r \rightarrow 1} (r+1)^{\alpha_3}(r-1)^{\beta_3} \left[\frac{1}{\rho_3} \frac{1}{2G_{xy}} \sigma_{1xy}(H_1, r) - i \sqrt{\frac{\rho_4}{\rho_1\rho_2\rho_3}} \frac{1-v_{xy}v_{yx}}{2E_x} \sigma_{1xx}(H_1, r) \right] \end{aligned}$$

then we obtain:

$$\frac{1}{\rho_3} \frac{1}{2G_{xy}} k_2(\pm 1) - i \sqrt{\frac{\rho_4}{\rho_1\rho_2\rho_3}} \frac{1-v_{xy}v_{yx}}{2E_x} k_1(\pm 1) = \mp \sqrt{1-\zeta^2} F_3^o(\pm 1) \quad (E.4)$$

In order to derive the expression for the strain energy release rate at the interface crack tip, we first express $\psi_3^o(r)$ in terms of k_1 and k_2 , then from (E.4), we have

$$\begin{aligned} \psi_3^o(r) &= - \frac{(r+1)^{-\alpha_3}(r-1)^{-\beta_3} e^{in\beta_3}}{\sqrt{1-\zeta^2}} \left[\frac{1}{\rho_3} \frac{1}{2G_{xy}} k_2 - i \sqrt{\frac{\rho_4}{\rho_1\rho_2\rho_3}} \frac{1-v_{xy}v_{yx}}{2E_x} k_1 \right] \\ &= - \frac{1}{\sqrt{1-\zeta_2}} \left[\frac{1}{\rho_3} \frac{1}{2G_{xy}} k_2 - i \sqrt{\frac{\rho_4}{\rho_1\rho_2\rho_3}} \frac{1-v_{xy}v_{yx}}{2E_x} k_1 \right] \left(\frac{1-r}{1+r} \right)^{in\beta_3} \frac{1}{\sqrt{1-r^2}} \quad |r| < 1 \quad (E.5) \end{aligned}$$

Noting also that:

$$\begin{aligned}
& \frac{1}{\rho_3} \frac{1}{2G_{xy}} \sigma_{xy} - i \frac{1 - v_{xy} v_{yx}}{2E_x} \sqrt{\frac{\rho_4}{\rho_1 \rho_2 \rho_3}} \sigma_{xx} \\
&= \lim_{r \rightarrow 1} (r+1)^{-\alpha_3} (r-1)^{-\beta_3} \left[\frac{1}{\rho_3} \frac{1}{2G_{xy}} k_2 - i \sqrt{\frac{\rho_4}{\rho_1 \rho_2 \rho_3}} \frac{1 - v_{xy} v_{yx}}{2E_x} k_1 \right] \\
&= \left[\frac{1}{\rho_3} \frac{1}{2G_{xy}} k_2 - i \sqrt{\frac{\rho_4}{\rho_1 \rho_2 \rho_3}} \frac{1 - v_{xy} v_{yx}}{2E_x} k_1 \right] \left(\frac{r-1}{r+1} \right)^{i\omega} \frac{1}{\sqrt{r^2 - 1}} \quad |r| > 1 \quad (E.6)
\end{aligned}$$

Assuming $\eta \ll 1$, where $\eta = r-1$, then (E.6) can be approximated by

$$\begin{aligned}
& \frac{1}{\rho_3} \frac{1}{2G_{xy}} \sigma_{xy} - i \frac{1 - v_{xy} v_{yx}}{2E_x} \sqrt{\frac{\rho_4}{\rho_1 \rho_2 \rho_3}} \sigma_{xx} \\
&\cong \left[\frac{1}{\rho_3} \frac{1}{2G_{xy}} k_2 - i \sqrt{\frac{\rho_4}{\rho_1 \rho_2 \rho_3}} \frac{1 - v_{xy} v_{yx}}{2E_x} k_1 \right] \\
&\quad \times \frac{1}{\sqrt{2}\sqrt{\eta}} \left[\cos(\omega \log(\frac{\eta}{2})) + i \sin(\omega \log(\frac{\eta}{2})) \right] \quad (E.7)
\end{aligned}$$

Similarly, letting $\zeta = 1-r$ and assuming that $\zeta \ll 1$, then (E.5) can be expressed as:

$$\begin{aligned}
\psi_3^o(\zeta) &\cong - \frac{1}{\sqrt{1-\zeta_2}} \left[\frac{1}{\rho_3} \frac{1}{2G_{xy}} k_2 - i \sqrt{\frac{\rho_4}{\rho_1 \rho_2 \rho_3}} \frac{1 - v_{xy} v_{yx}}{2E_x} k_1 \right] \\
&\quad \times \frac{1}{\sqrt{2}\sqrt{\zeta}} \left[\cos(\omega \log(\frac{\zeta}{2})) + i \sin(\omega \log(\frac{\zeta}{2})) \right] \quad (E.8)
\end{aligned}$$

Since $\psi_3^o(r) = \frac{1}{2} \frac{\partial}{\partial r} [(v_1 - v_2) - i \sqrt{\frac{\eta_1}{\eta_2}} (u_1 - u_2)]$,

then

$$\begin{aligned}
\psi_3^o(\zeta) &= - \frac{1}{2} \frac{\partial}{\partial \zeta} [(v_1 - v_2) - i \sqrt{\frac{\eta_1}{\eta_2}} (u_1 - u_2)] \\
&\cong - \frac{1}{\sqrt{1-\zeta_2}} \left[\frac{1}{\rho_3} \frac{1}{2G_{xy}} k_2 - i \sqrt{\frac{\rho_4}{\rho_1 \rho_2 \rho_3}} \frac{1 - v_{xy} v_{yx}}{2E_x} k_1 \right]
\end{aligned}$$

$$\times \frac{1}{\sqrt{2}\sqrt{\zeta}} [\cos(\omega \log(\frac{\zeta}{2})) + i \sin(\omega \log(\frac{\zeta}{2}))] \quad (\text{E.8}^*)$$

The oscillatory behavior in (E.8*) can be removed using the techniques described in [40,42]. Considering the fact that the stress intensity factors and the displacement derivatives just away from the interface crack tips should have definite values. Therefore we can chose η and ζ in such a way,

$$\omega \log(\frac{\eta}{2}) \cong 0 \text{ and } \omega \log(\frac{\zeta}{2}) \cong 0$$

In fact, for most material combinations, that above two quantities are indeed very small. Then from eqns (E.7) and (E.8*), we have

$$\sigma_{xy} \cong \frac{1}{\sqrt{2}\sqrt{\eta}} k_2 \quad \sigma_{xx} \cong \frac{1}{\sqrt{2}\sqrt{\eta}} k_1$$

$$\Delta v = (v_1 - v_2) \cong 2\sqrt{2} \frac{1}{\sqrt{1-\zeta_2}} \frac{1}{\rho_3} \frac{1}{2G_{xy}} k_2$$

and
$$\Delta u = (u_1 - u_2) \cong 2\sqrt{2} \frac{1}{\sqrt{1-\zeta_2}} \frac{1}{\rho_2} \frac{1-v_{xy}v_{yx}}{2E_x} k_1$$

Assume the crack front was closed along the interface by an amount Δa

then using the method given in [44], we obtain the increment of the strain energy:

$$\begin{aligned} \Delta E &= 2 \int_r^{r+\Delta a} [\sigma_{xx} \Delta u(r-\Delta a) + \sigma_{xy} \Delta v(r-\Delta a)] dr \\ &= 2 \frac{2}{\sqrt{1-\zeta_2}} \left[\frac{1}{\rho_2} \frac{1-v_{xy}v_{yx}}{2E_x} k_1^2 + \frac{1}{\rho_3} \frac{1}{2G_{xy}} k_2^2 \right] \int_r^{r+\Delta a} \frac{\sqrt{1+\Delta a-r}}{\sqrt{r-1}} dr \\ &= 2 \frac{2}{\sqrt{1-\zeta_2}} \left[\frac{1}{\rho_2} \frac{1-v_{xy}v_{yx}}{2E_x} k_1^2 + \frac{1}{\rho_3} \frac{1}{2G_{xy}} k_2^2 \right] \frac{\pi}{2} \Delta a \end{aligned}$$

Therefore, the strain energy release rate will be:

$$\frac{\Delta E}{\Delta a} = \frac{2\pi}{\sqrt{1-\zeta_2}} \left[\frac{1}{\rho_2} \frac{1-v_{xy}v_{yx}}{2E_x} k_1^2 + \frac{1}{\rho_3} \frac{1}{2G_{xy}} k_2^2 \right] \quad (\text{E.9})$$

For Isotropic materials we have:

$$\frac{1}{\rho_2} \frac{1-v_{xy}v_{yx}}{2E_x} = \frac{1}{\rho_3} \frac{1}{2G_{xy}}$$

then

$$\frac{\Delta E}{\Delta a} = \frac{2\pi}{\sqrt{1-\zeta_2}} \frac{1}{\rho_3} \frac{1}{2G_{xy}} [k_1^2 + k_2^2] \quad (E.9^*)$$

ii) Case of transverse crack touching the interface

Define the stress intensity factor

$$k(a_1) = \lim_{x_2 \rightarrow -H_2} 2^\gamma (x_2 + H_2)^\gamma \sigma_{2y}(x_2, 0) \quad (E.10)$$

from eqn (3.29b), we have

$$\sigma_{2y}(x_1, 0) = \frac{2\gamma_{14} E_y}{\pi(1 - \nu_{xy} \nu_{yx})} \int_{-H_1}^{H_1} K_{21s}(x_2, t) \phi_1(t) dt + \sigma_{2y}^o(x_2, 0) \quad (E.11)$$

where $\sigma_{2y}^o(x_2, 0)$ is bounded function and

$$\phi_1(t) = \frac{F_1(t)}{(H_1^2 - t^2)^\gamma} = \frac{F_1(t)e^{i\gamma}}{(t - H_1)^\gamma (t + H_1)^\gamma}$$

Again define:
$$\varphi(z) = \frac{1}{\pi} \int_{-H_1}^{H_1} \frac{\phi_1(t)}{t - z} dt$$

then we have:

$$\varphi(z) = \frac{F_1(-H_1)e^{i\gamma}}{(2H_1)^\gamma \sin \pi\gamma (z + H_1)^\gamma} - \frac{F_1(H_1)}{(2H_1)^\gamma \sin \pi\gamma (z - H_1)^\gamma} + \varphi_o(z) \quad (E.12)$$

Substituting (E.12) back into (E.11), and then from the definition of (E.10), we have:

$$k(a_1) = \frac{(H_1)^{2\gamma} \gamma_{14}^* E_y^* F_1^o(1)}{(1 - \nu_{xy}^* \nu_{yx}^*) \sin(\pi\gamma)} \left[\lambda_{101} \frac{|w_1|/\beta_5}{[w_1^* \| w_1|/\beta_5]^\gamma} + \lambda_{102} \frac{|w_1|/\beta_5}{[w_3^* \| w_1|/\beta_5]^\gamma} \right. \\ \left. + \lambda_{103} \frac{|w_3|/\beta_5}{[w_3 \| w_1^*|/\beta_5]^\gamma} + \lambda_{101} \frac{|w_3|/\beta_5}{[w_3 \| w_3^*|/\beta_5]^\gamma} \right] \quad (E.13)$$

The stress intensity factors at other crack tips and the strain energy release rate at the interface crack tip remain the same.

iii) H-shaped cracks

The derivation of stress intensity factors and of the strain energy release rates at the interface crack tip remain the same as those given in section i).